UNIVERSIDAD COMPLUTENSE DE MADRID
FACULTAD DE CIENCIAS FÍSICAS

TESIS DOCTORAL

Simulador Visual Binocular de Visión Simultánea : validación e implementación de la tecnología Sim+Vis en la clínica

Binocular Simultaneous Vision Simulator : validation and implementation of the Sim+Vis technology in the clinic

MEMORIA PARA OPTAR AL GRADO DE DOCTOR

PRESENTADA POR

Xoana Barcala Gosende

Directores

Carlos Dorronsoro Díaz
Susana Marcos Celestino

Madrid

UNIVERSIDAD COMPLUTENSE DE MADRID

FACULTAD DE CIENCIAS FÍSICAS

TESIS DOCTORAL

Simulador Visual Binocular de Visión Simultánea: validación e implementación de la tecnología Sim+Vis en la clínica.

Binocular Simultaneous Vision Simulator: validation and implementation of the Sim+Vis technology in the clinic.

MEMORIA PARA OPTAR AL GRADO DE DOCTOR

PRESENTADA POR

Xoana Barcala Gosende

DIRECTORES

Carlos Dorronsoro Díaz
Susana Marcos Celestino

INDUSTRIAL DOCTORAL THESIS

Binocular Simultaneous Vision Simulator: validation and implementation of the Sim+Vis technology in the clinic.

Simulador Visual Binocular de Visión Simultánea: validación e implementación de la tecnología Sim+Vis en la clínica.

Memoria presentada para optar al título de Doctor en Física por la Universidad Complutense de Madrid por:

Xoana Barcala Gosende

Supervised by:

Carlos Dorronsoro Díaz

Susana Marcos Celestino

VioBio Lab.

Instituto de Óptica

CSIC

2EyesVision S.L.

Madrid

Departamento de Óptica

Facultad de Ciencias Físicas

UCM

Madrid, July 2021

A todos los que me habéis acompañado
en este proceso de crecer y crear.
A mis miedos y mis monstruos.

"Only those who risk going too far can possibly know how far one can go."

T. S. Eliot

"Nunca he visto cumplirse un sueño en el que no he creído"

Coco Animaux

Acknowledgments

Creo que no llego a ser consciente de estar escribiendo esto y de pensar que esta etapa se termina. No diré que ha sido fácil, pero ha sido gratificante, y a pesar de pensar en desistir mil veces, aquí estoy, aquí estamos todas las Xoanas que he sido durante estos años, preparadas para cerrar esta etapa y comenzar una nueva aventura. Tengo mucho que agradecer a todas las personas que me han acompañado en este proceso.

A **Susana**, por brindarme la oportunidad de entrar en el grupo. Por dejarme fascinada con tu mente, tu esfuerzo y tu pasión por el trabajo. Por escucharme siempre que te lo he pedido. Por tu guía. Gracias por dejarme aprender de ti.

A **Carlos**, no se me ocurre mejor palara que decirte que GRACIAS. Gracias por tu entusiasmo y euforia. Gracias por creer en mí aun cuando a mí me costaba, gracias por los empujones y las broncas cuando tocaban. Gracias por enseñarme tu constancia, por dejarme fallar y ayudarme a aprender, por enseñarme tanto profesional y personalmente. Gracias por compartir reuniones y cañas, canciones de Spotify y fotos de viajes, lágrimas y risas. Gracias por ser inspiración.

A mi familia **2Eyes**, a la que he visto crecer y he crecido con ella. Creo que no podría haber mejores personas en este equipo, sin excepciones. Trabajar a vuestro lado ha sido (y es) realmente bonito. A **Enrique**, por su bondad y paciencia, por tu inteligencia que no para de sorprenderme. A **Álvaro**, por compartir risas y complicidad, por dejarme siempre asombrada con tu elegancia y confianza hablando. De mayor quiero ser como tú. Por ser el mejor compi de viajes. A ambos, por ser los mejores compis de booth y ferias que podría tener. A **Cris**, compañera infalible de iLab, por aguantar confesiones y apaciguar, por comprender siempre. Por esa luz que tienes, que siempre ves un pasito más allá. A **Lucie** por crear una red de intercambios de Gekkos en la misma manzana, por venir a visitarme al balcón con Emilio, por tener siempre un sitio en tu coche para mí. **Diana**, **Joshua**, **Yassine**, **Pilar**, **Carmen, Cándido, José**

Ramón, Ángel, Paula y **Edu**. Me siento siempre respaldada por todos vosotros aún en la otra punta del mundo. Gracias por ser **equipo**.

A **Jan Bonel**, por ver algo en mí que aún no sé qué es. Gracias por brindarme oportunidades, gracias por la confianza, gracias por dejarme aprender de ti.

A mi otra familia, **VioBio**. Realmente mi primer año en este laboratorio me enamoró, por cada una de las personas que lo componían, por transmitirme su pasión por lo que hacían. Ese fue realmente el inicio de todo esto, sois los culpables de que empezase este camino, y siempre os daré las gracias por ello. **María**, **Dani**, **Edu**, **Alberto**, **Andrea**, **Rocío**, **Sara**, **James**, **Andrés**, **Carmen**, **Elena**, **Clara**, **Judith**, **Miriam**, **Nohelia**, **Pablo**, **Víctor**, **Lekha, Ana, Iván, Merche, Amal,**… Sois tantos los que habéis pasado por ahí y me habéis enseñado y aportado algo, que lo siento si me he dejado a alguien.

Y cómo no, a **IOSA**. Gracias a **Rocío** y **Clara** por acompañarme en mi primera actividad, en Ubrique. Jamás algo tan altruista me había llenado tanto. Gracias a todos los que habéis ido pasando por la dirección del grupo, y a todos los miembros por hacerlo posible día a día. Os he ido nombrando en diferentes partes, pero no quería olvidarme de **Camilo**, **Carlos** y **Francesca**. ¡Ojalá podamos celebrarlo con unas cañas pronto!

Algo que compartimos en 2Eyes y VioBio, además del I+D, es la pasión por la música. No podía dejar sin mencionar a los **SinBises**, que llegaron y lo petaron en un único concierto. Pero lo bueno si es breve, dos veces bueno.

Gracias a **Clara**, por vivir a media canción de mí, por acogerme en tu casa y en tu vida. Gracias por cada abrazo. Porque sigamos sumando momentos, con viajes y bailes rumanos locos. Gracias a **Elena**, por iluminarme siempre con tu sabiduría, por ser vecina y compi de entrenos estoicos, por ser siempre sincera, por poder ser yo sin filtros. Gracias a las dos por los nuevos principios *di-vinos*. Gracias a **María**, por compartir cañas, familia, viajes a Galicia, experiencias, consejos. Gracias a las tres, por ser un pilar fundamental en los peores momentos, por ser compañeras de Mucca y vinos. Gracias a **Víctor**, que apareció sin contar y se queda como amigo. Por ser compi de despacho, porque podamos escribirnos siempre para desahogarnos, para que no se nos vaya la pinza, para que no trabajemos 16h al día, aunque luego lo hagamos. Gracias a **Sara**, por tu generosidad, por tu preocupación por los demás. Siempre te diré que me avises al llegar a casa.

Alessandra, gracias por aparecer para quedarte, por compartir cualquier clase de plan random, cóctel y sushi, o pensamiento científico. Gracias por ser un apoyo imprescindible, por tu sinceridad y tus consejos. Por ser inspiración, ejemplo de pasión, constancia y trabajo. Por quedar

aquí o en el fin del mundo. Por hacer planes juntas aún con un océano de por medio. Por entenderme hasta cuando gesticulo las palabras que no me sé y por darme tanta vida con tu risa. No sabes todo lo que te quiero. Gracias por venir acompañada de todo **RadioPatio**. **Gemma**, **Patri**, **María, Luz**, gracias por vernos siempre, por hacer que ni la distancia ni el tiempo importe. Por cada momento que he vivido con vosotras, en persona y por videollamada. Porque podamos coleccionar más elefantitos rosas juntas, vernos el cualquier país y ¡por todas las aventuras que nos quedan! Pero ya sabemos chicas, *Keep fucking going*.

A mi **Consejo de Sabias**. Las optometristas más top de Madrid. **Ainhoa**, **Caye**, **Estela**, ya sabemos que los domingos son los días en los que todo puede pasar y que *from lost to the river*. Gracias por cada quedada y desahogo que hemos hecho. Por tener orden del día para que no se nos olvide nada. Por vuestra luz interior.

Mis **Rollers**, ¡no me puedo olvidar de vosotros! **Edu**, **Pilar** y **Ana** que llegasteis en un momento complicado por la pandemia, pero me habéis dejado conocer lo maravillosas personas que sois. Gracias por cada quedada, risa compartida, juego de mesa y cómo no, salida en patines (que pronto retomaré). Por ser el grupo del **Sí**.

A mi compi de escritura de tesis por excelencia, **Jesús**, aunque fuese a distancia siempre encontrábamos desahogo y empatía. Al resto de amigos y compañeros que me han acompañado estos años, desde cualquier lugar, en Galicia, Letonia, Rumanía, ….

A **MariLuz**, porque sin ti no podría haber llegado hasta aquí. Gracias por ayudarme a comprender a cada Xoana, pero enseñarme a seguir, por ayudarme a crecer y que pueda intentar ser la mejor versión de mí. Gracias por cada abrazo, esos que tanto me reconfortan. Gracias por tu cariño. Qué suerte la mía por encontrarte.

E como non podía faltar, á miña familia de sangue, esa que está en Galicia ou desperdigada polo mundo, pero esa que sempre está a unha videochamada de distancia. A miña nai, **Belén**, a meu pai, **Manuel**, e a miñas irmás, **Catarina** e **Elisa**, gracias por sentirvos orgullosos de min. Gracias por ensinarme a esforzarme sempre, gracias por ter esa constancia e loita que tendes. Gracias por ser o meu principal apoio. Quérovos un mundo. Nenas, vos sempre. Gracias aos **meus avós**, que sempre teño presente, que me coidan na distancia, gracias por ser o mellor exemplo de persoa que me gustaría ser.

Funding

The research developed during this thesis would have not been possible without the funding received from the following public and private institutions:

- Madrid Regional Government (CAM). Industrial PhD Grant IND2017/BMD-76702 to Xoana Barcala.
- Instituto de Salud Carlos III from DTS16-00127 to Carlos Dorronsoro.
- Spanish Government Grant FIS2017-84753-R to Susana Marcos.
- Master Clinical Research Agreement between Johnson & Johnson Vision Care (USA), 2EyesVision, and IO-CSIC IP: Susana Marcos

Abstract

Binocular Simultaneous Vision Simulator: validation and implementation of the Sim+Vis technology in the clinic

With aging, the crystalline lens loses its ability to accommodate (a condition known as presbyopia), making necessary to use optical aids to see at near. Today, a wide variety of optical solutions for presbyopia (both surgical and non-surgical) are available, aiming at providing patients with satisfactory functional vision at different distances.

Prescribing presbyopia solutions is a difficult problem, as every patient has different needs, and it is difficult to convey to the patient how his/her visual quality is going to see with different corrections. Besides spectacles (progressive lenses or single focus positive lenses), multifocal contact lenses and intraocular lenses have emerged as popular solutions. Multifocal contact lenses are non-surgical solutions (and therefore easily reversible). However, the fitting process is lengthy. On the other hand, surgical solutions such as multifocal intraocular lenses, cannot be tried before implantation.

Visual simulators meet the need for non-invasive trying different corrections prior to prescription or implantation. The SimVis Gekko (based on the Sim+Vis technology) is the first see-through and binocular simulator, allowing patients to see the real world through different binocular combinations of monofocal and multifocal corrections.

The principle of the Sim+Vis technology is the temporal multiplexing of a tunable lens, which, through a custom-developed driver operating at 50 Hz, changes focus to produce multifocal retinal images of a static appearance. In this thesis, we present calibration set-ups and quality control benches developed to improve the control capacity of the tunable lens. In particular, we have improved the controllability of the tunable lens, by introducing corrections of dynamic and thermal effects, allowing precise simulations of commercial and generic lenses.

In this thesis, we have also developed a specific metric to evaluate perceived visual quality with presbyopic corrections: the Multifocal Acceptance Score to Evaluate Vision (MAS-2EV). This

metric represents a multifactorial evaluation of vision (through scoring of natural images) in different conditions of illumination (day and night) and distances, in addition to a stereopsis measurement. We have studied the repeatability of the metric and its performance on different groups of patients (presbyopic, simulated presbyopic, and cataract patients), in combination with the SimVis Gekko or contact lenses.

We have studied the accuracy of the SimVis Gekko to represent different commercial lenses. In a first study we compared through focus visual quality, perceived vision (MAS-2EV), and visual satisfaction (vision questionnaires) through real contact lenses or through these lenses represented in SimVis Gekko, showing a high degree of similarity between real and simulated lenses. Also, we compared through-focus visual quality with the SimVis Gekko representing state-of-the-art commercial multifocal intraocular lenses in a group of presbyopic patients with that of patients implanted with the same lenses (from the literature), obtaining a high degree of similarity. Finally, we evaluated (MAS-2EV) different presbyopia corrections administered in the SimVis Gekko in patients with cataracts, and in the same patients after implantation of a monofocal intraocular lens. We found similar rankings in the tested corrections before and after surgery, for patients with clear lens and to a relatively high degree of scattering, suggesting that SimVis Gekko can be reliably used even in patients with opacities.

In summary, we have calibrated and demonstrated the use of a novel commercial instrument, the SimVis Gekko, developed at the Visual Optics and Biophotonics Lab (IO-CSIC) and produced by 2EyesVision (the hosting research institution and company, respectively). The results of this thesis have therefore advanced the science of presbyopia correction and produced progress towards the clinical application of a technology-based product.

Keywords: presbyopia, quality of vision, visual perception, visual preference, multifocal lenses, EDOF lenses, visual simulators, simultaneous vision, temporal multiplexing, SimVis Gekko, ophthalmic corrections, contact lenses, intraocular lenses.

Resumen de la tesis en castellano

Simulador Visual Binocular de Visión Simultánea: validación e implementación de la tecnología Sim+Vis en la clínica.

Con el envejecimiento, el cristalino pierde su capacidad de acomodación (condición que es conocida como presbicia) haciendo necesario el uso de ayudas ópticas para ver de cerca. En la actualidad, existe una gran variedad de soluciones ópticas para la presbicia (tanto quirúrgicas como no quirúrgicas), cuyo objetivo es proporcionar a los pacientes una visión funcional satisfactoria a diferentes distancias.

La prescripción de soluciones para la presbicia es una tarea difícil, ya que cada paciente tiene necesidades distintas y es difícil transmitirle cómo va a ser su calidad visual con las distintas correcciones. Además de las gafas (lentes progresivas o lentes monofocales únicamente para cerca), las lentes de contacto multifocales y las lentes intraoculares han surgido como soluciones prometedoras. Las lentes de contacto multifocales son soluciones no quirúrgicas (y, por tanto, fácilmente reversibles). Sin embargo, el proceso de adaptación es largo. Por otro lado, las soluciones quirúrgicas, como las lentes intraoculares multifocales, no pueden probarse antes de su implantación.

Los simuladores visuales satisfacen la necesidad de probar de forma no invasiva diferentes correcciones de presbicia antes de su prescripción o implantación. SimVis Gekko (basado en la tecnología Sim+Vis) es el primer simulador visual binocular que permite a los pacientes ver el mundo real a través de diferentes combinaciones binoculares de lentes monofocales y multifocales.

El principio de la tecnología Sim+Vis es la multiplexación temporal de una lente optoajustable que, a través de un controlador desarrollado a medida que funciona a 50 Hz, cambia el enfoque para producir imágenes multifocales que tienen una apariencia estática en la retina. En esta tesis, presentamos montajes de calibración y bancos de control de calidad desarrollados para mejorar la capacidad de control de la lente optoajustable. En particular, hemos mejorado la capacidad de

control de la lente optoajustable, introduciendo correcciones de los efectos dinámicos y térmicos, lo que permite realizar simulaciones precisas de lentes comerciales y genéricas.

En esta tesis también hemos desarrollado una métrica específica para evaluar la calidad visual percibida con correcciones de presbicia: la Puntuación de Aceptación Multifocal para Evaluar la Visión (MAS-2EV, por sus siglas en inglés). Esta métrica representa una evaluación multifactorial de la visión (a través de la puntuación de imágenes naturales) en diferentes condiciones de iluminación (día y noche) y distancias, además de una medida de la estereopsis. Hemos estudiado la repetibilidad de la métrica y su rendimiento en diferentes grupos de pacientes (présbitas, présbitas simulados y pacientes con cataratas), en combinación con el SimVis Gekko o con lentes de contacto.

Hemos estudiado la precisión de SimVis Gekko para representar diferentes lentes comerciales. En un primer estudio comparamos la calidad visual a través del foco, la visión percibida (MAS-2EV) y la satisfacción visual (cuestionarios de visión) a través de lentes de contacto reales o a través de estas lentes simuladas en SimVis Gekko, mostrando un alto grado de similitud entre las lentes reales y las simuladas. Asimismo, se comparó la calidad visual obtenida a través de SimVis Gekko representando lentes intraoculares multifocales comerciales de última generación en un grupo de pacientes présbitas con la de pacientes implantados con las mismas lentes (obtenidos de la literatura), obteniendo un alto grado de similitud. Finalmente, evaluamos (MAS-2EV) diferentes correcciones de presbicia administradas en el SimVis Gekko en pacientes con cataratas, y en los mismos pacientes tras la implantación de una lente intraocular monofocal. Encontramos preferencias similares en las correcciones probadas antes y después de la cirugía, para pacientes con cristalino transparente y con un grado relativamente alto de dispersión, lo que sugiere que SimVis Gekko puede utilizarse de forma fiable incluso en pacientes con opacidades.

En resumen, hemos calibrado y demostrado el uso de un novedoso instrumento comercial, el SimVis Gekko, desarrollado en el Laboratorio de Óptica Visual y Biofotónica (IO-CSIC) y producido por 2EyesVision (la institución de investigación y la empresa anfitrionas, respectivamente). Los resultados de esta tesis han hecho avanzar, por tanto, la ciencia de la corrección de la presbicia y han producido un progreso hacia la aplicación clínica de un producto de base tecnológica.

Palabras clave: presbicia, calidad de visión, percepción visual, preferencia visual, lentes multifocales, lentes de foco extendido, simuladores visuales, visión simultánea, multiplexación temporal, SimVis Gekko, correcciones oftálmicas, lentes de contacto, lentes intraoculares.

List of most used abbreviations

A
Add = Addition
AO = Adaptive Optics
B
C
Cyl = Cylinder
CL = Contact Lens
CLUE questionnaire = Contact Lens User Experience vision questionnaire
D
D = Diopters
DFVA = Defocus Visual Acuity
DM = Deformable Mirror
DoF = Depth of Focus
E
EDOF = Extended Depth of Focus
F
FoV = Field of View
G
H
I
ICL = Implantable Collamer Lens
IOL = Intraocular Lens
J
K
L
Lasik = Laser Assisted Keratomileusis
LIRIC = Laser Induced Refractive Index Correction
M
M-CLs = Multifocal CLs

M-IOL= Multifocal IOL
MAS-2EV = Multifocal Acceptance Score to Evaluate Vision
MTF = Modulation Transfer Function

N

O

OD = Right Eye
OS = Left Eye
OSI = Objective Scatter Index

P

PRK = Photo Refractive Keratometry
PS = Perceptual Score

Q

QoV = Quality of Vision

R

RMS = Root Mean Square wavefront error
Sph = Spherical error
RS = Refractive Surgery

S

SimVis = Simultaneous Vision Simulator
SLM = Spatial Light Modulator

T

TL = Tunable Lens
TF = Through-focus

U

V

VA = Visual Acuity
VS = Visual Strehl

W

X

Y

Z

Table of contents

Chapter 1

Introduction

The visual system, and in particular the crystalline lens, undergoes alterations associated with aging that affect different aspects of the visual process. Presbyopia is one of the main processes that appear with aging and affects 100% of the population over 45 years old. Presbyopes progressively lose their capacity to focus near objects and consequently they need external solutions to see at intermediate and near distances.

Multiple solutions for presbyopia are available on the market, and many others are coming out trying to improve the performance of the current ones and the patient's outcomes. Additionally, this wide variety of options makes choosing the best solution for each patient a hard task. Different technologies have been developed in the last years, trying to facilitate the prescribing process for presbyopia corrections.

In the first chapter of this thesis, we present a brief revision of the state-of-the-art in the field of research and technologies, the motivation, open questions, goals of the thesis, and hypothesis. In particular, we address the aging eye, the different corrections available, and the strategies and technologies behind them. Current limitations to select the best solution for each patient in the clinic are also presented, as well as visual simulators and related technologies that arise trying to solve them.

This chapter is based on the published book chapter by Enrique Gambra Urralburu, María Viñas Peña, Lucie Sawides, Xoana Barcala Gosende, Carlos Dorronsoro Díaz and Susana Marcos Celestino, *Simuladores Visuales*, in *Cirugía refractiva del cristalino*, edited by Luis Fernández-Vega and José F. Alfonso. Monografías de la Sociedad Española de Oftalmología, 2020. ISBN: 9788489085756 [1].

1.1. The aging eye

The crystalline lens of the human eye is a transparent biconvex lens, with aspheric surfaces, located between the iris and the vitreous humor. It is held equatorially by elastic fibers of the zonula that attach it to the ciliary muscle and transmit the accommodation forces. The capsular epithelium regenerates the lens fibers throughout life forming the denser nucleus at the center, with a higher refractive index (1.44) and the relatively loosely packed cortex, with a refractive index of 1.36 [2].

The crystalline lens has the peculiarity of being able to change its shape and size with vergence. This process, known as accommodation, allows the visual system to focus on near objects. The first reference to accommodation is from Descartes in 1677 [3], but the most accurate and universally accepted theory of the accommodation process was proposed by Helmholtz in 1855 [4]. During the accommodation process, the ciliary muscle contracts relieving the tension on the zonular fibers and relaxing the forces transmitted to the crystalline lens, increasing its anterior curvature and in consequence its optical power. Figure 1.1 illustrates the differences between the accommodated and relaxed eye. The change in the lens curvature is accompanied by the convergence of the two eyes and constriction of the pupil (miosis) comprising the classic accommodative reflex [5,6].

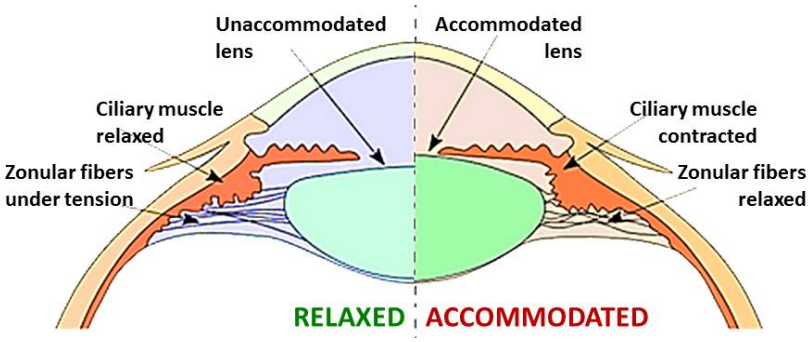

Figure 1.1 *Schematic representation of the accommodation process of the eye* [7]. *Left: Accommodation at rest (relaxed eye). The ciliary muscle is relaxed and the tension of the zonule fibers keeps the lens flattened, thus forming an image of distant objects. Right: Eye accommodating. The ciliary muscle contracts, releasing the tension of the zonule fibers, allowing the lens to curved to increase its optical power.*

The amplitude or range of accommodation is the total amount of accommodation that the visual system can bring into play, from the farthest point that the eye can see clearly when accommodation is at rest, to the closest point that can be seen clearly using the full amount of accommodation. This amplitude of accommodation ranges from 10-15 D in the young adult [8]. As the lens ages, it becomes harder and more sclerotic, resisting deformation when the ciliary muscle contracts. The loss of accommodative range is a gradual process that begins in childhood and affects 100% of the population but does not become a clinical problem until the age of 40 or 50 [9] when the subjective amplitude of accommodation falls below 3 D. This process is known as presbyopia and is defined as the loss of accommodative ability due to aging [10,11].

Cataract is a pathology mainly associated with aging, although environmental and genetic factors are also involved. Like presbyopia, it is also a gradual process, that begins with a loss of transparency until it reaches a total opacification of the crystalline lens that leads to blindness. This pathology affects 50% of the population over 65 years of age and is the leading cause of blindness in the world: 47.8% of blindness worldwide (17.6 million people) [12] is due to loss of vision due to cataracts. However, it is a reversible cause of blindness with the only possible solution so far, being a surgical intervention to remove the lens and implant an intraocular lens (IOL). Cataract surgery is the most performed surgical procedure worldwide. It was conducted over 4.3 million times in 2018 across the European Union. Approximately 828 operations were performed per hundred thousand inhabitants in Spain in that same year [13].

1.2. Ophthalmic corrections for presbyopia

The objective of correcting presbyopia is to restore, at least in part, the functionality of near vision. The first correction for presbyopia was a pair of convex lenses helping to focus at near distance. This solution is still one of the most widespread ones nowadays, despite the positive addition depending on the age and working distance, forcing presbyopic patients to continuously increase the addition of their near glasses. This traditional solution, like many others, only meets the basic needs since distance vision is blurred with near vision glasses. This is why many other alternatives have been developed throughout the years. Some of the current corrections for presbyopia, already available in optometry and/or ophthalmology clinics, are summarized in Table 1.1. Additionally, aging has increased worldwide in the last decades, and the prevalence of presbyopia is estimated to increase from 1.2 billion in 2010 to 1.8 billion in 2050 [14]. Although none of the current solutions can restore the full dynamic capacity of the young eye, different strategies try to provide good functionality for near and distance vision. The differences between them and their pros and cons are described in the following sections.

Method	Correction	Strategy
External Optics (non-surgical corrections)	Spectacles	Monofocal Alternating Vision
	Contact lenses (CLs)	Monofocal Multifocal EDOF Monovision Combined strategies
Surgical Corrections	Corneal refractive surgery (RS)	Monofocal Multifocal EDOF Monovision Combined strategies
	Intraocular lenses (IOL)	Monofocal Multifocal

		EDOF Monovision Combined strategies Accommodating IOLs

Table 1.1 *Main current solutions for presbyopia. Adapted from Charman et al. (2014) [15].*

1.2.1. Non-surgical corrections

Non-surgical corrections, using external optics in a non-invasive way, were the first solutions used, initially as spectacles and later using contact lenses.

Glasses are still the most common solution nowadays, in the form of monofocal lenses for near vision, or following alternating vision strategies (section 1.4.1), such as progressives or bifocals. Glasses are the more obvious choice for the patient when the first symptoms of presbyopia appear.

Soft contact lenses (CLs) as a solution for presbyopia are a minimally invasive method (unless otherwise noted, when referring to CLs, they are always soft CLs). The average age of the CLs wearers is increasing [16–18]. In fact, the reported percentage of patients using CLs as their presbyopia correction has increased from 16% in 2011 to 25–35% in 2019 [19,20]. Different strategies include spectacles over CLs, monovision (section 1.4.3), and multifocal CLs (M-CLs; section 1.4.2). However, the use of CLs to manage presbyopia, and in particular the penetration of M-CLs, is still low and subject to high regional variations [21]. Different variables introduce visual alterations concerning the lens design: interactions with the tear film, lens centration, up-gaze movement, and tightness due to the anterior face of the cornea, eyelids, and blink [22,23].

1.2.2. Surgical corrections

Surgical options for presbyopia, whether clear lens extraction, cataract surgery, or corneal refractive surgery (RS), are invasive procedures in which highly satisfactory patient outcomes are sought.

In corneal refractive surgery (RS) an excimer laser is typically used to compensate for ocular refractive errors. There are two major techniques: (1) photorefractive keratometry (PRK) and laser-assisted keratomileusis (LASIK). In the PKR technique, the stroma surface is ablated to the required curvature. In the LASIK procedure, a cornea flap is cut to perform the ablation on the deeper corneal stroma. The main advantage of LASIK over PRK is that the central corneal epithelium is better preserved, which is why LASIK is the dominant RS procedure [24,25]. Both techniques were first used to compensate myopia and hyperopia, and result in different ablation patterns to also compensate presbyopia (as in CLs, monovision, or modified monovision corrections -see section 1.4- are provided with RS). Lately, there is another specific technique that creates multifocal patterns on the corneal surface, known as presbyLASIK, aimed to reduce near vision spectacle dependency in presbyopic patients [26–28]. Lastly, there is a new technique called laser-induced refractive index correction (LIRIC) that creates diffractive profiles by altering the cornea's refractive index with a femtosecond laser [29].

However, the most frequently used surgical treatment for presbyopia is the use of intraocular lenses (IOLs) through clear lens extraction or cataract surgery. Cataract surgery is a non-elective surgery that patients must undergo to recover their vision and avoid blindness. However, as the hardness of the nucleus of the lens increases, the surgery becomes riskier. That is one of the reasons why clear lens extraction becomes popular for presbyopia correction, preventing the formation of cataracts. Both cataract and clear lens extraction surgeries are done using the same surgical technique. There are many different surgical techniques, but the most used nowadays is phacoemulsification.

This technique is performed through a small incision in the corneal limbus, which does not modify the preoperative corneal astigmatism. A circular aperture (capsulorhexis) is made on the capsular bag to proceed with the simultaneous fragmentation (using ultrasound waves) and aspiration of the crystalline lens. The IOL is folded and inserted, often using a cartridge, inside the capsular bag through the incision of the cornea and the capsulorhexis. Once inside the capsule, the lens is unfolded and its haptics rest on the edges of the capsule. By hydration of the tissue adjacent to the incisions, the incisions are sealed, without the need for sutures [30]. Figure 1.2 illustrates this technique during cataract surgery. There are several phacoemulsification techniques that usually depend on the hardness of the nucleus and the surgeon's preference.

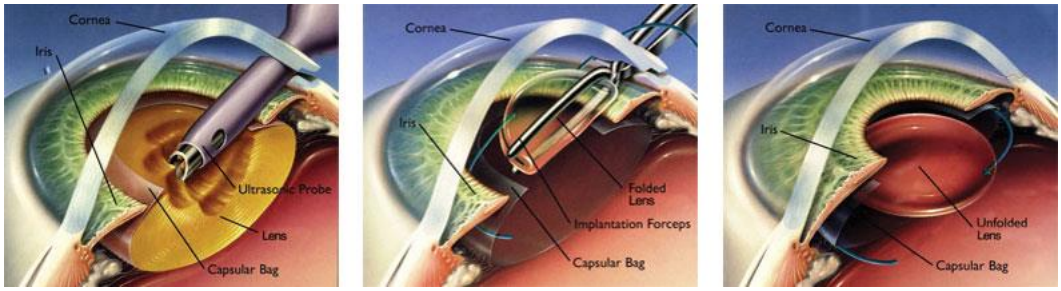

Figure 1.2 *Representative images of cataract surgery by phacoemulsification. Left image: Incision at the corneal limbus, the aperture in the capsular bag, fragmenting and aspirating of the lens. Middle image: insertion of the folded IOL. Right image: unfolded IOL placed inside the capsular bag. Image source: indoreeyecare.com*

There is a wide variety of IOLs designs, based on the number and distribution of the foci. They have normally split it into different groups: monofocal IOLs, M-IOLs, extended depth of focus (EDOF) IOLs, and accommodating IOLs [24]. They are explained in section 1.4.

Another type of IOLs that can be used for presbyopia corrections is the implantable Collamer lens (ICL), an IOL that is implanted on the anterior chamber of the eye, after the iris, and before the crystalline lens. ICLs are popularly known as implantable CLs and can have the same kind of designs as any other IOL. The main advantage is that the crystalline lens is not disturbed, so the surgical procedure is easier than a clear lens extraction or a cataract surgery, with a similar surgical procedure to the phacoemulsification. However, this solution is temporary as it does not prevent cataract development.

The main drawback of all these surgical corrections as a solution for presbyopia is their surgical nature and the risk of lack of adaptation due to loss of image quality, contrast, or monocular or

binocular blurring. Patient dissatisfaction may lead, in extreme cases, to a new surgery to exchange IOLs.

1.3. Strategies and technologies to compensate for presbyopia

As we have seen in the previous section, the compensation for presbyopia can rely on different ophthalmic solutions (glasses, CLs, IOLs, RS patterns, etc.). Each solution can be considered a platform in which different strategies can be implemented. While traditional monofocal corrections have a fixed focal position providing focused vision for only one specific distance, many other designs and strategies can provide focused images for different visual distances. This section describes some of the most common approaches to compensate for presbyopia.

1.3.1. Alternating vision

Alternating vision-based solutions comprised bifocal or progressive lenses, for its exclusive use in spectacles. Alternating vision CLs were a less frequently used option among rigid gas permeable CLs users for a few years but are no longer available. Changes in gaze and/or head position allow the selection of the viewing zone for the desired distance.

Conventional bifocal spectacle lenses offer two visibly differentiated zones, each of them with a fixed-focus for a different distance. Typically, a near vision segment is added on the lower part of a far vision lens. The discontinuity between zones normally produces an abrupt change in image size and location, known as image jump, as the line of sight passes between both regions [15,31].

Progressive lenses provide a continuous and smooth transition between the far-focus zone (upper part of the lens) and the near-focus zone (lower part of the lens), with an optical corridor for intermediate distances in the center of the lens. The continuous change in addition power is obtained at the expense of undesired optical degradations in the visual field outside of that corridor [32] (mainly optical distortion, astigmatism, and coma aberrations) producing visual discomfort, fatigue, and vertigo. The fitting process of progressive lenses and the education of the patients are particularly important to achieve a satisfactory vision and to minimize the rejection rate.

1.3.2. Monovision

In monovision, one eye is corrected for far distance and the other for near distance, both with monofocal lenses. Consequently, for each given visual distance at least one of the eyes is out of focus. The selection of the correction (visual distance in focus) for each eye is based on eye dominance, although there is a lack of standardization in the dominance test to use in clinical practice [33]. The selection of the wrong dominant eye can result in lower contrast images [34], additional discomfort, and increased rejection rates. Monovision relies on the selective neural suppression of the defocused images coming from the eye out of focus, while the brain processes the sharp images coming from the eye in focus.

Monovision is not a common solution in spectacles, due to the strong anisometropia and prismatic effects induced. However, monovision implemented with CLs, IOLs, and RS corneal ablation patterns is well accepted by the patients because the optical correction is placed near the principal points of the eye, reducing magnification, and well centered, reducing prismatic shifts [35].

This solution, in any of its implementations, has also some disadvantages caused by the interocular blur difference, mainly the loss of stereopsis [35] and other binocular vision abnormalities [36,37]. Despite the drawbacks, monovision correction is still the most popular spectacle-free presbyopic correction [15].

1.3.3. Simultaneous vision

Another spectacle-free solution is simultaneous vision [24], also referred to as multifocal corrections, which provides an alternative approach. Each simultaneous vision CL, IOL, or RS pattern has two or more foci, but as opposed to alternating vision spectacle lenses and monovision, simultaneous vision corrects each eye simultaneously for different distances. The correction moves with the eye and always produces the same effect, regardless of the gaze position. For each eye, simultaneous vision creates a superposition of image components in the retina, all of them with similar content, position, and magnification, but each one corresponding to a different visual distance. The goal is to always have one of those image components in focus: the one matching the visual distance of the object. However, the sharp component is always superimposed on a background of other defocused image components that reduce the overall contrast.

Generally, in multifocal design, some annular regions correct far distance vision while other annular regions have higher power for near and/or intermediate vision (Figure 1.3). The resultant retinal images with image components having different degrees of defocus provide sharp images of objects at different distances, at the expense of a reduction in optical quality (mainly contrast reduction, but also blur) [24,38]. Just as with monovision, the visual system beyond the optics is instrumental in the success of the multifocal vision. The neural processing of the image taking place along the visual pathway restores, at least to some extent, some key image features provided by the in-focus image (sharpness, contrast) and suppresses others from the defocused components (such as blur). The human brain is constantly re-normalizing new signals and conditions, which is why, after a certain period of time of constant exposure to multifocal images -from seconds to months-, neural adaptation takes place, adapting the brain to the new visual experience, and improving the perception of the images. Neural perception and neural adaptation are key processes in the acceptance of multifocal images.

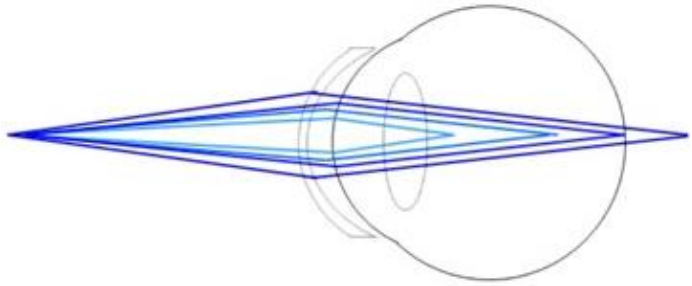

Figure 1.3 *Schematic representation of image formation with multifocal simultaneous vision lenses. When looking at a specific distance, a focused image is projected onto the patient's retina for that distance, superimposed with out-of-focus images for the other distances.*

The use of simultaneous vision is increasing, creating interesting market opportunities. There are many simultaneous vision correction designs, which can be classified based on the number of focal points: bifocal, trifocal, and extended depth of focus (EDOF) lenses.

Bifocal lenses have two foci, generally at far and near distances. Trifocal lenses add another focus at an intermediate distance. EDOF lenses are more difficult to define. The American Academy of Ophthalmology generated a consensus statement that defined EDOF lenses as M-IOLs that must provide excellent far and intermediate vision. According to the ANSI (American National Standards Institute), EDOF lenses have to provide increase depth of focus compared with monofocal lenses [39] in the defocus visual acuity (DFVA) curves. EDOF lenses came out to provide a better far and intermediate distance compared with bifocal and trifocal IOLs, with fewer dysphotopsia effects, where even the need for near spectacles may arise for near tasks. There are three ways to obtain an EDOF design: (1) using small apertures; (2) adding spherical aberration; (3) using discrete multiple foci in refractive and diffractive designs. Currently, there are at least 70 different M-IOLs (bifocal, trifocal, and EDOF) on the international market [40].

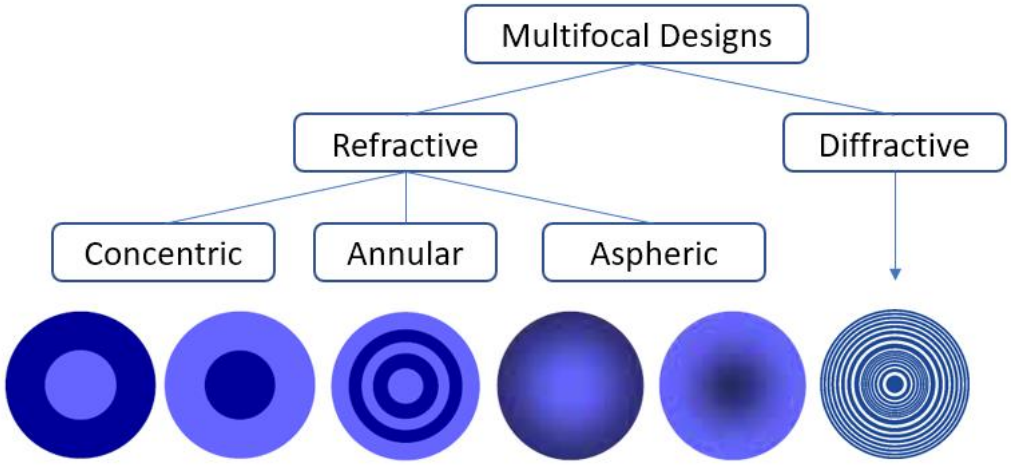

Figure 1.4 *Some examples of multifocal designs classification. The far and near zones are represented by different tones of blue.*

Simultaneous vision designs can also be classified according to the optical principle on which they are based (Figure 1.4): refractive, diffractive and, hybrid designs (combining both refraction and diffraction principles).

A. Refractive Designs

These designs are based on the fundamental optical principle of light refraction. A ray of light changes its direction upon passing through in the interface of two materials if the incidence angle is other than zero (oblique incidence according to the Snell's law or the law of refraction: $n \times \sin \varepsilon = n' \times \sin \varepsilon'$), and if the materials have different refractive indices, i.e., air and plastic which is often the case. The law of refraction can be applied only if the interfaces between the two optical media are smooth and undisturbed. Figure 1.4 illustrates some power maps corresponding to refractive designs. The different tones of blue indicate different optical powers. The transition between the far and near, or intermediate, distance zones can be gradual (aspheric designs), with segmented rings (concentric and annular designs) or a combination of both. In these designs, a part of the pupil is devoted for far, and another for near (either in the center or periphery).

In some aspheric designs, the progressive change in optical power is induced by conic surfaces, allowing the manipulation of the spherical aberration to expand the depth of focus. These designs comprise a power gradient that changes radially across the lens [41]. More complex aspherical surfaces entail free-form optics.

In concentric designs, the different optical powers are induced with different local surface curvatures in each zone. Refractive designs are usually highly dependent on pupil size, which changes the relative contribution of the different areas and, therefore, the distribution of energies in the different foci. Annular designs (see Figure 1.4) attempt to achieve pupillary independence with rings of optical power reducing the effect of different pupil diameters.

Aspheric designs are performed in PresbyLASIK RS, creating center-distance and/or center-near patterns with different asphericities [27].

Refractive M-CLs are typically a combination of bifocal concentric designs, either center-near or center-distance, and aspheric designs [42]. Some examples of commercial M-CLs, with their design approach, are listed in Table 1.2.

Brand	Manufacturer	Lens Design
Acuvue Oasys	Vistakon, Johnson & Johnson, USA	Center-distance concentric aspheric zones
1-Day Acuvue Moist		Center-near aspheric
Dailies AquaComfort Plus	ALCON, USA	Center-near aspheric
Proclear 1 day	Cooper Vision, USA	Center-near aspheric
PureVision 2	Bausch & Lomb, USA	Center-near aspheric

Table 1.2*. Some examples of M-CLs commercially available, with the brand, manufacturer, and lens design. Adapted from Kim et al 2017* [42].

Regarding refractive M-IOLs, some commercial lenses have asymmetrical segmented bifocal designs, such as the M-Plus (Oculentis BV, Netherlands) [43]. Others, such as the M-Flex (Rayner, UK) or the ReZoom (initially from Abbott Medical Optics Inc, nowadays property of Johnson & Johnson) [44], are M-IOLs with symmetric annular bifocal designs.

Considering EDOF lenses, the Lucidis lens (SAV-IOL SA, Switzerland) combines an aspheric central surface with a refractive peripheral surface [45]. The MiniWELL (SIFI, Italy) is a biconvex double aspheric design with three different zones [46]. Some promising refractive EDOF lenses have reached the market in the last years, such as the Vivity lens (Alcon Laboratories, TX, USA) and the Isopure (Physiol, Belgium) [47], both pupil independent designs. Another recent refractive EDOF, but pupil-dependent, is the EyHance (Johnson & Johnson, USA) [48,49]. Further descriptions of these designs and an exhaustive revision of the most popular ones, were done by Rampad and Gatinel in 2020 [40].

Additionally, there is a new IOL in the market called Light-Adjustable Lens (RxSight, California, USA), that can be shape modified after the surgery with ultraviolet light to improve patient outcomes [50].

B. Diffractive Designs

Diffractive designs are based on the principle of light diffraction when the light is understood as a wave. Diffractive surfaces are designed with the same magnitude as the wavelength of light. The optical path is modified once the light goes through the diffractive surface (also called steps) and different diffractive orders create near and/or intermediate foci [51]. Figure 1.5 shows a real diffractive IOL with an augmented image. Some of these lenses have apodized diffractive patterns, meaning that at some point in the periphery the height of the steps is progressively reduced so there is a continuous fade out of the diffractive foci.

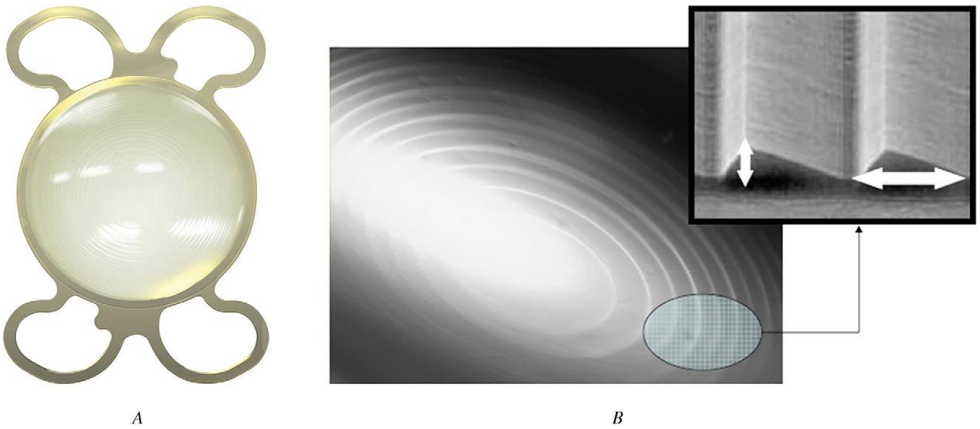

***Figure 1.5 A**. Real multifocal diffractive IOL. **B**. Augmented image of the diffractive M-IOL (microscope magnification x10)* [52].

In clinical practice, the main advantages of diffractive designs are that they provide excellent near vision [53] and that the image quality and the energy balance between the images at different distances do not depend on the pupil diameter. However, the perception of dysphotopsias, such as halos and glare at night, and chromatic effects are frequently reported [51].

Diffractive M-CLs are rare. There are only a few commercial designs based on diffractive steps, all of them in the posterior surface of the CL [20], probably due to the interactions between the tear film and the diffractive steps. Recently, non-superficial diffractive designs based on LIRIC technology (refractive index patterns inside the material) attempt to solve this problem.

Although they are not yet in the market, the company Clerio Vision (Rochester, USA) is currently developing them.

In the M-IOL market, however, we can find many more IOLs that introduce diffractive optics in their designs. Some lenses are based principally on diffractive optics including bifocal (Tecnis ZKB00 (+2.75D) [54], ZLB00 (+3.25D) [55], ZMB00 (+4.00D) [56] from Johnson & Johnson, Bi-Flex M from Medicontur), trifocal (AT Lisa from Carl Zeiss, RayOne tri from Rayner, FineVision from Physiol [40], Liberty from Medicontur), and EDOF lenses (Tecnis Symfony [57,58] and Synergy IOLs from Johnson & Johnson [59], AT Lara from Carl Zeiss [58,60]).

Hybrid designs using both refractive and diffractive principles to induce an addition compensating presbyopia are common options: bifocal (ReSTOR from Alcon, SeeLens from Hanita), trifocal (AcrySoft IQ PanOptix from Alcon), EDOF (EDEN and Harmonis from SAV-IOL SA [61], Diffractive Diff-Aa from HumanOptics and FineVision Triumf from Physiol) [40].

1.3.4. Corrections combining monovision and simultaneous vision

Binocular combinations of monovision and simultaneous vision, placing a different lens in each eye, open a new world of combinations. Modified monovision, mini-monovision, or blended vision [62] are corrections that require a smaller interocular dioptric power difference between eyes than traditional monovision. Among the wide variety of this kind of solutions, the most common ones are (1) a mix of a monofocal lens on the dominant eye and a multifocal correction in the non-dominant eye [63]; (2) the use of the same M-IOL (i.e., EDOF lenses) in both eyes with a myopic shift [64]; (3) the use of the same M-IOL (i.e., bifocal lens) in both eyes with different additions [55,65,66]; and (4) monofocal IOLs in both eyes with an interocular difference between 0.75 and 1.75 D [67,68]. These combinations attempt to improve several aspects of visual performance. Among them: binocular vision (and consequently stereopsis) in comparison to monovision contrast in comparison to M-IOLs alone and vision at intermediate distances.

Regarding M-CLs, modified monovision is usually performed by fitting a center-distance design on the dominant eye and a center-near design in the contralateral eye [15].

Mix and match strategies attempt to combine the advantages of refractive and diffractive designs, implanting one refractive IOL in one eye, and a diffractive design in the contralateral eye. This kind of combination tries to reduce the dysphotopsia effects (less glare and halos) while and improving the contrast sensitivity [69,70]. Although some ophthalmologists are skeptical about this mix and match of corrections, others see an opportunity to improve patient's visual performance and satisfaction.

1.3.5. Accommodation restoration

The most ambitious goal to provide an ultimate solution for presbyopia is the development of a lens that mimics the behavior of the crystalline lens, changing its shape to focus at one distance or another and thus restoring the accommodative capacity of the young crystalline lens.

Accommodative lenses are, in essence, monofocal lenses that aim to take advantage of the function of the ciliary muscle to change its focal length, making it possible to focus at different distances. This is possible because the ciliary muscle of presbyopic patients maintains its contraction capacity [71], at least in part.

Accommodating IOLs have an enormous economic and clinical interest. There have been several accommodative lenses designs on clinical trials, but only one of them has reached the market [72]: the Crystalens (Bausch & Lomb), based on axial displacements, and FDA-approved in 2009. Although there were reported clinical outcomes that showed an improvement in near vision with Crystalens, a few experimental studies showed that its mechanism did not function correctly on-eye and that the movement was often in the opposite direction of that was required to accommodate [73].

1.4. Selecting the best presbyopia correction in the clinic

The number of CLs, IOLs, or corneal ablation patterns available on the market is increasing, improving their designs and techniques to provide each patient with optimal vision. In addition to the multiplicity of designs, binocular combinations are possible, with the option of placing different lenses in each eye.

The first generation of M-IOLs was introduced in the 1980s with limited success, primarily due to less than stellar outcomes and visual trade-offs [74–76]. The latest generation of M-IOLs, such as the FineVision trifocal range and the M-Plus IOLs, have overcome many of the visual trade-offs that the 1st generation of designs had [77]. However, even with improvements in designs and visual outcomes, the uptake of presbyopia-correcting M-IOLs remains low, ranging from 10 to 15% globally. This is due to different factors: (1) surgeon skepticism resulting from poor results with earlier generations of these IOLs; (2) high patient expectations [78], difficult to meet.

Thus, the decision to implant one lens or another is currently based on the ophthalmologist's experience, combined with some data on the patient's visual habits and preferences, and on the patient's own personality [79]. Presbyopia surgery can give unexpected results due to various surgical reasons, but also due to the choice of an inappropriate optical solution for the patient. Although in the prescription process it is becoming common to analyze the results of other clinical measurements besides biometry (as aberrations or topography), in no case the decision on what lens to implant is based on the patient's actual visual experience with the type of correction to be implanted.

One method to assess a patient’s individual visual needs is to determine patient expectations and visual behavior pre-operatively to improve post-operative outcomes. To date, however, determining these requirements has been based almost solely on pre-operative questionnaires focusing on lifestyle and desired outcomes, and patient counseling [80].

It is well known that not all patients accept all optical corrections in the same way and that there are preferences for one or many corrections that depend on their visual system [81–83]. Although in recent years IOL exchange surgery has become increasingly common [84,85] it is an

option that should not be considered a priori when selecting the lens for the first surgery, to avoid the risks associated with successive surgeries. The priority should be to find the lens that best suits each patient individually and his or her daily visual needs, ensuring maximum visual satisfaction after surgery.

Similarly, in M-CLs the fitting process is performed over a three-day (or longer) period [86] and the average success rate for prescribing M-CLs is 67-83% after three months [20,87]. The main disadvantage is the current ineffective fitting strategy, based on a trial-and-error method to select the lens design, increasing the number of clinical appointments, and requiring too much chair time. Some practitioners do not offer the M-CL option to their patients, discouraged by the presumable compromise of visual quality experienced by patients [18,88] and the difficulty to manage patient expectations [89]. While recommendations for patient selection and fitting guides have been published [20,90] aiming at smoothing the process, there is a general consensus that a successful M-CL fitting is ultimately highly dependent on the patient's individual optics and visual tolerance.

1.4.1. Evaluating presbyopia corrections

Typically, the quality of vision provided by multifocal lenses, monovision, and combined strategies is tested using visual acuity (VA) at various distances or using defocus VA (DFVA) curves [91–94]. It is well recognized that high contrast VA is a limited descriptor of the quality of vision. Besides, the complexity and lack of personalized designs of multifocal vision [95] require wider and more sophisticated evaluation methods.

Quality of vision (QoV) is, in fact, multifactorial. QoV largely depends on the visual world projected onto the retina (luminance, spatial content, and contrast), on the response of the eyes to the three-dimensional visual scene (including the pupil diameter, the accommodation state -focus-, and the interocular convergence), on the optical quality of the eye or of the ophthalmic correction worn (optical aberrations, scattering) and, on the previous visual experience (neural adaptation) of the patient [96].

To date, the QoV is assessed clinically utilizing questionnaires that are given to the patient who self-report visual comfort and task performance in different situations (i.e. reading a restaurant menu, driving, sewing, etc...) [97]. Examples of these questionnaires include the NEI RQL-42 [98], a questionnaire with 42 questions that measure the patient's satisfaction at distance vision, clarity of vision, and severity and frequency of glare symptoms, along with the need for spectacles. Other questionnaires also include an assessment of the satisfaction with day and night vision (as the Functional Assessment of Visual Tasks (VISTAS) questionnaire [99,100]) or with night driving (as VF-14, the Visual Function Index). Some questionnaires (i.e., The Catquest-9SF questionnaire) address the perceived benefits of cataract surgery [101]. While the previous questionnaires were not specifically designed to evaluate the QoV with multifocal lenses, the CLUE questionnaire [102] developed by Johnson and Johnson targets specifically the QoV (as well as other comfort aspects) with M-CLs.

Drawbacks associated with vision questionnaires have been addressed before. For example, systematic psychometric evaluations showed that the NEI-RQL-42 questionnaire has deficiencies in most of its tested aspects [103]. All questionnaires, even those optimally designed, rely on the patient's memory, as they rate their vision for situations that they encountered over different days. Furthermore, the evaluations provided by the questionnaires may differ across patients, as not every patient is exposed to the same visual environment. There are no standardized validated questionnaires for IOL patients to report subjective symptoms.

1.5. Visual simulators and related technologies

Most of the presbyopic corrections mentioned in section 1.4, if not all, represent a novel visual experience for the patient. The final level of satisfaction, or even the rejection of the correction, depends, on one hand, on optical factors affecting retinal blur (as the aberrations of the eye, the optical coupling between the correction and the eye, or the pupil) that go beyond the design of the correction (distribution of energies at several distances) and; on the other hand, on the neural processing (interpretation in the brain and extraction of the relevant information) of the resultant retinal images often affected by spatially variant blur and contrast reduction. All these dependencies affecting visual performance and visual comfort interact with each other in different ways for every patient and, therefore, the final acceptance is difficult to anticipate.

The purpose of simulating optical corrections in the eye is the subjective experimentation by the patient of the corrections to be prescribed, dynamically. Visual simulators allow the comparison of different options, before the selection of the correction with which the patient obtains the best subjective vision. Within this option, one of the simplest and best-known visual simulators is the phoropter, which allows the patient to experience different spherical and cylindrical corrections. As ocular corrections become more sophisticated (i.e., correction of higher-order aberrations or simulation of presbyopia corrections) the possibilities of manipulating ocular optics through conventional lenses (spherical-cylindrical) become very limited, and, therefore, the phoropter can fall short in performance.

Visual simulators applied to the field of presbyopia are devices that allow the patient to experience different optical solutions before surgery or CLs fitting [82,91,104]. These devices are not virtual reality simulators based on computational manipulation of digital images, but instruments that faithfully replicate the optics of the solutions to be implanted. Therefore, the patient can experience their own vision through the replicated or simulated optics, and the interaction that exists between the object observed at a given distance, and the presbyopic solution being tested.

Visual simulators are particularly attractive for evaluating the patient's QoV with new optical designs before a CL fitting or their surgical implantation [81,83], and sometimes even before the lens has been manufactured. This extraordinary ability to simulate new ophthalmic corrections makes it possible to investigate the interactions between the ocular optics and a given optical

design, to evaluate the differences between lenses with different designs, and, finally, to select the correction that allows the best optical and visual quality in each patient [82,104,105].

Visual simulators can be used to determine the degree of acceptance to a generic type of correction (i.e., to a trifocal lens), to a particular commercial CL or IOL or, if the ophthalmologist deems it appropriate, to compare two or more corrections with each other; for example, a classic monofocal correction, a bilateral trifocal correction, and the combination of different lenses addition in each eye. Visual simulators are intended to help the ophthalmologist and contactologists to personalize the treatment offered to the presbyopic patient, improving the patient experience with better-informed decision making, increasing, and improving patient satisfaction by helping to identify the most appropriate optical solution for them. In the case of IOLs, visual simulators will reduce the risk of an explantation. For M-CLs, visual simulators will help to speed up the CLs fitting in a non-invasive way.

1.5.1. Adaptive Optics

Adaptive Optics (AO) was first developed in 1977 to compensate for the atmospheric turbulence affecting astronomic images [106]. Since then, AO techniques have evolved in a variety of applications requiring precise optical manipulations, mainly optical excitation or detection, in dissimilar fields such as free-space optical communications or microscopy. In the eye, AO has been used both for high-resolution imaging of the retina and for the simulation of optical corrections [107–109].

AO systems consist of a wavefront sensor (usually a Hartmann-Shack aberrometer) that measures optical aberrations in real-time and an active element that compensates for these aberrations. There are several types of active elements, including membrane electromagnetic Deformable Mirrors (DMs) or Spatial Light Modulators (SLMs). Other components of the AO system used in visual applications generally include a Badal system, for compensation of spherical errors, a psychophysical channel consisting of a monitor or mini display for the projection of psychophysical stimuli -and thus for the measurement of visual perception and function-, and a channel for monitoring pupil size and pupil centering.

The common principle of DMs is the use of multiple actuators located on the back of a flexible reflective membrane. Depending on the voltage applied to each actuator, they push or pull the surface, allowing the shape of the mirror to be controlled. DMs have the advantage of achromaticity and no significant light loss, but their main disadvantage is their inability to simulate patterns with abrupt phase changes as segmented and diffractive corrections [110].

SLMs consist of liquid crystal mirrors on a silica chip, in which an applied voltage allows to control the polarization state of each pixel on the screen. In combination with polarizers, it is possible to modulate a wavefront with pixel resolution. Compared to DMs, the spatial resolution of SLMs as active elements of an AO system is very high, allowing the rendering of segmented corrections or diffractive elements [82,111]. Their main disadvantage is that they are not achromatic, so they produce residual chromatic artifacts.

Some of the world's most recognized AO laboratories in visual science have developed visual simulators on optical benches with DMs and/or SLMs [112], proving that those systems can accurately replicate multifocal solutions, both IOLs [91] and CLs [113].

1.5.2. Commercial devices

In recent years, the technologies described above have led to the development of several visual simulators that, in some cases, have become commercially available.

The first visual simulators developed were based on AO, such as the CRX1 from Imagine Eyes (Orsay, France) [114], and the VAO from Voptica (Murcia, Spain) [115], although their use has not yet spread to clinical practice. However, the main disadvantage of these AO systems transitioned from research labs to clinical environments, is that they have large dimensions with a footprint difficult to fit in the clinical space, they are typically difficult to operate, requiring expert monitoring at all times, they are generally monocular, and, have a narrow-field-of-view black and gray stimulus computer-generated on a display [112]. Ideal visual simulators for clinical applications should be see-through and binocular, providing a natural observation of the rich visual environment around the patient, including the diversity of colors and distances, and with a wide field-of-view enabling different visual tasks and measurements of objective performance and subjective perception.

Additionally, there has been at least one attempt to develop a system based on the projection of the real IOL placed in a cuvette [116]. The device, called VirtIOL [117], has the advantage of allowing the outside world to be observed through the IOL projected onto the pupil plane of the eye. The field of view is wide, although static, as it is a table-top fixed instrument. Among its main disadvantages are the difficulty of changing the correction to be tested due to the alignment requirements of the equipment, and the fact that it is not programmable. It does not allow the quick alternation of different options adapted to the patient's visual needs and preferences. Furthermore, the instrument only allows monocular vision testing.

The latest device to appear on the market is called SimVis Gekko™ from 2EyesVision (Madrid, Spain) and is based on the use of temporal multiplexing with tunable lenses, a novel technology explained in the following section.

1.5.3. Sim+Vis Technology™

The Sim+Vis Technology™ was developed in the Visual Optics and Biophotonics Lab, starting with a monocular two-channel optical bench and ending on a miniaturized wearable binocular device. This sub-section addresses a review of the origins and evolution of this technology before this thesis.

A. Spatial multiplexing

The first version of the simultaneous vision simulator (SimVis) was developed in 2010 [118] (Figure 1.6) to assess visual perception and performance with pure binocular simultaneous vision corrections, and it was based on spatial multiplexing of two optical channels. A beam splitter

sends the optical projection of the stimuli through two independent Badal channels, one focused at far and the other focused at near distance, overlapping both images on the retina [118,119] without changing the magnification.

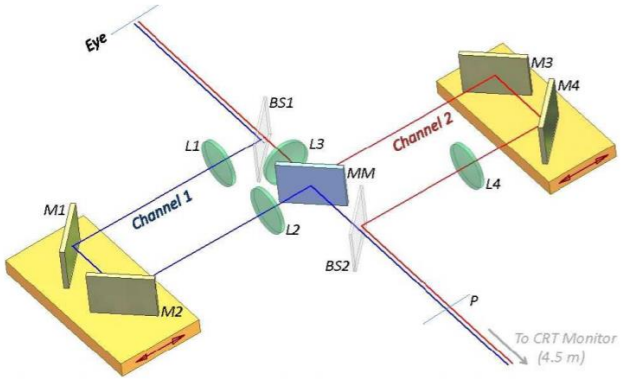

Figure 1.6 *Schematic diagram of the first SimVis system (spatial multiplexing SimVis simulator)* [119].

However, the system had limitations to simulate specific multifocal designs and a transmissive SLM was incorporated to introduce phase profiles corresponding to any segmented refractive multifocal design (angular or radial designs with different far-near energy ratios). Due to the limitations introduced by the SLM, the maximum extent of the retinal image that could be tested, without overlapping diffractive orders, was about 3 degrees [83]. The brightness of the stimuli used for psychophysical tasks was increased by adding a DLP projector instead of a CRT monitor, making the system more compact. A schematic representation of the improved spatial multiplexing SimVis is shown in Figure 1.7.

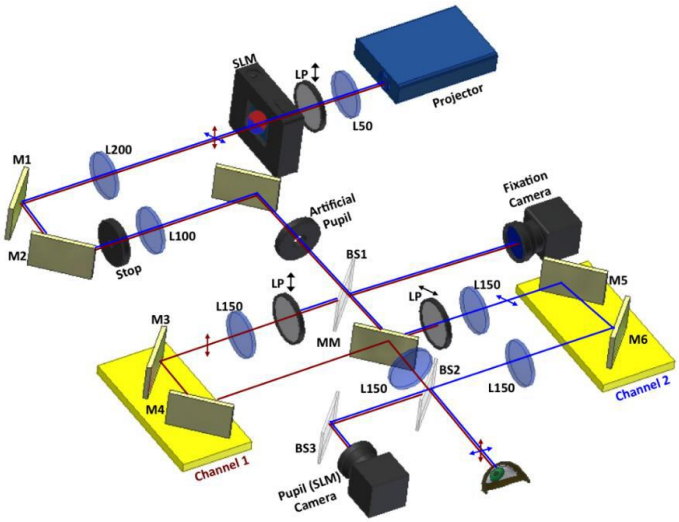

Figure 1.7 *Schematic representation of the improved spatial multiplexing SimVis simulator* [83].

B. Temporal multiplexing of tunable lenses

Temporal multiplexing is a novel technique for simultaneous vision simulation [105,120] that requires the use of an optical component that changes its focal length at high speed. Although it could in principle be implemented with DMs or SLMs, if these were fast enough, the only active

element that successfully reaches the speed criteria for visual applications are tunable lenses (TLs) [121] (see chapter 3).

TLs are active optical elements with the ability to change their optical power in response to an electric signal. They provide an additional degree of freedom in optical design and have only reached mass usage in recent years. These TLs have enabled new design strategies for optical systems allowing higher compactness due to the use of fewer optomechanical components, and fast frequency response [122]. The use of TLs is expanding in many applications including depth-scan optical coherence tomography [123], 3-D microscopy [124–126], and medical imaging [127]. They were proposed for SimVis simulation (following the temporal multiplexing concept) at the Visual Optics and Biophotonics Lab (VioBio lab) in 2015 [128].

Temporal multiplexing using TLs is based on inducing to the eye a periodic variation (in time) of optical power, i.e., a periodic variation of the vergence of the light beam passing through the lens. The different optical powers are repeated periodically and define different temporal channels, each one forming an image on the retina with a degree of defocuses corresponding to the optical power of the TLs at a given time, but without changing the position of the magnification of the retinal image. The temporal channels are temporally multiplexed at a frequency higher than the eye's fusion frequency [129] (50Hz, changing the optical powers of the tunable lens in a period of 20ms, preventing the eye from differentiating between different temporal images [130]), and consequently, a simultaneous vision image appears on the retina, with a static appearance, formed by the superposition of all the different images with different defocus.

For example, to simulate a bifocal lens with energy equally distributed between two foci, one for far vision (0 D, 50%) and one for near vision (3 D, 50%), the TLs will change their optical power throughout 20 milliseconds (ms) presenting an optical power of zero diopters for 10ms and an optical power of three diopters for the other 10 ms. This 20-ms period is repeated in a loop so that the two temporal channels are periodically projected onto the retina, and their superimposition is perceived as a static image of simultaneous bifocal vision. The energy balance between temporal channels, i.e., the assignment of different times to each optical power, allows simulating simultaneous vision with different optical power profiles (bifocal, trifocal, or EDOF) [120], matching any through focus optical quality curve, including those of commercial lenses [92].

Simultaneous viewing based on time multiplexing with TLs requires this lens to meet very demanding specifications in terms of operating speed and simulated power range. TLs are based on different technologies, most of them using fluids in combination with elastic membranes [122]. Due to their optomechanical nature, TLs inevitably have thermal effects and limitations in their temporal response. The output optical power of the lens does not perfectly follow the electrical input signal used to control it. When a change in power is requested, the lens needs a certain amount of time to provide stable optical power. During this settling time, which can vary between fractions of milliseconds and minutes, the output signal of the lens passes through a series of transient states including overshoots, undershoots, and/or oscillations. The response of

the lens during this time interval is defined as its transient response and is determined by the operation principle and design parameters of the TLs. The transient response describes dynamic artifacts, present in all TLs to a greater or lesser extent, which imposes the ultimate speed limitation in existing high-speed applications or in new developments to come. Additionally, internal variation of temperature affects the stability and precision of the optical power delivered by the lens [131]. This is a problem of temporal multiplexing, a limitation that will be addressed in this thesis (chapter 5).

Using TLs as the main element on a visual simulator would require the analysis and compensation of those thermal effects and the dynamic response. An accurate and high-precision simulation of any multifocal lens pattern will only be possible if the transient optical power is optimized, and the unwanted dynamic effects are corrected [132].

Multifocal simulations performed by temporal multiplexing have some unique peculiarities compared to those performed by spatial methods, including spatial multiplexing or AO-based approaches. The main advantage of temporal multiplexing is that each pupil position contains the full information of the multifocal design, ensuring that in presence of a local cataract, provided there is a region of transparency, all the information of the multifocal design will reach the retina through the most transparent regions of the lens (nowadays, cataracts are surgically removed long before the full opacification of the crystalline lens occurs).

C. Monocular Miniaturized SimVis (SimVis Mini)

The first SimVis simulator based on temporal multiplexing was an advanced prototype also developed at VioBio Lab (in 2015) called SimVis Mini, shown in Figure 1.8. It was a see-through, hand-held, and monocular. It used TLs model EL-10-30-C from Optotune AG (Switzerland). Besides a schematic diagram of the optical elements, Figure 1.8 shows pictures of the prototype in use [105].

The TL used has a clear aperture of 10 mm and can change the optical power from -1.50 D to +10.00 D, when used in combination with an offset lens. The TL (with the offset lens attached) was placed in a plane optically conjugated with the pupil of the eye, using a projection system comprising two identical achromatic doublets (focal length 75 mm). This projection by itself produces an image inversion both in the horizontal and vertical dimensions that, being a see-through system, is not acceptable. To get an erect image, 4 mirrors acted as a pair of Porro prisms, similar to those used in conventional binoculars. The magnification of the system was 1x, and the field of view 14 degrees (approx.). Temporal multiplexing, to implement multifocality with the TL, was programmed at 60 kHz using custom routines written in Visual C, and open-source electronics (Arduino hardware). The TL was calibrated against trial lenses, using a CCD camera and an ETDRS chart. The TL behavior, the voltage applied versus optical power, resulted to be highly linear [105,133]. The TL was also used to compensate for the refractive errors of the eye.

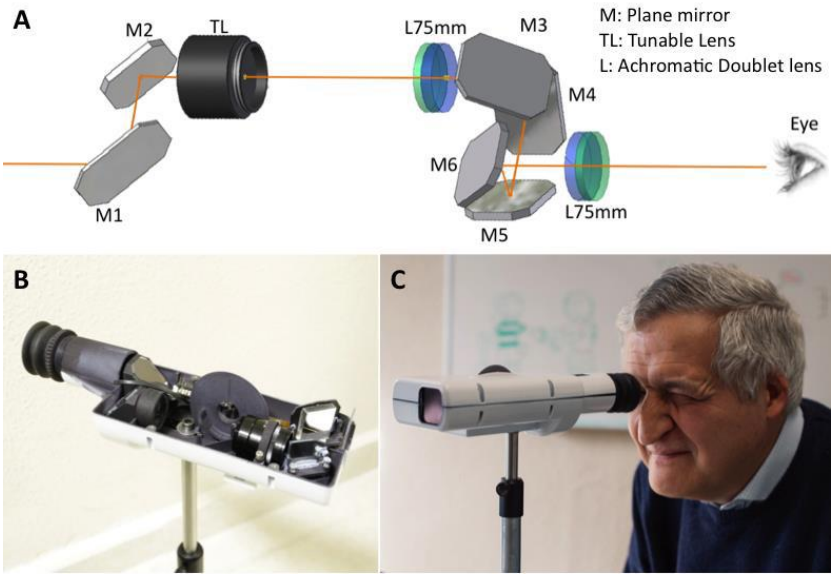

***Figure 1.8**. SimVis Mini: Miniaturized SimVis. (**A**) Schematic diagram of the optical elements. (**B**) Prototype and elements. (**C**) In use with subjects* [105].

D. Binocular SimVis (SimVis Bino)

Figure 1.9 shows another open-field vision simulator based on optical multiplexing, this time a binocular prototype called SimVis Bino, developed in 2016 at VioBio Lab. The prototype combines two similar channels, in which a Roof-Pechan prism was used to produce the image re-inversion. The projection system conjugating the TL and the subjects' pupil used achromatic doublets with reduced focal length (50 mm) to increase the visual field of view (FoV) up to 20º. The Schmidt-Pechan prism produces an erect image without changing the visual axis, thanks to the combination of a Roof prism and Half Pentaprism with an air interface. The prisms were taken from conventional compact binoculars. The image quality degradation reported when this type of prisms is used in precision imaging systems was not a problem in this visual application. No contrast reduction could be perceived. For mechanical simplicity, the prisms were placed between the object and the rest of the prototype, which allowed to test the solution although reduced the effective FoV from 20º to 12º. TLs control and static calibration were similar to SimVis Mini [134].

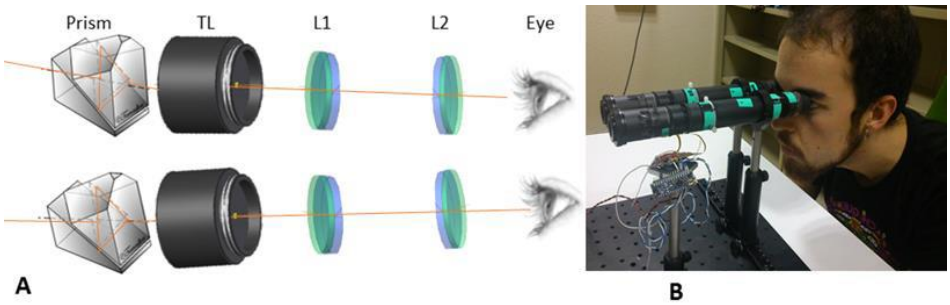

***Figure 1.9**. SimVis Bino: Binocular SimVis. (**A**) Schematic diagram of the optical elements. A Schmidt-Pechan prism was used to reverse the image. (**B**) Subject looking through the system (and performing psychophysical experiment)* [133].

1.6. Motivation

At the moment of starting this thesis, the emergence of the Sim+Vis technology had already been identified, not only at the level of the VioBio Lab but also in the visual optics scientific community, as a unique instrument that could enable very promising research related to presbyopic corrections. In parallel, after the first congress contributions, publications, and demos, and with the founding of 2EyesVision, the Sim+Vis technology was creating strong expectations in clinical communities (optometrists, ophthalmologists, and eye care professionals in general), as well as in lens manufacturers. The estimations of economic impact in the eye care market were supported in the potential benefits that the technology could deliver to the patients.

However, on the one side, important issues and bottlenecks were limiting the spread of the technology outside the research laboratories. It is well-known that tunable lenses suffer from temperature and dynamics effects. The critical consequences of those distortions in the behavior of the tunable lens are magnified by temporal multiplexing. There was an urging need for a better understanding of the Sim+Vis technology, of the behavior of tunable lenses used at high speed and its impact on the SimVis simulation, to learn about the feasibility, limitations, and improvement potential. It was clear that this knowledge would lead to new optical benches to control the optical quality of SimVis, to new compensation strategies of the tunable lens effect, and to the evolution of the Sim+Vis technology itself to provide accurate, robust, and realistic simulations of presbyopic corrections in the clinic.

On the other side, the encouraging opportunity (just discovered) of testing different presbyopia solutions in the clinic, especially multifocal lenses, in a natural visual experience allowing performing binocular visual tasks, brought the need for a new metric that can evaluate different visual dimensions including subjective perception and stereopsis besides defocus visual acuity (DFVA).

1.7. Open questions

In this thesis, we have developed different optical set-ups, validated and implemented different solutions as well as carried out different clinical experiments to answer the following questions:

1. Is it possible to improve the temporal multiplexing approach used in the visual simulation of presbyopic corrections? Are the tunable lenses available fast enough for implementing temporal multiplexing? Is their behavior linear, repeatable, and predictable? Is it possible to measure and compensate for the dynamic effects?

2. Is it possible to develop an accurate, cheap, and fast set-ups to check, characterize and calibrate the simulator in the clinic?

3. Is it possible to compensate for the temperature effects of tunable lenses? That is also critical for temporal multiplexing because the temperature effects modify the optical power during the simulation.

4. How good is the optical quality of the TLs in combination with the rest of the simulator? How stable is the optical axis? The simulator is an afocal system that induces different levels of blur, does it maintain unit magnification with all the optical powers? Is the system free of optical distortion or field curvature?

5. If patients can experience different presbyopic corrections in the clinic, which test would be best for the evaluation of those corrections? Can any test analyze the quality of vision while the patients experience the presbyopic corrections in natural and realistic environments?

6. How is the contact lens simulation performance compared to the real contact lens behavior?

7. How does the binocular IOL simulation compare, in terms of though focus visual acuity, to the reported data from implanted patients?

8. How is the simulation affected by the ocular opacity of a patient with cataracts? What is the level of cataracts that compromises the simulations?

1.8. Goals of this thesis

The main purpose of the thesis is to validate SimVis Gekko, a novel binocular simultaneous vision simulator based on Sim+Vis technology, and to demonstrate its capabilities in a clinical setting.

The specific goals are:

1. To explore the characterization and improvement of temporal multiplexing with tunable lenses.

2. To develop optical set-ups that guarantee the high precision and good quality of the simulations with SimVis Gekko.

3. To test and quantify the clinical similarities and differences of the simulations with the real lenses (CLs and IOLs).

1.9. Hypothesis

The hypotheses of this thesis are:

- Tunable lenses working under temporal multiplexing allow accurate simultaneous vision simulations. Dynamic and temperature effects can be compensated.

- The optical degradations of SimVis Gekko are negligible and small so that they do not affect the visual perception and the quality of the simulation of simultaneous vision corrections.

- Contact lens simulations are comparable to the visual experience with real contact lenses fitted on the eye, and multifactorial metrics provide an optimal comparison.

- The simulations of multifocal IOLs are also comparable to the vision of patients implanted with the same IOLs reported in the scientific literature. The presence of small cataracts will not affect the perception of multifocality through the simulator, as the temporal nature of temporal multiplexing can take advantage of the clear regions of the crystalline lens to induce the simulated lens, regardless of the position of those clear regions, or the spatial design of the lens.

1.10. Structure of this thesis

The body of this thesis is structured as follows:

Chapter 1, the current chapter, presented the background of the topic regarding presbyopia, the corrections and strategies available, as well as the current technologies to solve them, such as visual simulators, and their limitations. The motivation, open questions, goals, and hypothesis of the thesis are also presented.

Chapter 2 presents a description of the methods used throughout this thesis and common to the different studies. In particular, it includes a description of the standard optometric instruments and metrics for clinical evaluation. A description of the evolution (optical, mechanical, and electronic) of the SimVis Gekko simulator is presented, as well as the three optical set-ups developed during this thesis to evaluate it.

In **Chapter 3** we present the development of a high-speed focimeter to characterize different tunable lenses working under temporal multiplexing, and their dynamics effects. We study the repeatability and stability of the lens response. Other AO technologies are also evaluated under temporal multiplexing.

In **Chapter 4**, a low-cost and automatic focimetry system is presented for the characterization of tunable lenses. A closed-loop iterative algorithm was developed to optimize the tunable lens performance, following an automatic, experimental, granular, and customizable technique.

In **Chapter 5** we present, analyze and, characterize a method to correct the optical power deviations due to the variations in temperature of the tunable lenses in different working conditions.

Chapter 6 presents the characterization of the prismatic effect, magnification, distortion, field curvature, and image quality of afocal systems as the visual simulator, both theoretically with computationally simulations and experimentally with the development of an optical set-up and an automatic algorithm.

In **Chapter 7**, a new test of perceived visual quality was developed. The Multifocal Acceptance Score to Evaluate Vision (MAS-2EV) is a new perceptual metric based on natural images representing daily life scenes (daytime and nighttime, near and far distances, and stereovision). Its repeatability and sensitivity were evaluated in different patient groups, differentiating across different corrections, using both the SimVis Gekko and real CLs on eye.

In **Chapter 8**, we investigated the accuracy of representing M-CL designs using SimVis Gekko, comparing in presbyopic patients in a clinical setting, visual perception and performance with the simulated lenses and with the real M-CLs on. MAS-2EV metric was also compared to a standard questionnaire.

In **Chapter 9**, defocus visual acuity curves through the SimVis Gekko simulations in presbyopic subjects were compared with published data from patients implanted with those same lenses. Also, we directly compared visual performances (DFVA curves) of the preoperative simulation and the same lens surgical implanted in the same postoperative patients, binocularly on a small group of patients with cataracts.

In **Chapter 10** cataract patients compared their MAS-2EV preference through different presbyopic simulations before and after the cataract removal (with a monofocal IOL implantation).

Chapter 11 presents a summary of the major findings of this work, and their implications for the state-of-the-art, followed by the scientific activities developed during this thesis.

Chapter 2

Methods

This chapter describes the instruments, experimental techniques, developed set-ups, and clinical procedures used in this thesis.

The first section describes the evolution of the wearable SimVis Gekko during this thesis. The new developments and implementations were carried out in parallel to the work of this thesis and fed by the experiments presented here. This was a collaborative project led by the 2EyesVision R+D team, especially Dr. Enrique Gambra (CTO), Lucie Sawides (R+D engineer leading the lenses simulations and quality control), Ramón Alonso-Sanz (mechanical engineer), Yassine Marrakchi (biomedical engineer in charge of the firmware, software, and electronics) and Joshua Torrejón (leading the assembly of the SimVis Gekko devices).

The optical set-ups developed specifically during this thesis are briefly presented in this chapter and described in detail in their corresponding chapters throughout this thesis. The author of this thesis has been the main contributor in the development of the different optical set-ups:

1) The **high-speed focimetry system** (chapter 3) was built in collaboration with Enrique Gambra and Carlos Dorronsoro. This is the main system to characterize and calibrate the tunable lenses working under temporal multiplexing in the SimVis Gekko simulator.
2) The **low-cost and low-speed focimetry system** (chapter 4) was developed in collaboration with Iván Martínez-Ibarburu, Ángel G. López-de-Haro, Lucie Sawides and Carlos Dorronsoro. This system is the first approach for a calibration set-up thought to be placed in the clinical site.
3) Iván Martínez-Ibarburu and Carlos Dorronsoro had also contributed to the development of the **optical quality bench** (chapter 6). This optical bench is part of the assembly line check.

A Multifocal Acceptance Score subjective metric (chapter 7) was also developed in this thesis mainly by the author, in collaboration with Mercedes Romero, Carlos Dorronsoro, and Susana Marcos. This new metric was also used in subsequent studies (chapters 8 and 10).

2.1. Wearable Sim+Vis Technology™: SimVis Gekko™

SimVis Gekko™ (2EyesVision, Madrid) is a binocular wearable visual simulator based on the Sim+Vis Technology™ described in the 1.5.3 section of the introduction and developed after the SimVis Bino. Figure 2.1 shows both (a) the SimVis Bino and (b) the SimVis Gekko. Among its most outstanding features is that it is the first binocular visual simulator, it is see-through, with a very large field of vision (>20º in each eye) and that, as it is placed on the head (wearable) and works wirelessly, it allows patients to explore their visual environment by walking around, orienting their head and eyes as they would do under normal conditions. The instrument provides a natural vision to the patient through manipulated optics that emulates different presbyopia corrections. In this way, patients can observe stimuli with which they are familiar, such as their cell phone, a book, or the faces of their relatives, alternating between near and far vision while experiencing the visual perception provided by different presbyopia corrections.

The device is programmable, and the ophthalmologist can change the simulated lenses independently in each eye. With the push of a button on an iPad (Apple, California, USA) app, and while the patient has the device placed on their head, the temporal multiplexing temporal patterns corresponding to each eye will be sent into the TL. From these corrections, it is possible to change the curve through focus, i.e., where the different foci are placed, and with how much energy, even when there is a continuous transition between foci. For this purpose, the equipment is connected to the Internet and receives regular updates of simulations of new lenses. Generic corrections can be simulated in the unit, or specific commercial lenses can be emulated.

In addition, using the capabilities provided by binocularity, the system can simulate bilateral corrections, or combinations of different lenses in each eye such as monovision or modified monovision (where one eye is corrected with a monofocal lens and the other with a multifocal lens), among others.

SimVis Gekko™ is a see-through system, comparable to trial frames in portability, similar to a phoropter in the ability to switch between corrections, and superior to it in the number and types of corrections available (by incorporating the simulation of - potentially - any multifocal lens). Therefore, most kinds of clinical measurements can be performed on the patient, and at different distances, while experiencing different corrections: VA, contrast sensitivity, subjective preference between corrections, perceived quality, DFVA curves, or stereopsis.

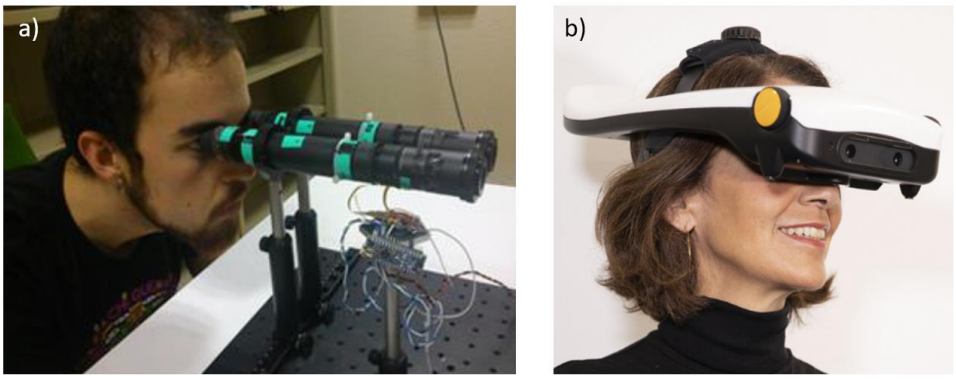

Figure 2.1 a) *A subject seeing through the SimVis Bino, binocular and fixed to the optical table.* ***b)*** *A patient wearing SimVis Gekko.*

2.1.1. Optical evolution

The first SimVis Gekko (version 0.0 – v0.0) device had the same optical components as the SimVis Bino presented in the introduction. The TL used was the EL-10-30-C model from Optotune AG (Switzerland) with an effective aperture of 10mm, and the optical projection system was designed with achromatic doublets of 50 mm focal length (unknown design) and an offset lens with a focal length of -75 mm (unknown design). Symmetrical projection systems produce less coma, astigmatism, and distortion.

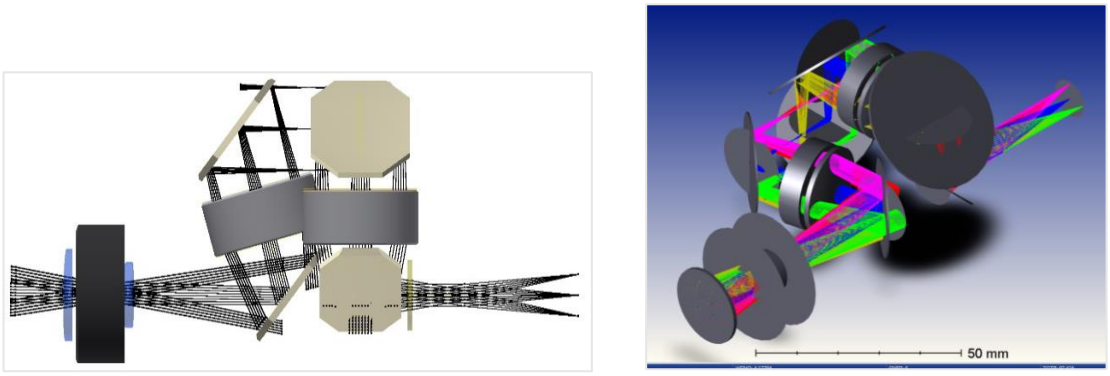

Figure 2.2 *Two views of the SimVis Gekko mirrors and lenses configuration, with the optical modeling performed in Optical Studio (**right**) and the posterior optomechanical integration (**left**).*

Six flat mirrors (Figure 2.2) were introduced to make the system more compact and reverse the imagen inversion made by the optical projection system, without introducing a prism. A pair of mirrors undoes the vertical inversion, while the second pair of mirrors overturn the horizontal image-inversion, and the third pair was necessary to have the same input and output optical axis.

Compared with the SimVis Bino, the SimVis Gekko is 40% shorter with a reading distance of 8 cm away from the eye position. The evolution of the different SimVis Gekko versions is briefly illustrated in Table 2.1.

Version	Year	Brief Optical Description	Connectivity
0.0	2017	TL: EL-10-30C. Achromatic lenses.	Cable
0.5	2018	TL: EL-10-30C. Aplanatic lens from Thorlabs	BT 2.0
1.0	2018	Aplanatic lenses made by Sun-Optics. No offset lens. New optical modules	BT 2.0
1.5	2019	Custom aplanatic lenses. New mirror thickness.	BT 4.0 (BLE)
2.0	2020	Different aplanatic lenses with an additional offset lens.	BT 4.0 (BLE)

Table 2.1 *Evolution of the SimVis Gekko device, with a brief description of the main differences of each version.*

The next SimVis Gekko version, v0.5, incorporated an optimization of the TL, based on the results shown in chapter 3 regarding the dynamic response (speed, overshoots and undershoots). The system incorporates the EL-10-30-C Optotune lens with a custom change. We have been using this model ever since and, although it is modified, it is still referred to as EL-10-30-C. Its range is +5.00 to +10.00 D and it has no internal offset lens. The effective aperture remains at 10 mm.

Regarding the optical projection system, the achromatic lenses were replaced by air-spaced commercial achromatic lenses (Thorlabs, USA) and an offset lens of -150 mm from Eksma Optics (Lithuania). The main reason for this was to improve the field curvature, as is demonstrated in chapter 6.

The following version (v1.0) maintains the same aplanatic lenses, although from Sun Optics Co. Ltd. (Changchun, China), reducing costs by 90%. The distance between both lenses was changed to introduce a -6.00 D defocus (as they were acting as a Badal System, changing the vergence) to remove the need for an offset lens, providing an optical range of -1.00 to +4.00 D. These inter-distance changes meant that a new optical module was needed to better fit all the components while maintaining a similar total size of the system.

The v1.5 (Figure 2.2) incorporated customized aplanatic lenses to further reduce the field curvature, provided by the same Chinese supplier. Additionally, to reduce the weight of the system, the thickness of the mirrors was reduced by 50%, from 3.00 to 1.50 mm.

The last version developed during this thesis, v2.00, had the goal of moving back the exit pupil of the instrument, as some patients reported flicker because the pupil and the TL were not correctly conjugated. The position of the exit pupil of the instrument was measured and compared with the average position of the eye's pupil in a group of 11 subjects, found to be 8.9 mm. Therefore, the new design shifts the exit pupil 9 mm away from the optical module. To maintain the same optical module housing and magnification x1 (both in the image and the TL projection in all the optical power range) the optical projection system was no longer symmetric incorporating two different aplanatic lenses, and a -2.00 D offset lens right behind the TL.

2.1.2. Mechanical evolution

The main requirements were to develop a head-mounted, see-though device that fits different head physiognomies. Different optical head-mounted systems, as 3D glasses and virtual reality systems, served as an inspiration to create the SimVis Gekko mechanical design.

Firstly, the incorporation of harnesses as a head-fastening system allows a wide variety of head and facial features (Figure 2.3). When resting on the forehead, the distance from the eye to the first window of the system remained fairly stable. The design distance is 11 mm. The harnesses were changed in different SimVis Gekko versions to improve their durability and quality. Likewise, they were reinforced with pads for improved comfort.

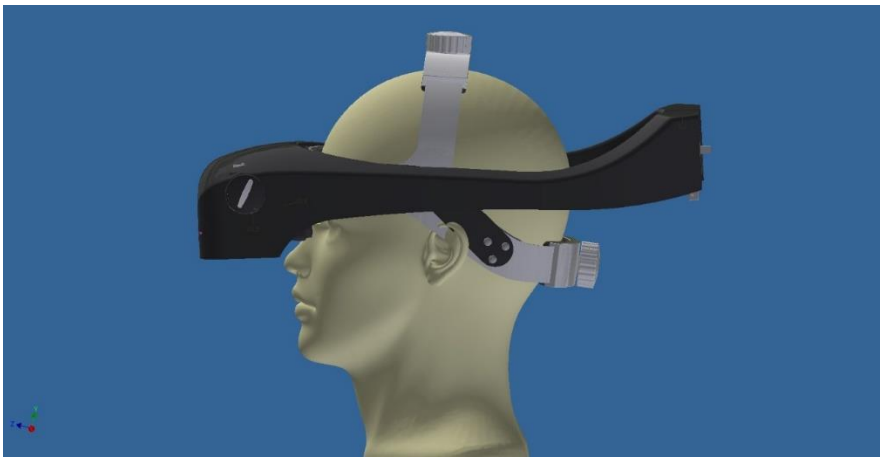

Figure 2.3 *Illustration of a dummy with a specific head structure with the SimVis Gekko adjusted to his head with the harnesses.*

As it is a binocular system, it should allow different interpupillary distances. Figure 2.4 shows the pupilar rulers above each ocular. The average value for adults is 63 mm, and the range selected to design the system was from 45 to 75 mm. This can be adjusted horizontally thanks to a pair of side wheels, with independent movements for each eye, and vertically, with the upper harness. Also, a pair of LEDs were placed to illuminate the pupil and make the alignment task easier.

Figure 2.4 *Pupilar rulers of the SimVis Gekko placed above each ocular.*

Additionally, the system must be able to fuse images from each of the channels for far, intermediate, and near objects. As a starting point, the convergence angle between channels was set and optimized for 80 cm, with an inclination angle of 2.25º for each channel towards the nose as illustrated in Figure 2.5. The distances and angles allow the patient to read at near distances and see distant objects without needing any alignment or repositioning changes, allowing to create of an integral system inside a helmet.

Figure 2.5 *Design of the optical module with the 2.25º convergence angle between channels optimized for 80 cm, and the lateral screw for the horizontal movement of the optical module to allow different interpupillary distances.*

To have a low-weight system was always a premise. As all the optical elements were placed on the front part of the helmet, when the harnesses were tightened, the system slipped forward, and it was quite uncomfortable. To solve that, different counterweights were tested in the backside of the helmet to find a balance without increasing the total weight of the system too much. The battery and the electronic (firmware) components were also placed on the backside of the helmet. The total weight of the v2.0 system is 1200 gr. All versions attempted to reduce the weight, but the weight of the two TLs and four doublets is around 350 gr and the same for the counterweights, so all the rest of the components amount to only 400 gr.

System design starts from the inside out. First, the parameters of the inner parts were established, and once they are designed, we moved onto the outer design of the system, which resulted in the final housing and external complements/accessories, such as the trial lens frames.

The TLs are used to simulate multifocality, but not to compensate for the refractive error of the patient. An additional system shown in Figure 2.6, similar to the commercial trial frames used in clinics, is designed to be placed in the SimVis Gekko. It was decided to introduce it externally to the helmet, employing magnets attached to the modules.

Figure 2.6 *Trial frames to compensate the refractive error of the patient, attached to the SimVis Gekko modules employing magnets.*

It was decided to choose additive manufacturing due to the dimensional tolerances, weight, and cost it provides. Different techniques were used, such as (1) stereolithography, used for elements

that need high precision such as trial frames; (2) sintering, for the optical modules housing; (3) precision machining for the metal elements; and (4) molding, both with silicone molds to make few units, and aluminum molds for many units. This last technique allows a more precise and delicate result, and it is used for the battery and housings. The combination of these techniques allowed us to achieve a light, small and cost-effective system that can be competitive in the market.

The development of each component is always in continuous evolution, growing towards logical parts for mass industrial development. In this sense, which completely conditions the design of the system, all parts that can be improved become parts that can be molded. Figure 2.7 shows a carving-up of the SimVis Gekko.

The company has been assessed and certified with the ISO 9001:2015 since September 2020 in the areas of Design, Development, and Manufacturing of ophthalmological equipment, among other areas.

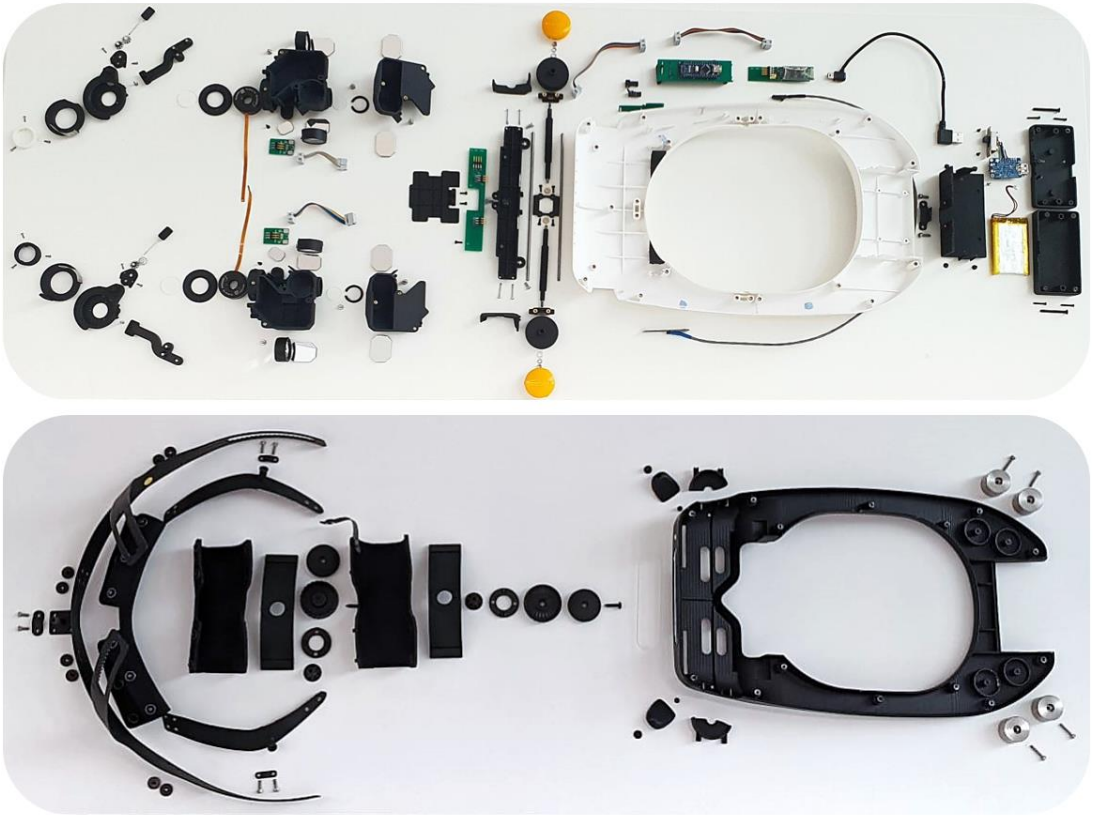

Figure 2.7 *Carving-up of a SimVis Gekko.*

2.1.3. Firmware and software

To simulate a lens or control the SimVis Gekko, a customized communication protocol has been developed that establishes a unified and flexible structure for information transmission and workflow execution, independently of the communication technology [135]. A host device (PC, tablet, or iPad) will be sending different frames to SimVis Gekko to manage every single functionality of the device.

Three main different connectivity technologies throughout this thesis were implemented in parallel to the SimVis Gekko versions. Even so, some elements were constant.

An Arduino nano is the microcontroller responsible for all the processing and signal handling required to control the components of the device. A custom current driver commanded by the Arduino is used to interface the lenses providing the necessary current to correctly cover the range of optical power of interest.

The electrical pinout of the lenses includes 2 driving pins and 4 I2C pins to access the internal temperature sensor which provides temperature warnings (chapter 5) that are useful to maintain the stability and precision of the lenses. All the electrical connections are accessible thanks to flexible flat cable (FFC). This kind of cable has many advantages as flexibility, it occupies less space and has greater electromagnetic interference (EMI) suppression. To connect the lenses to the driver a special FPC/FFC adapter is required to be able to use classical round cables.

The power delivery to the system is provided by a 2400 mAh lithium polymer with a 3.7V output voltage battery. The SimVis Gekko has relatively low energy consumption, with approximately a maximum total current needs of 500 mA for all the circuits with both TLs working simultaneously.

The first SimVis Gekko version, v0.00 was designed to be plugged into a computer able to send instructions through a custom Matlab (R2018, MathWorks Inc.) toolbox by a USB cable. The main inconvenience was the need to be always with a computer, which was also limited by the length of the cable.

In the following version (v0.5) a Bluetooth (BT) 2.0 was the technology chosen to transfer data from the host device to the SimVis Gekko, wireless. The BT 2.0 was compatible with Matlab and with Android devices. A tablet (from Samsung) was incorporated with a simple application to send some predefined optical corrections. On the way to getting a commercial SimVis Gekko, Apple iPad devices appeared to provide better security and stronger mobile device management (MDM) solutions for customization and remote updating.

Consequently, a different BT technology was integrated into the hardware of the SimVis Gekko v1.5. A BT 4.0, also called Low Energy Bluetooth (BLE) to allows the connectivity with Apple devices, like iPads, but could not be used with Matlab. The BLE is becoming the new standard, therefore it is more secure in the communication process and has lower consumption. Figure 2.8 shows a schematic of the electronic circuit of the SimVis Gekko with the exact distribution of each component along with the helmet. Deloitte had developed the first application to control the SimVis Gekko with an iPad.

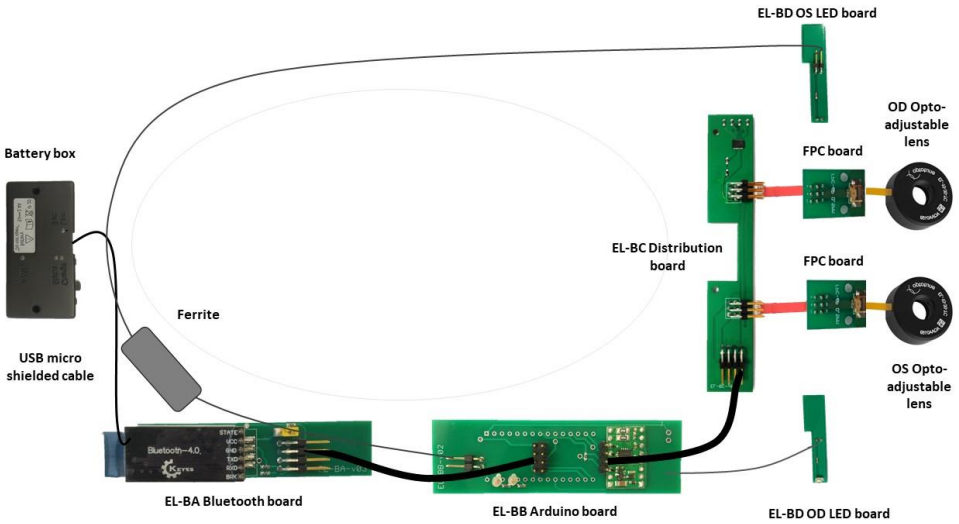

Figure 2.8 *Scheme of the electronics circuit of the SimVis Gekko.*

The current SimVis Gekko application allows to create a patient's profile, select the dominant eye, create combinations of lenses to simulate them. The alignment LED's can be switched on and off. The lenses can be changed between eyes (i.e., in a monovision correction, the far and near lenses), or between lens designs (i.e., change between a trifocal lens in both eyes, to an EDOF lens) in less than 30 seconds. When a simulation is running, the result of different standard clinical tests (VA, stereopsis, DFVA curves, …) can be safe inside the patient's profile. Among other functionalities.

2.1.4. Temporal coefficients and simulations of real lenses

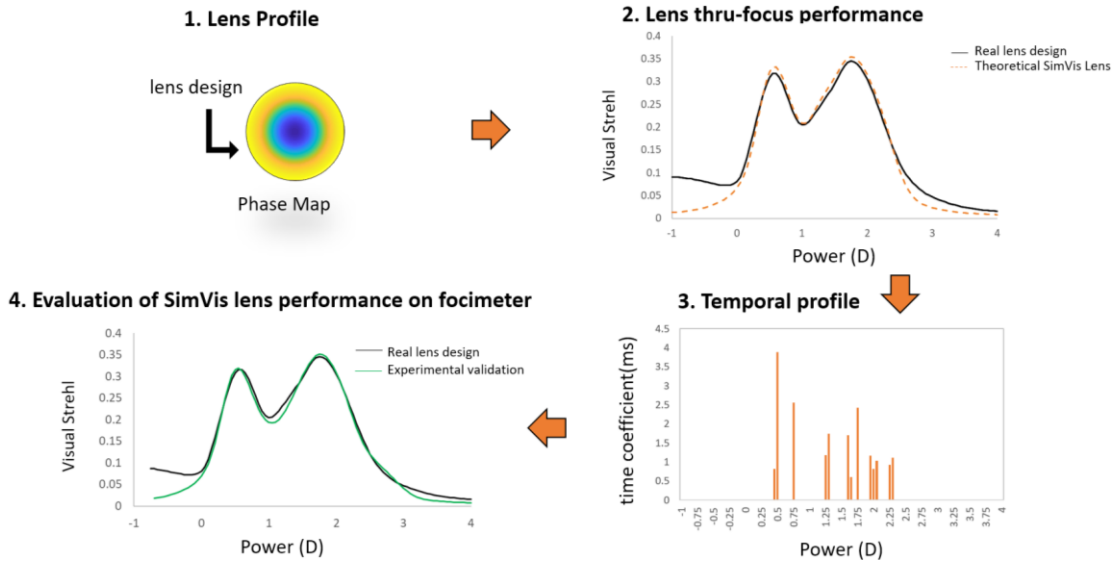

Figure 2.9 *Scheme of the steps needed to simulate a real lens from the theoretical design to the experimental SimVis Gekko performance measured in the focimeter.*

Figure 2.9 illustrates the process to simulate the temporal coefficients needed to send to the TL to reproduce the performance of a specific lens. The estimated trough focus Visual Strehl (TFVS) was obtained using different sources of data [136] that could be the phase map of the lens, the

refractive and/or diffractive real designs, or the power profile of the lens, normally provided by the lens manufacturer. Once we get the best estimated TFVS of the multifocal lens, we used custom-developed Matlab routines, previously described in [120] to calculate the first set of temporal coefficients, that best described the lens designs with temporal multiplexing through an iterative optimization process applied to the temporal coefficients. We obtained the theoretical SimVis Gekko lens performance mimicking the best estimated TFVS of the lens. Then, to compensate for the dynamic effect of the TL, new sets of temporal coefficients were calculated using custom-developed algorithms and an iterative optimization process was applied to the transitory temporal coefficients to obtain the corrected temporal coefficients that best simulate the lens design, and simulations were then validated in the high-speed focimeter (chapter 3).

2.1.5. Regulatory Status

The AEMPS (Spanish Agency for Medicines and Health Products) and the FDA (Food and Drug Administration) defined the SimVis Gekko as a non-medical device as is intended to simulate or provide a visual experience for any presbyopic correction, including multifocal corrections. SimVis Gekko is not intended to treat, prevent or diagnose any disease or medical condition. The selection of the CLs or IOL is the sole responsibility of the surgeon, based on the personal interpretation of the results and own criteria.

Additionally to the ISO9001:2015 certification, the SimVis Gekko complied with the applicable Essential Principles for Safety and performance of different European directives relative to electronic devices (restriction of certain Hazardous substances -RoHS 2011/65/EU + 2015/0863/EU, Electromagnetic compatibility Directive 2014/30/EU, Radioelectric Equipment Directive 2014/53/EU, and Low voltage Directive 2014/35/EU) and get the CE marked in September 2019.

2.2. Quality control and calibration of SimVis Gekko™

The work carried out during this thesis, and in particular, the methods developed, have resulted in assemblies and quality assurance procedures for the manufactured SimVis Gekko, its main components, and subsystems. This section introduces these methods, which will be detailed in the corresponding chapters. The development of a SimVis Gekko involves many more procedures and test benches, but only those related to this thesis are mentioned here because this thesis has been the origin that has given rise to these specific quality controls.

2.2.1. Dynamic behavior of tunable lenses

Previous studies have found that different model number from the same TL of the same manufacturer has different behavior and impulse response [132]. The first step in this process is to characterize the dynamic response of each TL, before its assembly. Chapter 3 presents a linear time-invariant model and a high-speed focimeter system as the first procedure for direct characterization of the transient response of tunable lenses and compensation of the temporal distortions introduced [137].

Later on, based on the high-speed focimeter, a closed-loop algorithm and a low-speed focimeter were developed able to characterize with the same accuracy the impulse response and dynamic behavior of TLs. It is presented and explained in chapter 4. After the TL characterization and dynamic effects correction, the final performance of the TLs, even with a different model number, when simulating a specific design remains the same [132].

2.2.2. Binocular check and optical power calibration

After the dynamic characterization of the TLs, the optical module is assembled. Two different set-ups are used in this stage of the process, the calibration set-up Cal-03 to evaluate the static and dynamic power check, and the calibration set-up Cal-04 to perform a binocularity evaluation and a FoV check.

The Cal-04 set-up consists of a collimator of 1-meter focal (Officine Galileo, Italy) that provides a wide FoV focus on infinite. On the object focal plane, a LED and a pinhole are located. A grayscale camera (DCC1545M, Thorlabs) and a 16-mm focal-length objective focused at infinite are placed behind the optical module to capture images through the SimVis Gekko. The FoV of each channel is measured individually by taking images of the pinhole. Figure 2.10 shows some images from a calibration procedure.

The matching of the binocular optical axes between channels is evaluated and must be within the tolerance established limits (the same as the American standards for binoculars [138]): <0.58º of divergence or convergence vertically; tolerance <1.66º if the axes are divergent horizontally and tolerance <0.83º if the axes converge horizontally. The field overlap is preset at 80 cm, and it is checked with a tolerance of <0.5º. The full field of view should be ≥ 20º.

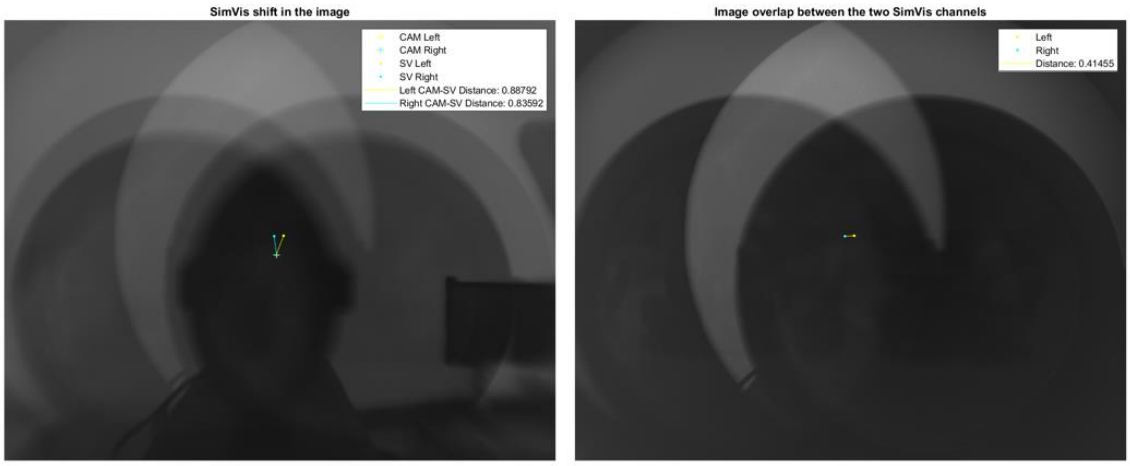

Figure 2.10 *Monocular images taken during a binocularity evaluation a FoV check superposed. The spot is the image of the pinhole through the collimator focused at infinite (yellow for the left eye, blue for the right eye). The superposition of each eyespot allows checking the field superposition and fusion of the system.*

Then, a static and dynamic power check is performed to evaluate the stability of the optical axis between 0 and 2 D. The DCC1545M Thorlabs camera and an achromatic doublet of 100-mm focal length provide great resolution but smaller field. At 50 cm from the TLs plane, a 5'' display

backpack (Adafruit, USA) is placed with a binary noise image. A flip-in/out lens of 40 cm focal length made possible the measurements at infinite (lens in) and at 2 D (lens out). Images are taken both at far distance and near (2 D) for each SimVis Gekko channel. A trough-focus is performed to select the best focus. In this step, the algorithm that allows the temperature control of TLs (chapter 5) is incorporated into the generation of the static powers and new monofocal and generic bifocal lenses are generated.

Figure 2.11 illustrates how the SimVis Gekko has placed on the calibration set-ups thanks to the magnets attached to the optical modules. As the axes are tilted due to the convergence, to evaluate the right and left channels centered, the SimVis Gekko needs to be placed in different positions (in the figure, the green SimVis Gekko illustrates the position of the system when the right eye is evaluated, and the white Gekko that of the left eye).

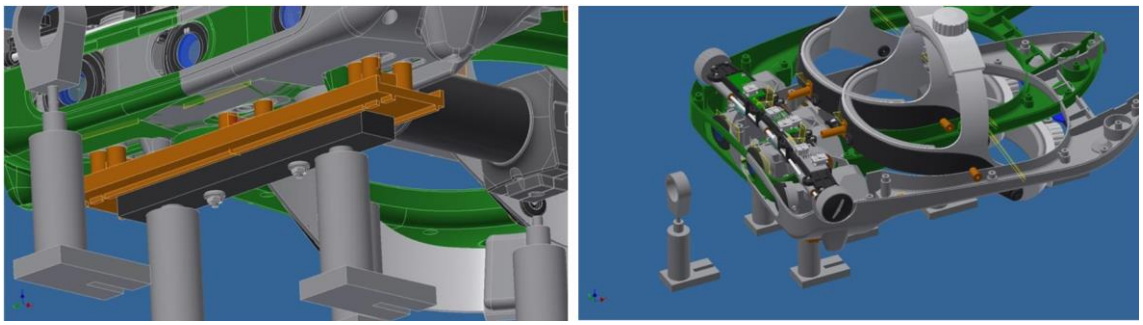

Figure 2.11 *Illustration of how the SimVis Gekko is placed in the calibration set-up. The green system illustrates the position of the system when the left channel is evaluated and the white one, the position while measuring the right channel.*

2.2.3. Optical quality evaluation

In the next step, once the simulated lenses are generated with the control of the temperature implemented, the SimVis Gekko undergoes an optical quality check control.

An analysis of the curvature, magnification, and distortion effect is checked to ensure the values are within the tolerable limits. In chapter 6, a description of the experimental set-up and comparison of two versions of SimVis Gekko is presented.

The established limits for the different parameters are:

- Curvature <0.12D in central 15º
- Magnification
    - x1 in the image, for all optical powers
    - x1 for the pupil, for all optical powers
- Distortion
    - 0.1% distortion throughout the FoV
    - Distortion increment between 0 and 3 D: 0.05%

2.2.4. External quality check and acceptance

An additional quality control and acceptance procedure are performed, checking sixty-five different items divided into five areas: traceability, the general appearance of the SimVis Gekko, connectivity, visual check of the device, and final optical performance measurements.

From the check of the correct stickers and traceability of the documents regarding all the performed calibrations and evaluations; passing through the checking of the pads, screws, logo impression, wheels movements, Bluetooth connection, LEDs operation, battery operation, and warnings, among others; to a final and double-check of the FoV, fusion, and superposition of both channels, working frames, and optical performance measurements using both Cal-03 and Cal-04 set-ups, are some examples of the items evaluated in this stage. Specific questions evaluated are shown in Figure 2.12.

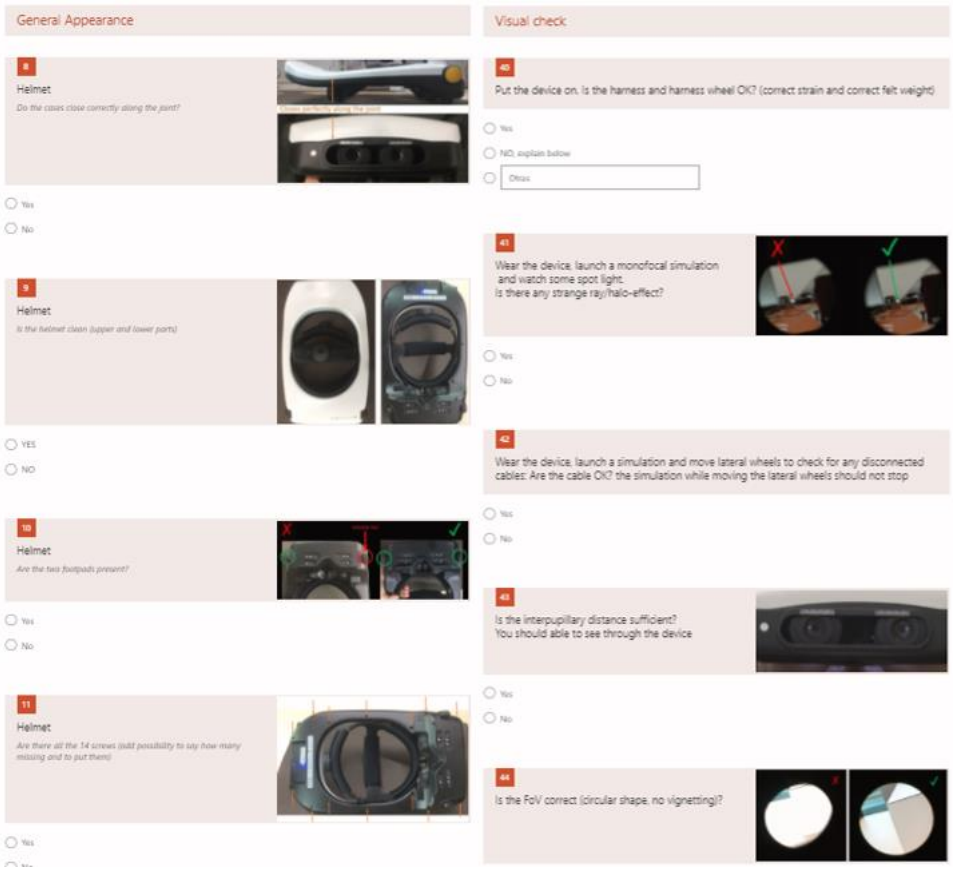

Figure 2.12 *Some questions from the quality control of a SimVis Gekko, regarding the general appearance and visual check.*

2.3. Clinical validation with patients

When evaluating the performance of a lens, especially a multifocal lens, the most widely metric used is the defocus visual acuity (DFVA) curve. However, and as we already mentioned in the introduction, the high contrast VA is a limited descriptor of the quality of vision. A new perceived visual quality metric, the Multifocal Acceptance Score to Evaluate Vision (MAS-2EV), was developed in this thesis (chapter 7). Both metrics, DFVA curves, and the MAS-2EV were the main

ones used in this thesis to evaluate the performance of different presbyopic, simulated and real, corrections.

2.3.1. Defocus visual acuity curves

Defocus Visual Acuity curves (DFVA) are often used to assess visual performance in pseudophakic patients. In this method, trial lenses are placed in front of the eye, to mimic different vergences, and high contrast VA is measured at each distance.

Typically, a VA chart is located at far distance (between 4 and 6 meters) and a subject wears his far refraction, so the chart is focused on the retina and the best VA can be achieved. When a trial lens is placed on a trial frame or a phoropter, a defocus blur is induced, and the vergence is changed based on the optical power of the lens (i.e., as Figure 2.13 illustrates, if a -2.50 D trial lens is placed in front of the eye, the vergence will change and brings the object to 40 cm). To evaluate the full performance of a lens design, DFVA curves are normally performed from +1.50 to +4.00 D in 0.50 D steps. The DoF has also been evaluated thanks to the DFVA curves, and it is defined as the range of powers through which a VA of 0.2 logMAR or better is maintained. Many reports compare post-operative DFVA curves (from different patients) to analyze the comparative performance of different multifocal or EDOF IOLs [139]

Despite some drawbacks of this method, which is time-consuming, uses targets with a frequency content and high contrast that may not be fully representative of natural targets and may be subject to VA underestimation associated with magnification, it still represents the most comprehensive assessment of the performance of presbyopic correction [140–142]. DFVA curves are used to estimate depth-of-focus.

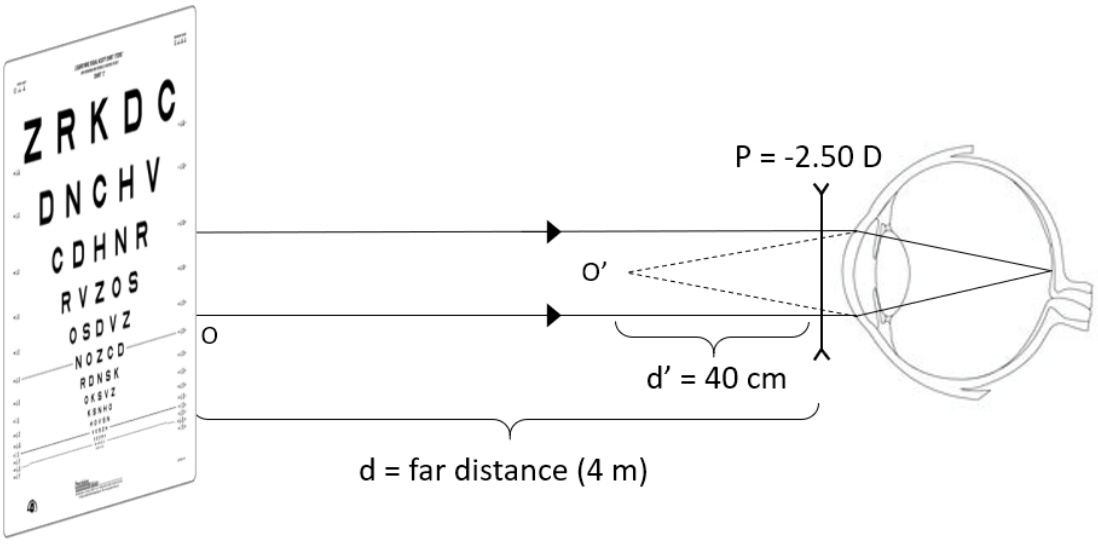

Figure 2.13 *Scheme of the vergence change during a DFVA curve measurement when a -2.50 D trial lens is placed on a trial frame.*

2.3.2. Multifocal Acceptance Score to Evaluate Vision: MAS-2EV™

We have developed and validated a new metric (MAS-2EV) to evaluate vision with presbyopic corrections. The MAS-2EV is based on a set of images representing natural visual scenes at day and night conditions projected in far and near displays and a near stereo target. Subjects view and gives a perceptual score (PS, between 0 and 10) to the images through different binocular corrections administered with CLs, implanted IOLs, or simulated with SimVis Gekko. MAS-2EV scores are visually represented in the form of polygons (Figure 2.14) and quantified using different metrics: overall visual quality, visual degradation at far, visual benefit at near, near stereo benefit, visual imbalance near-far, overall visual imbalance, and a combined overall performance metric. The development, repeatability, and validation of the metric are presented in chapter 7.

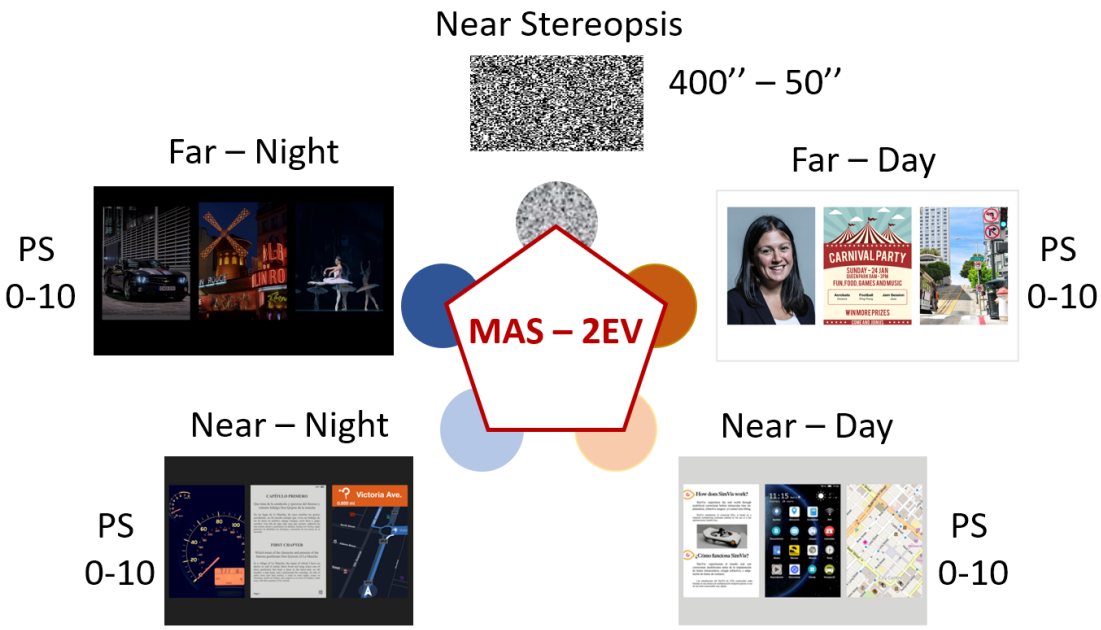

Figure 2.14 *Visual representation of the MAS-2EV metric in a polygon shape, with the images in each correspondent vertex.*

2.3.3. Clinical measurements

SimVis Gekko was used with seventy-eight human subjects in different studies presented along with this thesis: 5 young subjects, 49 presbyopes, and 24 cataract patients.

For each study, the protocol and experiments conformed to the tenets of the Declaration of Helsinki, getting the approvals from the correspondent Ethical Committee (in this thesis, the clinical studies get approval from the CSIC Ethics Committee and the Hospital Clinico San Carlos Ethics Committee). The subjects signed an informed consent after receiving an explanation of the nature and implications of the study and before starting the clinical measurements.

Chapter 3

Tunable lenses: dynamic characterization and fine-tuned control for high-speed applications

In the current chapter, we have developed a high-speed focimeter, characterize and analyze different active optical elements (TLs) at high speed, and validate a linear time-invariant model of optical power to compensate for the dynamic effects of tunable lenses.

This chapter is based on the paper by *Dorronsoro et al. "Tunable lenses: dynamic characterization and fine-tuned control for high-speed applications" in Optics Express (2019)*. The co-authors of the study are Xoana Barcala, Enrique Gambra, Vyas Akondi, Lucie Sawides, Yassine Marrakchi, Victor Rodriguez-Lopez, Clara Benedi-Garcia, Maria Vinas, Eduardo Lage and Susana Marcos.

The author of this thesis (1) performed the literature search, (2) developed the high-speed focimeter system, (3) performed the measurements with the tunable lenses, (4) collected the data, (5) analyzed the data (in collaboration with Carlos Dorronsoro and Enrique Gambra) and (6) contribute to prepare the manuscript.

The principle of this work is protected by a patent [143] licensed by 2Eyes Vision, in which the author of this thesis is a co-inventor.

This work was presented as an oral contribution at Visual and Physiological Optics (VPO) 2018 in Athens (Greece). Parts of this work were also presented as a poster contribution at the IONS 2017 in Paris (France) and IONS 2018 in Copenhagen (Denmark).

3.1. Introduction

TLs are based on different technologies, most of them using fluids in combination with elastic membranes: elastomeric membrane [122], mechanical actuators [144] or oscillators [145], electrowetting [146,147], dielectrophoresis [148], microfluidics in combination with stimulus-responsive hydrogels [149] or pneumatic pumps [150,151]. As any optomechanical system, TLs inevitably have limitations in their temporal response. The output optical power of the lens does not perfectly follow the electrical input signal used to command it. When asked to change its power, the lens needs a certain amount of time to provide stable optical power. During this period of time (settling time), which can vary between fractions of milliseconds and minutes, the output signal of the lens passes through a series of transient states including overshoots, undershoots, and/or oscillations. The response of the lens during this time interval is defined as its transient response and is determined by the operation principle and design parameters of the TL. The transient response describes dynamic artifacts, present in all TLs to a greater or lesser extent, which impose the ultimate speed limitation in existing high-speed applications or in new developments to come.

There are well-known strategies to model and control linear time-invariant systems [152] minimizing the distortions introduced by their transient response. These strategies assume repeatability and linearity. However, to our knowledge, the dynamic properties of TLs are for the most part unknown, as their transient response has never been directly characterized, nor indirectly measured with sufficient accuracy to provide precise estimations or predictions.

The new applications of TLs requiring fast dynamic measurements of optical power impose new requirements for measurement instrumentation, far beyond the existing techniques. The static power of a lens can be measured by changing optical inter-distances, between the lens and an object [150,151,153], an imaging screen or a camera [154,155]; or, as most ophthalmic lens meters do, by measuring the change in the inter-distances of a collimator [156]. Aberrometers as Laser Ray Tracing [157] or Hartmann-Shack [158] are another option that provide not only optical power measurements, but also detailed information about the optical quality of the lens. Unfortunately, Laser Ray Tracing is not sufficiently fast to measure the dynamic response of many TLs, which can change their power in fractions of milliseconds, and Hartmann-Shack has limited dynamic range for defocus. Dorronsoro et al. [105] used a laser scanning circular trajectory to demonstrate and evaluate the stability of two or three foci in a dynamic regime, although this method has some limitations due to mechanically moving parts. A faster method, although indirect, involves sensing the luminous intensity at the center of a laser beam [146,159] with a small photodiode or with an optical fiber. A more direct approach to test the dynamic performance involves imaging objects through the TL with a high-speed camera [160], although measuring the focal length poses challenges. As the current techniques cannot provide an accurate dynamic characterization of TLs, the compensation of dynamic effects of TLs has not been demonstrated to date. New dynamic characterization techniques, able to guide the

compensation of dynamic effects, will boost the performance of TLs in current applications, and open paths for new applications.

In this chapter, we present and validate a linear time-invariant model of optical power, for compensating the dynamic effects of TLs. As the model requires precise characterization of dynamic effects, we developed a novel fast focimeter that can measure optical power at high temporal sampling rates. The system uses a high-speed camera and a prism, providing direct and robust measurements of optical power, and it is insensitive to misalignments and decentrations (even those produced by the lens under test). It was calibrated in static measurements and validated in repeated dynamic characterizations of different TLs in the time and the frequency domains. The model also requires a predictable dynamic response of the TL, to provide reliable estimations of its temporal response. The focal length measurements performed with the focimeter showed that the lenses are repetitive and linear (and also the focimeter itself). Finally, using the model, we demonstrated the compensation of dynamic effects, both theoretically and experimentally. These experiments require a new level of precision in the control of the TL, which we achieved through the development of a custom electronic driver for fine-tuned control of the lens at high speed. The focimeter developed was used to quantify an important improvement in the performance of the TLs after the compensation of their dynamic effects. Finally, we used the instrument to validate the predictions of the model, demonstrating the feasibility of simple open-loop compensation strategies to minimize the effect of the transient response.

The focimeter was also used (see the Appendix of this chapter) to characterize other active optical elements (a deformable mirror -DM- and a spatial light modulator -SLM-).

3.2. Methods

3.2.1. Modeling temporal dynamics

The transient response of TLs introduces distortions in the temporal response of the lens concerning the intended input signal driving the lens. As generally encountered in electrical and mechanical engineering systems, we propose a description of the system inertia, load dump, and resonant frequency of the TL in terms of the temporal step response function [152]. The temporal step response function characterizes the dynamic performance of the TL and can anticipate its suitability for different applications. Moreover, the temporal step response function can ultimately predict the output of the lens to any input and therefore guide the compensation strategies to mitigate the transient effects or to evaluate tradeoffs between lens speed and control. Assuming that the system is linear (as discussed in section 3.3.2), the temporal response *s(t)* can be expressed as the convolution of any given input signal, *u(t)*, and the impulse response function, *h(t)*, as follows:

$$s(t) = u(t) * h(t) \qquad (3.1)$$

The impulse response function of the TL was calculated as the time derivative of the average temporal step response function measured with the focimeter (Sections 3.2.4 and 3.2.6) when

the electric input signal is an ideal step function. To avoid noise amplification in the differentiation operation, an analytical expression of *s(t)* may be obtained by fitting the measured response with a damped harmonic oscillator model. Once the impulse response is estimated, the true response of the TL can be predicted for any input wave (assuming a linear time-invariant system). This prediction capability will enable (Section 3.2.7) compensation strategies for dynamic effects, based on the fine-tuning of the predicted optical power output by optimization of the input electrical signal.

3.2.2. High-speed tunable lens driver

As already seen in section 2.1.3 of the previous methods chapter, we developed a custom high-speed driver for TLs (including hardware and firmware, and a new data frame for the input wave), to achieve the temporal accuracy required to compensate for the dynamic effects. The hardware comprises an Arduino Nano 3 (Arduino, Italy) and a DRV8833 Dual Motor Driver (Texas Instruments, TX). The signal driving the TL is based on pulse width modulation (PWM at 32 kHz) and typically provides a temporal sampling of 0.1 ms along with a periodic signal of 20 ms, although other configurations are also possible. The high-speed driver is compatible with the TLs used in this study (see Section 3.2.6) and can read the temperature sensor included in some of them.

3.2.3. Operation of the high-speed focimeter

When an object, for example, a slit, is imaged through a TL, the position of the image changes along the optical axis as the lens changes its optical power. This study proposes the use of a prism to transform the axial displacements of the image (slit) into lateral displacements. A fixed camera can then measure the focal length (optical power) of the TL in just one frame, by capturing the lateral displacement produced on the image of the slit. Figure 3.1 illustrates the principle, reminiscent of the prism-based focusing screens of manual-focus cameras. As the optical axis is deviated by the prism, each optical power of the TL produces a lateral displacement of the image (slit) depending on its axial position. Snell's law predicts the deviation of the principal ray as follows:

$$\theta = \arcsin [n \sin(\alpha)] - \alpha \qquad (3.2)$$

where θ is the deviation angle in radians, *n* is the refractive index of the prism material, and *α* is the prism angle (in radians). Under small-angle approximation, Eq. 3.2 can be simplified as follows:

$$\theta = \alpha [n-1] \qquad (3.3)$$

Equation 3.3 shows that the higher the refractive index, *n*, of the prism and the angle, *α*, the higher is deviation angle. The lateral image displacement d is obtained as $r \cdot sin(\theta)$, being *r* the distance between the prism and the real or virtual image of the slit, that changes with the optical power. For small angles, *d* is proportional to *r* (and to the changes in the optical power):

$$d = r \cdot \alpha [n-1] \qquad (3.4)$$

In the high-speed focimeter presented here, a fast camera (with a high frame rate) is used to record the transient displacement of the slit's image as the power of the TL changes. As shown

in Figure 3.1, the prism only covers half of an intermediate image plane. The other half is used to obtain a reference, preventing the measurements to be affected by vibrations, decentrations, and misalignments.

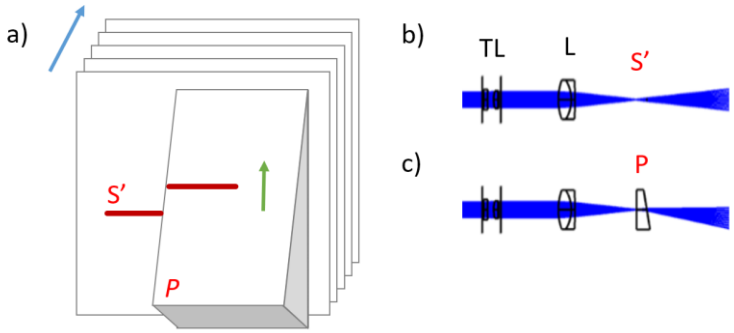

Figure 3.1 *Principle of the high-speed focimeter. (**a**) The image of the intermediate image of the slit (S') through the prism (P) is laterally displaced (right side of the image plane) concerning the reference without prism (left side of the image plane). The displacement increases (green arrow) when the distance between the prism and the image plane increases (blue arrow). (**b**) The tunable lens (TL) creates an intermediate image of the slit. (**c**) The prism (P) deviates from the optical axis.*

3.2.4. Optical set-up

OpticStudio (Zemax LLC, WA, USA) was used to simulate the arrangement of the optical elements and to optimize the parameters (focal lengths, prismatic powers, optical inter-distances, and diaphragm diameters) that provide the best balance between the displacement of the slit with optical power change and slit widening due to defocus. Figure 3.2 shows a diagram of the experimental set-up, to scale, with (b) and without (a) the prism. An incoherent source of polychromatic light illuminates a diffuser in front of a tilted slit (25 µm wide; 3 mm long). A 4f projection system (lenses L1 and L2, f=50 mm) creates a pupil plane in which the electrically TL under evaluation is placed. A second 4f system (lenses L3 and L4, f=50 mm) creates a second pupil plane optically conjugated to the TL. Trial lenses (TrL; positive and negative thin lenses from an optometry trial lens set) are placed in this second pupil plane for calibration/validation purposes, allowing for inducing known magnitudes of optical power in the optical system. A prism (P; see details in Figure 3.1(a) and in section 3.2.3) is placed at the focal plane of L2, covering one-half of the intermediate image (S') of the slit. The base of the prism is orthogonal to the optical axis of the instrument. Due to the prism, the image of the slit appears to split in the high-speed camera (IL5S; Fastec Imaging, USA), provided with a macro-objective (MO; 100mm f/3.5; Cosina). The light passing through the prism forms a displaced image (DI), and the rest provides a reference image (RI).

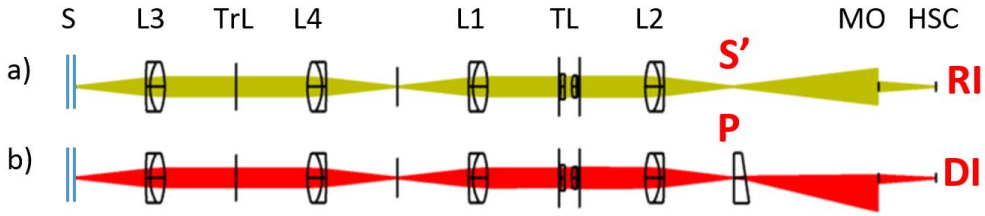

Figure 3.2 *Optical set-up. S: Slit (an incoherent polychromatic light source and a diffuser are not shown); L1 and L2: 4F projection system; L3 and L4: 4F additional projection system for calibration; TL: Tunable lens; TrL: Trial lenses; S': Intermediate slit image; P: (prism); MO: Macro objective; HSC: High-Speed camera. (**a**) Configuration without the prism providing a reference image RI. (**b**) Configuration with a prism in the region of the intermediate image S', providing a displaced image DI, with a displacement (concerning the reference) that changes with the axial position of the intermediate slit image S' and therefore changes with the optical power of the tunable lens TL. Both configurations co-exist in the same set-up, as the prism P only affects one-half of the intermediate image S'.*

Figure 3.3 shows examples of the displaced out-of-focus slit images in comparison with reference in-focus slit images. For each frame, the left side of the slit provides a reference, and the right side is displaced upwards. The vertical distance between the displaced and reference images is directly proportional to the optical power of the TL. The lateral displacement of the slit is calibrated with the help of trial lenses.

For dynamic characterization, the camera is configured at a speed of 3823 frames per second (with 320 × 256 pixels per frame). The position of the slit can be estimated every 0.26 ms with an initial spatial resolution of 5 µm per pixel, which is improved later with a superresolution algorithm (described in Section 3.2.5). By tracking the distance between the reference and displaced slit images, the instrument characterizes the transient response of the lens.

3.2.5. Image processing

The slit is intentionally tilted to reduce the effect of spatial sampling (aliasing) due to image pixelation and to simplify an automatic superresolution algorithm. After measuring the slit angle with a Radon transform, the region of the image containing the slit is cropped, bilinearly interpolated, and rotated (to compensate for the tilt). The different luminance profiles along the slit (sampled by the pixels with different shifts due to the original tilt) are then averaged. This procedure provides a simple and robust estimation of the luminance profile of the image of the slit (combining the data of more than 100 rows of the image, each row providing an independent 'observation' of the slit position), with subpixel resolution (8x). The peak positions in the super-resolved luminance profiles (corresponding to the displaced image and the reference image) provide an accurate measurement of the displacement, which in turn provide an independent observation of the transient optical power of the lens at a given time point. The procedure is repeated for the stack of images corresponding to the successive frames (during which time the TL changes its shape), tracking in this manner the temporal response of the TL that generates the addressed input signal. The measurement and the processing are automatic, providing a unique combination of simplicity, temporal discrimination, speed, robustness, and accuracy that surpasses other instruments able to measure dynamic optical power.

3.2.6. Samples and measurements

Three different models of Optotune AG (Switzerland) TLs were measured in the study (Table 3.1): EL-10-30-C (4 units labeled 30C#1 to 30C#4), EL-10-30-TC (3 units: 30TC#1 to 30TC#3) and EL-16-40-TC (1 unit: 40TC#1). The TLs were tested together with an offset lens to bring their lower power close to zero diopters (D).

The temporal step response function of each TL was obtained by measuring the response to a square electric input wave with periodic temporal steps (rise time < 30 µs), upwards and downwards. For a reference quantitative description of the temporal response function and settling time, we used 3 D amplitude waves with a 100-ms period. A series of 9 cycles of the temporal response from the same lens were superimposed to evaluate the repeatability of the response of the lens, as well as the precision of the instrument. The linearity of the lenses was assessed by measuring other wave amplitudes (different step heights): 1.00, 1.50, 2.00, 2.50, and 3.00 D; and normalizing the response between 0 and 1. Further, we measured the frequency response of the lens by driving it at a fixed step size and variable frequency (10, 50, 100, 250, and 500 Hz).

Specifications

Lens model	**EL-10-30-C**	**EL-10-30-TC**	**EL-16-40-TC**
Aperture (mm)	10	10	16
Tuning range (D)	+5.0 to +10.0	+8.3 to +20	-2.0 to 3.0
Wavefront error (@530 nm, 0 mA) Optical axis vertical / horizontal (RMS)	<0.15/<0.25 λ	<0.25/<0.60 λ	~ 0.25/~0.5 λ

Nominal values

Rise time [a] (ms)	<2.5	<2.5	~ 5
Overshoot (%)	-	-	-
Settling Time (ms)	<15	<15	~ 25

Measurements

Units Labels	4 30C#1 to 30C#4	3 30TC#1 to 30TC#4	1 40TC#1
Rise time [a] (ms)	1.3-2.1	2.3	46.2
Overshoot (%)	13.7-24.3	10.6	0
Settling Time [b] (ms)	8.6-12.4	20.1	>50

[a] Rise time was defined in the 10%-90% step.
[b] Settling time is defined as the time needed for the step response to reach and stay within 2% of the steady-state value.

Table 3.1 *Tunable lenses used.*

3.2.7. Model validation and compensation transient response

The validation of the high-speed optical power measurements obtained with the focimeter is not straightforward, as a gold standard is lacking. To assess the accuracy of the measured transient optical power response, we used the model described in section 3.2.1. The predicted transient response of the lens to an electric input wave including positive and negative steps (of 1 D) was compared to the corresponding transient response measured with the focimeter. The procedure not only validates the measurements, but also the model used to obtain the predictions.

This validation enabled strategies to compensate for the transient response of the TLs. As a first demonstration of the capability to manipulate the temporal response of the lens, a simple compound waveform was generated by inserting to the transitions of a square wave a short and small correction step (2 ms, 0.20 D), reducing the overshooting in the measurements.

The final strategy to compensate for the transient response was based on automatically generating input waves of higher complexity, using an optimization algorithm (implementing the linear model described in 3.2.1) to minimize the deviations in the predicted response of the lens [132]. In particular, we minimized the root mean square error between the theoretically estimated response and the target curve, with constraints: the maximum and minimum optical power available, the temporal resolution of the device (Section 3.2.2), and the sampling of the optical power dynamic range. By definition, the compensated waveform produces a temporal response close to the target curve when the transient response is taken into account, both in predictions and experiments.

This approach can be applied to any target curve and in this study, it was demonstrated with a 50-Hz waveform including successive positive and negative increments of 1D.

3.3. Results

3.3.1. Computer optical simulations

The amount of light that reaches the high-speed camera determines the performance of the instrument and its design. Computer ray-tracing simulations predict an increase in image displacement with higher prismatic powers, and therefore an increase in measurement sensitivity, at the expense of a reduction in the amount of light reaching the camera. On the other hand, defocus, inherent to the changes in the measured optical power produces a widening in the slit image and reduces the measurement precision. A reduction of the effect of the defocus can be achieved by reducing the diameter of the camera objective (that increases the depth of focus), at the cost of additional reduction in light. With a focal length of F = 50 mm for the projection lenses L1 to L4, a good compromise is achieved with a prism of 10 deg (5.71 Δ), a camera objective with a focal length of 100 mm, and 5-mm pupil diameter. The computer simulations predict a displacement of 18.1 pixels per diopter with a widening of 3.3 pixels per diopter while allowing 0.6 % of the light to reach the detector. Opening the pupil diameter of the

camera objective to 12.5 mm increases the light to 3 % without affecting the displacement, but it increases the widening to 8 pixels per diopter.

3.3.2. Experimental validation and calibration

Figure 3.3 illustrates the displacement of the slit image in the experimental set-up when trial lenses of different powers are placed in the plane indicated by TrL in Figure 3.2. To compensate for the light loss predicted by the simulations, a 25 µm wide slit (magnified to 40 µm in the plane of the camera) was used, directly illuminated with a high-power white LED source. The left side of the slit image corresponds to the light that does not propagate through the prism, and this portion of the image is used as a reference since it is unaffected by changes in optical power. The right side of each image is imaged through the prism, and the slit image suffers a vertical displacement that is directly proportional to the optical power, as shown later in this section.

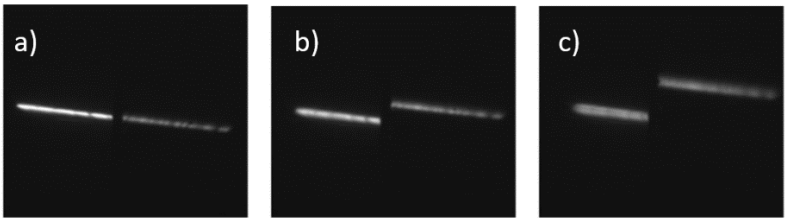

Figure 3.3 *Raw tilted slit images when trial lenses are measured. Left side of each image: reference (no displacement). Right side: displaced images through the prism:* ***a****) 0 diopters (D) -without trial lens-;* ***b****) -0.75 D;* ***c****) -1.75 D. Besides relative displacement, the defocus causes some widening in the image of the slit. The images were taken through the prism (right-half of the slit images) are weaker due to reflection and transmission losses, and due to the prismatic deviation of the light.*

The automatic 8x super-resolution algorithm detected slit tilts between 0.5 and 5 deg, and by digitally inverting the rotation was able to overcome the limitations imposed by the sampling resolution of the camera, even when 2 × 2 binning was used. The ultimate limit to the estimation of the slit position was imposed by the optical quality of the image (mainly defocus) and, to a lower degree, to the irregularities in the slit and the illumination, and was estimated to be 0.5 pixels (0.8 pixels with a defocus of 3 D).

The instrument translates the different optical powers (induced by the trial lenses in this case) into lateral displacements of the image of the slit. Panels b) and c) show some widening in the slit image due to defocus. That widening (under 3 pixels per D in the measurements) affects the estimation of the peak position (<1 pixel as described before), but it is relatively lower than the displacement (16 pixels per D in the measurements), allowing accurate measurements (high displacement-to-widening ratio, i.e., high signal-to-noise).

The complete static calibration (with trial lenses) of the instrument showed a highly linear relationship ($R^2 > 0.99$) between optical power and image displacement. The static calibration with TLs showed a linear relationship between steady voltage and optical power ($R^2 > 0.99$ in all the tested TLs), from which a calibration equation (optical power versus input voltage) was obtained for each lens unit and model.

3.3.3. High-speed focimetry

In Figure 3.4(a), corresponding to lens 30C#2, deviations from the ideal response are restricted to the region around the transition between the two states (high power and low power). The focimeter is sufficiently fast to track the transient optical powers between states and describes a smooth transition. The maximum speed of the TL is 1.27 D/ms. This TL converges to the desired optical power of 6.80 ms after the beginning of the transition following an overshoot (11.47 % of the step height), and damped oscillation. The lens is free of dynamic artifacts (in one of the two stable positions) 86.40 % of the time (for a duty cycle of 100 ms). A detail of the transient response of the same lens is shown in Figure 3.4(b) and (c) (without and with super-resolution algorithm, respectively). Super-resolution (based on Radon transform) softens the transient response curve and removes quantization artifacts due to image pixelation. Figure 3.4(d) shows the superposition of 9 different cycles (each one shown in a different color) for a different unit (30C#3) and 20-ms cycles. For each temporal sampling position, the figure represents 9 points. The high degree of superposition (RMS 0.05 D) demonstrates the high repeatability in the measurement of the transient response of the lens (as already evidenced in Figure 3.4(a)), as well as the high precision of the proposed instrument.

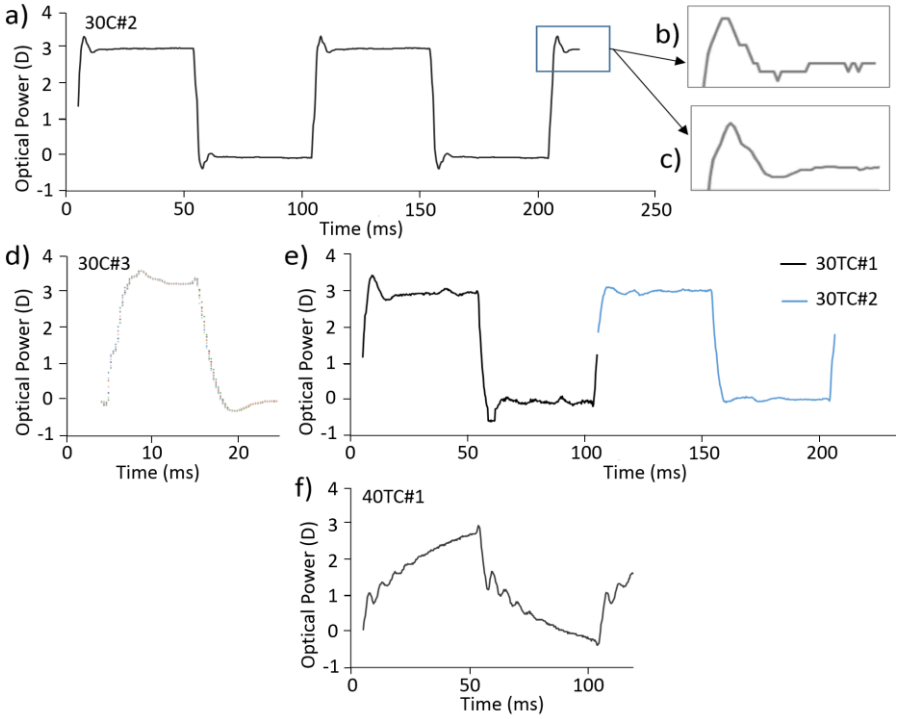

Figure 3.4 *High-speed focimetry measurements. The graphs represent the measured response of the tunable lens (optical power as a function of time) when a square electric input wave is used. The wave period is 100 ms for all the plots, except for (**d**), which has a period of 20 ms. The step height is 3 D in (**a**)-(**f**) and 2 D in (**g**)–(**i**). (**a**) Measured temporal response for tunable lens 30C#2. (**b**) Measured temporal step response function when the slit is not tilted. (**c**) Measured temporal step response function when the slit is tilted and the superresolution algorithm is applied. (**d**) Measured temporal response of a different unit (30C#3) obtained from a superposition of 9 cycles (20 ms). Results with: (**e**) two other units of a different tunable lens model (30TC#1 in black, representing a tunable lens with strong and asymmetric dynamic*

*artifacts; 30TC#2 in blue, with a moderate dynamic behavior) and (**f**) large aperture lens (40TC#1; slow average speed).*

Figure 3.4(e) and (f) show characterization results for other TL models. Figure 3.4(e) shows lenses with a less stable plateau (noise and oscillations) and illustrates the capability to detect differences across units (30TC#1 and 30TC#2; see figure caption for details). A large aperture lens is shown in Figure 3.4(40TC#1). This model is not intended for high-speed applications and shows strong distortions with oscillations, and a settling time over 50 ms, with a low average speed of 0.04 D/ms.

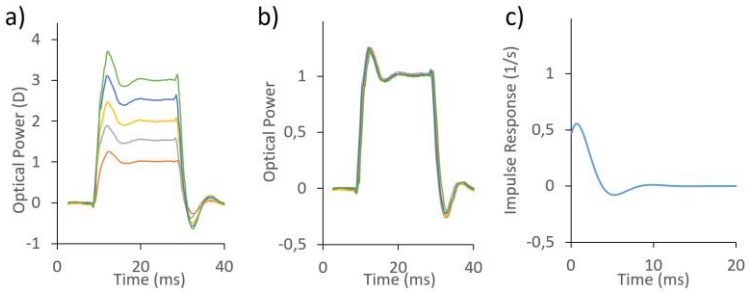

***Figure 3.5** Transient response of tunable lens 30C#4 for a cycle of 40 ms and different steps heights (1 to 3 D in 0.5 D steps). (**a**) Absolute response: measured optical power as a function of time. (**b**) Normalized transient response to justify the linearity of the response with varying optical power. (**c**) Impulse response.*

Figure 3.5(a) shows the transient response of a lens 30C#4 TL for different step heights (1 to 3 D in 0.5 D steps). Figure 3.5(b) shows the normalized transient responses (mean RMS difference 0.055 D) and illustrates that all the curves in Figure 3.5(a) are approximately directly proportional to the step height. This validates the hypothesis that the transient response of the TL under consideration is linear. This assumption makes the process of correcting the input signal to achieve the desired output simple. Figure 3.5(c) shows the corresponding impulse response (Section 3.2.1).

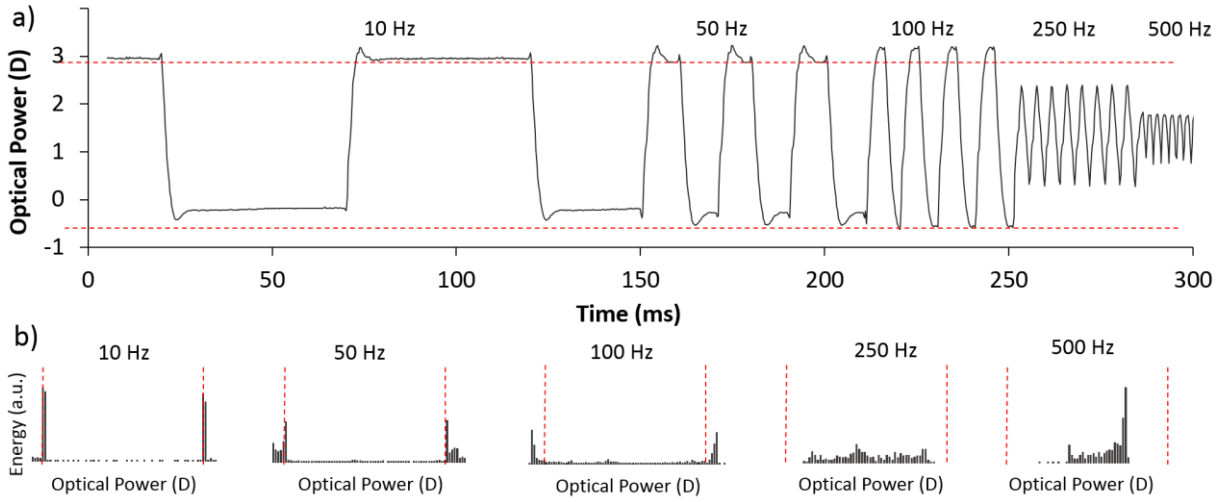

***Figure 3.6 a**) Transient response of tunable lens 30C#3 at different excitation frequencies for a square wave of 3 D of amplitude. **b**) The corresponding histograms showing the distribution of focal positions of the temporal response.*

Figure 3.6(a) illustrates the transient response of lens 30C#3 at different excitation frequencies (10, 50, 100, 250, and 500 Hz). A slow 10 Hz cycle provides a histogram of the temporal response (Figure 3.6(b)) close to two Dirac delta functions, as the TL is in a stable state most of the time and the relevance of the transient response is minor. At 50 Hz, a significant percentage of the energy is spread across optical powers beyond the 0-3 D range, and the energy at the peaks decreases. Beyond 100 Hz, the peaks at nominal powers are lost, either due to overshooting or due to a lack of compliance of the TL to the frequency of the input signal.

3.3.4. Compensation of transient response

The results are shown in Figure 3.4(d), Figure 3.5(b), and Figure 3.6(a) demonstrate high repeatability, linearity, and predictability in the behavior of the TLs (RMS < 0.05 D), confirming the possibility of using linear-system design strategies to compensate for transient response and to improve the expected performance of the lens by manipulating the input wave.

As a proof-of-concept, Figure 3.7(a) shows a modified input wave with softened transitions aiming at modulating the lens response and reducing the overshooting. Figure 3.7(b) compares the outputs measured in the focimeter for a TL (30C#4), with a square input wave (in black) and with the modified softened input wave (in orange). This simple example shows that the transient response can be locally adjusted and could be fine-tuned by applying a step-by-step correction of the electric signal to improve lens compliance. As the distortions introduced by transient response are known to be systematic, we can predict them using the linear model described in Section 3.2.1. Once the behavior of the TL is predicted, we can use inverse problem modeling approaches to optimize the input signal to generate the desired response in a design step.

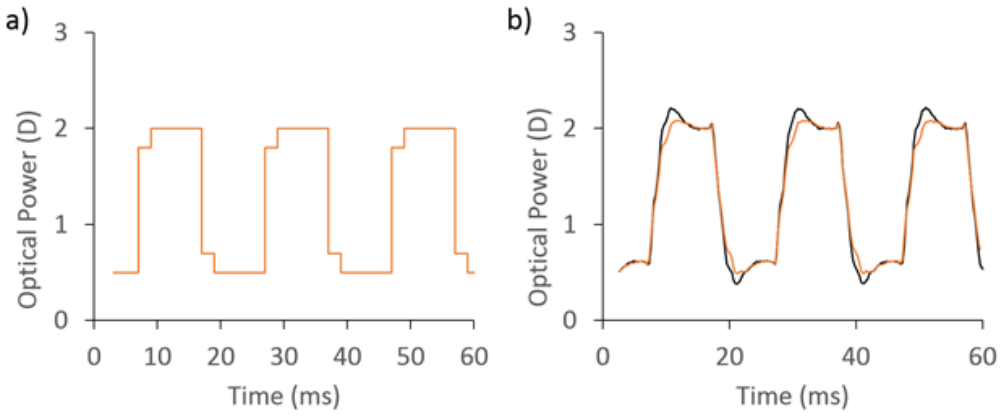

***Figure 3.7 a**) Modified square input wave with a transient correction step (2 ms, 0.2 D), to generate an improved square step response. **b**) The corresponding measured temporal response (tunable lens 30C#4) showed a reduced overshoot (orange curve) in comparison with the measured step response to a square input wave (black curve).*

Figure 3.8(a) shows results for another input wave, in which 3 different focusing states (1 D, 2 D, and 3 D) are sequentially scanned at high speed (50 Hz). This scenario mimics, for example, an artificial vision system or a camera focused at 0.5 m, but periodically seeing or recording objects at 1 m and 0.33 m. The nominal input signal, shown in blue, is severely degraded by the transient

response effects of the TL. The gray curve shows the predicted transient response, using the data in Figure 3.5(c) in the linear invariant model (*h(t)* in Eq. 3.1). The difference between the predicted transient response and the nominal wave is higher than 0.05 D (the reported RMS due to repeatability) 50% of the time, with a RMS difference of 0.34 D. The transient response of the corresponding lens (30C#4) was experimentally measured (black curve in Figure 3.8(a)). The high degree of superposition between the measured response (black) and the predicted response (gray) in Figure 3.8(a) (less than 0.05 D RMS difference) validates the model and the inherent assumption of linearity of the TL transient response with optical power. The small discrepancy is compatible with the repeatability of the lens and the measurements in the focimeter (see Figure 3.4(d) and Figure 3.5(b)). Due to the considerable distortions in the transient response concerning the nominal wave (Figure 3.8(a)), the TL without compensation of transient response could not be used in this application as it would be unable to image all the objects in focus.

Figure 3.8(b) shows the optimal compensated input wave (orange) that minimizes the distortions in the temporal response. This compensated input wave results from an iterative optimization (Section 3.2.7) using the linear model (Section 3.2.1) and shows two main features: an abrupt pulse right before each step transition, to produce the maximum acceleration of the lens, and a progressive slow down following each transition. These features are not forced by a particular compensation strategy. They appear in the minimization and result to be approximately symmetrical in upwards and downwards steps.

Figure 3.8(c) shows, in red, three repetitions of the temporal response experimentally measured with the focimeter when the transient response is compensated. The compensation of transient response improves the fidelity of the lens in scanning different optical power steps at high frequencies (RMS 0.07 D with compensation vs 0.23 D without compensation). Figure 3.8(d) shows the histograms of focus positions, with compensation (in red) –showing three clear foci of energy measured at exactly their nominal positions (1, 2, and 3 D)- and without compensation (in gray) –showing broadened peaks, with less energy, and displaced concerning their nominal positions.

The procedure summarized in Figure 3.8 validates the focimeter, justifies the description of the transient response of the lens in terms of step response and impulse response, and supports the hypothesis of considering the TL a linear time-invariant system in the model, and the strategy to compensate the transient response. Figure 3.8 also shows that although it is not possible to break the fundamental limit set by the maximum speed of the TL, it is possible to improve the transient response of the lens, reducing the settling time and the overshooting, by adjusting the input signal taking into account the transfer function of the lens measured with the developed focimeter.

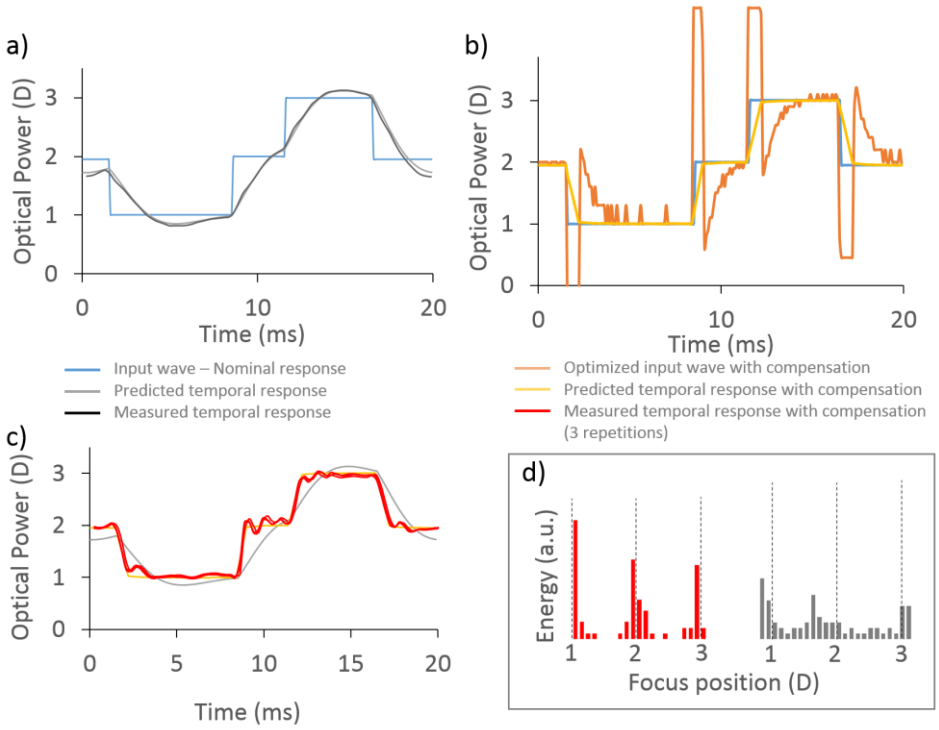

Figure 3.8 *Compensation of transient response. (**a**) Nominal response of the tunable lens (blue); predicted (gray) and measured (black) transient response of tunable lens 30C#4. (**b**) Compensated input wave (orange) that minimizes the effect of the transient response, providing a predicted temporal response with compensation (yellow) close to the nominal (intended) response (blue). (**c**) Measured temporal response with compensation of transient response, 3 superimposed repetitions. (**d**) Histograms of focus positions measured with (red) and without (gray) compensation of transient response.*

3.4. Discussion

We have presented a new approach to measure and compensate for the dynamic behavior of fast TLs. The potential of TLs is remarkable in the fields of machine vision and inspection, microscopy and ophthalmology, and in applications requiring fast and automatic focusing. The proposed new fast focimeter device relies on simple optics (a prism and a slit) in combination with a high-speed acquisition camera. The method has proved to be robust and has demonstrated direct measurements of optical power with high temporal sampling.

Configuration. The optical configuration was optimized to maximize measurement precision (<0.05 D), following a trade-off between image widening due to defocus of the slit, image displacement due to the beam deflection by the prism, and amount of light (i.e., measurement signal in the detector). The optics were tailored to ease image processing. The tilted slit enables a fast and automatic super-resolution algorithm that overcomes the limitation imposed by pixelation (and binning) and improves the estimation of the slit position (resolution in optical power). The sampling rate of the camera, 3823 fps, was sufficient to measure the fastest lens at maximum speed (1.27 D/ms).

Measurements. The new focimeter was able to provide, besides static calibrations, dynamic measurements at 3.8 kHz. It has proven to be versatile with the ability to measure at high speed, a range of active transmissive and reflective (Appendix of this chapter) optical elements that are

known to be subject to transient response [121,161]. The availability of a reference image during the measurements, inherent to the approach, contributes to the precision of the instrument (0.05 D), making it robust against TL positioning. The additional pupil plane allows a channel for calibration. The technique captures subtle differences in the dynamic behavior, both across lens models and across units of the same model, suggesting that the approach could be used for quality control. The instrument could be used to measure TLs with different principles of operation. Among others, it can also detect time-dependent abnormalities in the TL and the driving electronics with a temporal resolution of 0.2 ms.

Predictability and compensation of transient response. The response of the lenses understudy was shown to be systematic and linear: they have a similar normalized response for different step heights, i.e., the same transient response (although scaled) with different amplitudes. This linearity enables precise predictions of the output of the lens, for any input, with simple linear models, and further design compensation strategies to dump the overshoots. We have shown the strong potential of the instrument in combination with a linear model of the temporal response of TLs. The impulse responses of the TLs were obtained from measurements of the temporal step response function with the focimeter. The focimeter was also used to experimentally measure the output response, which was successfully compared with the predictions of the model. A numerical optimization [132] demonstrated that the compensation of transient response is possible, and experimental measurements proved that applying this compensation represents a significant improvement in the performance of TLs working at high speed.

The capability to detect differences across lens models and units of the same model (Table 3.1) enables compensation strategies at an individual level, that would require measuring the transient response of each lens.

TLs are prone to power drifts with temperature changes that can be external (environmental), but also internal, owing to different energy dissipations at different dynamic regimes. These power drifts introduce additional dynamic variability, reducing long-term repeatability, that could be compensated with more sophisticated models incorporating temperature measurements (already available in commercial lenses with temperature sensors). A focimeter like the one presented can be envisioned as part of a compensation arm of an optical instrument using TLs to provide real-time testing and closed-loop compensation of transient response. On the other hand, focimeters are also instrumental in the evaluation of presbyopic corrections mapped by temporal multiplexing in simultaneous vision simulators [105]. The quality of a simulation will rely on an accurate representation of the multifocal optics.

Advantage over the state-of-the-art. There are other methods to evaluate TLs that can work at high speed. In methods relying on focused energy, (normally at the peak or at the center of the point spread function), the measurements are affected by optical quality: through-focus energy changes due to aberrations and diffraction spread of energy that typically overestimate the transient response. Methods relying on light pencils, as deflectometry or phase-detection are

quite independent of the image quality, but are sensitive to lens geometry and position, and therefore not suitable with active optical elements such as TLs. Hartmann-Shack aberrometry does not rely on energy and is robust against lens position and can work in combination with a high-speed camera. In comparison with Hartmann-Shack, the focimeter presented in this study has a larger dynamic range, is simpler, and the processing is straightforward.

While optical quality has not been explored as an outcome, it could also be estimated with the focimeter. If the slit is sufficiently narrow, the energy profile provides the Line Spread Function of the system (LSF), following background subtraction and normalization. The LSF is a fundamental optical image quality descriptor, that provides common metrics like the Strehl ratio (the value of the LSF peak) and the modulation transfer function (by Fourier Transform). As defocus blur and motion blur degrade the slit image quality, the estimation of optical quality is only valid for the static optical power of the lens that brings the slit to focus. The measurement of optical quality is obtained at no cost and provides additional evaluation capabilities.

Applications. TLs are becoming ubiquitous in optical instruments (artificial vision, 3D displays, microscopy, OCT [123], visual simulation [105]) and are often used to scan a range of through focus positions at high speed. As they are prone to suffer from dynamic artifacts, commercial TLs can exhibit inaccurate responses (slowed down hardware or electronic driver) designed to avoid overshooting and oscillations, at the expense of slower responses. The high-speed focimeters like the one presented here will stimulate designing strategies for TL manufactures and for application developers, compensating the transient response associated with the operation of TLs at high speed. Within the limits of repeatability and linearity, the TL (based on any working principle, or any other variable focus active optical element) can be pushed to the limits of its potential, after characterization and optimization of the driving electrical signal.

3.5. Appendix: Deformable mirror and spatial light modulator

Besides TLs, other technologies that can produce a rapid change in focus are deformable mirrors -DM-, where piezo-actuators deform a reflective membrane normally in a closed-loop operation with inputs from a wavefront sensor, and liquid crystal spatial light modulators -SLM-, where about 1 million or more pixels arranged in a 2-dimensional array can independently change their phase in response to an input electrical or optical signal.

In this study, we also measured with the focimeter the transient response of a DM with 52 actuators (miraoTM 52-e, Imagine Eyes, France) and a reflective phase-only liquid crystal SLM (PLUTO-VIS; Holoeye Photonics AG, Germany). The design of the focimeter was modified due to its reflective nature. After calibration of the focimeter in its initial configuration (Fig. 3.2), the slit (S) and the measuring arm (Prism (P), Macro Objective (MO) and High-Speed Camera (HSC)) were moved to an adaptive optics system [104], where they were coupled to the existing projecting elements creating an intermediate slit image (S'). We measured temporal waves with steps of 2 D, also in cycles of 100 ms. To account for potential chromatic effects, both active elements were measured in green monochromatic light (555 nm).

Figure 3.9(a) illustrates the dynamic behavior of the adaptive optics DM (membrane with actuators). The estimated speed is comparable to that of the TL of Figure 3.4(a), but with more oscillations. Figure 3.9(b) shows the behavior of the liquid crystal SLM. This device has a completely different dynamic behavior. Using the same camera parameters, the image of the slit does not move progressively from one position to another (as in the TLs and the DM). Instead, the image of the slit progressively fades out from one position, without moving, and at the same time, it progressively appears in the second position, without a transition through intermediate foci. These fade-in/fade-out events are represented by gray scales in Figure 3.9(b). The period of co-existence of foci is four times longer for the excitation (20.80 ms to change from 0 to 2 D) than for the relaxation (5.03 ms to change from 2 to 0 D). The different times needed by each pixel of the SLM, dependent on the phase induced, can explain this singular bimodal behavior without intermediate foci.

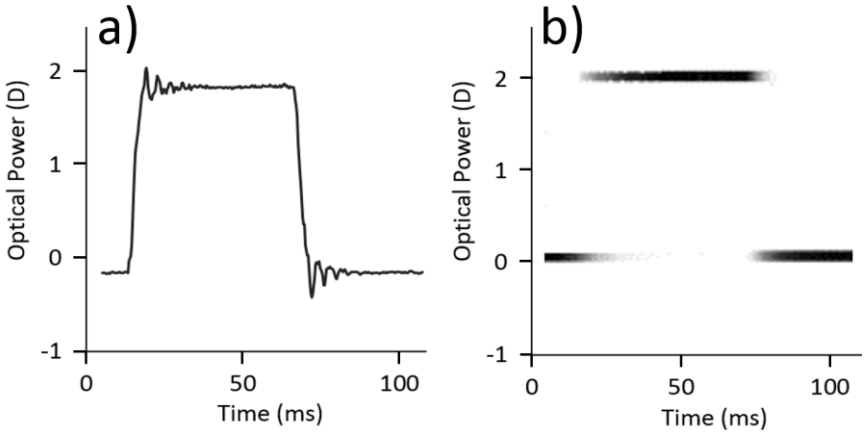

Figure 3.9 *High-speed focimetry measurements of other active optical elements. (**a**) Deformable mirror with monochromatic light (555 nm), and (**b**) spatial light modulator (555 nm).*

The combination of the linear time-invariant model and the fast focimeter presented in this study enables the first procedure, to our knowledge, for direct characterization of the transient response of TLs and compensation of the temporal distortions introduced. This allows accurate control of the operation of TLs working at high speed. In the next chapter, optimization and implementation of a closed-loop iterative algorithm validate a low-cost and low-speed focimetry system for TLs characterization.

Chapter 4

Closed-loop experimental optimization of tunable lenses

In the current chapter, we present a low-cost focimeter, able to characterize the dynamic response of TLs, but using a conventional low-speed and low-cost camera.

This Chapter is based on the paper by *Lopez-de-Haro et al. "Closed-loop experimental optimization of tunable lenses" in preparation*. The co-authors of the study are Xoana Barcala (equal contribution to the first author), Ivan Martinez-Ibarburu, Yassine Marrakchi, Enrique Gambra, Victor Rodriguez-Lopez, Lucie Sawides, and Carlos Dorronsoro.

The author of this thesis (1) conceived the ideas along with Carlos Dorronsoro and Lucie Sawides, (2) provided guidance, coordination, and clinical orientation, (3) contributed to the evolution and calibration of the optical setup along with Ivan Martinez, (4) supervised the experimental measurements (Ivan Martinez and Angel G. Lopez-de-Haro), (5) participated in the data analysis and, (6) contributed to the preparation of the manuscript (with Carlos Dorronsoro and Angel Lopez-de-Haro).

4.1. Introduction

As explained in chapter 3, an accurate assessment of the TL's temporal response and the characterization of its dynamic effects are key elements in the design of specific applications involving fast changes of the optical power of a TL. Chapter 3 presented the development of a high-speed focimeter, an instrument able to measure the TL impulse response. Furthermore, the instrument enabled the development strategies to compensate the dynamic effects of the lenses, to match the nominal optical power wave even in time regimes with important distortions. These strategies can dramatically improve the performance of TLs when close to their temporal limits. However, the compensation strategies require the use of a high-speed focimeter that integrates a high-speed camera (3800 fps), not affordable in all facilities using TLs. Besides, the compensation strategy previously proposed involves complex calculations modeling the dynamic behavior of the TL, to reach precise a priori predictions of its response. These important limitations reduce the universal availability of the technique.

In this study, we present an alternative approach, a low-cost focimeter able to characterize the dynamic response of TLs but using a conventional low-speed camera. With that instrument, we implement a closed-loop iterative algorithm for the experimental, automatic, and heuristic optimization of TLs. Finally, we demonstrate, in a depth scanning prototype, the benefits of compensating the dynamic effects following the new procedures.

4.2. Methods

4.2.1. Experimental set-up: low-cost focimeter

The low-cost focimeter is designed (Figure 4.1) to take measurements of the dynamic optical power induced by the TL. Of the different elements of the set-up (shown in Figure 4.1B and detailed below) the most important one is the prism, which induces a displacement in the image of a slit, proportional to the optical power induced by the TL. Similarly to the high-speed focimeter, a camera captures the displacement of the slit while the TL is driven with a periodic signal (typically square) as in the static examples of Figures 4.1C and 4.1D. Figure 4.1E shows the reconstruction of the dynamic response in optical power of the TL, showing the dynamic effects. Only one line of each frame is used, and the same line is represented for different time positions sampled.

The light source is made of a laser source (λ=650 nm ± 10nm) coupled to an optical fiber (thickness 480 um and 2cm length) whose properties had been chemically altered with acetone [162] to induce important optical losses in a specific portion (Figure 4.1B shows the red light emitted from the optical fiber). This emitting portion of the fiber defines a robust and low-cost slit object that is imaged through the system. The slit object is placed 200 mm behind a collimating lens. Right after the collimator, we place the TL under study (EL-10-30-C; Optotune AG, Switzerland [163]) inside a SimVis Gekko module that acts as an optical projector, optically conjugating the TL with a trial lens holder. A 50 mm lens focused the beam onto the prism (10º, PS814-A) that gauges the dioptric power of the TL into the displacement of the slit image [137]

captured in a low-cost CMOS camera (Thorlabs DCC 1545) with a 16 mm objective lens (Navitar, MVL16M23). This process follows the same procedures of lens characterization and instrument calibration as the previously developed high-speed focimeter (see chapter 3).

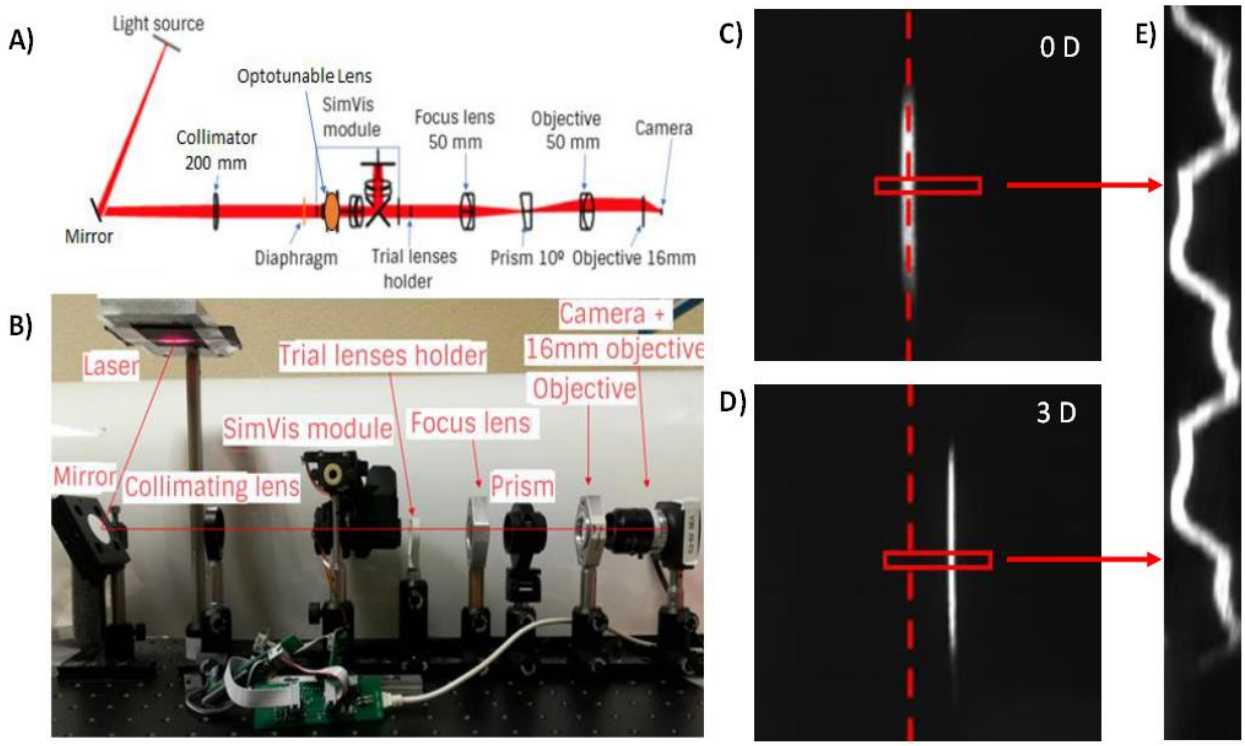

Figure 4.1. *(**A**). Schematic view of the low-cost focimetry system for TL characterization. (**B**) Picture and elements. (**C-D**) static positions of the image of the slit when captured by the camera at two different optical power values of the tunable lens: 0D (**C**) and 3D (**D**). (**E**) Reconstructed signal when a bifocal profile 0-3D is induced in the tunable lens. The same line of the image is represented for different time positions.*

4.2.2. Tunable lens characterization with low-cost focimeter

Previous studies have shown that the response of the TL is stable, producing a repetitive signal when driven with a periodic input signal (see chapter 3). Repeatability is instrumental in this low-cost instrument that uses a conventional camera since it enables the full registration of the TL response (dynamic optical power) sampling it at low frequency. By knowing the frequencies of the original and sampling signals and, consequently, the existing delay between both, it is possible to rebuild the original profile from the measured samples, spanned along with different cycles. Figure 4.2 shows the reconstruction (red line) of the original signals (blue line) from the sampled measurement (red dots).

Custom automatic algorithms in Matlab (Mathworks, US), enabled to control of the low-cost camera parameters, and capture images at specified frequencies and with precise integration times. To register 6 periods of a 50 Hz wave, a periodically sampled is performed every 21 ms. That registration spans over a time interval of 25 seconds and 1180 sampling points are measured. An exposure time of 0.64 ms was found to provide a good exposition of the moving slit, with enough signal, but without motion blur, achievable thanks to the vertical electronic rolling shutter of the camera.

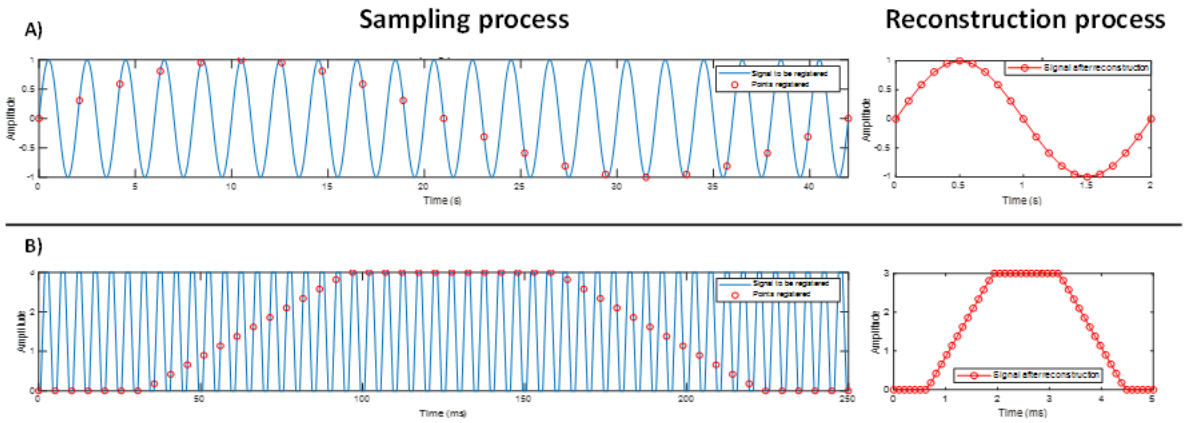

Figure 4.2 *Reconstruction method of an original signal sampled at low frequency. (**A**) For an ideal sinusoidal profile. (**B**) For an ideal soft step profile. The blue line represents the original signal to be reconstructed. The red dots correspond to the sampling signal. The red lines (right panels) show the reconstructed signals.*

Figure 4.3 shows the measurement of a 0 – 1D bifocal profile (square driving signal with abrupt steps) at 50Hz. Figure 4.3.A shows the reconstructed signal after image processing to retrieve the slit position, from the images capture by the low-cost focimeter (Figure 4.3B). The dynamic effects of the TL over- and under-shooting are very apparent.

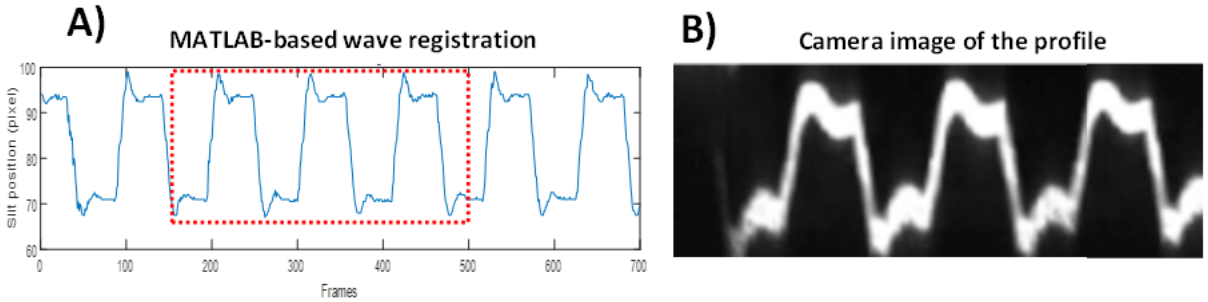

Figure 4.3 *(**A**) Measurement of six periods of a bifocal 0-1D profile (blue signal) using the sampling method proposed in this study. (**B**) Corresponding focimeter images were taken by the camera (similar to Figure 4.1.E). The three periods shown in the red box in (A) correspond to those shown in (B).*

4.2.3. Closed-loop experimental optimization algorithm

The developed closed-loop experimental optimization algorithm is based on four main steps, as shown in Figure 4.4: (1) The optical power response produced by the TL is measured using the low-cost focimeter, (2) the images are reconstructed and post-processed, (3) the response is compared to the target wave and a specific merit function is built accordingly. If the response is optimal and, thus, the established merit function's value is below a predefined threshold, the process concludes. Otherwise, (4) the original input signal is modified, and a new iteration takes place.

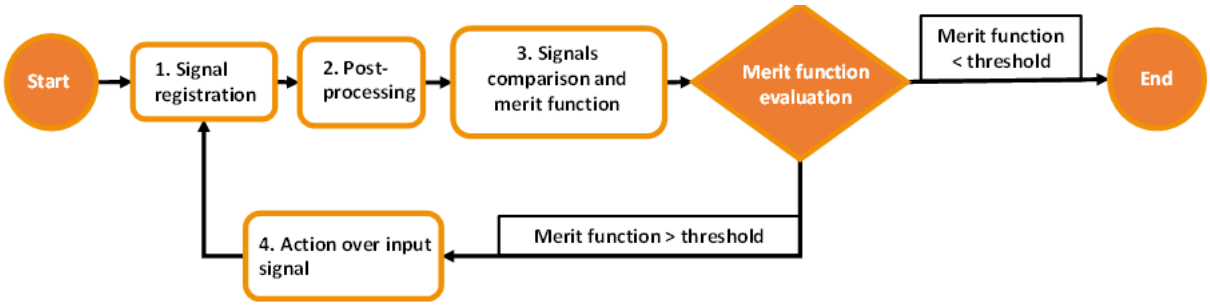

Figure 4.4 *Scheme of the proposed closed-loop algorithm for experimental optimization of TL. This algorithm presents four main steps by which the induced profile is optimized experimentally and on a granular basis.*

As shown in the example of Figure 4.5A, the algorithm identifies the regions of the signal located above their targeted value (red regions) and below that value (green regions). Then, as depicted in Figure 4.5B, the method will transduce these regions to the input signal and act accordingly. The red regions (located above the targeted value) are compressed, and the green ones (those below the targeted value) are amplified. This method acts over the TL response on an automatic, experimental, and granular basis: (1) the algorithm works autonomously and concludes only when the obtained response is optimal (automatic); (2) it measures the TL's performance in every iteration and acts over the empirically obtained response (experimental); (3) it acts only on the specific regions showing deviations (granular).

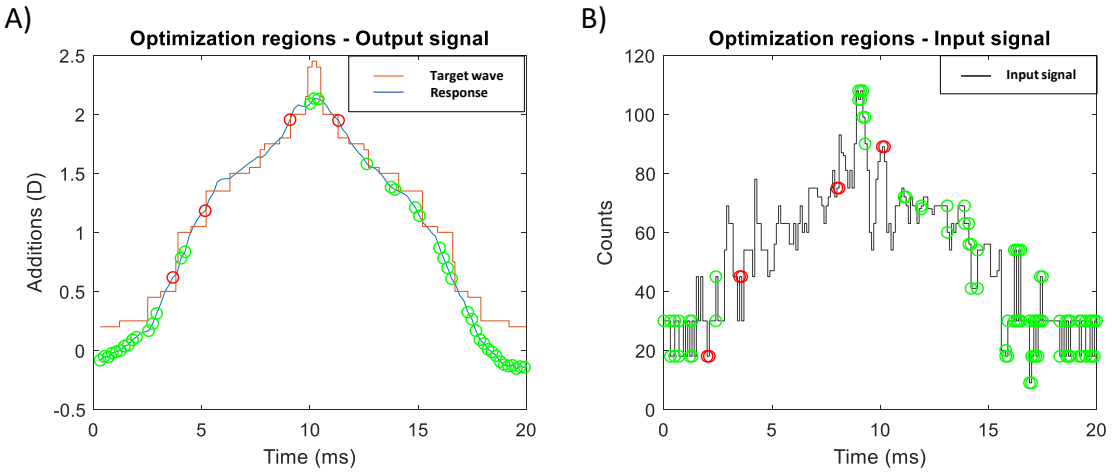

Figure 4.5 *Scheme depicting the regions to be corrected in the output (**A**) and input (**B**) signals of the TL. In (**A**), the orange line corresponds to the target wave and the blue line, to the TL response. In (**B**), the black line corresponds to the input signal introduced in the lens. In both figures, red dots correspond to the areas to be compressed and the green ones to the ones to be amplified.*

As shown in the example of Figure 4.5, the closed-loop experimental optimization can be implemented with any signal, any nominal through focus temporal trajectory of the TL. For demonstration purposes, in this study, the method was implemented in two specific profiles shown in Figure 4.6: a trifocal profile, and a staircase profile. The time regime (50Hz) was below the temporal limit of the TL, but sufficiently close to induce important dynamic effects. The trifocal profile has two plateaus of 5.25 ms. The staircase profile has four plateaus of 3 ms.

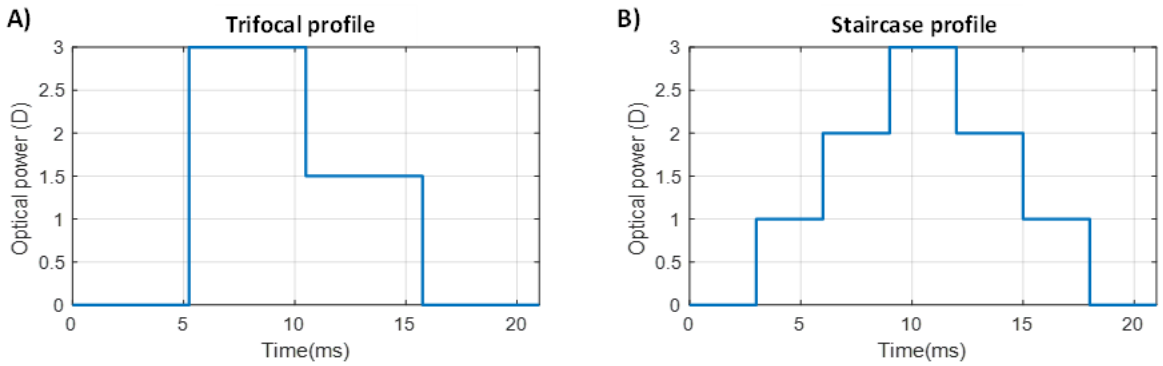

Figure 4.6 *Optical power profiles of trifocal (A) and staircase (B) waves.*

Three different metrics were evaluated to obtain a quantitative measurement of the process, summarizing the performance of the proposed algorithm in each iteration:

- Area under the error curve. Difference between the target wave to response, as shown in equation 4.1.

$$error\ curve = response\ - target\ wave \qquad (4.1)$$

- Effective time ratio. Proportion of time spent by the response in the targeted optical power values. The ratio is calculated considering a tolerance of ±0.09 D. This value is subclinical in ophthalmic applications.
- Standard deviation of the mean, which represents the variation of the profile with respect to its mean.

4.2.4. Illustrative application of tunable lenses: depth scanning

We applied the closed-loop experimental optimization method in a depth scanning experiment. By placing two objects at given distances to a TL, a depth scanning scheme is reproduced, as objects at different distances are focused [164]. The set-up used in this experiment is illustrated in Figure 4.7 and comprises:

- The high-speed camera IL5 Fastec Imaging (USA). This device can take frames at high velocities and allows to monitor the focus change produced by the TL, in ms scale.
- Tunable lens (TL) EL-10-30-C AQAA4517 (Optotune). The TL produces the change in focus allowing the depth scanning.
- Objective AF micro Nikkor 200mm, 1:4D (Nikon ED, Japan). The objective, which allows to identify of very small variations in focus, facilitates the detection of slight changes in the focus of the system.
- Two conventional rulers: (1) They have been selected because of their high degree of detail, letting to detect focus changes precisely. (2) Their axial position is changed depending on the optical power induced by the TL.
- Light source to illuminate the objects.

Figure 4.7 *Diagram of the set-up built to mimic a depth scanning scheme.*

Two different optimization experiments were carried out: (1) using the trifocal wave profile, where the two objects were placed at the distances corresponding to 1.50 D and 3.00 D (67 and 33 cm); and (2) using the staircase wave profile, where both objects were placed at the distance corresponding to 2.00 D (50 cm). At this optical power value, two different regions of the profile were targeted: 2.00 D uphill and downhill steps.

Raw signal in the lens without optimization and inducing the optimized signal were measured in both experiments. As indicated above, the images were taken at specific optical power values, coincident with specific regions of the profiles. In those specific regions, two images were taken: (A) an individual frame and (B) a "step frame". This step frame corresponds to a wider region of the profile and was obtained by summing together a given number of individual frames, which depends on the specific shutter time of the experiment's high-speed camera. In the case of the trifocal profile experiment, both types of images were taken, whereas in the case of the staircase wave only the individual frames are captured. For visualization purposes, for the staircase profile, the camera frame rate was 6150 Hz, and the shutter time 0.151 ms. For the trifocal profile, the camera frame rate was 7694 Hz, and the shutter time 0.127 ms.

To quantitively measure the difference between the images of the optimized and non-optimized profiles, they were compared to a reference optimally-focused image using the structural similarity (SSIM) metric [165,166]. This index quantifies the resemblance between a given image and a reference picture, spanning the values from 0 (no resemblance) to 1 (same image).

4.3. Results

4.3.1. Closed-loop experimental algorithm implementation: trifocal profile

The TL undergoes 21 iterations to achieve optimal performance in the case of the trifocal profile. This optimal performance is revealed by the dramatic increase in the curve matching between the induced and the targeted profiles, shown in Figures 4.8A and 4.8C. The implementation of the algorithm mitigates the undesired deviations shown in the initial cycle, producing a major enhancement of the lens performance. This enhancement takes place gradually along the process, as shown in Figure 4.8B.

The error magnitude undergoes a major decrease along with the 21 cycles of the optimization process, from 8.202 ms·D to 2.483 ms·D (69.7% drop) (Figure 4.8D). This metric decreases gradually following a quadratic curve fitting of amplitude 0.010 ms·D, reaching a plateau around 2ms·D. The existence of this plateau suggests that further improvement may be unreachable

even if more cycles are implemented. At cycles #4 and #16, the error magnitude suffers sharp increases that contradict the general trend of the curve, suggesting the existence of errors in the post-processing of the signal.

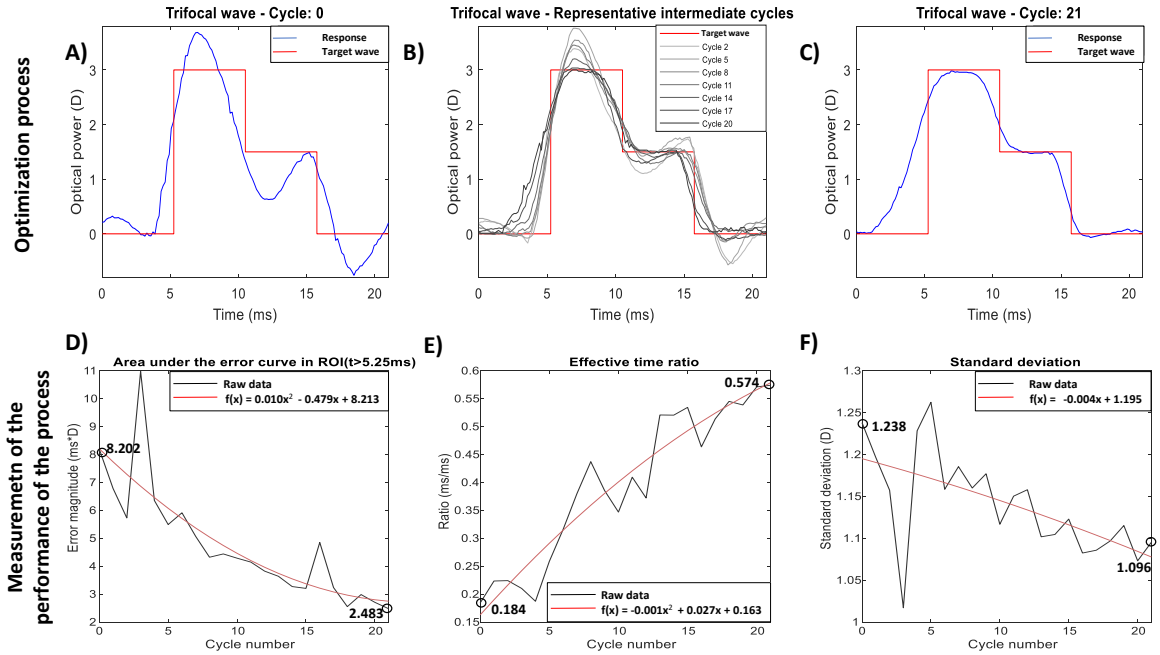

Figure 4.8 *Optimization of the trifocal profile in lens Optotune AQAA4517. (**A**) and (**C**) initial and end state (cycles 0 and 21) of the profile during the whole process; red curves represent the target wave and blue curves the response. (**B**) Evolution of the profile during the iterative procedure, showing the state of the wave in seven illustrative cycles (gray) compared to the target wave (red). Evolution of the metrics being monitored throughout the process, from the beginning (cycle 0) to the end of the optimization (cycle 21) for (**D**) the area under the error curve for a given region of interest. (**E**) The effective time ratiometric and (**F**) the standard deviation. In figures **D-F**, the black line shows the raw data and the red one, their corresponding quadratic regression fits: (**D**) f(x) = 0.010x² – 0.479x + 8.213 (R^2 = 0.720), (**E**) f(x) = -0.001x² + 0.027x + 0.163 (R^2=0.908) and (**F**) f(x) = – 0.004x + 1.195 (R^2=0.363).*

Figure 4.8E illustrates how the effective time ratio at each cycle increases from 0.184 to 0.574. That is, this value undergoes a 211% improvement in 21 cycles, following a quadratic trend (f(x) = -0.001x^2 + 0.027x + 0.163 (R^2=0.908)) that indicates a plateau is likely to be reached around ~0.60. Meanwhile, Figure 4.8F shows the change of the standard variation of the response. This metric undergoes a small change from an initial value of 1.24 D to a final figure of 1.10 D, representing a moderate decrease of 11.4% in the 21 cycles of the process. The metric evolves following a slightly linear pattern, although it is not strong enough to consider it an accurate trend (R^2 = 0.363).

4.3.2. Closed-loop experimental algorithm implementation: staircase profile

The staircase profile takes 23 cycles to improve its performance until it reaches an optimal outcome. As shown in Figures 4.9A and 4.9C, the curve matching increases especially on the right-hand side of the graph, in the three steps containing the 3.00 D to 0.00 D drop. The transition between the initial and final states is shown in Figure 4.9B. It can be observed how the changes

take place especially in the right region of the wave, where the response gradually gets closer to the targeted step value. The optimization process takes place in small steps between cycle 0 and cycle 23, producing moderate improvements in every individual iteration.

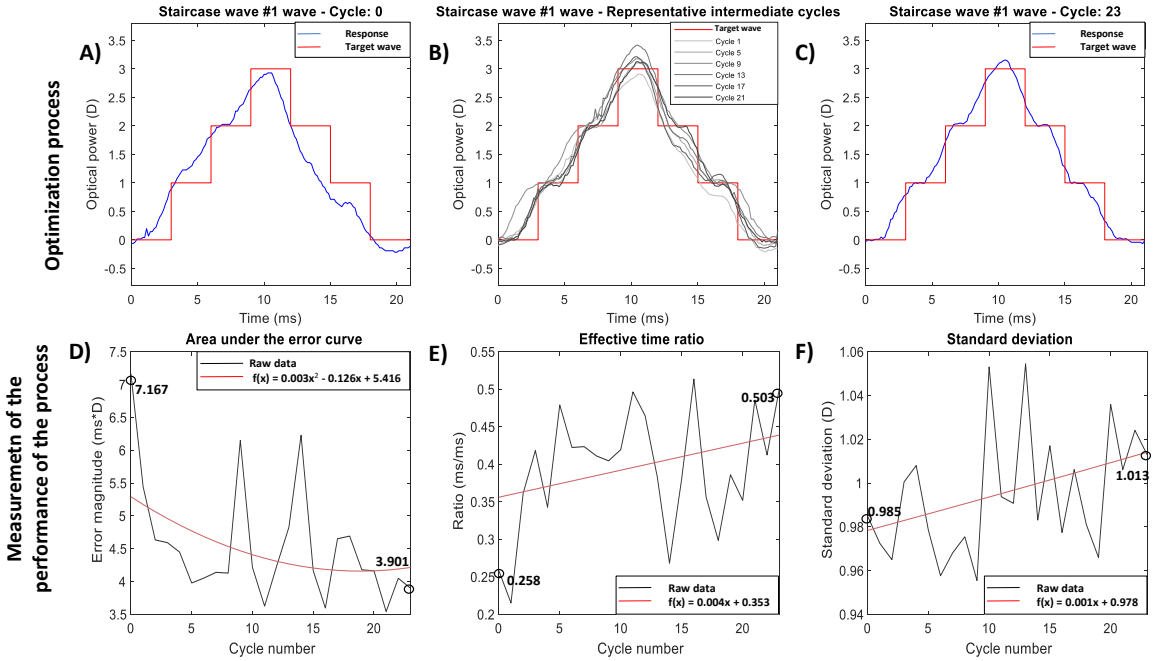

Figure 4.9 *Optimization of the staircase profile in lens Optotune AQAA4517. (**A**) and (**C**) initial and end state (cycle 23) of the profile during the whole process; red curves represent the target wave and blue curves the response. (**B**) Evolution of the profile during the iterative procedure, showing the state of the wave in seven illustrative cycles (gray) compared to the target wave (red). Evolution of the metrics being monitored throughout the process, from start (cycle 0) to end of the optimization (cycle 21) for (**D**) the area under the error curve, (**E**) the effective time ratiometric, and (**F**) the standard deviation. In figures **D-F**, the black line shows the raw data and the red one, their corresponding quadratic regression fits: (**D**) f(x) = 0.003x² - 0.126x + 5.416 (R^2 = 0.204), (**E**) f(x) = 0.004x + 0.353 (R^2=0.102) and (**F**) f(x) = 0.001x + 0.978 (R^2=0.150).*

The area under the error curve metric decreases from an initial error value of 7.167 ms·D at cycle 0 to a value of 3.901 ms·D at the last iteration (cycle23) (figure 4.9D), producing an improvement of 45% in the metric. Figure 4.9E indicates how the effective time ratio of the profile reaches a relevant value of 0.503 at cycle 23, improving dramatically from the initial value of 0.258. Thus, the profile's effective time at the last cycle almost doubles with respect to the evaluated at cycle 0 (95% improvement). This metric undergoes a gradual enhancement along the whole process, although a consistent trend is not produced (R^2 = 0.102). At the same time, the value for the standard deviation of the signal suffers almost no variation throughout the whole of the process, starting at 0.99 D and finishing at 1.01 D, with no consistent trend (R^2 = 0.150).

4.3.3. Depth scanning experiment: trifocal profile

Figure 4.10 shows the results of the depth scanning experiment implemented in the trifocal profile for the initial cycle (Figure 4.10 A, B, E, and F) and for the end cycle (Figure 4.10 C, D, G, and H) of the iterative algorithm.

Figures 4.10 A-D illustrate the frames taken in the “3.00 D step” both for the non-corrected (cycle 0) and the optimized wave (cycle 21). It can be observed how both the step frame and the individual frame undergo a clear improvement in the 21 cycles of the process. On the one side, the individual frame, taken in the middle point of the step suffers a dramatic improvement, evolving from an inaccurate value of 3.68 D to a focused state at 3.01 D. On the other side, the step frame also improves strongly. It evolves from a blurry state to a stable step where the wave remains at a value of 3.00 D for the whole duration of the image capture. This improvement produces the evolution from a blurry image in the initial cycle to a nitid image in the end cycle. Quantitatively, the structural similarity index (SSIM) reveals a sharp improvement undergone from cycle 0 to cycle 23. The SSIM of the individual frame changes from a low 0.394 (39.4% of structural similarity with respect to the targeted, focused image at 3.00 D) to a high 0.976 (97.6% of structural similarity), whereas the SSIM of the step frame experiments a moderate increase from 0.560 to 0.663.

Similarly, Figures 4.10 E-H illustrate the frames taken at the same conditions but the “1.50 D step” and reflect a huge improvement in the performance of the lens. In the case of the non-corrected wave (cycle 0), the lens does not remain stable in the target period, resulting in a blurry image both for the step and individual frames (Figures 4.10E and F). After 21 cycles of the optimization process, the curve matching between the target wave and the response is optimal, producing nitid images for both the step and the individual frames as shown in Figures 4.10G and H. This important enhancement is measured quantitively using the structural similarity metric, with an improvement of 0.598 points (from 0.367 to 0.966) in the individual frame and of 0.525 points (from 0.322 to 0.847) in the step frame.

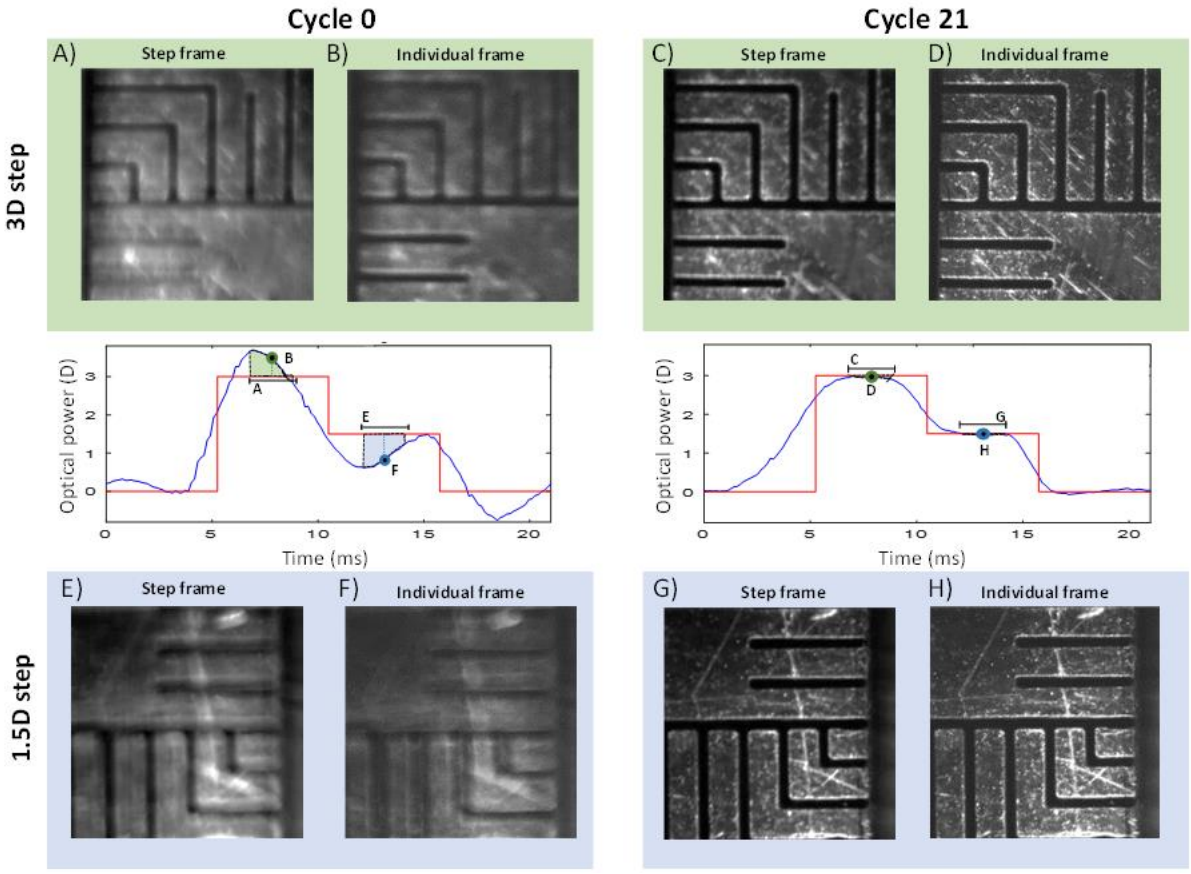

Figure 4.10 *Depth scanning experiment performed on the trifocal profile in lens Optotune AQAA4517. For visualization purposes, all images have been edited: for individual frame images, brightness and contrast were increased by 20%; for step frame images, brightness was increased by 20% and contrast was reduced by the same value.* ***B****,* ***D****,* ***F*** *and* ***H*** *are individual frames taken at the highlighted green and blue dots.* ***A****,* ***C****,* ***E*** *and* ***G*** *are referred to as "step frames" and are built by the sum of various individual frames.* ***A****,* ***B****,* ***E****, and* ***F*** *show the images taken for the case of the initial cycle of the process (cycle 0) when the response has not been optimized.* ***C****,* ***D****,* ***G****, and* ***H*** *show the images taken for the case of the end cycle of the optimization process, when the response has been optimally enhanced. The highlighted regions in green and blue correspond to the 3.00 D and 1.50 D steps, respectively.*

4.3.4. Depth scanning experiment: staircase profile

Figure 4.11 shows the results of the depth scanning experiment implemented in the staircase profile and applied to the two regions, "2.00 D uphill" and "2.00 D downhill" steps, for initial cycle 0 and the end cycle 23 of the iterative algorithm.

Figures 4.11A and B depict the results obtained when taking an individual image at the middle point of the 2.00 D uphill step, both for the non-corrected (cycle 0) and the optimized (end cycle 23) profiles. This instant represents the 2.00 D uphill step, where the non-corrected profile already shows an accurate matching to the target wave. Consequently, it can be observed how Figures 4.11A and B show similar quality images, being both sharp frames, and the structural similarity index metric undergoes only a slight improvement of 0.029 points, from 0.908 (non-corrected – cycle 0) to 0.937 (optimized – 23rd cycle). In the 2.00 D downhill step with individual frames taken at time 13.5 ms (Figures 4.11C and D), the 23-cycle process produces a relevant

improvement in the profile, improving this value from 1.35 D to an optimal matching of 2.02 D. Consequently, Figure 4.11D shows a sharp image where details of the object under study can be observed, whereas figure 4.11C shows a less-focused image. The structural similarity index shows a relevant improvement (0.182 points) in the downhill step, jumping from 0.663 to 0.845.

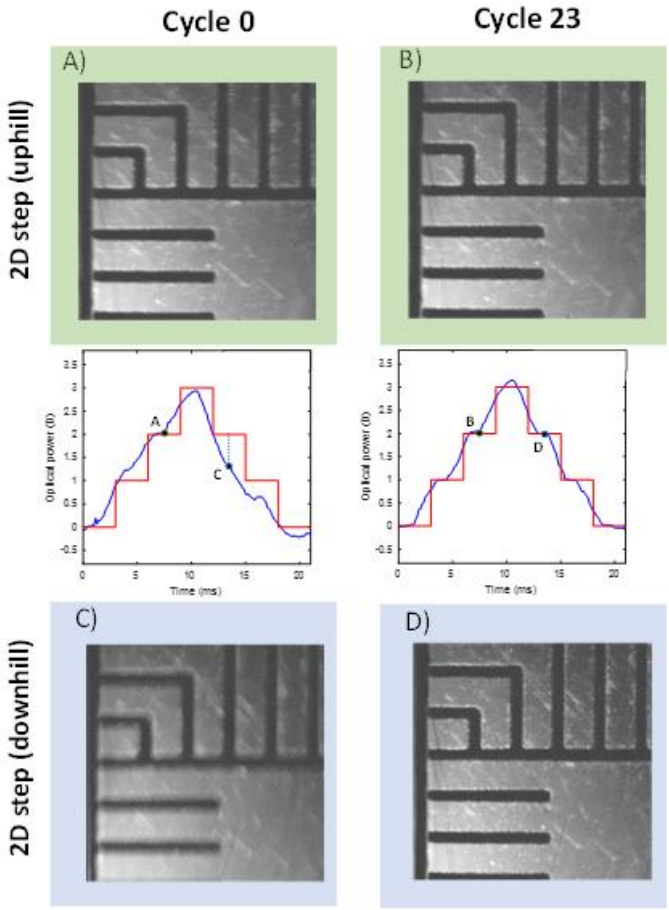

Figure 4.11 *Depth scanning experiment performed on the staircase profile in lens Optotune AQAA4517. For visualization purposes, the brightness and contrast values of the images were increased by 40% and 20%, respectively.* ***A***, ***B***, ***C*** *and* ***D*** *are individual frames taken at the highlighted green and blue dots – A; B (green) and C, D (blue)-.* ***A***, *and* ***C*** *show the images taken for the case of the initial cycle of the process (cycle 0) when the response has not been optimized.* ***B*** *and* ***D*** *show the images taken for the case of the end cycle of the optimization process, when the response has been optimally enhanced. The highlighted regions in blue and green correspond to the 2.00 D downhill and 2.00 D uphill steps, respectively.*

4.4. Discussion

The proposed method for TL characterization and the implementation of the low-cost focimeter has proven to be successful, providing results comparable to those of the high-speed focimeter. But this new system entails less cost and complexity and is more compact and robust. It, therefore, has more potential to evolve into a prototype or instrument that could be present in all kinds of clinical sites, laboratories, or facilities using TLs at high speed.

The optimization experiments have demonstrated the advantages of the method being automatic, granular, and experimental. Being automatic, its potential integration in an industrial procedure is feasible. Automation enables the optimization of the TL response to a given profile

in short periods with virtually no human intervention. The two cases under study took between 21 and 23 cycles, representing 18.4 – 20.1 minutes (a time that can be drastically reduced in future versions of the software). The experimental nature of the optimization, as opposed to the computational approach of previous approaches, makes the procedure easy and accessible. As it does not require previous knowledge on TLs or linear systems control to model and optimize the behavior of the lens, we can consider the approach heuristic, or agnostic. Additionally, the optimization works with less accurate measurement systems, because the impulse response is not needed for the optimization, and the measurement errors are not propagated, but corrected, in subsequent optimization cycles. The granularity contributes to the optimization in just a few cycles, as the method acts exclusively on those regions that empirically deviated from the target wave, leaving unaltered regions behaving correctly. In addition, the algorithm is customizable, and the response of the TL can be adapted to any application.

The implementation of the closed-loop optimization algorithm showed optimal results in the two profiles evaluated. In both cases, the iterative method produced an optimal curve matching between the response and the target wave, in contrast with the curve matching obtained by the raw non-optimized signal. This enhancement in curve matching (and, consequently, in lens performance) was observed empirically and quantitatively: the three monitored metrics improved their values in both profiles. On the one side, the standard deviation metric does not produce relevant insights on the process' performance and can be neglected in the analysis ultimately. On the other side, the two other metrics (area under the error curve and effective time ratio) do reveal critical facts on the algorithm implementation. Especially relevant is the evolution of the effective time ratio metric, which improves in 211% in the case of the trifocal profile (from 0.184 to 0.574) and in 95% in the case of the staircase wave (from 0.258 to 0.503). This fact reveals how the tunable lens's performance is highly stable when the profile has been optimized following the proposed technique.

The optimization of the trifocal profile showed better results than that of the staircase profile. This fact shows how the algorithm produces a better performance when optimizing profiles presenting fewer optical power value changes and longer plateaus. Whereas the trifocal profile is composed of three optical power values, the staircase figure (4.6B) presents six steps, and the algorithm faces barriers when adjusting to the target wave. Despite these limitations, the implementation of the algorithm showed great results. As previously mentioned, the monitored metrics dramatically improve along the process (area under the curve drops around 70% in the case of the trifocal profile and 45% in the staircase wave, whereas the effective time ratio increases 211% in the trifocal profile and 95% in the staircase one).

The depth scanning experiment provides a strong visual illustration of the benefits of the experimental optimization algorithm on the performance of the TL. It confirms that the optimized profile presents a considerably higher stability than the raw one, and an optimal match to the target wave. The visual result was quantitatively corroborated. The SSIM metric improved an average of 92% in the cases under study. The depth scanning experiment also confirmed that

lens optimization was more effective in the case of the trifocal wave than in the staircase profile. Additionally, it showed the potential of this method to be applied in real-life functionalities, being depth scanning of great interest in various science and industry fields such as microscopy.

In summary, a new approach to TL optimization was proposed and demonstrated. The novelty of the proposed method is driven by three main aspects: its automatic, granular and experimental character. To assess the success of this technique, the algorithm was implemented in TL EL-10-30-C AQAAA4517 from Optotune and reproduced in two different profiles (trifocal and staircase). The implementation of this algorithm has shown satisfactory results, as the iterative process produced a relevant enhancement in the TL performance. This enhancement was shown by two aspects. First, the improvement in curve matching between the response and the target wave. Second, the visual evidence provided by the depth scanning experiment. The success of this implementation opens the possibility of applying this technique to TL aiming diverse functionalities.

The low-cost low-speed focimeter presented in this chapter have evolved and the first prototype of the SimVis Gekko Dock was developed (in a collaborative project with the Universidad Autónoma de Madrid). The SimVis Gekko Dock (Figure 4.12) performs automatic and periodic verifications of the SimVis Gekko, checking binocularly the calibration and quality control (see chapter 6) of the TL and lenses simulations.

Figure 4.12 *First prototype of the SimVis Gekko Dock, based on the low-speed low-cost focimeter presented in the current chapter.*

In the following chapter, temperature effects are characterized and a method to compensate for them is proposed.

Chapter 5

Characterization, prediction, and compensation of temperature effects in tunable lenses

In the current chapter, a compilation and analysis of the heating effects that TLs suffers are presented. After their characterization, different experiments were carried out to present a method that corrects the optical power deviations due to the variations in temperature of the TLs in various working conditions.

This Chapter is based on the paper by *Marrakchi et al. "Characterization, prediction, and compensation of temperature effects in tunable lenses" submitted in Optics Express (2021)*. The co-authors of the study are Xoana Barcala, Enrique Gambra, Ivan Martinez-Ibarburu, Lucie Sawides, and Carlos Dorronsoro.

The author of this thesis (1) conceived the ideas along with Carlos Dorronsoro and Lucie Sawides, (2) provided guidance, coordination, and clinical orientation, (3) contributed to the evolution and calibration of the optical setup along with Ivan Martinez, (4) supervised the experimental measurements (Ivan Martinez and Yassine Marrakchi), (5) participated in the data analysis and, (6) contributed to the preparation of the manuscript.

5.1. Introduction

The performance of TLs is critical for the correct functioning of the devices and instruments that rely on them. Their application requirements include stability over time, and speed to shift from a focus state to another, especially in rapid scanning applications [124] and temporal multiplexing [120]. But more important are the precision and accuracy that they have to achieve in terms of optical power, and the robustness against modifications of the internal or external environment conditions as temperature. Some specific lenses exploit the property of dielectric liquids to expand with an increase of temperature [167]. However, for most TLs available internal or external temperature changes represent an unresolved issue inducing important instabilities and reducing the precision of the optical power delivered by the lens [131]. Driving a lens at medium or high currents, or due to absorption of high-power laser light, produce heating of the internal temperature [163]. These deviations are important and often not linear with the change in the temperature. As an example, in the lens model under study in this article (10-30-C; Optotune AG, Switzerland), according to the specifications of the manufacturer, the optical power increases in average 0.07 D each 1º C increment on temperature [163], when the temperature is around 25º C. Commercial lens manufacturers have developed some hardware strategies to decrease the magnitude of the deviations, but they are limited to small dioptric ranges [168,169]. On the other hand, software compensation based on characterization of individual lenses at different temperatures and interpolation, require specific drivers and therefore have limited options in the design of the corrections.

This chapter presents an analysis, characterization of a method to correct the optical power deviations due to the variations in temperature of the TLs in various working conditions. Thus, providing enough evidence about the feasibility and advantages of correcting thermal effects in liquid lenses.

5.2. Methods

Static power variations, hysteresis measurements, random optical power variations and dynamic states experiments were carried out to obtain a full characterization of temperature effect on TLs. A custom electronic driver of the lens was developed to perform those experiments. A low-cost low-speed version of a focimetry system (presented in chapter 4) was used to accurately measure the transient optical power of the TL s during the temperature changes.

5.2.1. High-speed tunable lens driver and temperature registering

In chapter 3, a custom high-speed driver for TLs was specifically developed for temporal multiplexing applications, and it is also used for the experiments presented in this chapter. The TL is driven with a voltage pulse width modulation (PWM) signal at 32kHz to achieve high temporal accuracy for generating fast dynamic optical power profiles (in the order of milliseconds; ms). It can also work in a dual channel, with synchronization for binocular

applications. The amplitude of the PWM voltage signal ranges from 0V to 5V and is specified in digital counts that go from 0 to 255 (an 8-bit timer is used to generate the signal). The 'digital counts' notation is used in the calibration of the lens and during the experiments. The custom driver fulfills all the compatibility requirements of the TL model used in this study (see section 5.2.4). Also, it uses the temperature sensor included (SE97B) to register internal temperature data with 0.125 ºC resolution. The firmware is configured to retrieve the internal temperature of the TLs each half-second using the I2C protocol. The control interface is developed in Matlab (Mathworks, Natick, MA) and can drive the tunable lens in different modes and display its internal temperature as well as some flow monitoring messages.

5.2.2. Samples and specifications

The experiments in this study were carried out using 2 custom units of EL-10-30-C tunable lens model from Optotune AG (Switzerland). The optical power ranges from 5 to 12 D. According to the technical specifications of the TL model [163], internal temperature variations have two effects: when heating up, first the refractive index of the fluid decreases, producing a decrease in optical power. Second, the internal fluid of the lens expands in volume ending up in an increase of the optical power. The second effect prevails and the resulting increase in optical power has been evaluated to be approximately 0.7 D for a 10ºC temperature increase. Also, according to the TL manufacturer, the sensitivity in optical power to temperature changes along the dioptric range. The sensitivity is higher (around 10 %) when the lens is driven at low currents, and lower when the lens is driven close to its higher current limit. The study was performed using one specific lens model, but the methods and strategies we are presenting can be applied to other TLs that have similar working principles and suffer from temperature variation effects.

5.2.3. Measurement system

To estimate the TL's optical power, we used the custom optical low-cost focimeter presented in the previous chapter 4. The images are processed using custom Matlab routines, applying the results of a calibration performed a-priori (see 2.4). The TL is mounted in an optical module that reduces the offset optical power of the lens by 6 D to bring the minimum power close to 0 D. Also, it makes the system more compact, encapsulating the sample lens in a plastic case that will retain heat, simulating the use of the TL in real world applications.

5.2.4. Calibration of the measurement system and driver

The characterization of the system is done in two steps: First, we obtain a direct relationship between the lateral displacement of the stimulus image (in pixels) and the optical power (in diopters, D), by using trial lenses at a secondary pupil plane optically conjugated to the TL under study. Positive and negative power lenses induce known values of optical power covering the whole dioptric range of the sample TL. The result of this calibration is a linear equation plotted in Figure 5.1 (a) where the zero-diopter point corresponds to the position of the reference slit

when the sample lens is at idle state (no current). This calibration is used to process every measurement performed in the system.

Once the measurement system is calibrated, we calibrate the driver and TL set without any trial lens in the system. This way, we estimate the optical range of the lens and the relationship between the voltage applied to the lens and the optical power it provides (from 0 to 160 counts). To obtain robust results, we maintain the internal temperature of the TL stable during the whole process, by including a rest time of 20 seconds between each measurement. The mean internal temperature is registered since it is part of the calibration parameters. At this point, we have a relation between voltage applied to the lens (in digital counts) and the position of the stimulus (in pixels). Finally, making use of the previous characterization of the measurement system, we can obtain the relation between the optical power in diopters and the voltage applied to the lens as illustrated Figure 5.1 (b).

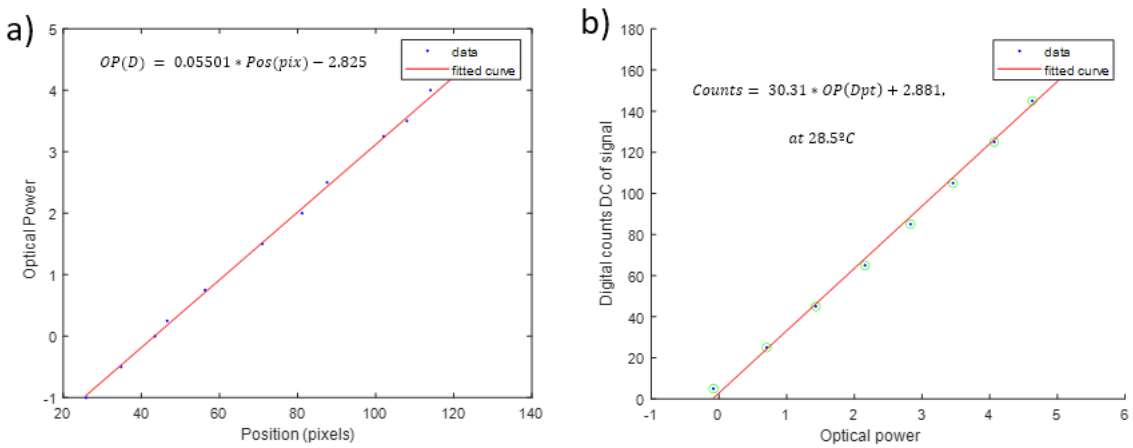

Figure 5.1 *Examples result of a calibration of the measurement system (**a**) and the driver (**b**).*

5.2.5. Experiments to characterize the effect of the TL temperature

We performed four experiments to characterize the effect of the variations in internal temperature on the optical power of the TL, in the complete range of optical power and in different situations, and to guide, adjust, and evaluate the compensation strategies introduced in section 5.2.6.

A. Static experiment

In this first experiment the lens was driven with a predefined voltage signal for 40 minutes and then with a home value (corresponding to 1 D) for other 40 minutes. Nine predefined voltage signals were measured, corresponding to optical powers 1.50 to 5.00 D, in 0.50 D steps. The whole experiment took 12 hours per lens, providing a complete and precise characterization of the temperature variations and the lens behavior during heating and cooling. The results of this experiment were used to adjust the mathematical models guiding the compensation of temperature effects, described in section 5.2.6.

B. Hysteresis experiment

In this second experiment, the TL input was a stair of states (digital counts), starting from 30 counts and ending at 180 counts in steps of 10, then a descending from 180 to 30, to close the cycle. Each state was driven during 30 seconds in which the temperature and optical power are registered every 0.5 seconds. Each cycle was repeated 5 times, to test the hysteresis of the TL.

C. Random experiment

To perform the third experiment, an array of 1000 randomly ordered optical counts, corresponding to optical powers in between 1.00 and 5.00 D (in steps of 0.50 D) was created according to the initial calibration. Each power state was maintained for 5 seconds while the temperature was registered.

D. Dynamic states experiment and step response

In some applications, as in temporal multiplexing for the simulations of multifocal corrections, or in-depth sectioning of a volume, it is necessary change the optical power of the TL every few milliseconds, with abrupt transitions. The dynamic behavior of the lens is critical, as well as the drift induced by temperature variations.

In the first part of this last experiment, we programmed a bifocal simulation (a bistate wave of nominal optical shifting between 1.00 and 4.00 D every 10 ms), run it for 40 minutes while the internal temperature changes were registered, and compared to a monofocal simulation (a stable state).

The second part of this fourth experiment consisted in measuring with a high-speed camera(see chapter 3), at three internal temperatures (21, 27 and 33 ºC) that are expected to be reached during operation of the lens at room temperature: 1) the step response describing the dynamic behavior of the TL; and 2) a complex multifocal pattern simulation very sensitive to the shape of the step response [113]. The multifocal simulation is very similar to the bifocal simulation but have different additions or optical power coefficients and the electrical signal is optimized to compensate the transient response of the lens measured at 21ºC [132]. The performance of the TL simulation at different temperatures was evaluated in terms of the through-focus Visual Strehl ratio (TFVS), and compared with the real physical lens simulated [170].

5.2.6. Compensation strategies and mathematical models

Besides to evaluate the stability of the lens in time, we used the long heating and cooling cycles of alternating static power (section 5.2.5.A) to obtain mathematical models of the behavior of the TL in a 3-dimensional (3D) space of optical power, internal temperature, and electrical signal. The models were used to guide strategies to characterize, predict, and compensate the effect of temperature. We tested many non-linear equations, that were evaluated considering the

goodness of the fit to the experimental data. Three models were finally developed and are referred to as the optimized, the polynomial and the experimental.

Once the model equations were fitted, the compensation strategy was implemented in the TL driver by storing the equation in the memory of the microcontroller. The algorithm developed, checks the temperature every 0.5 seconds. Each time the temperature increases or decreases 1ºC or more, the voltage driving the lens is recalculated according to the equation and applied to compensate the temperature effects. The temporal sampling period was chosen to correctly trace the temperature variations without overcharging the microcontroller. The temperature variation limit was set considering the resolution of the timer (8 bits) generating the PWM voltage signal, to avoid unnecessary calculations providing variations below the rounding threshold.

It is important to mention that the manufacturer have developed a custom method to compensate the temperature effects [163]. It is based on an interpolation algorithm that makes use of an internally stored calibration of the lens' optical power versus current at two temperatures (20ºC and 50ºC). The results are very good but requires using a specific current driver that limits the design possibilities. For example, driving the lens with a voltage signal, binocular applications, or the need of using the TL integrated in an optical system requiring a specific characterization.

5.2.7. Prediction of temperature variations

In case it is not possible to access the internal temperature sensor of the TL, we developed an equation that can be used to predict the temperature variation due to driving the lens considering the ambient temperature. In section 5.3.1.A the equation is described based on the results obtained from the characterization experiments. To show the application of this principle and test the accuracy of the equation, it is applied on the hysteresis (Figure 5.7 (a)) and random (Figure 5.7 (c)) experiments.

5.3. Results

5.3.1. Mathematical Models

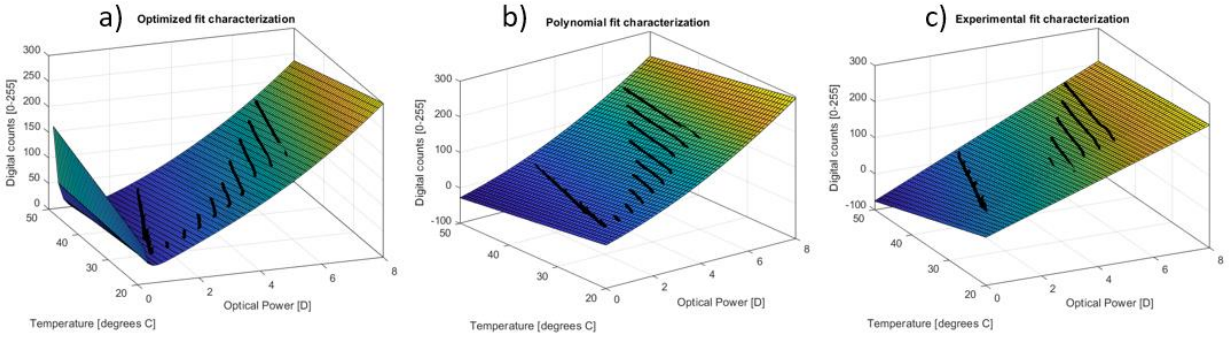

Figure 5.2 *Graphical representation of the 3D fitting models tested as a compensation method for temperature effects on the tunable lens. Optimized model (**a**), Polynomial model (**b**) and experimental equation model (**c**).*

Figure 5.2 shows the graphical representation of the three models developed.

A. Optimized model

The optimized model, providing the best results, follows with equation:

$$Counts(x,y) = A + B*x + C*x^2 + D*y + E*\frac{y}{x} + F*\sqrt{x}, \qquad (5.1)$$

where *x* corresponds to optical power in diopters (D) and *y* corresponds to the temperature of the lens in degrees (ºC). The 3D curve representation is illustrated in Figure 5.2.A. The coefficients providing the best fit were: *A* = -23.76, *B* = -19.23, *C* = 3.338, *D* = -2.265, *E* = 0.8523 and *F* = 108.9.

To compare the models, three different standard indicators evaluating the goodness of the fitting were used: Sum of squared estimate of errors (SSE), Coefficient of determination (R-square) and Root mean square error (RMSE). For the Optimized model we got SSE 5.167 $\times 10^4$, R-square 0.9997, and RMSE 0.7943.

B. Polynomial model

The polynomial model, illustrated in Figure 5.2.B, followed a second-order polynomial equation in optical power and a first-order polynomial in temperature, with a first-order cross term:

$$Counts(x,y) = A + B*x + C*y + D*x^2 + E*x*y, \qquad (5.2)$$

where *x* corresponds to optical power in D and *y* refers to the temperature of the lens in ºC. The coefficients obtained were: *A* = 55.99, *B* = 20.1, *C* = -1.676, *D* =1.904 and *E*= -0.06397, and the goodness parameters SSE 6.921 $\times 10^4$, R-square 0.9996 and RMSE 0.9193. If added, other polynomial terms result in non-relevant coefficients (<10-5), inducing confusing dependencies without improving the goodness of the fit.

Even though the polynomial model provided worse fit indicators, it also resulted in a better representation at low optical powers. While the polynomial model represents near 0 D values with a lower electrical signal, the optimized model equation diverges near 0 due to the $\frac{y}{x}$ coefficient.

C. Experimental model

The first two strategies of compensation (optimized and polynomial) can be used as a characterization procedure for a given lens in laboratory. However, they represent important practical limitations if extended to the compensation of thermal effects in any lens: the calibration is slow (it takes over 12 hours to complete); the implementation is costly in memory for simple microcontrollers; and the performance is not robust against small variations in the behavior of the lenses. Therefore, one characterization is not expected to work for all the lenses without additional modifications in the model.

The model describing the experimental method is based on the simple calibration of the driver presented in section 5.2.4: a linear equation relating optical power and voltage, obtained at a reference temperature. To compensate the effects of temperature, two components were added in the equation. The first one, *C*, is a fixed coefficient that introduces a linear dependence with the temperature increment, and the second one, *D*, introduces a cross term between temperature increment and target optical power. The resulting equation is the following:

$$Counts(x,y) = A + B * x - (y - T_C) * (C + D * (1 - (x+1)/x_{max})), \quad (5.3)$$

where *x* corresponds to optical power in D, *y* refers to the actual temperature of the lens in ºC, T_C is the reference temperature at which the calibration was performed and x_{max} is the maximum value of optical power of the lens. The coefficients *A* and *B* are defined by the calibration, in this case, *A* = 2.88 and *B* = 30.31. The compensation coefficients were optimized considering the electrical driver resolution and the smallest variation in temperature producing a noticeable deviation in optical power, resulting in optimal values C = 0.5 and D = 1.5. This model provides a SSE 2.234 ×10^6, a R-square 0.9878 and a RMSE of 5.223.

5.3.2. Static experiment

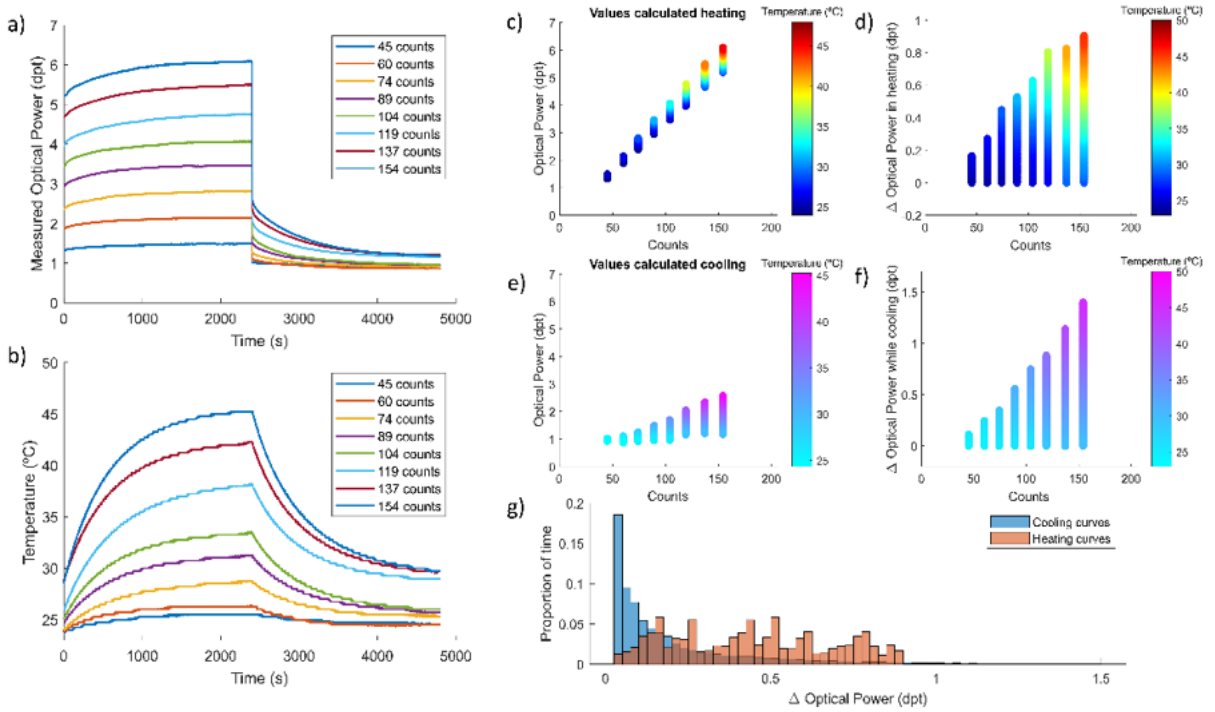

Figure 5.3 *Characterization of temperature effect in a TL during long static states of different optical power. (**a**) Graphical description of the static experiment showing the optical power variation with time due to temperature variation. (**b**) Profile of the lens internal temperature during the experiment with different voltage driving signals. Measured optical power of the lens while heating (**c**) with different driving signals and cooling (**e**) at rest state. Estimated deviation, calculated from the difference between the initial point and measured optical power in the heating (**d**) and cooling (**f**) processes. (**g**) Histogram of optical power deviation while heating (red) and cooling (blue) to show the proportion of time the lens diverges a certain magnitude.*

Figure 5.3 illustrates the results of the characterization of the temperature effect in the TL. We can see in Figure 5.3(a) that as we increase the current flowing through the lens, the optical power is higher and the variation due to temperature is more noticeable. Moreover, as can be observed in Figure 5.3(b), the temperature increases faster and reaches a higher stability point, when the driving signal is higher. This happens in the first situation, which is the heating curve. In this phase, the temperature increases gradually starting from an initial point that depends on the ambient temperature and the previous state of the TL in the last few minutes before the experiment starts.

From the results obtained in the static experiment, we can derive the equation to predict the temperature variations due to driving the lens. The heating process of the TL when driving it at a specific voltage signal can be well described with the following equation 5.4:

$$\mathrm{T}(\mathrm{t}, \mathrm{T}_{env}, \mathrm{x}) = \mathrm{T}_0 + ((Ax + Bx^2) + \mathrm{T}_{env} - \mathrm{T}_0) * (1 - e^{-t/C}) \quad (5.4)$$

Where T is the internal temperature of the lens at a certain time, T_{env} is the environment temperature, T_0 is the initial temperature (which can correspond to the environment temperature or any else if the lens has been driven before) and t refers to the time (in seconds). A = 0.02357 and B = 0.0005752 are constants that define the maximum temperature that the lens can reach depending on the magnitude of the driving signal x. Finally, the C = 560 constant corresponds to the decay constant of the exponential function and describes the speed at which the temperature reaches the plateau. The deviations magnitude during the heating is presented in Figure 5.3(c) and (d) and have a maximum of 1.00 D.

The internal cooling of the lens can be approximated by the same exponential decay equation, similar to the discharge of a capacitor. The sign of the exponential factor is defined by the $((Ax + Bx^2) + \mathrm{T}_{env} - \mathrm{T}_0)$ multiplying term. In Figures 5.3(e) and 5.3(f), the effect of the cooling process on the optical power of the lens is described. In this case, the variations are evaluated when the lens is driven to a home state. We can observe that the fluctuations due to temperature have a different magnitude in the top and the bottom part of the optical range. During the cooling process the maximum deviation reaches 1.60 D. Each time, a different electrical signal is applied to the TL, the previous equation represents the expected temperature evolution of the lens depending on the signal applied to the lens the ambient temperature. Therefore, in case it is not possible to access the internal temperature sensor of the TL, this equation can be used to predict the temperature variation due to driving the lens. To show the application of this principle and test the accuracy of the equation, it is applied on the hysteresis (Fig. 5.7(a)) and random (Fig. 5.7(c)) experiments.

In Figure 5.4, we present the results obtained in the same experiment but using the optimized fit model correction. We can observe that although the temperature increases with time Figure 5.4(b), the optical power is compensated by adjusting the electrical signal driving the TL. If we observe the curves of Figure 5.4(a), we can see a sawtooth pattern that represents the small

correction steps performed each time a variation in temperature of 0.5ºC is detected and the recalculation is performed by the software.

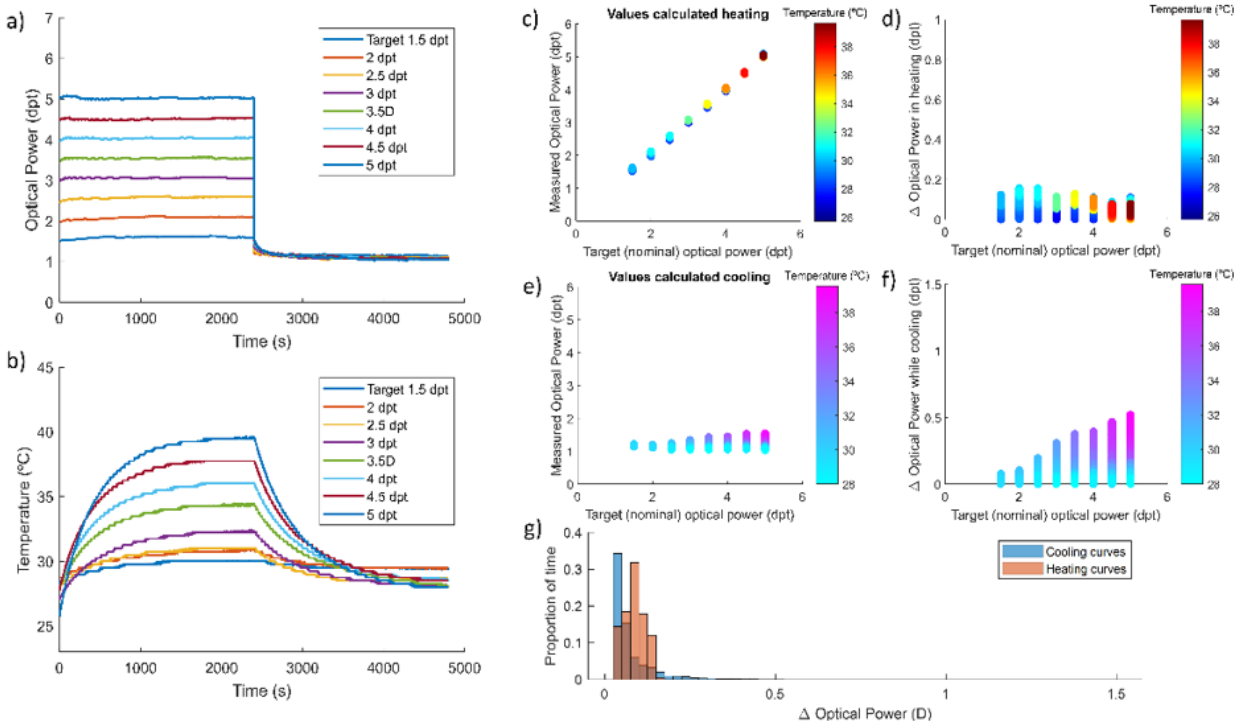

Figure 5.4 *Optimized model compensation of temperature effect in a TL during long static states of different optical power. (**a**) Graphical description of the result of compensation strategy showing the optical power stabilization in time. (**b**) Internal temperature profile of the lens during the experiment with different target power states. Measured optical power of the lens while heating (**c**) with different driving signals and cooling (**e**) at rest state. Estimated deviation, calculated from the difference between target power and measured optical power in the heating (**d**) and cooling (**f**) processes. (**g**) Histogram of optical power deviation while heating (red) and cooling (blue).*

The plots showing the deviation between the target optical power and the measured one also show a great performance of the correction procedure in the heating process of the lens (less than 0.20 D deviation against 1.00 D deviation for non-corrected measurements). Concerning the cooling curves, the deviations are more important but if we observe the transition to a home state in Figure 5.4(a) and the histogram in Figure 5.4(g) this only happens at the first few seconds after the lens is returned to the rest state. In any case, the deviation magnitudes remain smaller than for the non-corrected experiment (maximum value of 0.50 D against 1.60 D).

The next results, Fig. 5.5 correspond to the polynomial equation fit. In this case, the home power corresponds to 0.00 D instead of 1.00 D since the equation covers a wider range, and it is interesting to increase the demand for the lens. In this case, the correction works a little bit worse than in the optimized fit model on the heating curves. The maximum value is around 0.25 D against 0.20 D for the optimized fit and 1.00 D for non-corrected. Also, in the first part of the cooling curves, Figure 5.5(a), an important deviation is observed. It is evaluated quantitatively in Figure 5.5(f) with a maximum of 0.90 D but in the histogram Figure 5.5(g) is shown that this deviation occurs in a small proportion of time corresponding to the optical power step down.

This could be explained by the fact that the home power state (the position in which the lens cools) is closer to 0.00 D and is lower than in the previous model. Values around zero give less range in the correction since when we reach the minimum electrical signal we can generate; we cannot compensate further.

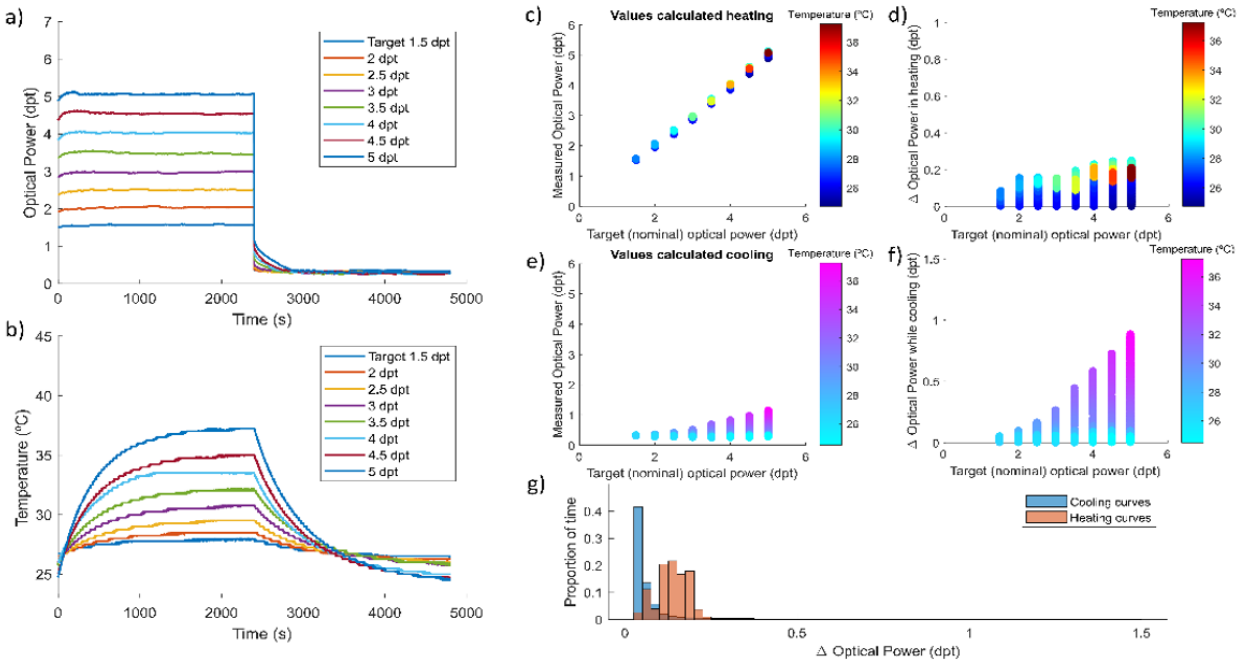

Figure 5.5 *Polynomial model compensation of temperature effect in a TL during long static states of different optical power. (**a**) Graphical description of the result of compensation strategy showing the optical power stabilization in time. (**b**) Internal temperature profile of the lens during the experiment with different target power states. Measured optical power of the lens while heating (**c**) with different driving signals and cooling (**e**) at rest state. Estimated deviation calculated from the difference between target power and measured optical power in the heating (**d**) and cooling (**f**) processes. (**g**) Histogram of optical power deviation while heating (red) and cooling (blue).*

The last correction method is the experimental. In the temperature curve, Figure 5.6(a), we can see that some of the measurements start at different initial temperatures. The results of the deviations are very good for the experimental method. Less than 0.18 D in maximum amplitude deviation in the heating process and less 0.35 D in the cooling process.

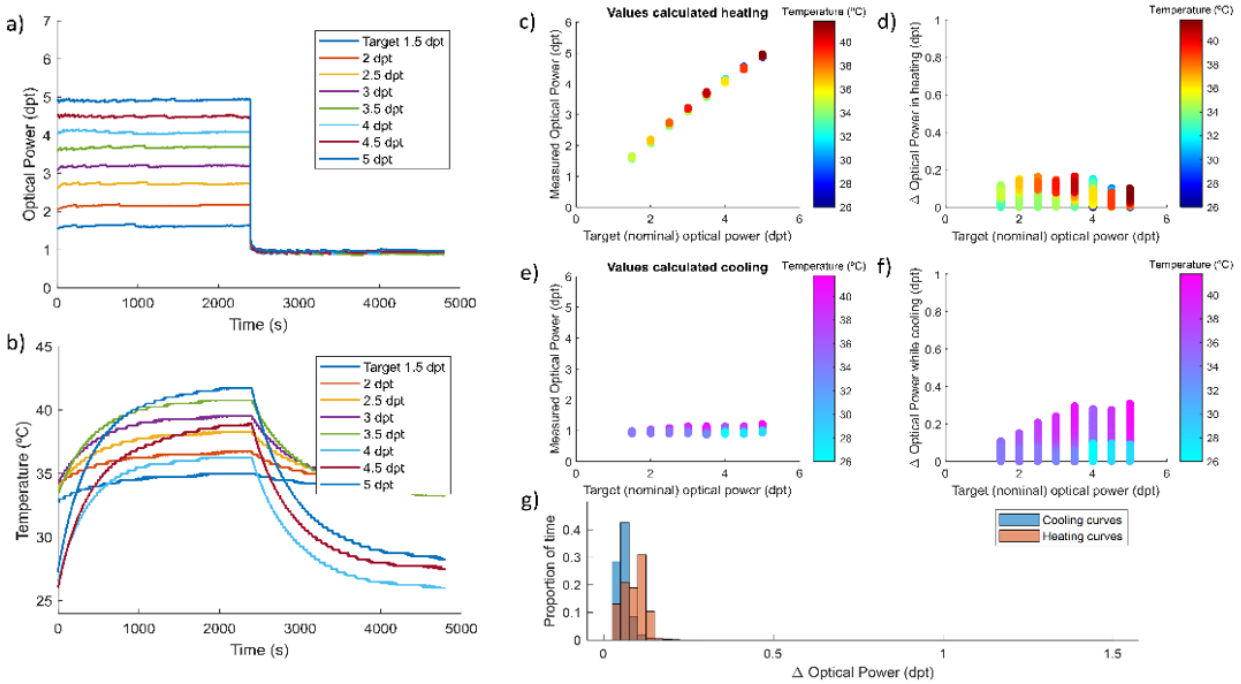

Figure 5.6 *Experimental model compensation of temperature effect in a TL during long static states of different optical power. (**a**) Graphical description of the result of compensation strategy showing the optical power stabilization in time. (**b**) Internal temperature profile of the lens during the experiment with different target power states. Measured optical power of the lens while heating (**c**) with different driving signals and cooling (**e**) at rest state. Estimated deviation calculated from the difference between target power and measured optical power in the heating (**d**) and cooling (**f**) processes. (**g**) Histogram of optical power deviation while heating (red) and cooling (blue).*

To verify the results obtained in the previous experiments and as a repeatability test was performed with a second TL of the same model. The characterization procedure was not performed again since the objective was to test if the correction methods could be directly applied to other lenses in a production environment or some adjustments must be done. In this case, only the polynomial equation and experimental model were used. The results are presented in Table 5.1.

Correction method	Maximum ΔTP heating	Maximum ΔTP cooling
No correction	1.00	1.60
Optimized fit	0.16	0.50
Polynomial fit	0.25	0.90
(2 lenses)	0.12	0.70
Experimental correction	0.18	0.35
(2 lenses)	0.27	0.45

Table 5.1 *Summary results of optical power deviation for the three models and repetition measurements.*

When testing the method in the second lens, we observed that the compensations work well. The only difference is that target values are not reached precisely in all the states. This is due to a different offset of the TL. Nevertheless, the temperature effect seems to be very similar for different samples of the same TL mode. This points out an advantage in the experimental method because the calibration procedure is faster (does not need a full characterization) and could be done for each lens to adjust offset variations.

5.3.3. Hysteresis experiment

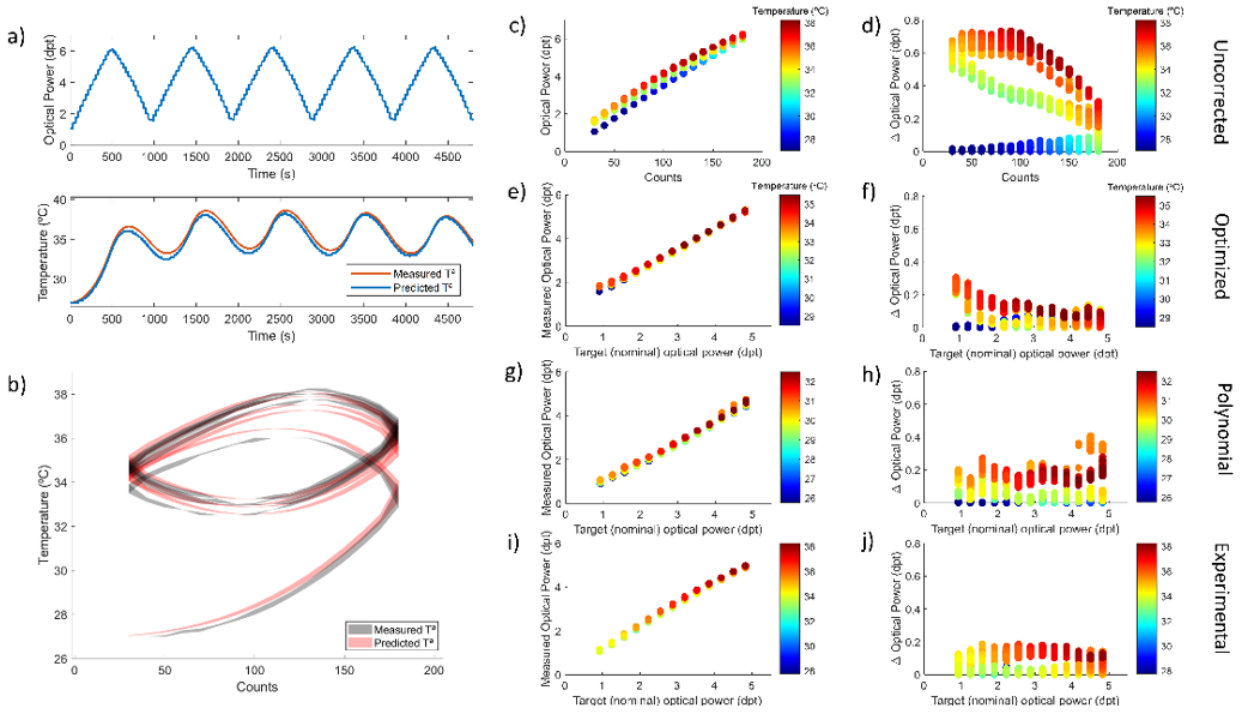

Figure 5.7 *Hysteresis experiment description and performance of the three compensation methods used to correct temperature effect. (**a**) Optical power and temperature profile of the lens during a hysteresis experiment. (**b**) Internal temperature variation and stability region. (**c**) Optical power measured values and deviations concerning nominal value in characterization measurement (**c**, **d**), optimized model compensation (**e**, **f**), polynomial model compensation (g, h), and experimental model compensation (**i**, **h**).*

Figures 5.7(a) and (b) are intended to explain graphically the experiment. The pattern of optical power states and the temperature profile can be observed. It is interesting to see how the temperature increases when the lens is driven at a higher current and decreases when driven at lower currents reaching a stability range that is several degrees higher than the initial ambient temperature. Figures 5.7(c) and (d) are represented the optical power deviations due to differences in the internal temperature of the lens when no compensation method is applied. These are the reference values with a maximum deviation of 0.80 D and an important dispersion. The next graphs of Figure 5.7 are results of the application of the three correction models: optimized fit (e, f), polynomial fit (g, h), and experimental equation (i, j). If we analyze the graphs from Figure 5.7, we can make the following statements:

The optimized fit model seems to be very precise (less than 0.35 D deviation) but has some problems in the lower powers near the origin, due to the nature of the equation model. The polynomial equation seems to be a little bit less precise (less than 0.45 D), especially at higher temperatures and optical power values. However, it does not suffer from distortions around 0.00 D. Both models require a long characterization process, unlike the experimental compensation. The experimental model works also very well in hysteresis conditions, with a deviation smaller than 0.20 D. Also, the residuals do not follow a pattern and are quite homogeneous across the optical range of the lens.

5.3.4. Random experiment

Figures 5.8(a), (b), and (c) illustrates the purpose of the random experiment: (a) shows the optical power measurements for randomly ordered prefixed points when no compensation is applied; (b) shows the same phenomena but with the polynomial compensation applied as an example to illustrate the working principle. If we compare both figures, we can see that the optical power points that correspond to the same driving signal are more stable when the correction is applied and that the distortion due to changes in temperature, Figure 5.8(c), are less noticeable.

In figures 5.8(d) and (e) the optical power deviation is represented due to differences in the internal temperature of the lens when characterization is intended, no correction method is applied. These are the reference values with a maximum deviation of 1 D and an important dispersion. The next graphs are results of the three correction models: optimized fit (f, g), polynomial fit (h, i), and experimental equation (j, k). The results of the three compensation methods are similar to the ones obtained in the hysteresis experiments and the same conclusions could be extracted: Optimized fit suffers from distortions in low power states. Polynomial is robust and covers a wide range but may have less precision. Finally, experimental show small deviations in the calibration, that can be improved easily, but is more practical for mass characterization and has a robust compensation of the effect of temperature in the whole range of optical power of the TL.

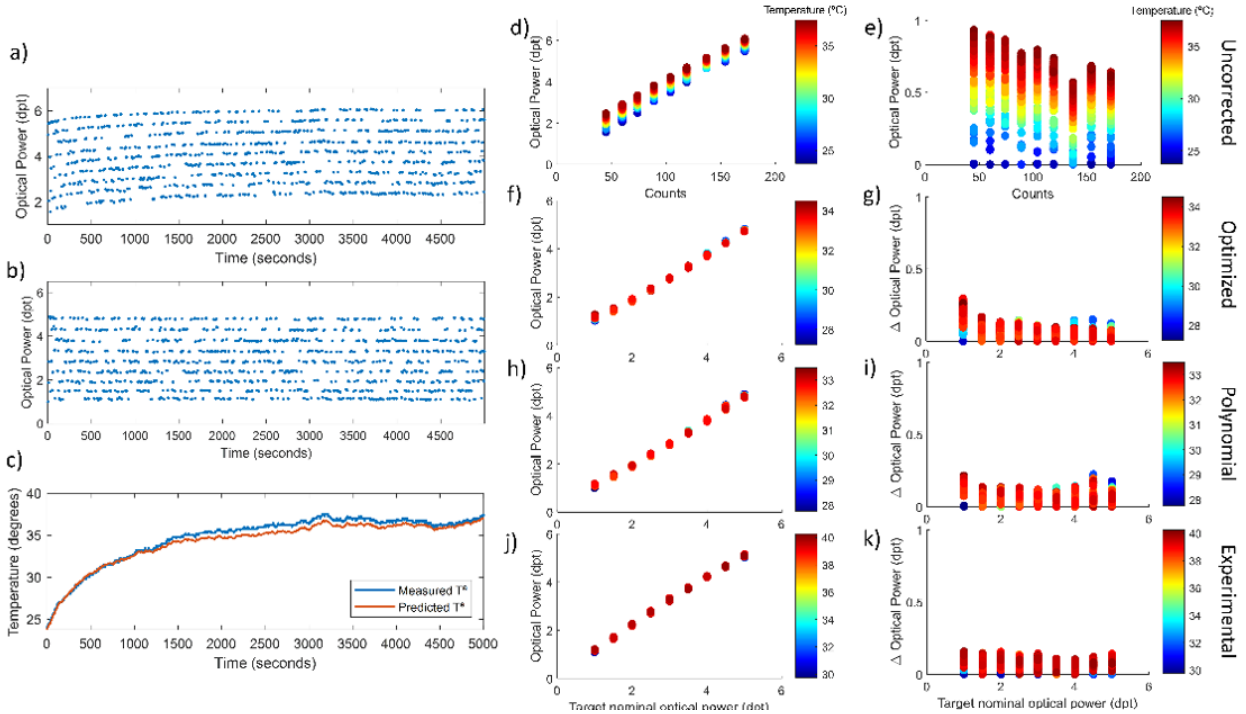

Figure 5.8 *Random experiment description and performance of the three compensation methods used to correct temperature effect. Optical power and temperature profile of the lens during a random sequence of power states for characterization without compensation strategy (**a**) and with the polynomial correction as an example (**b**). Internal temperature variation and stability region. (**c**) Optical power measured values and deviations concerning nominal value in characterization measurement (**c**, **d**), optimized model compensation (**e**, **f**), polynomial model compensation (**g**, **h**), and experimental model compensation (**i**, **h**).*

5.3.5. Dynamic experiment

When driving the lens in a dynamic situation, we may expect the internal temperature of the lens to increase further since there is more movement in the liquid and the membrane forming the lens. In the results presented in Figure 5.9(a) (yellow), the lens is shifted from a 1.00 D state during 10 ms to a 4.00 D state during another 10 ms. Since the speed of variation of the optical power of the lens is faster than the minimum capture period of the camera, it is not possible to register the whole path of the lens. Instead, we are capturing random points that can be used to observe a sample of the optical power points that the lens has gone over. The increase in temperature when using this signal to drive the lens, Figure 5.9(b) (yellow) is compared to when the lens is driven with the static optical power states: 1.00 D (blue) and 4.00 D (orange). The bifocal simulation generates an increase in the internal temperature of the lens that is almost equivalent to driving the lens in a static power state corresponding to the weighted mean of the states forming the bifocal simulation. These results confirm that the internal temperature of the lens is not affected by driving the lens dynamically or statically but by the total amount of current flowing through it.

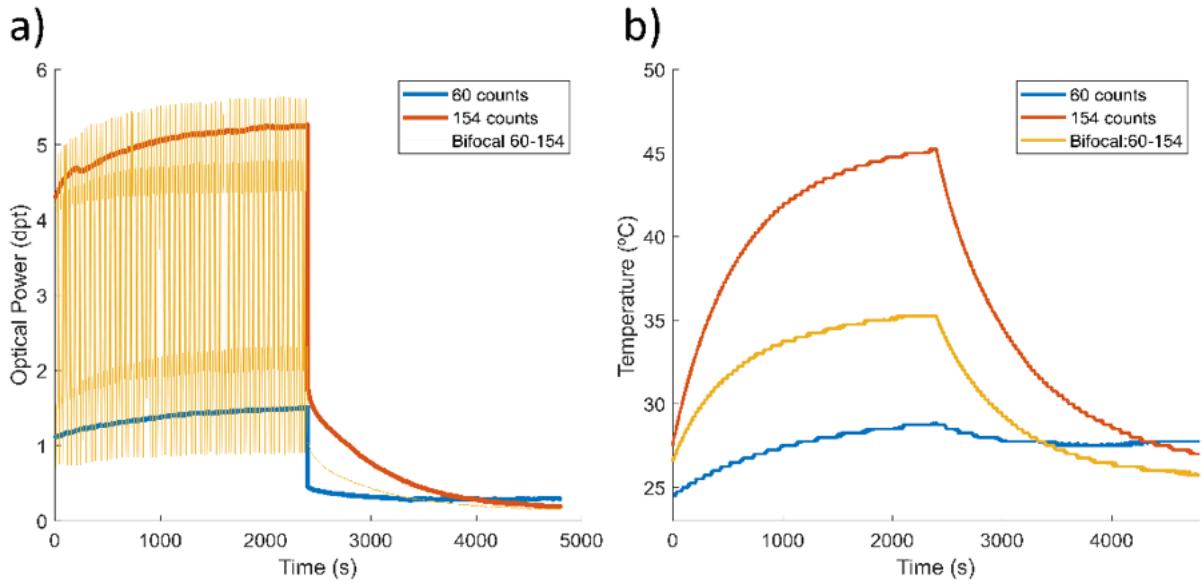

Figure 5.9 *Dynamic experiment description. (**a**) Optical power profile of a static state of 154 counts (orange), a low static state of 60 counts (blue), and a bifocal driving signal (yellow) comprising both states. (**b**) Lens internal temperature profile for each signal.*

Regarding the dynamic behavior of the TLs, the second part of the experiment was to measure the step response at different temperatures. In Fig. 5.10(a) the results are illustrated. From an overview, the magnitude of the distortions in the transient response seems to increase. The overshoot increases with the internal temperature of the TL. At 21ºC the overshoot has a value of around 25 %, while at 33ºC the value increases to 50 %. Also, the settling time is greater at higher temperatures going from 10 ms at 21ºC to around 15 ms at 33ºC. To analyze the consequences of the variations in the transient response of the TL due to temperature, a multifocal pattern simulation was measured with internal temperatures of 21ºC, 27ºC, and 33ºC.

Fig. 5.10(b), (c), and (d) represent the results of this simulation in the TFVS metric without applying any compensation strategy. We can observe that as temperature increases, the defocus profile is shifted to higher optical power values showing a deviation comparable to the one observed in the characterization of the TL in static experiments. A maximum of 0.40 D deviation at 27ºC and 0.80 D at 33ºC. In Fig. 5.10(e), (f), and (g) the same simulation is measured but, in this case, the experimental compensation strategy is applied to quantify the performance in fast dynamic situations. Much better accuracy on the simulations is observed. The shift due to temperature increase and consequently the internal fluid expansion is compensated. However, there is a difference in the shape of the TFVS profile.

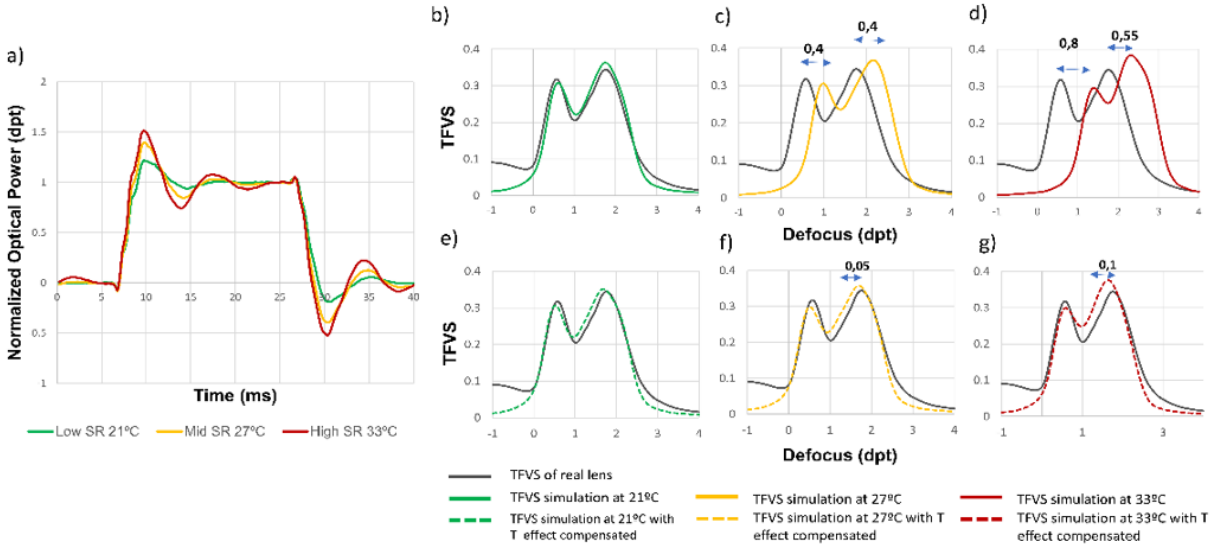

Figure 5.10 *Characterization of TL dynamic behavior at different temperatures. (**a**) Step response measurement of the TL at 3 temperatures 21ºC, 27ºC, and 33ºC. TFVS ratio of the simulation of a multifocal lens design at (**b**) 21 ºC (**c**) 27 ºC and (**d**) 33ºC. The same simulations are performed applying the experimental correction to compensate for the deviation in optical power due to temperature (**e**) 21 ºC, (**f**) 27 ºC, and (**g**) 33ºC.*

5.4. Discussion

As the initial hypothesis suggested, the variations in the internal temperature of the TLs can considerably affect their performance and stability. The main purpose of the experiments carried out was to characterize these phenomena and try different methods to attempt to correct them and improve the precision of the lenses.

Concerning the characterization procedure, the following statements summarize the results obtained: (1) The internal temperature of the lens depends on the ambient temperature and the previous simulations/signals in the previous minutes. (2) The temperature of the lenses increases when driving the lens at medium/high currents. At an initial temperature of around 25ºC, the lens can reach a temperature higher than 45ºC. This can suppose almost 1.5 D in the deviation of the TL. This deviation is due to the expansion of the internal fluid that make possible their unique working principle. (3) Temperature affects more the low power states or when the electrical driving signal is lower. That is, the magnitude of the deviations is higher at the lower

part of the optical range. (4) During a multifocal simulation (fast dynamic driving), the temperature increases in a similar way than when driving the lens in a static power state that corresponds to the weighted mean of the different states covered in the multifocal simulation. (5) Also, about the dynamic operation of the TL, unexpectedly, the temporal distortions of the transient response increase as the internal temperature of the lens increases. This phenomenon can be explained by the fluid nature of these TLs. It could be that unlike what happens with the fluid volume, the viscosity of the liquid seems to be lower as the temperature increases. In this way, the fluid and consequently the membrane movements are amplified generating additional temporal distortions. Still this effect is only noticeable in fast applications.

When the temperature correction strategies are applied, the internal temperature of the lens reaches on average lower values since the current is reduced to compensate the effect of the temperature. This can be explained by the fact that as temperature increases, the optical power delivered by the TL is bigger. However, when the compensation is applied, the lens requires less current to achieve the target power states. Since the temperature increase depends directly on the applied current, the overall increase in temperature is lower.

All the compensation methods described (optimized, polynomial and experimental fitting) provide an improvement in the performance of the lenses. The polynomial equation gives a little worse result in some experiments/conditions than the optimized fit. However, it describes better the behavior of the lens in the complete optical range, especially near 0.00 D. The experimental method gives similar results and even better in some conditions. This is encouraging since it is not necessary to do a complete characterization of the lens to obtain a good calibration. The only drawback for the experimental method is some deviation in reaching the target nominal power values showing a curvature in the relation between measured power against target nominal power in Fig.5.8 (i). This can be explained by the fact that the calibration in this method was performed with the hypothesis that the relation between optical power delivered by the TL and the value of voltage of the driving signal is linear. However, after analyzing the results of the different experiments, a second order term would improve the calibration.

In some temperature curves (see Fig.5.6 (a) for example), we can see that some of the measurements start at different initial temperature. This is because the ambient temperature varies during the 24 hours of a day and the measurements require more than 12h. Some of them are done while air conditioning is on and in different moments of the day. This should not be a problem since the correction method considers it.

The repetition of the experiments in a second lens showed a correct performance reinforcing the idea that the TLs have a similar behavior in terms of temperature, where only an offset in the idle power state and small variations can be observed.

We presented a method to quantify and correct with success the temperature variations effect on liquid TLs. The compensation methods worked well in the four experiments (static states,

random states, hysteresis and dynamic states) and reduced considerably the precision error showing great performance in the conditions and requirements tested, including fast dynamic operation. Achieving in this way, positive results in the typical simulations of multifocal lenses used in SimVis Gekko.

In the following chapter, an optical quality evaluation is presented, analyzing optical effects (prismatic shift, magnification, distortion, and curvature) that affect the quality of the simulations and need to quantify and within the standards.

Chapter 6

Optical quality evaluation for active afocal systems

In the current chapter, the image quality of different SimVis Gekko versions was evaluated at different optical powers, measuring and quantifying the prismatic shift, angular magnification, image distortion, field curvature and image quality. Theoretical simulations and experimental measurements, with an automatic custom-developed algorithm, were done and presented hereinafter.

This chapter is based on the published proceeding by Barcala et al. *"Optical quality evaluation for active afocal systems"* in SPIE Optical Systems Designs (2021) [171]. The co-authors of the study are Enrique Gambra, Lucie Sawides, Ivan Martinez-Ibarburu, Angel G. Lopez de Haro, Yassine Marrakchi, and Carlos Dorronsoro.

The author of this thesis (1) conceived the ideas behind the project (with Carlos Dorronsoro), (2) performed the first algorithm coding (with the help of Carlos Dorronsoro), (3) developed the optical quality bench system, (4) performed the measurements with the SimVis Gekko devices, (5) collected and analyzed the data, and (6) prepared the manuscript (in collaboration with Carlos Dorronsoro).

This work was presented as a poster contribution at the IONS 2019 conference (Barcelona) and SPIE Optical Systems Designs 2021 (Madrid).

6.1. Introduction

Afocal visual systems, like binoculars or telescopes, are optical systems with some distinctive features. These systems do not have defined principal planes nor focal points [172]. The rays of light entering and exiting the system are collimated, and for a given pencil o rays the exit angle equals the entrance angle times the angular magnification. The simplest afocal system comprises two lenses, being the distance between them equal to the addition of their focal lengths (f'1=f2). This configuration allows having a constant angular magnification: when moving an object, its image changes its angular position, but the angular size is maintained.

The combination of TLs with afocal systems results in active afocal visual systems. One specific example of these active optical systems is a novel simultaneous vision simulator, SimVis Gekko (2EyesVision, Madrid).

One of the main problems of active afocal visual systems, and particularly of temporal multiplexing, is the need of presenting superimposed images with the same magnification and position, without distortion or curvature, while the active optical element induces controlled amounts of optical power. Otherwise, the transient image suffers displacements and the combined image is degraded, in some cases inducing a perception of flicker or ghost images [130]. Additionally, the instability of the axial and lateral eye position with respect to the optical axis of the instrument, in many cases not coincident with any mechanical reference, introduces more complexity to the instrument and more image degradation.

Traditional methodologies and metrics to evaluate the optical quality at a single optical power, such as the Modulation Transfer Function (MTF), distortion and curvature, or the displacement in the optical axis [173],should be reviewed for the particularities of active afocal visual systems able to change the optical power of at least one optical element.

In this study, the image quality of three different designs of a 4-f afocal system was modeled and experimentally evaluated for different optical powers of a TL inducing defocus, measuring the prismatic shift, magnification, image distortion and field curvature.

6.2. Methods

6.2.1. Samples: optical systems under evaluation

Two different tentative designs of the 4-f relay lens system (linear version and v0.5, see chapter 3) were analyzed in this study and compared with the final configuration (v2.0, see chapter 3) of the lens system. The first version (linear version) was a linear set-up (Figure 6.1.A), using the TL EL-10-30-C model from Optotune AG (Switzerland) with an effective aperture of 10 mm. This version was used as a proof of concept and feasibility. The optical projection system comprised two achromatic doublets of 50 mm (unknown design) and an offset lens (to shift the optical power range of the TL) with a focal length of -75 mm (unknown design). Although the image was reversed, it had no impact on the measurements due to the symmetry of the object. The second version (v0.5; Figure 6.1.B) introduced six flat mirrors. The achromatic lenses were replaced by

air-spaced commercial achromatic lenses (Thorlabs, USA) and an offset lens of -150 mm (Eksma Optics, Lithuania). The diagram in Figure 6.1.B also shows the position of the eye (E, represented with an ideal lens) and the windows (W) of the optical system. The third and final version developed (v2.0, see chapter 3) has a longer eye relief, shifting the exit pupil 9 mm away further from the optical module that has, essentially, the same layout as Figure 6.1.B. To reach a 1x magnification (both in the image and the TL projection in all the optical power range) while maintaining the same optimized mechanical dimensions in the optical module, the optical projection system in v2.0 was no longer symmetric and incorporated two different custom aplanatic lenses, and a -2.00 D offset lens right behind the TL.

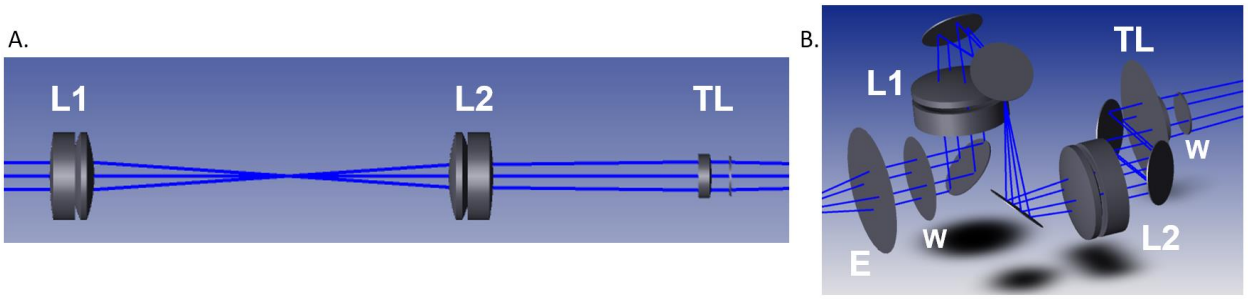

***Figure 6.1 A**. Linear version of a tentative version of the 4-f visual simulator system. L1 and L2: achromatic doublets. TL represents the tunable lens. **B**. Folded version v0.5 of the 4-f system with six flat mirrors. L1 and L2: aplanatic doublets. E: ideal eye. W: window.*

6.2.2. Computer optical simulations

The linear version was not simulated since the design of the projection system and offset lens was unknown. The folded optical systems (v0.5 and v2.0) were simulated with OpticStudio (Zemax LLC, USA), using a model eye composed of a paraxial lens of 25 mm of focal length with a flat retina at its focal plane. A stop aperture of 6 mm in diameter in the pupil plane was used for the simulations. In all designs, prismatic shift, angular magnification, spot size and field curvature were evaluated up to 16 degrees of FoV. The theoretical simulation of both folded versions of the optical system were compared across them and with the experimental evaluations.

6.2.3. Experimental set-up and protocol

An image quality bench, based on artificial vision, was developed to capture monocular images through the different versions of the visual simulator. The system comprises a DCC1545M grayscale camera (Thorlabs Inc., USA) and an objective lens (19-mm focal-length) with an adjustable diaphragm, placed on a motorized XYZ translation stage allowing the analysis of different eye decentrations. A high-resolution screen was placed at one meter of the afocal system with two different targets: (1) a checkerboard pattern (Figure 6.2.A), used to measure the prismatic shift, magnification, and image distortion; (2) a binary noise pattern (Figure 6.3.A), used to measure the local residual defocus (field curvature) and image quality.

The simulator and the camera software are controlled with custom routines developed in Matlab (MathWorks, USA), displaying the image in real-time and synchronizing the optical power of the

TL. The checkerboard images were taken first, with the diaphragm of the objective set to an aperture of 1 mm to achieve extended depth of focus. Secondly, the binary noise images were taken with the objective diaphragm opened to 5-mm, to achieve high defocus sensitivity in the measurement of field curvature and image quality.

As explained in chapter 5, the TL is driven with a voltage pulse width modulation (PWM) signal at 32kHz to achieve high temporal accuracy for generating fast dynamic optical power profiles (in periods of 20 ms). The amplitude of the PWM voltage signal range from 0V to 5V and is specified in digital counts that go from 0 to 255 (an 8-bit timer is used to generate the signal). The 'counts' notation is used in the calibration of the lens and during the experiments.

Images were taken for both stimuli from 0 to 100 counts in 10 counts steps (static states), equivalent approximately to a 2 D range, from 1 D to 3 D, steps of 0.20 D. With this configuration, the screen was focused when the combination of the TL power and the respective offset lenses was 1 D.

6.2.4. Software and image processing

The images were processed using custom Matlab routines. The main optical problems of active afocal systems with variable optical power are prismatic shift, magnification changes, optical distortion, field curvature and image quality. To quantify these optical effects in relation to the continuous optical power variation, two different algorithms were developed:

Algorithm 1. Checkerboard pattern. To analyze the shift, magnification, and distortion, we developed an algorithm to automatically detect all the corners in the checkerboard, with an accuracy of 3 arcmin (3 pixels) and compare their positions across different optical-power images. Figures 6.2.A to 6.2.D summarize the procedure. Figure 6.2.A shows the full screen with the checkerboard corners automatically detected (red crosses). Figure 6.2.B shows more detail. Images were taken every 0.20 D for a 2.00 D range. Figure 6.2.C shows the first and last images, superposed in different colors. Figure 6.2.D illustrates, using optic flow vectors, the movement of the corners (amount and direction) between the first and the last image, as the optical power increases.

Prismatic shift, magnification and optical distortion were quantified using a geometric transformation fit of the horizontal and vertical positions of the corners to two second-order polynomial equations:

$$U = A_1 + B_1 x + C_1 y + D_1 xy + E_1 x^2 + F_1 y^2, \quad (6.1)$$

$$V = A_2 + B_2 x + C_2 y + D_2 xy + E_2 x^2 + F_2 y^2, \quad (6.2)$$

Where U represents the fitted horizontal positions of all the corners. In Equation 6.1, the horizontal prismatic shift is quantified by A_1, horizontal magnification by B_1, horizontal linear distortion by D_1 and horizontal quadratic distortion by E_1. V represents the fitted vertical positions: vertical prismatic shift is quantified by A_2, vertical magnification by C_2, vertical linear

distortion by D_2 and vertical quadratic distortion by F_2. For U we did not consider C_1 and F_1 because they represent vertical components. Similarly, for V we did not consider B_2 and E_2 because they represent horizontal components.

Panels E to H in Figure 6.2 illustrates how the combination of equations 6.1 and 6.2 represent the different optical effects isolated: Figure 6.2.E illustrates the prismatic shift -changes in A_1 and A_2- Figure 6.2.F shows an increment in magnification -B_1 and C_2- and Figure 6.2.G and 6.2.H linear distortions -D_1 and D_2-; positive in Figure 6.2.G (also known as barrel distortion) and negative in Figure 6.2.H (pincushion distortion). Blue crosses represent the checkerboard corners in the reference image, without any effect, and red crosses demonstrate the different ideal effects of changing the correspondent terms.

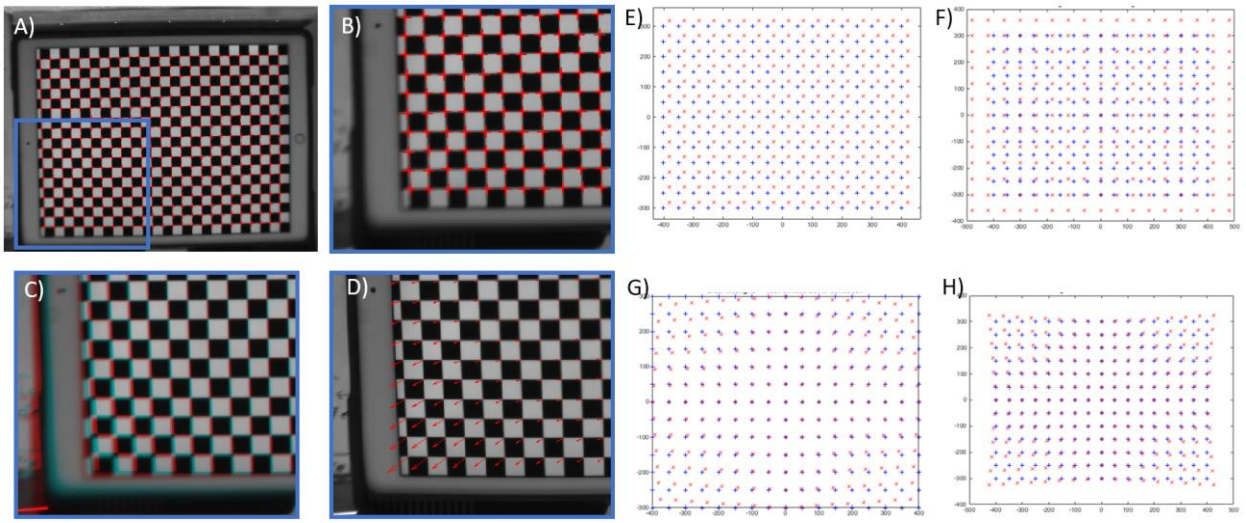

***Figure 6.2 A**. Full screen with the checkerboard corners detected, with an accuracy of 3 arcmin (3 pixels). **B.** Augmented area from figure 6.2.A. **C**. First and last images of a 2.00 D range are superposed; position differences are colored in cyan (for the first image) and red (for the last image). **D**. Same differences as in figure 6.2.C are illustrated with magnified optic flow vectors that show how the last image differs from the first one. **E.** Demonstration of the prismatic shift represented by the A_1 and A_2 coefficients (red crosses) compared to a reference image (represented with blue crosses). **F.** Demonstration of the magnification effect with the B_1 and C_2 terms (red crosses) in comparison with a reference image (blue crosses). **G-H**. Demonstration of the positive and negative linear distortion effect represented by the D_1 and D_2 coefficients (red crosses) superimposed with a reference image free of distortion (blue crosses).*

Algorithm 2. Binary noise pattern. To analyze field curvature, through-focus images of a binary noise pattern (Figure 6.3.A), with the same increasing optical powers, were automatically processed. The image was block-processed in 16x16 pixel blocks and the best focus for each block was obtained (Figure 6.3.B), using a local gradient-contrast metric applying the Sobel method [174]. This algorithm provides an accurate estimation of best defocus (±0.02 D) and can also provide a quantitative indicator of image quality in focus. An analytical description of the field curvature of the system was obtained by fitting the block-processed local focus positions along the field of view to an asymmetric paraboloid (equation 6.3). Figure 6.3C shows a graphical representation of the residual defocus. The fitted paraboloid provides an accurate estimation of the field curvature center (<1 arcmin) and can be used to quantitatively describe the center region free of residual defocus, and its dependence on the optical power.

$$Field\ Curvature = K + Lx + My + Nxy + Ox^2 + Py^2, \qquad (6.3)$$

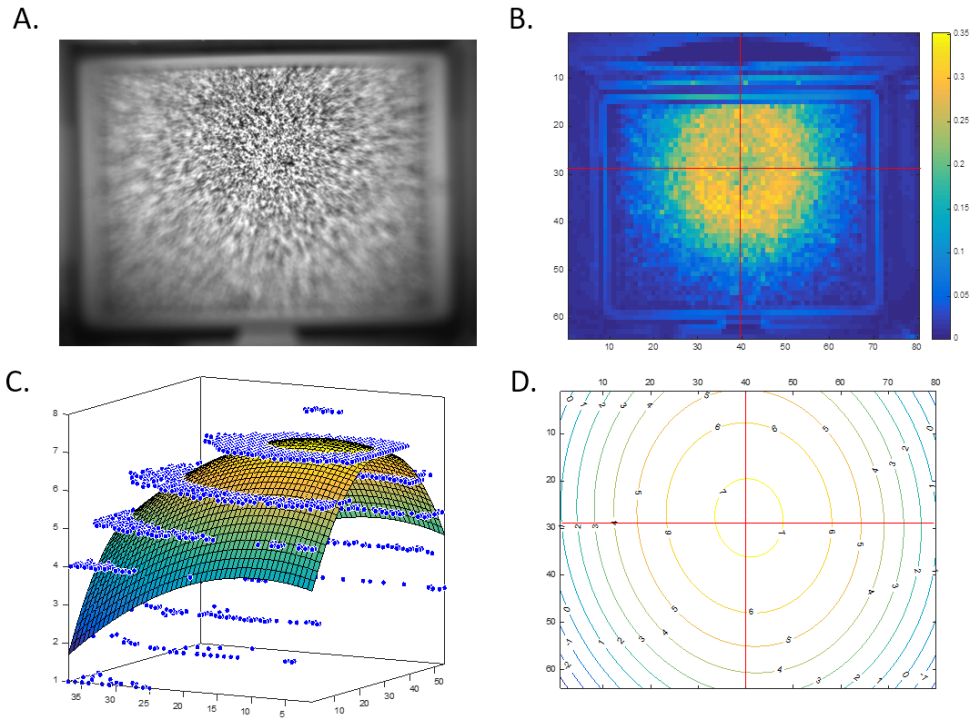

***Figure 6.3 A**. Image captured during the measurements with the simulator focused on far distance. **B**. Block-processed single image illustrating the local defocus (color coder corresponds to diopters). **C**. Graphical representation of the stack of through focus images, indicating the best focused image for each 16x16 pixel block, and the fitting to a paraboloid. The horizontal axes represent the block indices and the vertical axes the image number. **D**. Contour map for the calculated local residual defocus.*

6.3. Results

6.3.1. Computer Simulations

The computer simulations of the folded systems (v0.5 and v2.0) show that the theoretical prismatic shift is negligible. The angular magnification is 0.97 and 1.00 for the v0.5 and v2.0 systems, respectively. The computer simulations also showed that the systems are free of distortion effects.

Figures 6.4 and 6.5 show the theoretical spot sizes and field curvature of the two different versions (v0.5 and v2.0) of the commercial optical system.

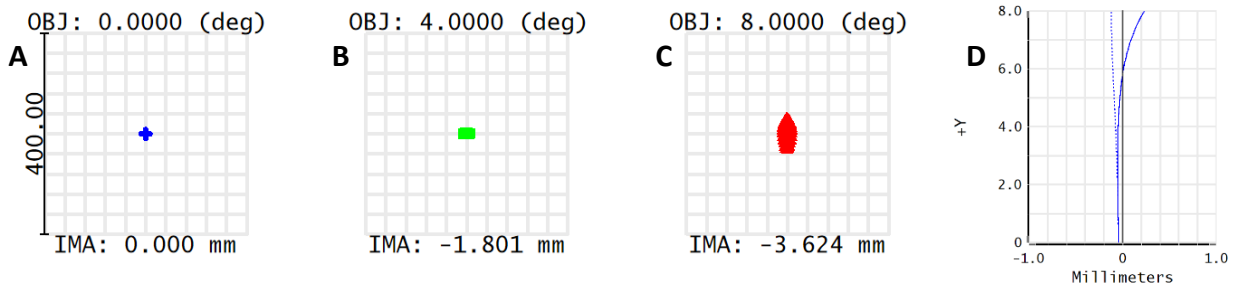

Figure 6.4 *Spot size for 0 degrees (**A**), 4 degrees (**B**) and 8 degrees (**C**) of half field of view and field curvature (**D**) of the SimVis v2, with commercial air-spaced doublets. RMS radius is 3.684 µm, 4.453 µm and 18.161 µm for 0, 4 and 8 degrees of half FoV respectively. At 8 degrees of half FoV, sagittal field curvature (dotted line) is -0.0767 mm and tangential field curvature (solid line) is 0.2845 mm.*

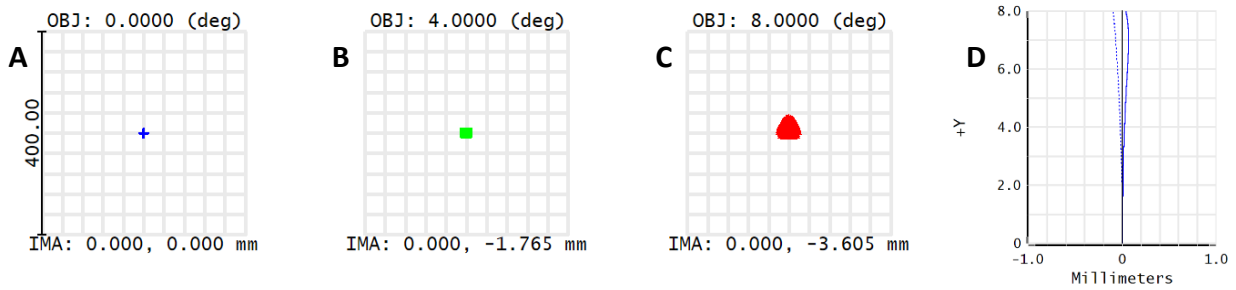

Figure 6.5 *Spot size for 0 degrees (**A**), 4 degrees (**B**) and 8 degrees (**C**) of half field of view and field curvature (D) of the SimVis v3, with commercial air-spaced doublets. RMS radius is 1.027 µm, 1.805 µm and 11.213 µm for 0, 4 and 8 degrees of half FoV respectively. At 8 degrees of half FoV, sagittal field curvature (dotted line) is -0.1006 mm and tangential field curvature (solid line) is 0.0367 mm.*

As expected, the computer simulations demonstrate that the use of air-spaced achromatic doublets provides lower field curvature: from 0.2 D in the v0.5 version to 0.1 D in the v2.0 version, evaluated at a full field of view of 16 degrees.

The optical quality for the central field (0 degrees) did not improve when using commercial air-spaced doublets (v0.5 system), but the use of custom-design air-spaced doublets (v2.0) decrease the spot size from 3 µm to 1 µm.

6.3.2. Prismatic shift, magnification, optical distortion, field curvature and image quality for the different designs

Figure 6.6 shows the results for the linear version measured.

Figure 6.6.A shows the total prismatic shift variation with different optical powers of the TL when the camera is centered with the nominal axis of the instrument given by mechanical references. The total shift variation, in this case, is different for the horizontal and the vertical axes, with a variation of x=0.12º/D and y=0.22º/D, respectively. This result changes with the position of the camera, and there is always a position for which the total shift variation is 0 and constant with optical power, corresponding to the optical axis of the afocal system. We measure important total shift variations due to deviations of the optical axis with respect to the mechanical reference

used to place the camera. These deviations have their origin in the manufacturing mechanical and optical tolerances of the elements of the instrument, especially in the TL, and in the assembly process without fine-tuning. In practice, these deviations are not so important because the eye can be aligned with the real optical axis, using references as the instrument pupil.

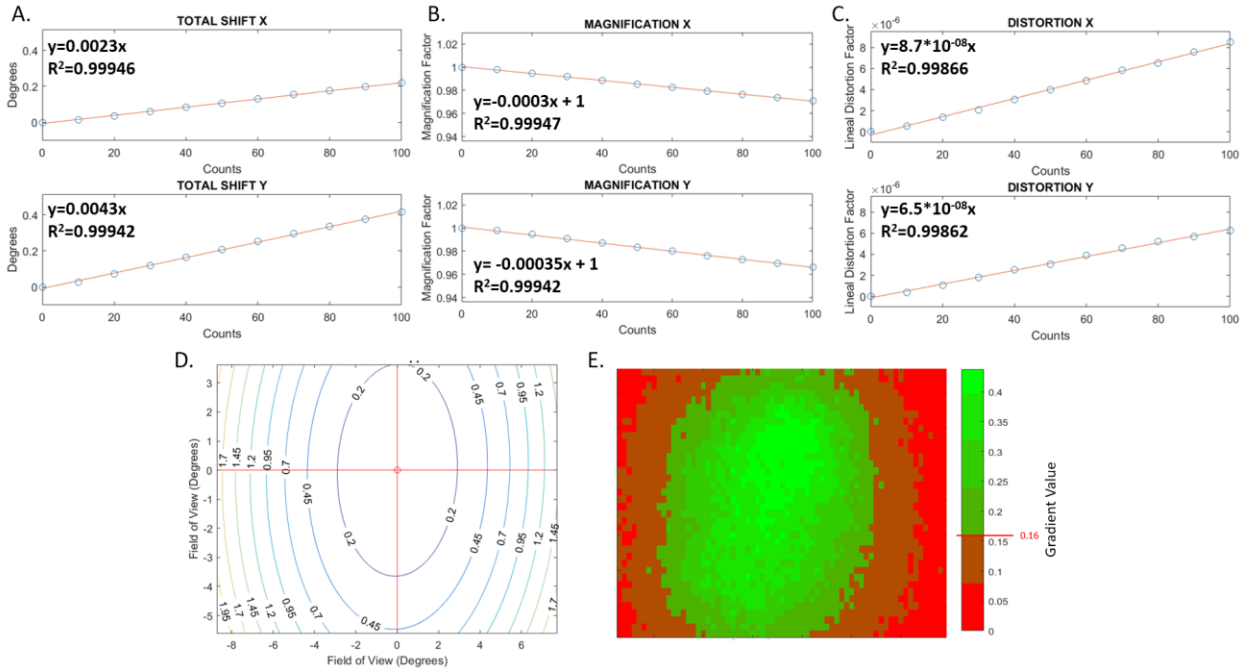

Figure 6.6 *Optical quality evaluation of the linear optical system, with the achromatic doublets.* ***A****. Total prismatic shift variation with the optical power sent to the TL, x=0.12º/D and y=0.22º/D. This effect changes with the alignment of the system in relation to the camera or the eye of a subject.* ***B****. Magnification variation of the system -1.5%/D and -1.75%/D. Magnification is inherent to the design and cannot change.* ***C****. The system is free of distortion. The linear distortion measured is <0.00005%/D.* ***D****. Contour map of the field curvature. Each contour line shows the optical power variation. The area with less curvature (<0.2 D) covers a FoV of ±2.50º horizontally and ±3.50º vertically. This system has a FoV of 25.24º.* ***E****. Local image quality in focus. The color code represents the maximum local gradient value, in arbitrary units.*

By contrast, magnification changes, optical distortion, and curvature (described below) are inherent to the design, and although they can be affected by the centering of the eye or the camera, when present there is no position correcting them.

Figure 6.6.B shows the variation of the magnification with the optical power. Although magnification should ideally remain constant, we measured important magnification changes with the optical power that were similar in the vertical (-1.75%/D) and in the horizontal (-1.5%/D) directions.

Figure 6.6.C shows the linear distortion changes with the optical power variation. It should be noted that the vertical axis has a $x10^{-6}$ factor. Linear distortion is below 0.00005%/D both for the horizontal and the vertical axis. The quadratic distortion coefficients were negligible.

Figure 6.6.D shows the contour map of the field curvature, with the change of the curvature in diopters shown in each contour line, in relation to the field of view. In this case, the curvature is not centered in the field of view and is not symmetrical (has an oval shape). The area with almost

no curvature (<0.2 D) covers a FoV of ±2.50º horizontally and ±3.50º vertically. Field curvature increases very rapidly, achieving 1.95 D at 8º on the horizontal FoV. For this system, a total FoV of 25.24º was measured.

Figure 6.6.E illustrates the local image quality metric in focus, based on the local gradient-contrast metric. The color code represents the maximum local gradient value, i.e., the image quality in focus, in arbitrary units. The image quality is not stable across the area analyzed and runs in parallel with the field curvature.

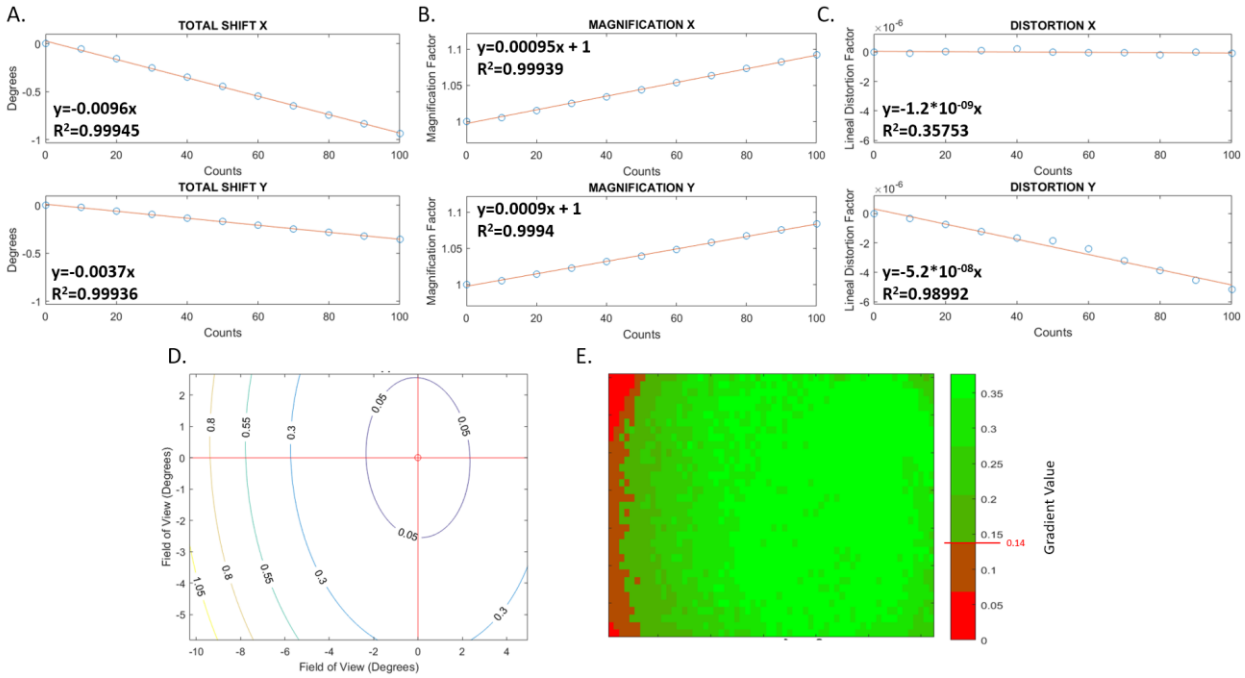

Figure 6.7 *Optical quality evaluation of the folded system v0.5, with the commercial air-spaced achromatic doublets.* ***A.*** *Total prismatic shift variation with the optical power sent to the TL, x=-0.48º/D and y=-0.19º/D. This effect changes with the alignment of the system in relation to the camera or the eye of a subject.* ***B****. Magnification variation of the system 4.75%/D and 4.50%/D. Magnification is inherent to the design and cannot change.* ***C****. The system is free of distortion. The linear distortion measured is <0.00005%/D.* ***D****. Contour map of the field curvature. Each contour line shows the optical power variation. The area with less curvature (<0.01 D) covers a FoV of ±2.25º horizontally and ±2.50º vertically. This system has a FoV of 20.32º.* ***E****. Local image quality in focus. The color code represents the maximum local gradient value, in arbitrary units.*

The total shift variation for the version v0.5 is, in this case, larger (Figure 6.7.A), and different in magnitude and sign for the horizontal and vertical axis (x=-0.48º/D and y=-0.19º/D). The total prismatic shift variations have increased compared with the linear system, and it can be related to the incorporation of the mirrors and the increased of internal misalignments.

Figure 6.7.B shows the variation of the magnification with the optical power. Compared with the previous system, the magnification has increased 3%/D.

Figure 6.7.C shows the linear distortion changes with the optical power variation. It should be noted that the vertical axis has a $x10^{-6}$ factor. Linear distortion is below 0.00005%/D both for the horizontal and the vertical axis. The quadratic distortion coefficients were negligible.

Figure 6.7.D shows the contour map of the field curvature, with the change of the curvature in diopters shown in each contour line, with the field of view. In this case, the curvature is not centered in the field of view and is not symmetrical (has an oval shape). The area with almost no curvature (<0.01 D) covers a FoV of ±2.25º horizontally and ±2.50º vertically. Compared to the previous system configuration, the curvature decreases a 41%. For this system, a total FoV of 20.32º was measured.

Figure 6.7.E illustrates the local image quality metric in focus, based on the local gradient-contrast metric. The image quality is more stable than the previous system.

The results regarding the last measured version, v2.0, are shown in Figure 6.8.

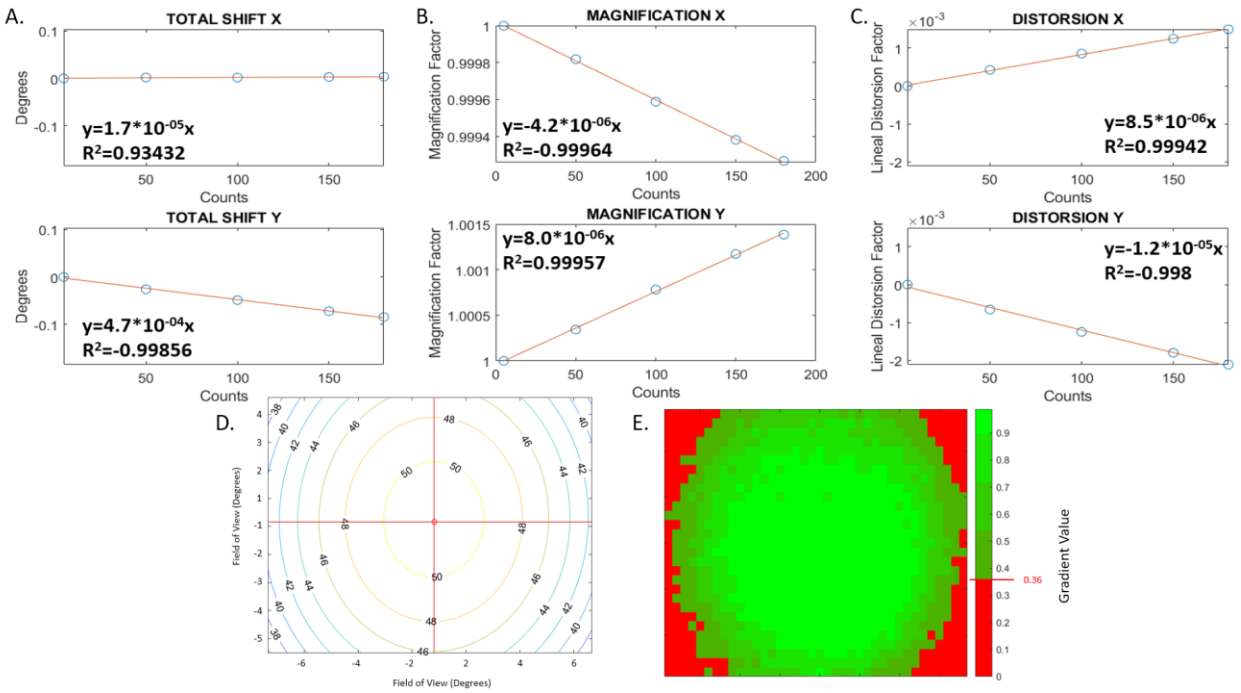

Figure 6.8 *Optical quality evaluation of the folded v2.0 optical system, with the air-spaced custom achromatic doublets.* ***A****. Total prismatic shift variation with the optical power sent to the TL, x=0.00085º/D and y=0.024º/D.* ***B****. Magnification variation of the system -0.021%/D and 0.04%/D.* ***C****. The linear distortion measured is <0.0007%/D.* ***D****. Contour map of the field curvature. Each contour line shows the optical power variation in digital counts. The area with less curvature (<0.24 D) covers a FoV of ±7 horizontally and ±5º vertically. This system has a FoV of 20.32º.* ***E****. Local image quality in focus. The color code represents the maximum local gradient value, in arbitrary units.*

The alignment system was improved between versions v0.5 and v2.0. The total shift variation measured were x=0.00085º/D and y=0.024º/D (Figure 6.8.A).

The magnification remains constant, with a variety of -0.021%/D horizontally and 0.04%/D vertically shown in Figure 6.8.B The magnification was reduced 1.4%/D compared to v0.5 and 4.4%/D compared to the linear version.

The vertical axis of the linear distortion shown in Figure 6.8.C has a $x10^{-3}$ factor. For the v2.0 the linear distortion has increased compared with the previous two versions of the system, although is still below 0.0007%/D both for the horizontal and vertical axis and not relevant.

Figure 6.8.D shows the contour map of the field curvature, with the change of the curvature in digital counts shown in each contour line, in relation to the field of view. In this case, the curvature is centered in the field of view and is symmetrical. The maximum area of the image covers a FoV of ±7º horizontally and ±5º and presents a curvature of 0.24 D. The curvature has decreased an 85% compared with the linear version and 28.75% compared with the v0.5. The total FoV of this system is the same as the one of the v0.5.

Figure 6.8.E illustrates the image quality metric, based on the local gradient-contrast metric. A symmetrical and stable optical quality metric can be observed. The maximum quality of vision increases to 0.99 (arbitrary units of gradient), from 0.43 and 0.37 in previous versions, and run in parallel with the improvement in field curvature.

6.4. Discussion

Both the optical bench developed and the custom algorithms demonstrated to provide enough sensitivity during the measurements and quantification of the optical quality of visual simulators implemented on afocal systems with active optical elements. The linear behavior of the prismatic shift, magnification, and distortion makes possible a faster measurement procedure, taking only the first and last image of the optical range to be analyzed.

The linear system, with the achromatic doublets, had an important amount of field curvature and therefore provided poor image quality in the periphery. When changing the achromatic doublets for the air-spaced commercial achromatic doublets in the folded system (v0.5), we expected an important improvement in field curvature with a magnification factor x1. However, when the v0.5 system was experimentally measured, important magnification changes were measured with the optical power. The measuring system allowed to detect a problem in the assembly of this particular system, that was confirmed afterward. The last version measured, v2.0, is free of significant optical effects that may degrade the image quality during the visual simulation (prismatic shift, magnification, and optical distortion), as demonstrated both theoretically and experimentally. Despite some of the field curvature is compensated with the natural curved shape of the retina, it is still visually noticeable for the expert eye, but only in the far periphery of the field of view. More importantly, the measurements show that there is a huge central area free of field curvature, and with high optical quality. That central area is the one used for observation and perceptual judgements, while the far periphery of the image, close to the edge of the field, is only used to give context to the image.

By incorporating a XYZ translation stage, the system could also allow the study of tolerances in the eye positioning. But those measurements do not seem to be necessary because the eye is

intuitively self-aligned to look through the center of the system, using optical references (not mechanical) such as the amount of light, the pupil position, or the image quality.

In conclusion, the optical quality evaluation system developed can measure and quantify the (1) prismatic shift, (2) angular magnification, (3) optical distortion, (4) field curvature, and (5) image quality of afocal visual systems and visual simulators. The artificial vision system developed can automatically quantify their through-focus image quality. This system could guide the design, assembly, and fine adjustment of active afocal optical systems and visual simulators.

Chapter 4 showed the development of a low-cost focimeter that is the starting point for a prototype for its use in the clinical site. Measurements of the dynamic response of the TL and the calibration of the SimVis Gekko were always requirements the prototype had to meet. However, after the analysis and measurements presented here the analysis of the optical quality will be added to the calibration prototype for the clinic, to ensure the quality of the simulations.

In the next chapter, a metric for assessing multifocal vision in the clinic is presented.

Chapter 7

Multifocal Acceptance Score to Evaluate Vision: MAS-2EV

In the current chapter, we present de development of a new subjective visual quality metric to evaluate vision with presbyopic corrections. It is based on a set of images representing natural visual scenes at day and night conditions projected in far and near displays and a near stereo target. Two groups of subjects performed the clinical experiments analyzing their visual satisfaction both with simulated corrections and real contact lenses. The repeatability of the metric is also presented.

This Chapter is based on the published paper by Barcala *et al. "Multifocal Acceptance Score to Evaluate Vision: MAS-2EV" in Scientific Reports (2021)*. The co-authors of the study are Maria Vinas, Mercedes Romero, Enrique Gambra, Juan Luis Mendez-Gonzalez, Susana Marcos, and Carlos Dorronsoro.

The author of this thesis (1) conceived the ideas for the definition of the MAS-2EV metric along with Carlos Dorronsoro and Susana Marcos, (2) design and implemented the experimental procedure, (3) performed the measurements, (4) analyzed the data, and (5) prepared the manuscript (in collaboration with Susana Marcos).

This work was presented as an oral contribution at the European Society of Cataract and Refractive Surgery (ESCRS) annual meeting (September 2018) in Vienna (Austria) and in the Association for Research in Vision and Ophthalmology (ARVO) annual meeting (May 2019) in Vancouver (Canada).

7.1. Introduction

Typically, the quality of vision provided by multifocal lenses, monovision, and combined strategies (i.e. modified monovision where the dominant eye is corrected with a monofocal lens at far and the non-dominant eye is corrected with a multifocal lens [15]) is tested using visual acuity (VA) at various distances or using DFVA curves [91–94]. It is well recognized that high contrast VA is a limited descriptor of the quality of vision. Besides, the complexity and unfamiliarity of multifocal vision [95] require wider and most sophisticated evaluation methods.

Quality of vision is, in fact, multifactorial, and largely depends on visual conditions that affect luminance, pupil diameter, and the spatial content and contrast of the visual world [96].

To date, the quality of vision is assessed clinically through questionnaires that are given to the patient who self-report visual comfort and task performance in different situations (i.e. reading a restaurant menu, driving, sewing, etc...) [97]. Examples of these questionnaires include NEI RQL-42 [98], a questionnaire with 42 questions that measure the patient's satisfaction at distance vision, clarity of vision, and severity and frequency of glare symptoms, along with the need for spectacles. Other questionnaires also include an assessment of the satisfaction with day and night vision (as the Functional Assessment of Visual Tasks (VISTAS) questionnaire [99,100]) or with night driving (as VF-14, the Visual Function Index). Some questionnaires (i.e. The Catquest-9SF questionnaire) address the perceived benefits of cataract surgery [101]. While the previous questionnaires were not specifically designed to evaluate the quality of vision with multifocal lenses, the CLUE questionnaire [102] developed by Johnson and Johnson targets specifically the quality of vision (as well as other comfort aspects) with M-CLs.

Drawbacks associated with vision questionnaires have been addressed before. For example, systematic psychometric evaluations showed that the NEI-RQL-42 questionnaire has deficiencies in most of its tested aspects [103]. All questionnaires, even those optimally designed, rely on the patient's memory, as they rate their vision for situations that they encountered over different days. Furthermore, the evaluations provided by the questionnaires may differ across patients, as not every patient is exposed to the same visual environment.

In this chapter, we present for the first time a perceived visual quality test (Multifocal Acceptance Score to Evaluate Vision, MAS-2EV) that combines the systematicity and accessibility of those tests conducted using visual displays in the clinic (such a VA), with the multi-component description of the visual world that is captured in the questionnaires. In MAS-2EV, natural images representing scenes that can be encountered in daily life (daytime and nighttime, near and far distances, and stereovision) are scored by the patient.

The metric can be applied to patients already implanted with a M-IOL, or fitted with CLs of various designs, similarly to the indicated VA tests or questionnaires. However, the real value of the metric relies on the possibility to perform these tests pre-operatively or before fitting real CLs on eye. Pre-operative or pre-fitting simulations are now possible with the use of visual simulators.

Adaptive optics visual simulators typically based on deformable mirrors or spatial light modulators have been used to replicate various multifocal lens designs [82,91,104,175,176]. Alternatively, SimVis Gekko is targeted to prospective M-IOL and M-CLs patients.

The new Multifocal Acceptance Score to Evaluate Vision (MAS-2EV) presented here is ideally administered in combination with binocular visual simulators such as SimVis Gekko. The patient experiences through different presbyopic corrections (simulating prospective contact or intraocular lenses) realistic daytime and nighttime natural scenes at near and at far, representative of different situations that the patient may encounter in his/her daily life (with different illuminations, distances, contrasts, glare sources, and spatial content). We evaluated the repeatability and sensitivity of the metric in differentiating across different corrections, using both the SimVis Gekko and real CLs on eye.

7.2. Methods

7.2.1. Multifocal Acceptance Score to Evaluate Vision (MAS-2EV)

MAS-2EV is a custom-developed metric defined as a multi-component vector, comprising five perceptual scores (PS; 0 to 10) of multi-stimuli images of day and night scenes, at far (4 m) and near (40 cm) distance, and of a stereovision target at near. The perceived image quality of the global visual scene at far and near distances through a given correction was judged by the subject using a perceptual scoring technique [177] ranging from very blurred (score 0) to very sharp (score 10).

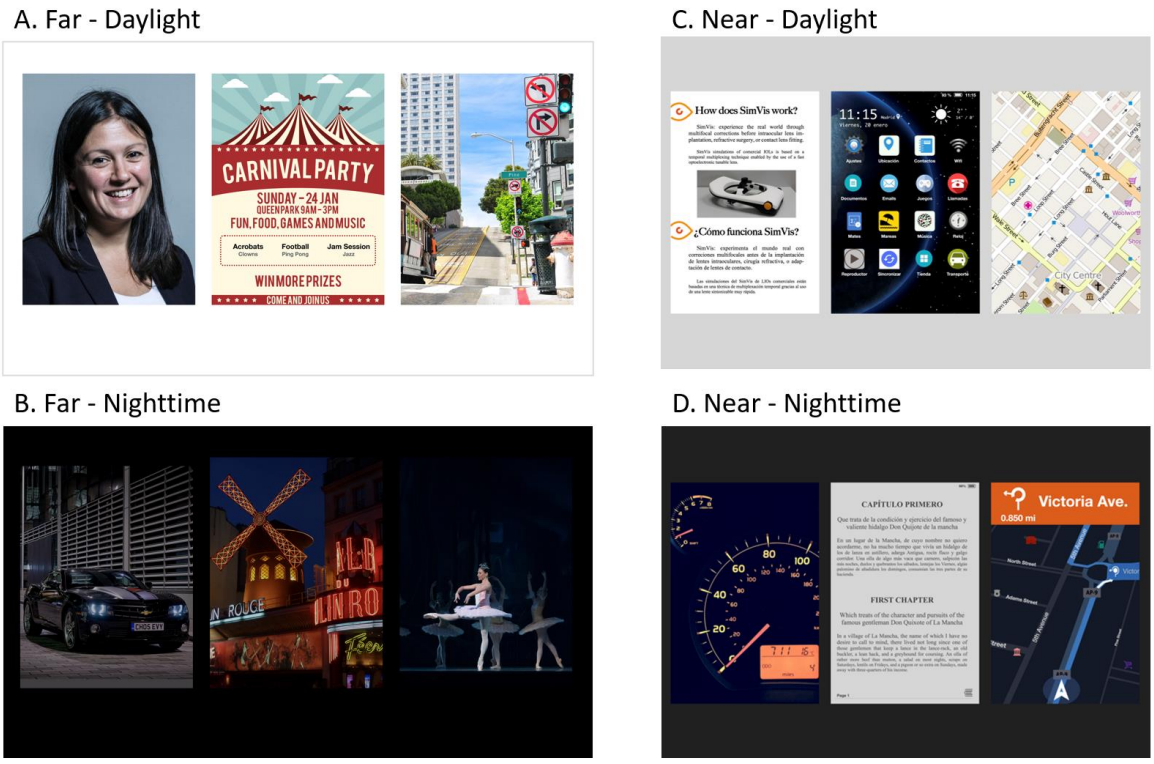

Figure 7.1 *Set of images of MAS-2EV.*

The selected images, shown in Figure 7.1, represent four different daily-life visual activity areas: far-day, far-night, near-day, and near-night. The images are available to distribute and either come from public repositories of images (details of the sources, licenses, and attributions can be found on the acknowledgments) or have been specifically generated for this study.

The far-day image (Figure7.1A) set consists of a female portrait; a poster with different letter fonts and sizes; and an urban street view. The far-night set (Figure7.1B) represents urban scenes at night: a view of a stopped car with the lights on and a readable license plate, with a pair of bright superimposed white LEDs (18 cd/m^2) simulating real headlights introducing glare, a street scene with neon signs of different sizes; and an indoor ballet show. Near-day (Figure7.1C) activities are represented by a flyer with different text sizes; a smartphone screen with app icons and text; and a digital city map. The near-night (Figure7.1D) set consisted of a car's glowing dashboard at night; an electronic book screenshot with low contrast and different letter sizes; and a GPS navigation map in night mode. The power spectra of the face and street scene images followed roughly the 1/spatial frequency of natural images with a spatial frequency range between <0.25 and >40 cpd. The objects shown were designed to be seen at a specific distance and to represent habitual visual scenes for a patient, the size of the text in the images ranged from 0 to 1 logMAR VA. The contrast and color of each image were carefully selected to match with the light condition and distance.

Additionally, near stereo-acuity targets are presented, consisting of a Random-dot anaglyph with seven in-depth Snellen-E letters with different orientations and different crossed disparities (400 to 50 arcsec). For the stereo test, the score corresponds to the number of letters whose orientation the subject can detect at 40 cm, ranging from 0, for stereo disparities equal or above 400 arcsec, to 10, for a disparity of 50 arcsec. The anaglyphs are presented in an iPad Pro 12.9" with Retina Display (by Apple Inc) and observed with cyan / red glasses.

The MAS-2EV stimuli were designed to be presented on a standard monitor screen of 42" for far distance, and on a standard iPad screen of 9.8", being possible a resize to fit them on higher screens without modifying the size of the stimuli. In this study, they were presented on a 48.5" display (3840x2160 pixels, 49UH850V, LG) at 4 meters for far distance and an iPad Pro (2732x2048 pixels) at 40 cm for near distance. With the displays switched off, the room illumination was above 400 lux for day-time conditions and below 2.5 lux for night-time conditions. The average luminance of the MAS-2EV stimuli presented on the displays was measured with a colorimeter ColorCal (MKII, Cambridge Research Systems). The average luminance was 120±51.21 cd/m^2 (for far-day), 131.67±17.28 cd/m^2 (for near-day), 5.40±5.79 cd/m^2 (far-night) and 1.86±0.30 cd/m^2 (near-night). The brightness control of the displays was not changed between day and night conditions for far distance. The brightness control of the iPad was changed from the maximum (day condition) to the minimum (night condition) for near distance.

7.2.2. Subjects

Measurements were performed in ten healthy subjects: five young subjects (age: 29±6 years; spherical error (sph.): -2.23±2.07 D) and five presbyopic subjects (age: 61±4; 1.20±0.45D). Astigmatism was lower than 0.75 D in all subjects. Anisometropia was lower than 1.50 D in all subjects. All presbyopic subjects wore reading glasses, but they were spectacle-free for far distance. Presbyopia was pharmacologically simulated in young subjects by instillation of one drop of 1% tropicamide 15 minutes before the measurements, and then every hour. The accommodation amplitude (A.A.) in presbyopic subjects was measured using a Power Refractor 2 (PlusOptix, Germany), and was 1.35±0.33 D, on average. The subject profiles are shown in Table 7.1 with individual data of age, gender, sphero-cylindrical refraction, eye dominance, and accommodation amplitude.

	Subject	Age	Rx OD (Sph, cyl)	Rx OS (Sph, cyl)	Dominance	A.A. OD/OS
Young	S1_ F	26	0.00, -0.50 x 30	-0.25, -0.50 x 150	OD	Cyclopleged
	S2_F	26	-3.75, -0.50 x 30	-5.00, -0.50 x 65	OD	Cyclopleged
	S3_F	29	-2.00, -0.25 x 95	-2.50, -0.25 x 40	OD	Cyclopleged
	S4_M	24	-4.00, -0.50 x 35	-4.75, -0.50 x 165	OS	Cyclopleged
	S5_F	38	0.00, -0.75 x 180	0.00, -0.75 x 170	OD	Cyclopleged
Presbyopes	S6_M	57	+0.25	+0.75, -0.50 x 70	OS	1.56 / 1.30
	S7_F	68	+1.25, -0.25 x 80	+1.50, -0.25 x 80	OS	0.93 / 1.07
	S8_F	59	+1.00, -0.75 x 100	+1.00, -0.75 x 80	OS	1.61 / 0.93
	S9_F	60	+1.50, -0.50 x 55	+1.50, -0.50 x 105	OS	1.29 / 1.92
	S10_F	61	+1.75, -0.50 x 80	+1.50, +0.25 x 55	OS	1.27 / 1.67

Table 7.1 *Individual data of gender (_M male; _F Female); age (years); Sphero-cylindrical refraction (Rx, sph and cyl in D, x astigmatic angle in degrees) in right (OD) and left (OS) eyes; eye dominance (OD right eye; OS left eye) and amplitude of accommodation (A.A, in D for OD/OS, only in presbyopes).*

7.2.3. Experiments

All young subjects were measured both with CLs and SimVis Gekko. Presbyopic subjects only performed measurements with SimVis Gekko. Subjects were divided into three different groups: (1) young subjects measured with SimVis Gekko; (2) young subjects measured with CLs; (3) presbyopic subjects measured with SimVis Gekko. The experimental protocol was the same for all groups.

The experiments conformed to the tenets of the Declaration of Helsinki, with protocols approved by the Consejo Superior de Investigaciones Cientificas Ethics Committee. The subjects signed an informed consent after receiving an explanation of the nature and implications of the study.

7.2.4. Tested binocular presbyopic corrections

Four binocular presbyopic corrections were tested, both with CLs and simulated using SimVis Gekko in young subjects, and SimVis Gekko in presbyopic subjects: (1) Monofocal far in both eyes (FF); (2) Bifocal lenses in both eyes (BB); (3) Monovision (FN; dominant eye with monofocal far

and non-dominant eye with monofocal near); and (4) Modified Monovision (FB; dominant eye with monofocal far and non-dominant eye with a bifocal lens). The near add in bifocal corrections was +2.50 D, and the interocular refraction difference was +2.50 D in the monovision correction.

7.2.5. Contact lenses

In one experiment, patients wore monofocal and M-CLs (Biofinity, CooperVision, USA) [42]. The lenses were silicone hydrogel (Comfilcon A) with standard geometry parameters (Base Curve: 8.6, Lens diameter: 14.0) and monthly disposable. Distance power ranged from -0.25 to -5.00 D in both monofocal and bifocal lenses. M-CLs had a central near add of +2.50 D, with an aspheric front surface and a mono-curve back surface.

CLs were fitted following the manufacturer's guide and checked for lens damage under the slit-lamp before proceeding with lens settling. Evaluation of the lens centration, primary gaze movement, upgazed movement, and tightness was carried out following routinary standard practice [178]. CLs had a settling time of at least 4 minutes before proceeding.

7.2.6. SimVis Gekko

A SimVis Gekko v0.5 visual simulator (see chapter 2) was used in this study. This wearable device can simulate, in either eye, programmable multifocal corrections. In this study, we used generic multifocal profiles with an energy distribution of 50% for far distance (0.00 D) and 50% for near distance (+2.50 D) programmed in the SimVis Gekko. Trial lenses inserted in a dedicated slot in the system were used to correct the far distance refraction in the multifocal designs (from -1.00 D to +4.50 D, in 0.25-diopter steps) and to replicate a monofocal correction.

The calibration of the device was checked weekly to guarantee the stability of the simulation throughout the study (see chapter 2). It should be noted that the lens designs used in this study correspond to generic monofocal and bifocal (pure simultaneous vision) designs, and do not aim at reproducing the specific CLs designs of subsection 7.2.5.

7.2.7. Experimental protocol

The measurements were conducted by two experienced optometrists. Conventional non-cyclopleged subjective refraction was obtained using Optonet Vision Unit (Optonet Ltd, United Kingdom).

The patient's sphero-cylindrical refraction was corrected with the spherical equivalent by the CLs power (in the measurements with CLs) or by trial lenses placed in the dedicated slot in the SimVis Gekko device. Natural binocular vision was tested using a 4-dot Worth test to discard fusion dysfunction, which was an exclusion criterion. Eye dominance was determined by the +1.50 D blur test.

A preparatory trial using SimVis Gekko allowed the subject to set the range for their perceptual scoring by viewing the MAS-2EV far-day images through a simulated far-distance corrected monofocal lens (10 PS) and an additional +2.50 D monofocal lens (0 PS).

Figure 7.2 illustrates and summarized the methodology followed in the study. The set of four presbyopic corrections described in section 7.2.4 was tested first with the SimVis Gekko in the young and presbyopic subjects, and then with CLs only in young subjects (in different sessions). Within each method, corrections were tested following a preset random series.

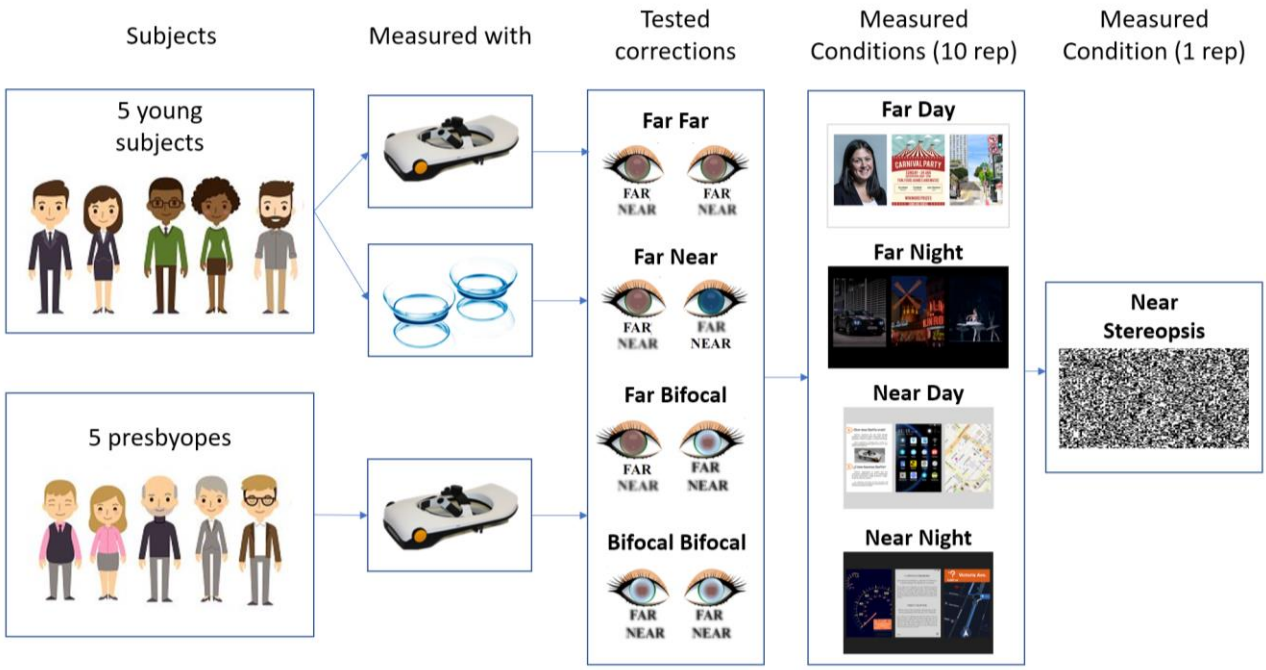

Figure 7.2 *Illustration summarizing the methods, showing the subjects measured divided into three groups depending on the simulator/contact lens, the corrections tried by each group, and the measured conditions.*

For a given correction, the stereopsis at near was first tested (yielding a 0-10 score), according to the description in subsection 7.2.1. Then MAS-2EV scorings were first obtained for far-day and near-day. Patients were then allowed to settle into the night-time setting for 4 minutes, after which MAS-2EV scorings were obtained for far-night and near-night.

A total of 1640 trials were conducted in young subjects (SimVis Gekko and CLs), and 820 trials in presbyopic subjects (SimVis Gekko), corresponding to 4 corrections, 2 light conditions, 2 distances, each repeated 10 times, and 4 stereo responses. A full MAS-2EV task takes 2 min to be completed per correction. Measurements were performed in two different experimental sessions, lasting 5 hours (SimVis Gekko) or 10 hours (CLs).

7.2.8. Data analysis and visualization

MAS-2EV is graphically represented as a polygon, with the Perceptual Scores (PS) in each vertex: the measured stereopsis (upper vertex) and the four PS measured for far-day, far-night, near-

day, and near-night (an example is shown in Figure 7.3). The geometrical center of the polygon corresponds to score 0 and the maximum separation of the vertex to score 10.

A metric of the overall visual quality with a specific correction is given by the unweighted average (MAS-2EV Modulus) of the five vertices. Alternatively, the overall visual quality can be calculated as the normalized area enclosed by the MAS-2EV polygon (MAS-2EV Area), defined as (*area* - *area_min*) / (*area_max* - *area_min*) where *area* is the area enclosed by the MAS-2EV polygon for a given subject and correction, *area_max* is the maximum area obtained across subjects and corrections, and the *area_min* the minimum area obtained across subjects and corrections.

The visual imbalance across distances (near and far) for a given correction was obtained by subtracting the PS at near from the PS at far. Additionally, the overall visual imbalance across conditions (near/far, day/night, stereo) for a given correction was calculated as the standard deviation across all PS (normalized to the maximum) and represented the asymmetry of the MAS-2EV polygons.

Metrics of visual compromise were also obtained from the MAS-2EV scores, concerning the PS for the bilateral monofocal corrections (FF): (1) Visual degradation at far, defined as (*PS Far for each presbyopic correction – PS Far FF*)/*PS Far FF*; (2) Visual benefit at near, defined as (*PS Near for each presbyopic correction – PS Near FF*)/*PS Far FF*; (3) Near stereo benefit is defined as (*Stereo with FF – Stereo for each presbyopic correction*)/*Best Near Stereo* for that subject.

The intra-subject repeatability was calculated as the mean of the standard deviation across repetitions for each subject. Inter-subject differences were calculated with the standard deviation of the MAS-2EV Modulus.

Statistical analysis was performed in IBM SPSS Statistics v26 to (1) to analyze the statistical relevance of each variable (subject, correction, distance, and illumination) using a Mixed Model Analysis: Main effect and all two-way; (2) analyze the reliability and the consistency in the scoring criteria used by the subjects with an Alpha Cronbach; (3) analyze the significance of the difference between two variables across the same group using a Related-Samples Friedman's 2-way ANOVA by Ranks with pairwise comparison-adjusted by the Bonferroni correction; (4) analyze the significance of a variable between groups using an Independent-Samples Kruskal-Wallis Test with pairwise comparison-adjusted by Bonferroni correction; (5) analyze the repeatability of the metric using a Repeated Measures ANOVA analysis between factors.

7.3. Results

Section 7.3.1 (below) presents the statistical analysis and relevance of each variable, as well as the reliability of the metric. Section 7.3.2 presents 1) an example of how to construct the MAS-2EV polygon that represents the ten perceptual score repetitions for each subject (figure 7.3); 2) all MAS-2EV polygons for all subjects (figure 7.4) showing differences across corrections and groups; 3) MAS-2EV Modulus and Areas averaged across subjects (figure 7.5) and; 4) a comparison between day and night conditions (figure 7.6). Section 7.3.3 presents: 1) visual

imbalance for each correction (figure 7.7); 2) visual compromise across distances (figure 7.8); 3) near stereo benefit (figure 7.9); 4) overall visual imbalance and; 5) overall visual quality metrics (table 7.2 and table 7.3). Section 7.3.4 presents the MAS-2EV inter- and intra- subject variability. Finally, section 7.3.5 shows the repeatability of the proposed metric.

7.3.1. Analysis of the variables and reliability of the metric

A Mixed Model Analysis (Dependent: PS; Fixed Factors: distance, light condition, correction; Random: Subject; Repeated: distance, light condition, correction, repetition) reveals that all main effects were statistically significant (subject $p<10^{-10}$; correction $p<10^{-10}$; distance $p<10^{-10}$; light condition $p<0.01$) in all groups, and the two-way effects involving distance (near/far) were also significant ($p<0.05$) in all groups.

The reliability and the consistency in the scoring criteria used by the subjects were high (Cronbach's Alpha > 0.95 for each group, distance, and light condition).

7.3.2. MAS-2EV polygons, near stereopsis and perceptual scores

Figure 7.3 shows an example of MAS-2EV polygons (Fig. 7.3A), near stereovision (NS) scores (Fig 7.3B), and individual perceptual scores (PS, Fig. 7.3C and D) in one subject (S01) for four presbyopic corrections (FF in blue, BB in orange, FN in grey, FB in yellow) simulated by SimVis Gekko. Data are averaged across ten repeated measurements. Figure 7.3C shows the average individual PS for far-day (Fig. 7.3C, left columns) and near-day (Fig. 7.3C, right columns) and far-night (Fig. 7.3D, left columns) and near-night (Fig 7.3D, right columns). As expected, the FF correction (Monofocal far in both eyes; blue columns) provided better scores at far distance than at near distance (62.5%). For BB (bifocal lenses in both eyes; orange), the scores were 23% lower than FF but similar at both distances (6.92 and 8.05, respectively). For FN (Monovision; gray) the scores were high at both distances (65% higher than FF for near). For FB (Modified monovision; yellow) the scores were higher for far distance than for near distance (27.5%), and more balanced across distances than with FF. Although the trends for day and night PS were similar, scores were on average 4.25% higher for day than for night.

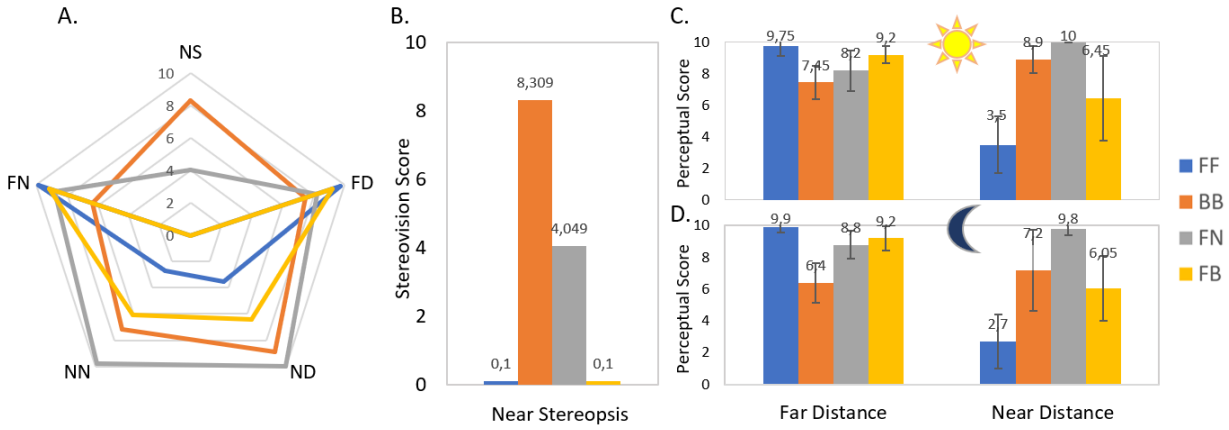

Figure 7.3 *MAS-2EV polygons, near stereovision and perceptual scores for subject S1_SV, with presbyopic corrections simulated with SimVis Gekko. (**A**) MAS-2EV polygon. The upper vertices represent stereopsis*

*score (NS), and the four lower vertices perceptual scores for far-day (FD), near-day (ND), near-night (NN), and far-night (FN) counter-clockwise. (**B**) Near stereovision scores. (**C** and **D**) Perceptual scores (PS) for far distance (left columns) and near distance (right columns), for day stimuli (upper graph), and night stimuli (lower graph) for the different corrections. In all graphs Blue stands for both eyes corrected for far (FF); Orange both eyes corrected with bifocal lenses (+2.50 D add, BB); Gray stands for monovision (monofocal for far distance in the dominant eye and +2.50 D monofocal in the non-dominant eye, FN); Yellow stands for modified monovision (monofocal for far distance in the dominant eye and bifocal lens with +2.50 D near add in the non-dominant eye, FB). Each data point is the average across 10 repeated measurements, and error bars represent standard deviations.*

Figure 7.4 shows the MAS-2EV polygons for all measured subjects and conditions: young subjects with SimVis Gekko (Fig. 7.4A, left column), young subjects with CLs (Fig. 7.4B, middle column), and presbyopic subjects with SimVis Gekko (Fig. 7.4C, right column).

In all subjects, FF correction (blue line) provided the highest PS at far distance for day and night (PS=9.38±0.73), which was 75.27% on average higher than at near distance (PS=2.32±2.40). NS (near stereopsis) with FF was low in almost all subjects (NS=2.76±2.96). Unlike FF, which produced similar polygons across subjects, BB bilateral correction (orange line) produced a larger inter-subject variability in the response (1.71 PS). NS with BB correction (NS=7.58±0.72 PS) was 63.59% higher than with FF. The FN correction (grey line) provided good visual quality at near distance (PS=7.64±2.27) for all subjects except S2_SV and S3_SV, and in general, good quality at far distance (PS=7.66±0.87). However, FN seriously compromised NS (NS=3.38±2.87 PS, on average) in 12 out of 15 subjects (except in S3_SV, S9_SV, and S10_SV, whose NS was not affected). The FB (yellow line) was nearly as good as FF for far (only 12.3% lower). However, FB was 26.4% higher than FF for near. FB compromised NS (NS= 4.28±3.17 PS) in all subjects (except in S6_SV), although NS with FB was 20.05% higher than FF and 11.87% higher than FN, but 43.54% lower than BB. Despite common trends across subjects, differences in both the shape and the area polygons between subjects suggest different responses to different corrections depending on the subject.

An average metric for vision quality was calculated as the unweighted average (MAS-2EV Modulus, Fig. 7.5A) of the PS scores and the polygons normalized area (MAS-2EV Area, Fig. 7.5B). The similarity of the individual polygons for SimVis Gekko and CLs in most of the subjects indicates that SimVis Gekko captures similar trends as the real CLs, even if SimVis Gekko was not programmed to mimic the actual design of the lens.

Both in young and presbyopic subjects, the FN correction produced the best overall visual quality (highest MAS-2EV Modulus and Area). The FF correction produced a significantly lower MAS-2EV Modulus ($p<0.03$; paired-sample t-test) than FN and FB in young subjects, but not in presbyopic subjects. The difference between the best and the worst correction was FN-FF=1.94±1.00 for the young group with SimVis Gekko, FN-FF=2.26±0.74 for the young group with CLs, and FN-BB=1.21±0.93 for presbyopes. The overall visual quality (MAS-2EV Area) was lowest for FF (0.25±0.16), followed by BB (0.42±0.14), FB (0.46±0.16), and highest (with higher STD) for FN (0.60±0.21).

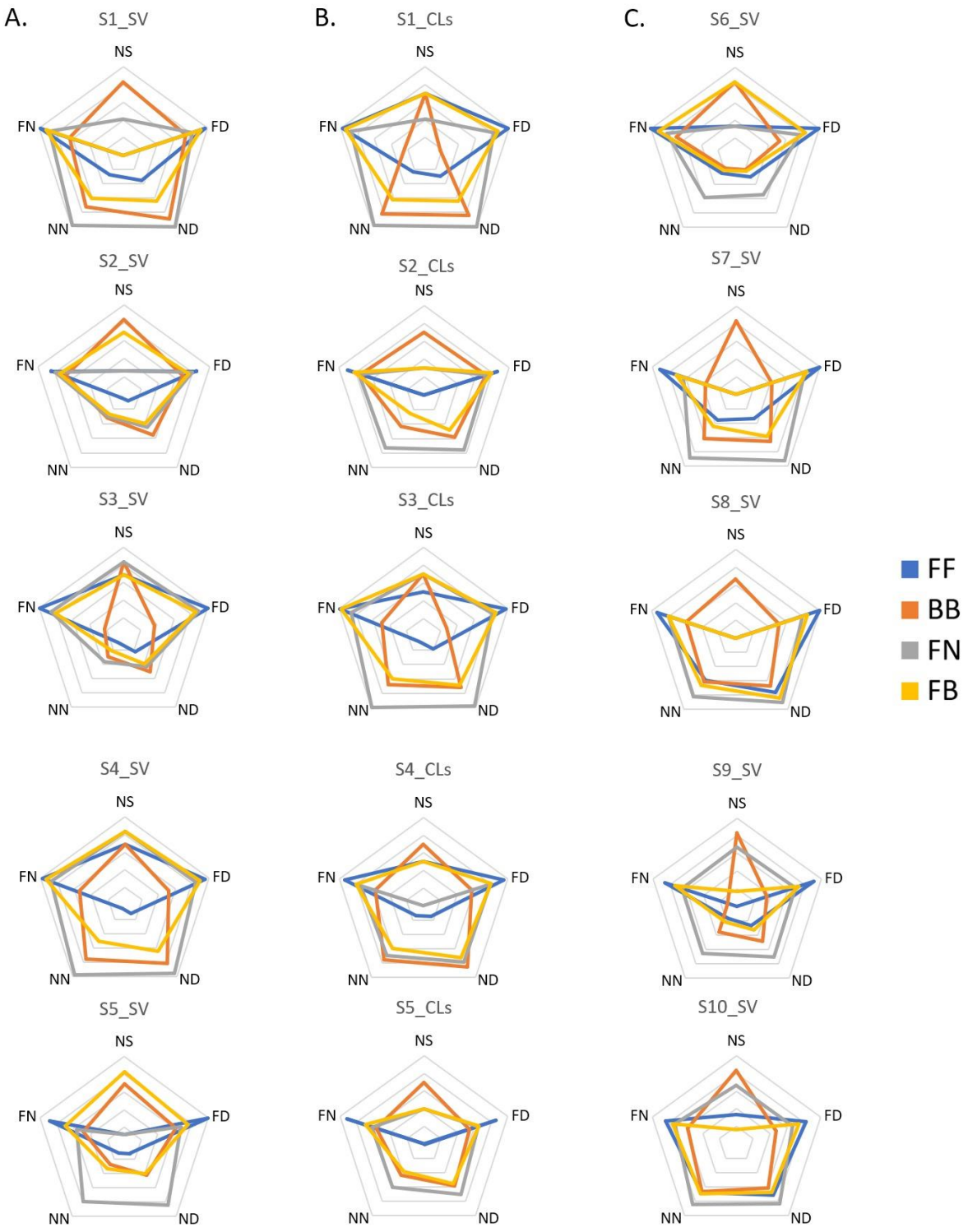

Figure 7.4 *MAS-2EV polygons.* ***A.*** *for young subjects measured with SimVis Gekko.* ***B.*** *for young subjects measured with CLs.* ***C****. for presbyopic subjects measured with SimVis Gekko. Blue line corresponds to bilateral monofocal correction for far (FF), orange line to bilateral bifocal (BB), gray line to monovision (FN), and yellow line to modified monovision (FB).*

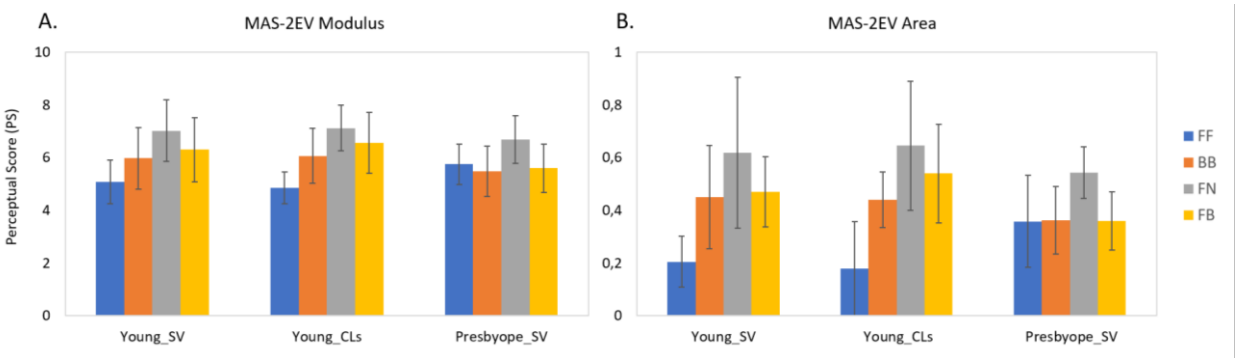

***Figure 7.5 A**. MAS-2EV Modulus (average of the five polygon vertices: NS and the four PS averaged across subjects for each group), for all corrections. **B**. MAS-2EV Area (normalized areas averaged across subjects for each group), for all corrections.*

Figure 7.6 shows the mean PS across subjects and distances, itemized by group, far/near, and day/night conditions. For each group, FF correction was statistically significantly different than BB at far distance both at day and night condition (p=0.001; Related-Samples Friedman's 2-way ANOVA by Ranks with pairwise comparison-adjusted by the Bonferroni correction). However, FF was statistically significantly different than BB at near distance (both at day and night condition) only for young subjects, both with SimVis Gekko (p=0.02; Related-Samples Friedman's 2-way ANOVA by Ranks with pairwise comparison-adjusted by the Bonferroni correction) and CLs (p=0.042; same test). Very consistently, PS for FF at near was lower in young (by 71.27%, p<0.04 -for both illuminations-; Independent-Samples Kruskal-Wallis with pairwise comparison-adjusted by Bonferroni correction) than in presbyopic subjects. PS were almost identical for day and night (the average PS difference across distances, corrections, and subjects was 0.32).

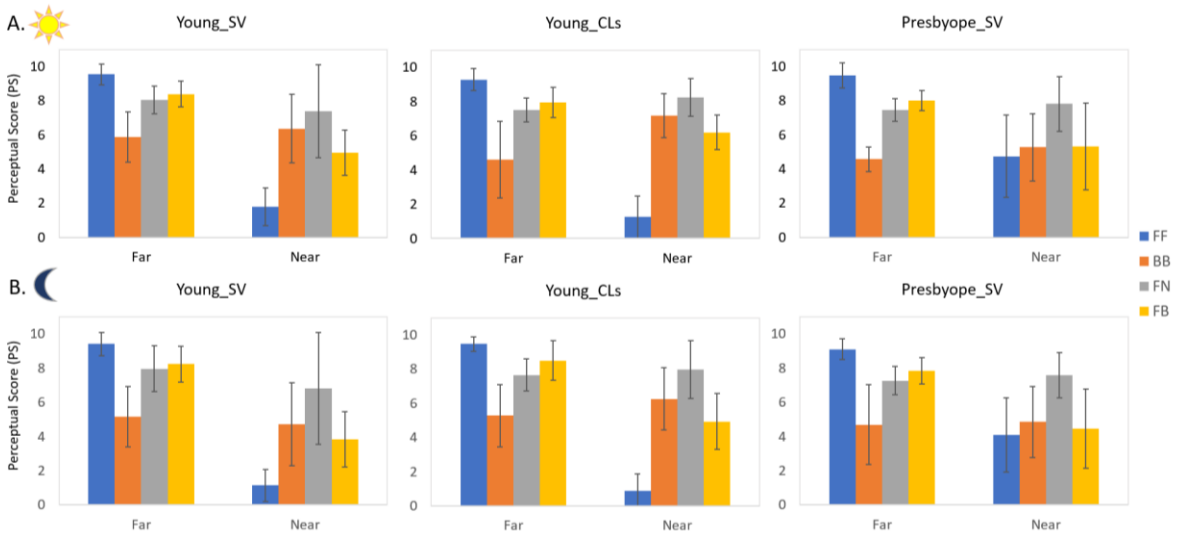

***Figure 7.6** Mean PS across subjects for day (**A**, upper row), night (**B**, lower row) conditions, at far and near distances.*

7.3.3. Visual imbalance and compromise of different presbyopic corrections

Figure 7.7A shows the visual imbalance across distances, calculated as far-near PS difference (averaged across subjects and day/night conditions), for each correction. FF and FB corrections provided statistically significant imbalances between far and near distances in all groups ($p<0.005$; paired-sample t-test), although those were significantly lower for presbyopes than for young subjects. The lowest far-near imbalances (not statistically different from zero) occurred in all subjects for BB and FN. On average, the largest overall visual imbalance (Fig. 7.7B) was found for FF (0.84±0.12) followed by FB (0.48±0.13) and FN (0.39±0.25), with the lowest visual imbalance found for BB (0.33±0.17).

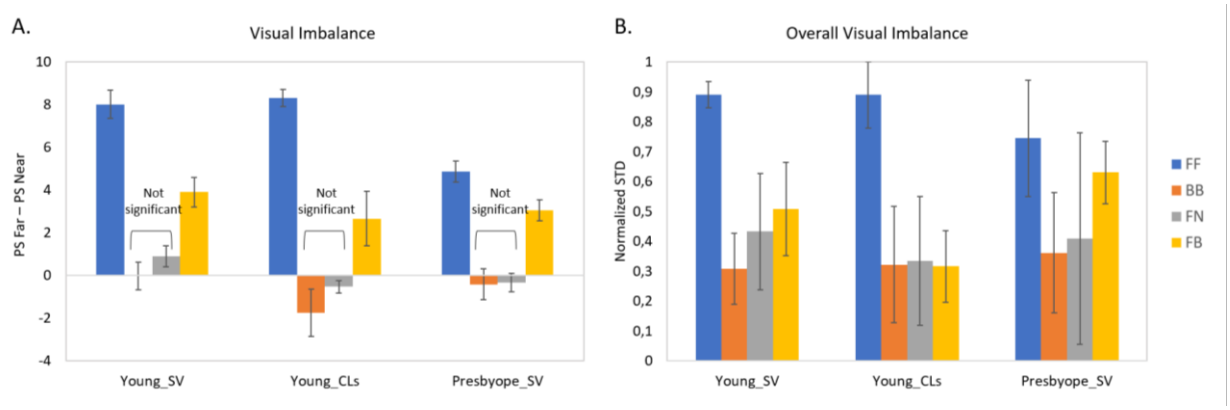

***Figure 7.7 A**. Visual imbalance between distances (difference PS Far-PS Near) for each correction and group (averaged across light conditions and subjects). **B**. Overall visual imbalance (normalized standard deviation in PS, averaged across subjects) for each correction and group.*

Figure 7.8 shows the visual compromise (degradation at far distance versus visual benefit at near distance) for each correction and each subject. The ideal correction will lie in the (0, 1) coordinate, i.e., low degradation at far and high benefit at near. Points above the -1:1 line are indicative of a positive compromise (more benefit at near than degradation at far).

Out of the 30 evaluations (3 groups x 5 subjects x 2 light conditions) per correction represented in Figure 7.8, 28 showed a positive compromise for FN, 20 for FB, and 13 for BB. Figure 7.8 also shows histograms representing the distribution of degradation at far (horizontal axis) and benefit at near (vertical axis) for the three presbyopic corrections. FN produced the highest benefit at near distance across subjects and light conditions (56.38±25.79%; with a peak at of the histogram at 0.69); followed by BB (36.79±27.60%; peak at 0.57), and by FB (28.10±20.89%; peak at 0.33). The degradation at far distance was lowest for FB (-12.03±5.71%; peak at -0.14); followed by FN (-18.26±7.00%; peak at -0.19); and it was highest for BB (-45.51±18.38%; peak at -0.47).

An important aspect not reflected in visual quality at near and far distances is stereo vision, the fifth parameter in the MAS-2EV metric. Figure 7.9 shows the near stereo benefit as a function of visual benefit at near, for all subjects and presbyopic corrections. The ideal correction will have both high near vision and near stereo benefits. We found the largest near stereo benefit for BB (61.92±38.31%; peak at 0.84, followed by FB (22.80±30.12%; peak at 0.02) and FN

(17.23±35.21%; peak at 0.04). On average across subjects, near stereo benefit for BB was 0.45±0.38 higher than near stereo benefit for FN, and 0.39±0.42 higher than near stereo benefit for FB, indicating that in most subjects BB provided the best stereo near vision, which on the other hand was compromised in FB and FN.

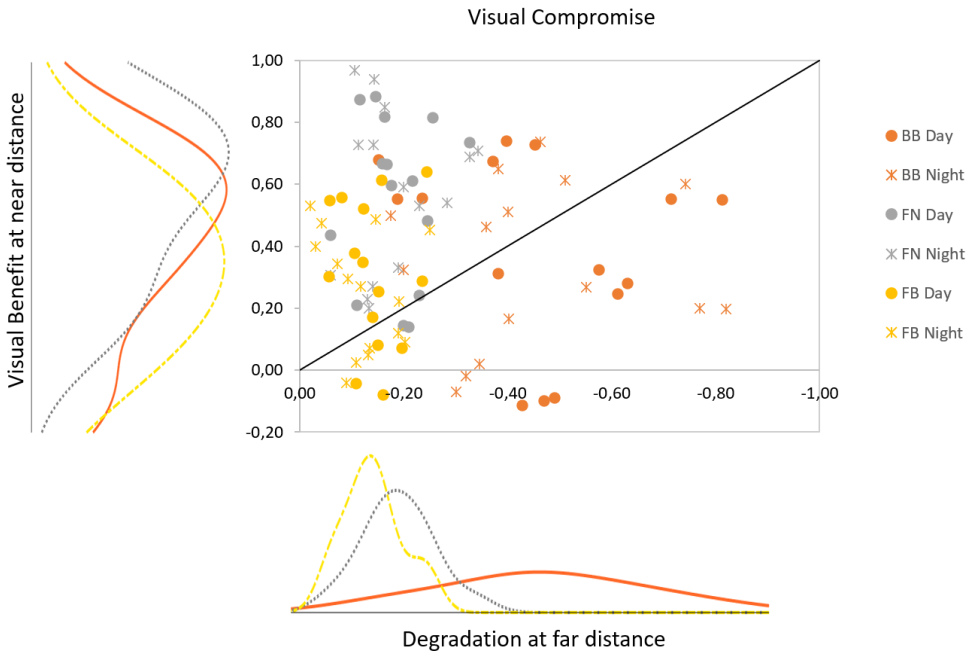

Figure 7.8 *Visual compromise: Visual degradation at far vs Visual Benefit at Near, concerning a bilateral monofocal correction (FF), for all presbyopic corrections (bilateral bifocal BB, monovision FN, modified monovision FB). Symbols represent each subject measured at day (spots) and night (asterisks) conditions. The histograms show the distribution of the data for each axis.*

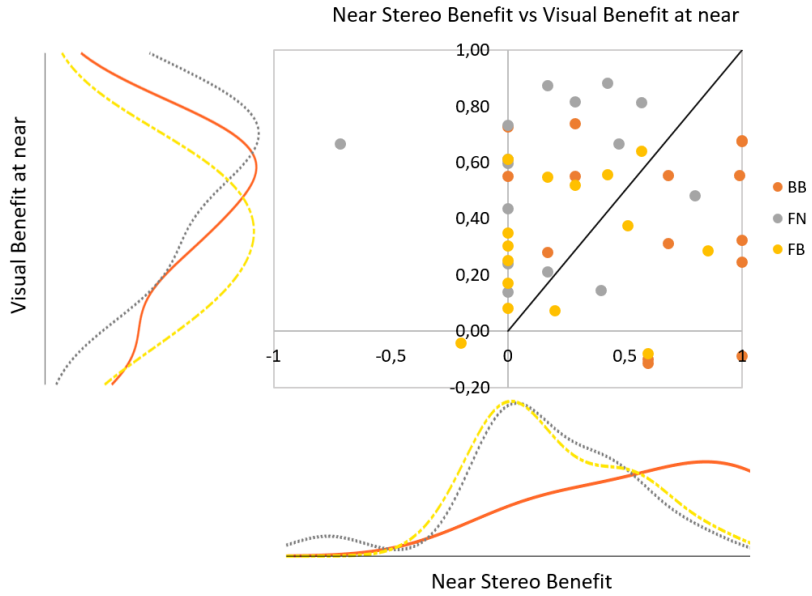

Figure 7.9 *Near Stereo Benefit as a function of Visual Benefit at near for each presbyopic correction. The histograms show the distribution for each axis.*

Figure 7.10 shows the MAS-2EV overall visual imbalance (polygon asymmetry) as a function of overall visual quality (MAS-2EV Area). For all corrections there was a significant negative correlation between overall visual imbalance and overall visual quality (r=-0.78; p=0.0005 for FF; r=-0.74; p=0.002 for BB; r=-0.54; p=0.04 for FN and r=-0.56; p=0.03 for FB), indicating that overall quality increases as visual imbalance decreases.

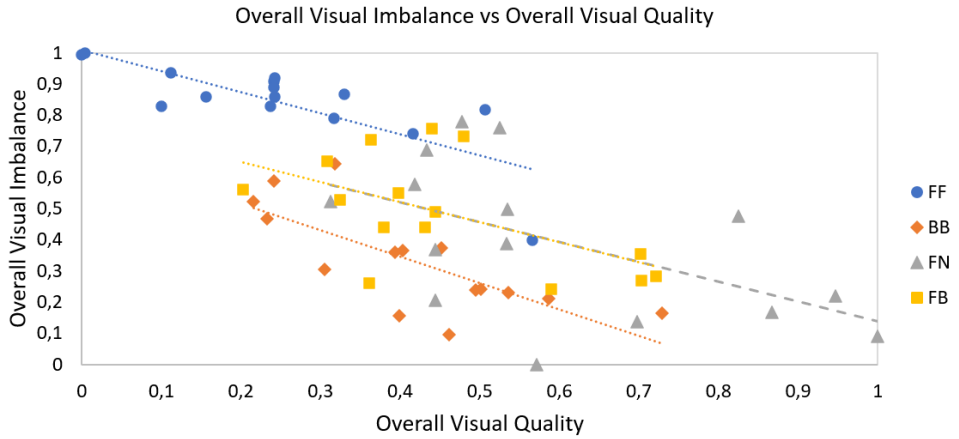

Figure 7.10 *Overall visual imbalance (MAS-2EV polygon asymmetry) vs overall visual quality (MAS-2EV Area), for all tested corrections (Far-Far; Bifocal-Bifocal; Far-Near and Far-Bifocal).*

Figures 7.3-10 allow visualizing overall trends with the different corrections and their average performance. However, the parameters at the individual level may have an important predictive power to aid in the selection of a correction or discard corrections not suitable for a patient. Table 7.2 (for SimVis Gekko) and Table 7.3 (for CLs) show the ranking of corrections based on the combination (addition) of all parameters: visual degradation at far, visual benefit at near, near stereo benefit, visual imbalance (multiplied by -1) and overall visual quality (MAS-2EV Area). The corrections marked in bold meet the threshold (0) in the overall performance parameter. The circled number indicates the correction ranked as best for each subject. In 40% subjects with SimVis Gekko and 60% subjects with CLs the BB was ranked 1, in 50% (SimVis Gekko) / 40% (CLs) FN was ranked as 1, and 10% (SimVis Gekko) / 0% (CLs) FB was ranked as 1.

Subject	Correction	Degradation @Far	Benefit @Near	Benefit Stereo	- Overall visual imbalance	Overall visual quality	Overall Performance Parameter	Ranking
S1_SV	FF	0.00	0.00	0.00	-0.91	0.24	-0.67	4
	BB	-0.30	0.51	0.99	-0.16	0.73	**1.77**	①
	FN	-0.14	0.70	0.48	-0.48	0.82	**1.38**	2
	FB	-0.06	0.32	0.00	-0.76	0.44	-0.06	3
S2_SV	FF	0.00	0.00	0.00	-0.83	0.10	-0.73	4
	BB	-0.19	0.44	0.68	-0.37	0.45	**1.01**	①
	FN	-0.06	0.37	0.00	-0.52	0.31	**0.1**	3
	FB	-0.11	0.32	0.51	-0.44	0.38	**0.66**	2
S3_SV	FF	0.00	0.00	0.00	-0.87	0.33	-0.54	4
	BB	-0.70	0.24	0.17	-0.47	0.23	-0.53	3
	FN	-0.13	0.24	0.17	-0.50	0.53	**0.31**	①
	FB	-0.17	0.15	0	-0.55	0.40	-0.17	2
S4_SV	FF	0	0	0	-0.92	0.24	-0.68	4
	BB	-0.46	0.73	0	-0.23	0.54	**0.58**	3
	FN	-0.11	0.92	0.17	-0.09	1.00	**1.89**	①
	FB	-0.05	0.51	0.17	-0.35	0.70	**0.98**	2
S5_SV	FF	0	0	0	-0.94	0.11	-0.83	4
	BB	-0.39	0.24	0.68	-0.30	0.30	**0.53**	2
	FN	-0.33	0.71	0	-0.58	0.42	**0.22**	3
	FB	-0.21	0.25	0.85	-0.44	0.43	**0.88**	①
S6_SV	FF	0	0	0	-0.79	0.32	-0.47	4
	BB	-0.39	-0.09	0.60	-0.59	0.24	-0.23	3
	FN	-0.21	0.29	0	-0.37	0.44	**0.15**	①
	FB	-0.13	-0.06	0.60	-0.72	0.36	**0.05**	2
S7_SV	FF	0	0	0	-0.86	0.24	-0.62	4
	BB	-0.56	0.30	1.00	-0.36	0.40	**0.78**	①
	FN	-0.23	0.57	0	-0.78	0.48	**0.04**	2
	FB	-0.18	0.17	0	-0.65	0.31	-0.35	3
S8_SV	FF	0	0	0	-0.82	0.51	-0.31	4
	BB	-0.42	-0.04	1.00	-0.10	0.46	**0.9**	①
	FN	-0.17	0.19	0	-0.76	0.53	-0.21	2
	FB	-0.14	0.08	0	-0.73	0.48	-0.31	3
S9_SV	FF	0	0	0	-0.86	0.16	-0.7	4
	BB	-0.72	0.22	1.00	-0.52	0.22	**0.2**	2
	FN	-0.24	0.51	0.80	-0.00	0.57	**1.64**	①
	FB	-0,16	0.06	0.20	-0.56	0.20	-0.1	3
S10_SV	**FF**	0	0	0	-0.40	0.57	**0.17**	3
	BB	-0.37	-0.07	0.60	-0.24	0.50	**0.42**	2
	FN	**-0.17**	**0.17**	**0.40**	**-0.14**	**0.70**	**0.96**	①
	FB	-0.11	-0.01	-0.20	-0.49	0.44	-0.37	4

Table 7.2 *Individual data of visual degradation at far distance, visual benefit at near distance, near stereo benefit, overall visual imbalance (negative), overall visual quality, overall performance parameter, and ranking. Corrections in bold indicate acceptable overall performance. Circled correction ① indicates the highest ranking. Data correspond to measurements performed with SimVis Gekko.*

Subject	Correction	Degradation @Far	Benefit @Near	Benefit Stereo	- Overall visual imbalance	Overall visual quality	Overall Performance Paramenter	Ranking
S1_CL	FF	0	0	0	-0.74	0.42	-0.32	3
	BB	-0.78	0.58	0	-0.64	0.32	-0.52	4
	FN	-0.18	0.67	0	-0.17	0.87	**1.19**	①
	FB	-0.08	0.37	0	-0.27	0.70	**0.72**	2
S2_CL	FF	0	0	0	-0.99	0.00	-0.99	4
	BB	-0.16	0.59	1.00	-0.24	0.50	**1.69**	①
	FN	-0.15	0.87	0.43	-0.39	0.53	**1.29**	2
	FB	-0.09	0.43	0.43	-0.53	0.32	**0.56**	3
S3_CL	FF	0	0	0	-0.89	0.24	-0.65	4
	BB	-0.61	0.58	0.29	-0.36	0.39	**0.29**	3
	FN	-0.15	0.88	0.29	-0.22	0.95	**1.75**	①
	FB	-0.07	0.53	0.29	-0.28	0.72	**1.19**	2
S4_CL	FF	0	0	0	-0.83	0.24	-0.59	4
	BB	-0.39	0.69	0.29	-0.21	0.59	**0.97**	①
	FN	-0.18	0.63	-0.71	-0.69	0.43	-0.52	3
	FB	-0.15	0.55	0.00	-0.24	0.59	**0.75**	2
S5_CL	FF	0	0	0	-1.00	0.00	-1	4
	BB	-0.39	0.59	1.00	-0.16	0.40	**1.44**	①
	FN	-0.30	0.76	0.57	-0.21	0.44	**1.26**	2
	FB	-0.25	0.55	0.57	-0.26	0.36	**0.97**	3

Table 7.3 *Individual data of visual degradation at far distance, visual benefit at near distance, near stereo benefit, overall visual imbalance (negative), overall visual quality, overall performance parameter, and ranking. Corrections in bold indicate acceptable overall performance. Circled correction ① indicates the highest ranking. Data correspond to measurements performed with CLs.*

7.3.4. Inter- e intra-subject variability

MAS-2EV was highly repetitive across the ten repetitions of each measurement. The intra-subject repeatability of the scoring was consistent in all subjects, with an average standard deviation of 0.97 PS. The standard deviation across repetitions (intra-subject variability) was similar in the different groups (young 1.00 PS; presbyope 0.91 PS), light condition (day 0.99 PS; night 0.93 PS), corrections (FF 0.73 PS; BB 1.05 PS; FN 0.98 PS; FB 1.09 PS) and distances (far 0.78 PS; near 1.14 PS).

However, the inter-subject variability was significantly higher ($p<0.02$, paired-sample t-test) for near distance (2.74 PS) than for far distance (1.92), being the difference across distances much higher in young (1.05 PS) than in presbyopic subjects (0.34 PS). Across all subjects, BB at far showed the highest inter-subject variability (1.71 PS).

7.3.5. Metric repeatability

Given the high repeatability of the responses (Alpha Cronbach's factor 0.95), we studied the theoretical minimum number of repetitions of a MAS-2EV test that would provide reliable information on the perceived quality of a given correction, and establish a ranking of corrections. A Repeated Measures ANOVA analysis between factors (for a medium effect size of 0.25) estimated that 3 repetitions provide enough statistical power to show significant differences in

perceived quality, influenced by the fixed factors (correction, distance, and light condition). However, a parametric approximation would entail a higher number of subjects per group.

7.4. Discussion

We have presented a new visual metric (MAS-2EV) that captures the multidimensionality of vision, measuring the perceptual quality at different distances, light conditions, and stereo. Instead of relying on visual acuity charts or contrast sensitivity targets, judgments of the quality of vision are made on a total of 12 natural images representing habitual visual scenes that the patient can recognize, and that are relevant to his/her daily visual tasks. The test fulfills time requirements in clinical practice both regarding materials (only requires a monitor to display the images at distance and a tablet for images at near, and two LEDs to couple with the night scene), room dimensions (being compatible with the settings of other visual tests) and time of application (evaluation of each correction takes 3 minutes). The metric has proved repetitive (only 3 repetitions needed to obtain sufficient sensitivity) and provides multiple parameters (including, visual degradation at far, visual benefit at near, near stereo benefit, visual imbalance, and overall visual quality) onto which the selection of a correction can be based. The metric is particularly suitable to evaluate and compare multiple presbyopic corrections on the same patients. In the current study, four binocular presbyopic corrections (bilateral monofocal corrections at far, monovision, modified monovision, and bilateral bifocal corrections) were evaluated using the MAS-2EV.

The study was conducted on cyclopleged young subjects (i.e., with simulated presbyopia) and a presbyopic group. While presbyopes are the natural users of presbyopic corrections, multifocal corrections have been proposed for myopia control in young patients [179]. In this study, we paralyzed accommodation in the young group, although a similar study could be envisioned for this group also under natural conditions as a way to study vision with these lenses before their prescription. Interestingly, on average across groups, we found similar perceptual scores for the same presbyopic corrections and conditions between young and presbyopic subjects (see for example Fig. 7.5). Only the perceptual scores for the FF correction at near distance were significantly higher in the presbyopic subjects than in the young subjects. This may indicate a higher tolerance to blur at near in presbyopic subjects, likely as a result of neural adaptation [177]. Consequently, the imbalance of far and near vision for FF was significantly higher in young subjects than presbyopes (Fig. 7.7).

Perceptual scores between day and night conditions (Fig. 7.6) were small (0.32 PS) but statistically significantly in all groups ($p<0.01$). This effect is likely due to the influence of the pupillary dynamics in the study design. On the one hand, measurements in young subjects were performed with a dilated pupil (therefore not reacting to light and potential differences in vergence). On the other hand, the simulations with SimVis Gekko were performed for a fixed pupil diameter of 4 mm in all conditions.

MAS-2EV allows a comparison of different presbyopic corrections, including multiple parameters (Fig. 7.8-10), and to perform that comparison of the performance of each correction for each subject (Table 7.2 and 7.3). While visual benefit at near was highest for monovision (FN), the inclusion of other parameters such as stereo vision, visual imbalance, and overall quality (MAS-2EV polygon area), increased the value of bifocal corrections (BB). At the individual level, BB resulted in the first option in 46.67% of the subjects, FN the first option in 46.67%, and FB in 6.67%.

MAS-2EV allows the evaluation of the visual quality of the real visual world, making it closer to the information collected in the quality of vision questionnaires [97]. However, to date, typical questionnaires are passed after contact lenses are prescribed or after intraocular lens or corneal surgery, and rely, to a large extent, on the patient's memory, particularly on evaluations of their current quality of vision in comparison with their previous corrections (i.e. monofocal contact lenses or pre-operatively). The value of the MAS-2EV metric presented here is that it is defined to be performed before final prescription, and allows in situ comparison of prospective corrections, while still experiencing a realistic environment that samples different situations of the patient's visual world (faces, street scenes, theater, driving, navigating a map, reading, halos at night, and stereo tasks).

A goal with the MAS-2EV metric is to aid in the selection of the most suitable correction for a patient. In the current study, the ranking, and hence the optimal correction, is based on a simple addition of parameters, which are blind to the patient lifestyle or preferences. It is conceivable to weight the retrieved parameters with factors accounting for the importance of time spent by the patients on near, far, daytime, or nighttime activities, requiring stereovision or benefiting from constant visual quality. The information from these weights could be extracted, from lifestyle questionnaires or devices attached to the patient that measure light exposure and work distance over a period of time[80].

The MAS-2EV metric has been applied in patients both wearing real contact lenses (monofocal and multifocal, and their combinations) and the SimVis Gekko representing monofocal and bifocal contact lenses. The simulation of the exact design of the real contact lens was not attempted. Even with this approximation, the visual experience of the patient with SimVis Gekko with all corrections (bilateral far monofocal, bilateral bifocal, monovision, and modified monovision) captures to a large extent that provided by similar corrections in the contact lens form, as revealed by the similarity of the MAS-2EV–based parameters obtained with SimVis and CLs (Fig. 7.5, 7.6). At the individual level (Table 7.2-3) the exact ranking of corrections obtained with SimVis Gekko was only strictly the same as with CLs in one subject, although the acceptable corrections (overall performance parameter) were captured similarly by SimVis Gekko and by CLs in 70% of the cases. In the young group, where the study was performed with CLs and SimVis Gekko, performing the MAS-2EV study with 4 CLs based conditions to 2-3 times longer than performing the MAS-2EV with 4 SimVis-simulated conditions (369 vs 164 min per session), as the former requires interchanging of the contact lenses while the latter passes rapidly across the

programmed corrections. Similarly, SimVis Gekko + MAS-2EV can be used to guide the selection of presbyopic corrections in intraocular lens form, allowing the patient to experience the world with those corrections before implantation. The use of the MAS-2EV metric in combination with visual simulators, such as the SimVis Gekko, therefore serves to reduce chair time in contact lens fitting as well as to reduce uncertainties in intraocular lens surgeries.

In conclusion, MAS-2EV is a suitable metric for its use in the clinic due to its high repeatability, high sensitivity, and short administration time (3 min for subject/ condition/correction). Also, the images were designed to be presented in standard displays (or projectors). Further studies are currently underway, including a comparison between MAS-2EV and validated visual quality questionnaires [102,180], evaluation of the MAS-2EV metric in cataractous patients, evaluation of the sensitivity of the metric in a larger population, evaluation of the metric in patients with other visual limitations and pathologies, study of the effect of pupillary dynamics (in particular, its impact on differences between perceptual scores at near and far) and a direct comparison of perceived visual quality with real contact lenses and their specific programmed design in the visual simulator using MAS-2EV.

In the next chapter, we investigated the accuracy of the representation of M-CL designs in SimVis Gekko. For that, comparisons of real and simulated lenses were performed using VA, the MAS-2EV metric, and patient-reported visual quality questionnaires.

Chapter 8

Comparison of vision with a binocular visual simulator and the actual M-CLs in a clinical site

In the current chapter, we used SimVis Gekko to simulate binocular presbyopic correction strategies and compared them with the actual M-CLs. We performed visual performance and perceived visual quality measurements to compare the real and simulated lenses.

This chapter is based on the paper by *Barcala et al. "Comparison of vision with a binocular visual simulator and the actual multifocal contact lenses in a clinical site" submitted to Contact Lens and Anterior Eye (2021)*. The co-authors of the study are Maria Vinas, Sofia Ruiz, Fernando Hidalgo, Derek Nankivil, Tom Karkkainen, Enrique Gambra, Carlos Dorronsoro and Susana Marcos.

The author of this thesis (1) collaborate on the definition of the experiments along with the J&J team and Susana Marcos, (2) performed the measurements from the pilot study, (3) performed the necessary training and support to the optometrists from Centro Boston de Optometría, (4) supervised half of the measurements from the full study, (5) collect the data, (6) analyze the data and (7) prepared the manuscript (in collaboration with Susana Marcos).

This work was presented as an oral contribution at the Association for Research in Vision and Ophthalmology (ARVO) annual meeting (May 2020) celebrated remotely.

8.1. Introduction

This chapter describes some clinical measurements performed with SimVis Gekko simulating M-CLs. To provide some context of the clinical environment during this study, it is worth revisiting some ideas already addressed in chapter 1. In particular: (1) The low penetration of M-CLs (8-16% [19,20]); (2) Patients can achieve high satisfaction with M-CLs (for example, when M-CLs are fitted, they are prescribed 3.6 times more than monovision lenses [20]); (3) Fitting M-CLs generally requires a strong time commitment from the doctor and patient - the selection of the distance and addition power is performed over a three-day period [86] and the average success rate for prescribing M-CLs is 67-83% after three months [20,87]-.

Simultaneous Vision Simulators have been evaluated in previous studies. One study incorporated a monocular on-bench SimVis channel into a multi-channel AO visual simulator, and cross-validated for simulation of commercial multifocal IOLs (M-IOLs), against a simulator based on a spatial-light-modulator and the physical lens placed in a cuvette [91,92]. Very recently [113], the same monocular on-bench SimVis channel was used to represent M-CLs (center-near aspheric designs, of low, medium and high adds) and through-focus quality was measured in subjects with actual and simulated M-CLs. Both, through focus optical (on bench and in vivo) and visual (*in vivo*) quality measurements captured the expected extended depth of focus with increasing add. Monocular defocus curves with the monocular on-bench SimVis-simulated and the actual M-CLs on eye showed significant similarity, demonstrating that monocular on-bench SimVis captured the through-focus optical and visual performance of the M-CL in most of the subjects.

An advantage of the Sim+Vis simulations over other approaches is its see-through nature, which has allowed the development of a compact binocular instrument, suitable for tests in the clinic. The SimVis Gekko has been demonstrated in patients before intraocular lens surgery with diffractive M-IOL, comparing pre-operative simulated through-focus visual acuity pre-operatively with that post-operatively with the implanted IOLs [92].

Besides, the Multifocal Acceptance Score to Evaluate Vision (MAS-2EV) (chapter 7) is well suited to evaluate patient’s visual quality with multifocal corrections.

In this paper, we used SimVis Gekko to simulate binocular presbyopic correction with M-CLs. We assessed visual performance and perceived visual quality with M-CLs placed on eye. Both sets of measurements were performed in the clinical environment. M-CLs were fitted in patients according to the manufacturer fitting guidelines. Conversely, the M-CLs were programed in SimVis Gekko, following prior validations on bench and in patients in an AO system, presented earlier. Comparisons of actual and simulated lenses were performed using visual acuity (high-contrast), the MAS-2EV metric, and patient reported visual quality questionnaires.

8.2. Methods

Defocus visual acuity curves (DFVA), visual acuity (VA) at different distances, perceived visual quality (MAS-2EV metric[181]) and visual questionnaires (ProVision [102]) were performed on patients with the SimVis Gekko simulating commercial M-CLs (1-Day ACUVUE® Moist Brand Multifocal, Johnson & Johnson Vision Care, Jacksonville, FL, USA) and the actual lenses on eye.

In a pilot study, DFVA curves were measured with simulated lenses in SimVis Gekko. In a follow-up study, VA at far, intermediate and near distance, MAS-2EV scores and ProVision Questionnaire responses were obtained with the actual M-CLs and the M-CLs represented in the SimVis Gekko. The measurements were obtained in two different sessions on different days, in random order (SimVis Gekko or M-CLs in the first session). Unless otherwise noted, the tests were done binocularly.

8.2.1. Subjects

Ten patients participated in the pilot study (age: 53±4 years; spherical error: -0.19±2.15 D; astigmatism≤0.75 D) and 27 patients participated in the follow-up study (age: 52±7 years; spherical error: -0.74±2.49 D; astigmatism<0.75 D). None of the patients participated in both studies. All patients had good ocular health, except for their refractive errors. Inclusion criteria for the study were: age ranging between 40 and 70 years old; distance spherical equivalent refraction in the range of +4.00 D to -6.00 D in each eye; cylinder ≤0.75 D; required add power between +0.75 D to +2.50 D; and best corrected visual acuity of 20/20-3 or better in each eye. Natural binocular vision was tested using a 4-dot Worth test to discard fusion dysfunction, which was an exclusion criterion. Eye dominance was determined by the +1.00 D blur test.

¡Error! No se encuentra el origen de la referencia. shows the demographic and refractive profiles of the patients, along with the tested lenses in each patient. The optical power for the M-CLs and SimVis Gekko was selected based upon initial selection recommended by the 1-Day Acuvue Moist Multifocal fitting guide [182].

	Subject ID	Age	Gender	Sph. Equiv. (OD/OS)	Lenses Add	Eye Dominance
Pilot study	001	54	M	+3.50 / +1.25	Medium	OS
	002	51	M	-3.75 / -3.75	Low	OS
	003	58	M	-4.00 / -4.25	Medium + High	OS
	004	49	M	+1.00 / +1.75	Low	OD
	005	57	F	-2.25 / -1.75	Medium + High	OS
	006	54	F	0.00 / 0.00	Medium	OS
	007	55	F	+1.50 / +1.00	Medium	OS
	008	53	F	+0.75 / +1.50	Medium	OS
	009	52	M	0.00 / +0.25	Low	OD
	010	55	F	+1.25 / +1.25	Medium + High	OD

Follow-up study	011	59	M	+0.75 / +0.25	Medium + High	OD
	012	56	F	+0.75 / +0.75	Medium + High	OD
	013	55	M	-1.50 / -1.25	Medium	OS
	014	49	F	-2.00 / -2.00	Medium	OS
	015	59	M	+1.75 / +1.75	Medium + High	OD
	016	46	F	-3.00 / -3.25	Low	OD
	017	60	F	-4.00 / -4.00	Medium + High	OS
	018	54	F	-2.00 / -2.00	Medium	OD
	019	48	M	-3.50 / -3.00	Medium	OS
	020	50	M	-3.25 / -3.25	Medium	OD
	021	52	F	+1.50 / +1.50	Medium	OD
	022	67	F	+1.50 / +1.25	Medium + High	OS
	023	53	F	+2.75 / +2.50	Medium + High	OD
	024	55	F	+3.00 / +2.50	Medium	OD
	025	54	F	-0.75 / -1.00	Medium	OD
	026	41	F	-4.75 / -3.00	Low	OD
	027	66	F	+2.00 / +2.25	Medium	OD
	028	48	F	-2.75 / -2.75	Medium	OS
	029	52	F	+1.75 / +1.75	Medium + High	OD
	030	53	M	+0.75 / +0.75	Medium	OD
	031	43	F	-3.75 / -4.00	Low	OS
	032	48	M	-3.00 / -2.50	Medium	OD
	033	53	M	-2.75 / -2.50	Medium	OD
	034	41	F	-1.00 / -1.25	Low	OS
	035	61	F	+3.75 / +3.75	Medium + High	OD
	036	48	M	+1.00 / +1.00	Low	OD
	037	42	F	-4.75 / -4.50	Low	OS

Table 8. 1 *Sample's profile, with their subject ID, age (years old), gender (F: female, M: male), spherical equivalent (Sph. Equiv.) for the right (OD) and left (OS) eye, the addition (add) needed for 1-day moist lenses and the ocular dominance.*

The measurements in the pilot study were performed at the Visual Optics and Biophotonics Lab (Consejo Superior de Investigaciones Cientificas, CSIC) The measurements of the follow-up study were performed in Centro Boston de Optometría, Madrid. The protocol and experiments of both studies conformed to the tenets of the Declaration of Helsinki, with protocols approved by CSIC Ethics Committee. The subjects signed an informed consent after receiving an explanation of the nature and implications of the study.

8.2.2. Multifocal Contact Lenses (M-CLs)

The M-CLs used in this work were 1-Day ACUVUE® Moist Brand Multifocal (Johnson & Johnson Vision Care, Jacksonville, FL, USA). The lenses are Etafilcon A, center-near aspheric with a hybrid back curve design with standard geometry parameters (Base Curve: 8.4 mm, Total diameter: 14.3 mm) and are daily disposable. Distance power ranged from -6.00 to +4.00 diopters, in 0.25 D steps, with three different add powers: low, +1.25 D; medium, +1.75 D and high, +2.50 D. Further details on the power profiles can be found in a previous publication: Vinas et al. 2020 [113].

In the pilot and the follow-up studies, the actual and simulated M-CLs were fitted following the manufacturer's guide [182]. No refraction enhancement over the selected base power was performed. Patients were examined under the slit-lamp before and after measurements, to check for their eligibility and to confirm no effect of lens wear during the study. A lens settling time of 10 minutes was allowed before measurements. Evaluation of the lens centration, primary gaze movement, up-gaze movement, and tightness was carried out following routine standard practice [183].

8.2.3. SimVis Gekko and simulated CLs

The SimVis Gekko™ v1.0 (2018 version) visual simulator (see chapter 2) was used in this study to simulate non-invasively the corresponding M-CLs (1-Day Moist; Low, Medium, and High add) for a 4-mm pupil diameter. In a previous publication [113] we showed the temporal profile for the simulated 1-Day Moist M-CLs in the Sim+Vis technology, we validated it on bench as well as reported measurements of VA in presbyopic patients with the Sim+Vis technology incorporated in a channel of an AO System.

The calibration of the optical power was checked weekly performing the procedures explained in chapter 2. No recalibration of the SimVis Gekko was performed during the study.

8.2.4. VA measurements

ETDRS 2000 series high contrast retro-illuminate charts at a distance of 4 m from the patients were used to measure the baseline VA of patients (to check their inclusion criteria), VA in DFVA curves measurements (pilot study) and to measure VA at far in both studies. Guillon-Poling charts were used to measure intermediate (64 cm) and near (40 cm) VA in both studies [184]. Measurements were performed binocularly. Three different charts were interchanged during measurements to avoid learning effects. LogMAR VA corresponding to the minimum legible letter was recorded with the best correction at far, and (with best far correction in place) for intermediate and near distance with the multifocal lenses (both actual and simulated).

Charts luminances and room illumination were controlled and checked before each measurement using a L-858D-U Light Meter (Sekonic Corporation, Japan). Far ETDRS chart luminance was kept between 181 – 208 cd/m2 and near charts luminance was kept between 222 to 275 cd/m2 and the room illuminance between 394 and 597 lux.

8.2.5. MAS-2EV

The Multifocal Acceptance Score to Evaluate Vision (MAS-2EV™) is a new metric to evaluate the global quality of vision presented in chapter 7. The metric comprises five perceptual scores (PS) of multi-stimuli images of day and night scenes, at far (4 m) and near (40 cm) distance, and a stereovision target at near. The patient gives perceptual scores [177] according to his/he

perceived image quality of the visual scenes through a correction, from very blurred (PS:0) to very sharp (PS:10).

The stimuli of MAS-2EV were displayed on a standard monitor screen of 42" for far distance (4 m), and on standard iPad screen of 9.8" at near distance (40 cm). For far distance, the brightness of the displays was not changed between day and night conditions. For near distance, the brightness of the iPad was changed, for day condition it was at the maximum level (218.07±0.62 cd/m^2) and for night condition was at the minimum (1.99±0.006 cd/m^2).

Additionally, near stereo-acuity was measured at 40 cm. Random-dot anaglyphs (observed through cyan/red glasses) with seven in-depth Snellen-E letters were presented with different orientations and different crossed disparities, ranging from 400 to 50 arcsec. Stereo-acuity was converted to a 0 (disparities above or equal to 400 arcsec) to 10 (disparity of 50 arcsec) scale.

The sequence of MAS-2EV measurements were near stereopsis, far and near daylight scoring, 4 minutes of dark adaptation, far and near night scoring.

8.2.6. ProVision questionnaire

The CLUE^{TM} questionnaire is a standard questionnaire developed by Johnson & Johnson [102]. In this study, responses were limited to the twenty-two questions of the CLUE^{TM} questionnaire that address quality of vision (and not other domains of CLUE^{TM} such as comfort and handling). As the questions were selected specifically for this study, we referred to the questionnaire as a standard Patients Reported Outcomes Vision (ProVision) questionnaire. Patients completed the questionnaire after removal of M-CLs fitting or SimVis Gekko, at the end of each session.

¡Error! No se encuentra el origen de la referencia. shows the 22 questions (left column), where questions in green were classified for this study as positive (scored between 1 to 5) and questions in black are classified as negative (scored from -1 to -5). There are five different possible answers: Strongly Disagree; Disagree; Neither agree nor disagree; Agree; Strongly Agree. Questions that were answered as "Not applicable" were not quantified. For this study, the overall ProVision questionnaire response (from weighted individual responses) can range from +50 (if all positive questions were scored as +5 and negative questions as -1) to -38 (if all positive questions were scored as +1 and negative questions as -5).

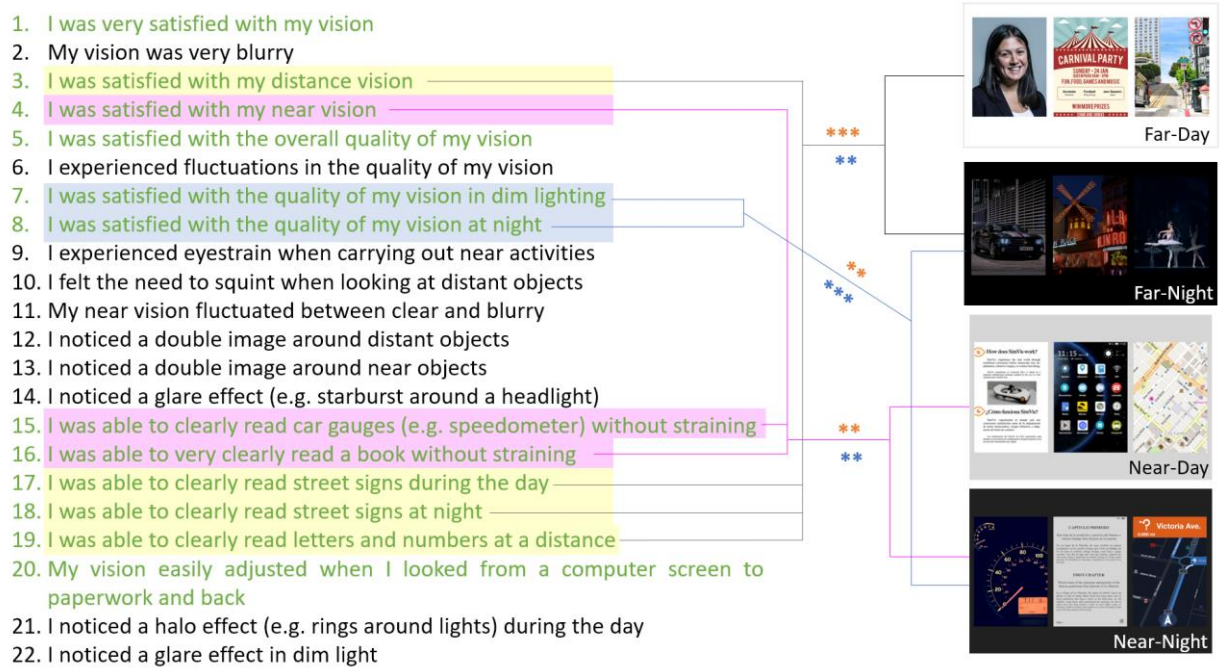

Figure 8.1 *ProVision questions (left column) with the positive (green) and negative questions (black) and MAS-2EV images (right column) from top to bottom: Far-Day; Far-Nigh; Near-Day and Near-Night. Highlighted ProVision questions were correlated (**p<0.005; ***p<0.0005) with some MAS-2EV scores, specifically for far distance, near distance and night illumination, both with actual M-CLs (blue asterisks) and SimVis Gekko (orange asterisks).*

8.2.7. Measurements

Pilot study: DFVA, MAS-2EV & Vision Questionnaire through SimVis Gekko simulated M-CLs

In the pilot study, measurements were performed on 10 patients (Table 8.1) using the SimVis Gekko only. The purpose of this study was to characterize the full DFVA curves with the M-CLs and evaluate the correspondence between MAS-2EV and ProVision questionnaire. The tests were administered at the Visual Optics and Biophotonics Lab by an experienced optometrist.

LogMAR VA was measured using a VA ETDRS 2000 chart (as described in Section 8.2.4) at 4 m, changing the vergence with trial lenses placed in the SimVis Gekko in a range from -4.50 D to +2.00 D in 0.50 D steps [185], relative to the far distance correction, also corrected by trial lenses in the device. In addition, logMAR VA was measured using Guillon-Poling charts at intermediate (64 cm) and near (40 cm) distances (as described in Section 8.2.4).

MAS-2EV (day/night; far and near) was measured using MAS-2EV metric protocols [181] (chapter 7). Finally, the subject responded to the ProVision questionnaire (Section 8.2.6) after the removal of the SimVis Gekko.

Follow-up study: VA at different distances, MAS-2EV & Vision Questionnaire with SimVis Gekko simulated and Real M-CLs

In the follow-up study, measurements were performed on 27 subjects (Table 8.1) in two different visits. In one visit the patient was measured with the SimVis Gekko, and in another visit with the M-CLs on eye. The order of the visits was randomly assigned. The visits were on average separated by a week (7±1 days). The tests were administered in an optometry clinic ("Centro Boston de Optometría") by two experienced optometrists.

The patient's sphero-cylindrical refraction was corrected with the far distance power of the M-CLs (in the measurements with CLs) or by trial lenses placed in the dedicated slot in the SimVis Gekko device (in the simulated M-CLs).

LogMAR VA was measured at distance (4 m), intermediate (64 cm) and near (40 cm), using ETDRS 2000 and Guillon-Poling charts (as described in Section 8.2.4), followed by MAS-2EV (with M-CLs or SimVis Gekko) scoring. The ProVision questionnaire was completed after removal of M-CLs/SimVis Gekko), as per protocols described above.

8.2.8. Data analysis

Depth of Focus (DoF), defined as the dioptric range for which VA is 0.2 logMAR [186] or better was obtained for the DFVA curves performed in the pilot study.

LogMAR VA at far (4m), intermediate (64 cm) and near (40 cm) was measured both with SimVisGekko and with the actual M-CLs. Comparisons between simulated and actual M-CLs were performed in terms of logMAR differences (95% confidence intervals and paired t-test).

MAS-2EV modulus (chapter 7) was calculated from scores obtained with the real and SimVis Gekko-simulated M-CLs. The ProVision questionnaire mean scores were also calculated for responses obtained with the actual and SimVis Gekko-simulated M-CLs. Differences between scores obtained with simulated and M-CLs were calculated, and the statistical significance of the differences were obtained using paired-sample-ttest ($p<0.05$ significance level).

Linear correlations were analyzed between VA at far and near distance and MAS-2EV mean PS for far and near (averaged for day and night), both for CLs and SimVis Gekko. Linear correlations between MAS-2EV and ProVision questionnaires were analyzed for average scores, as well as for far, near, night and day specific questions. The statistical significance of the linear correlation was tested using the Pearson correlation coefficient ($p<0.05$ significancy level).

8.3. Results

8.3.1. DFVA curves with SimVis Gekko-simulated M-CLs

Figure 8.2 shows the DFVA and VA results for all subjects. Data are displayed by rows, according to the magnitude add of the SimVis Gekko-simulated lenses (low add in both eyes: upper row, figure 8.2A; medium add: middle row, figure 8.2B; medium add in the dominant eye and high

add in the non-dominant eye: bottom row, figure 8.2C). The dotted line represents the logMAR DFVA and the isolated diamonds represent the logMAR VA measured placing the target at different distances: far (4 m = 0D), intermediate (64 cm = -1.50 D) and near (40 cm = -2.50 D). On average across subjects, the VA difference between the isolated VA and the DFVA was -0.03±0.04, 0.03±0.01, 0.00±0.00 at far distance, 0.04±0.14, 0.03±0.10, 0.02±0.00 for intermediate and -0.08 ±0.16, -0.01±0.14, -0.05±0.05 for near distance, for low, medium and medium+high add lenses simulation respectively.

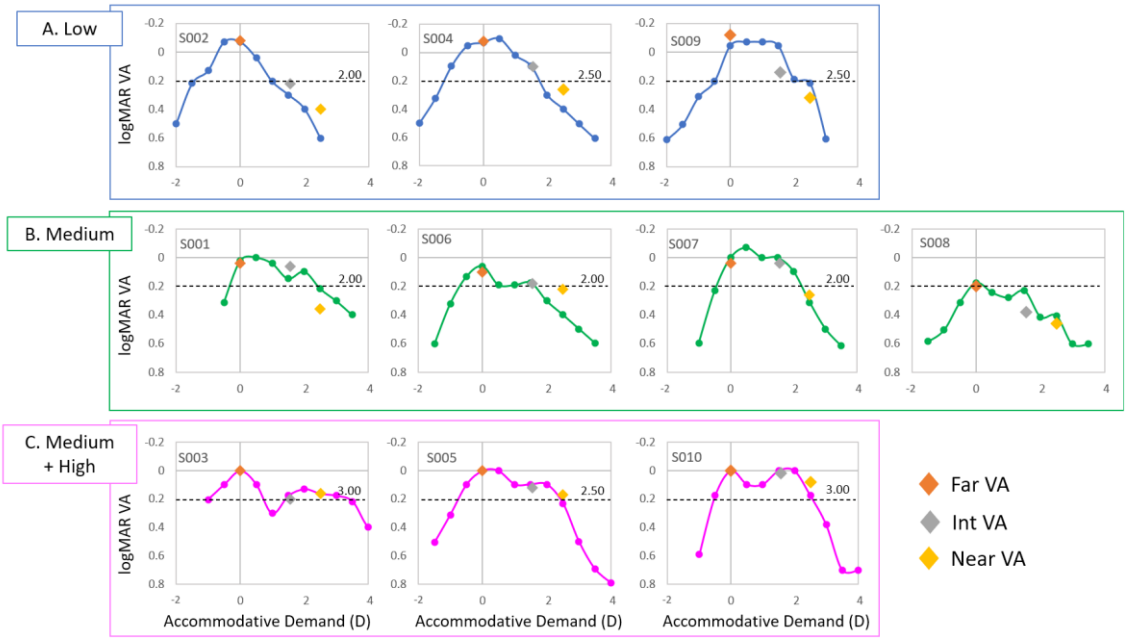

Figure 8.2 *DFVA and VA measurements obtained with the SimVis Gekko simulating M-CLs: upper row, low add in both eyes; middle row, medium add in both eyes; bottom row, medium add in dominant eye and high add in non-dominant eye. The solid lines (and same-colored circles) represent logMAR measurements performed with vergence induced with trial lenses. The isolated diamonds represent the VA measured at far (4 m), intermediate 64 cm) and near (40 cm) distances. The dashed horizontal black lines represent logMAR VA=0.2. Depth of focus (DOF), defined as the dioptric range for which VA is above this line, is indicated by the value on the right above the line (in D).*

The DFVA curves for low add lenses show a single peak centered between +0.50 D and -0.50 D, while the medium add and medium+high add lenses generally produce two differentiated peaks, with the far focus centered between -0.50D and 0.00D, and the intermediate/near peak is centered between -1.50 and -2.00 for medium add, and between -2.00 and -2.50 D in medium add+high add lenses. VA at the best focus was above 0.00 logMAR VA in all cases, except for S#6 and S#8 with medium add lenses.

DOF was on average 2.33±0.29 D for the low add, 2.00±0.00 D for the medium add and 2.83±0.29 D for the medium+high add. S#8 was excluded from the average, as the entire range was below 0.2 logMAR VA.

8.3.2. VA with actual M-CLs vs SimVis Gekko-simulated M-CLs

Figure 8.3 shows some representative examples of binocular VA at far, intermediate, and near distance, with SimVis Gekko simulated lenses (closed circles) and real M-CLs (asterisk). In general, there is a similar variation of VA with distance with simulated and actual M-CLs, with some patient showing a very close match in absolute values (i.e., S#14, S#21 and S#34).

On average, the VA achieved with the simulated-CLs were -0.08±0.10 at far distance, 0.06±0.06 at intermediate distance and 0.12±0.06 at near distance. The VA values obtained with the fitted CLs were -0.13±0.07 at far distance, -0.06±0.08 at intermediate distance and 0.03±0.07 at near distance. The average logMAR VA difference between the simulated and the actual MCLs was: for far distance, 0.07±0.01, 0.07±0.01 and 0.04±0.08 for the low, medium and medium+high add respectively; for intermediate distance, 0.15±0.03, 0.08±0.01 and 0.10±0.01 for the low, medium and medium+high add respectively; for near distance, 0.09 ±0.00, 0.09±0.03 and 0.07 ±0.00 for the low, medium and medium+high add lenses respectively.

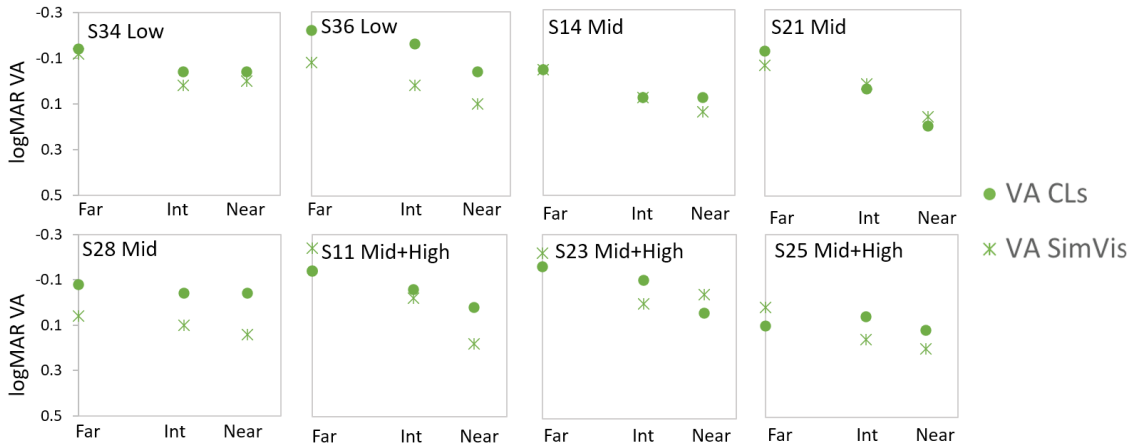

Figure 8.3 *Some subject's examples for the binocular logMAR VA measurements with SimVis Gekko (asterisk) and M-CLs (spot) at far, intermediate, and near distance.*

Mean logMAR VA difference between M-CLs and SimVis Gekko was estimated with the 95% confidence intervals (Table 8.2) for all subjects. Mean VA difference (simulated - actual) was 0.08±0.01 logMAR VA for far, 0.12±0.01 logMAR VA for intermediate and 0.1±0.01 logMAR VA for near distance, averaged across patients. Although these VA differences are statistically significant ($p<0.005$, paired-sample t-test) at all distances, performance with simulated lenses tended to mimic the salient features of performance measured with M-CLs. Namely, acuity was better at distance than at intermediate and acuity was better at intermediate than at near.

	Alpha	Mean	StdError	Sample	Lower Conf.Lim.	Upper Conf.Lim.	t-test
Distance	0.05	0.0785	0.0122	27	0.0547	0.1024	p<0.005
Int.	0.05	0.1200	0.0133	27	0.0939	0.1461	p<0.005
Near	0.05	0.1015	0.0107	27	0.0806	0.1224	p<0.005

Table 8.2 *Mean Estimates and 95% Confidence Intervals for (Binocular, High Luminance, High Contrast) logMAR Visual Acuity. StdError: standard error, Conf.Lim.: confidence limits.*

8.3.3. MAS-2EV and ProVision questionnaire with SimVis Gekko-simulated M-CLs (pilot study)

Overall ProVision questionnaire scores were 22.67±8.62 with the low add lenses, 14.74±4.99 with the medium add lenses, and 14.33±17.56 with medium+ high add lenses.

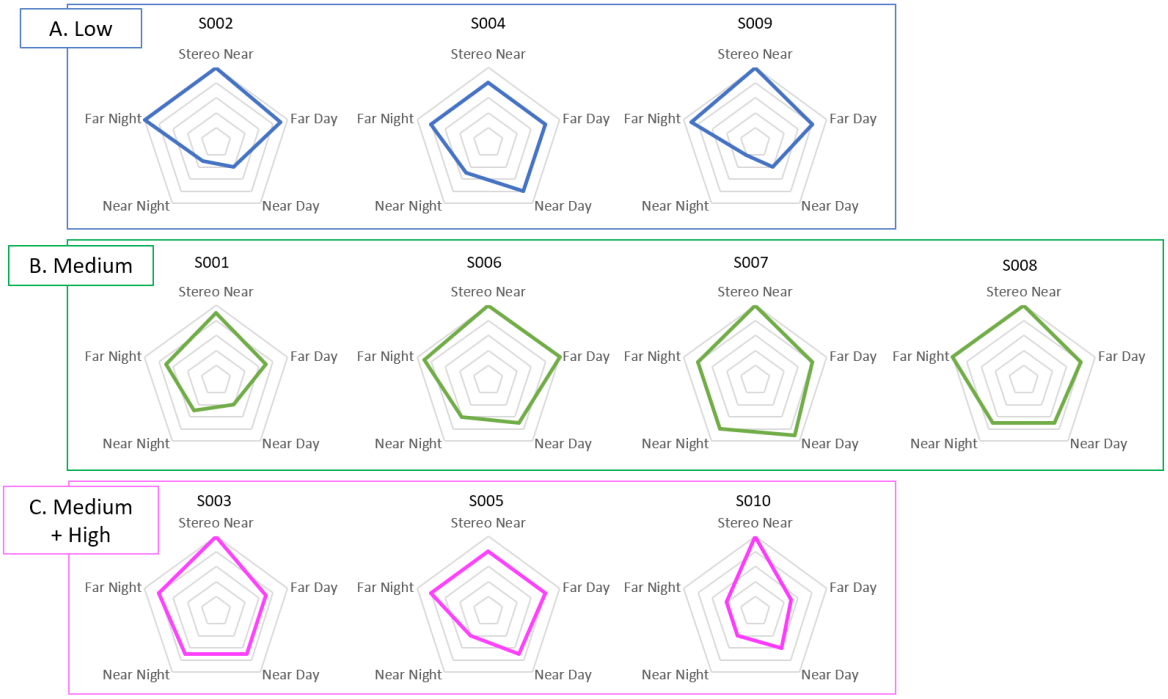

Figure 8.4 *MAS-2EV questionnaire for all subjects with the recommended simulation on SimVis Gekko: subjects with low add lenses (**A**, in blue), with medium add lenses (**B**, in green) and with medium and high add lenses (**C**, in pink).*

Figure 8.4 shows the MAS-2EV polygons for all subjects. Simulated low add M-CLs show relatively higher scores at far distance (8.67±0.82 PS, averaged across patients), at low scores at near (2.07±2.07 PS), consistent with an almost monofocal performance. Conversely, scores at near increase with medium (6.63±1.60 PS) and medium+high add (5.83±1.47 PS) simulated M-CLs, at the expense of reducing the score at far (8.38±1.19 PS and 6.67±1.75 PS, respectively).

8.3.4. MAS-2EV with actual M-CLs vs SimVis Gekko-simulated M-CLs

Figure 8.5 shows some examples of the MAS-2EV polygons both with actual M-CLs (in blue) and SimVis Gekko-simulated M-CLs (in orange). In some subjects MAS-2EV polygons with simulated lenses differed from those with actual lenses (S020, S021; S022 or S035, with a maximum intra-subject MAS-2EV Modulus difference of 3.40±2.19), while in other subjects there was a close match (S016, S017 or S031, with a minimum MAS-2EV Modulus difference of 0.00±1.00). S013 and S024 showed the same polygon shape with actual and simulated lenses, but different size.

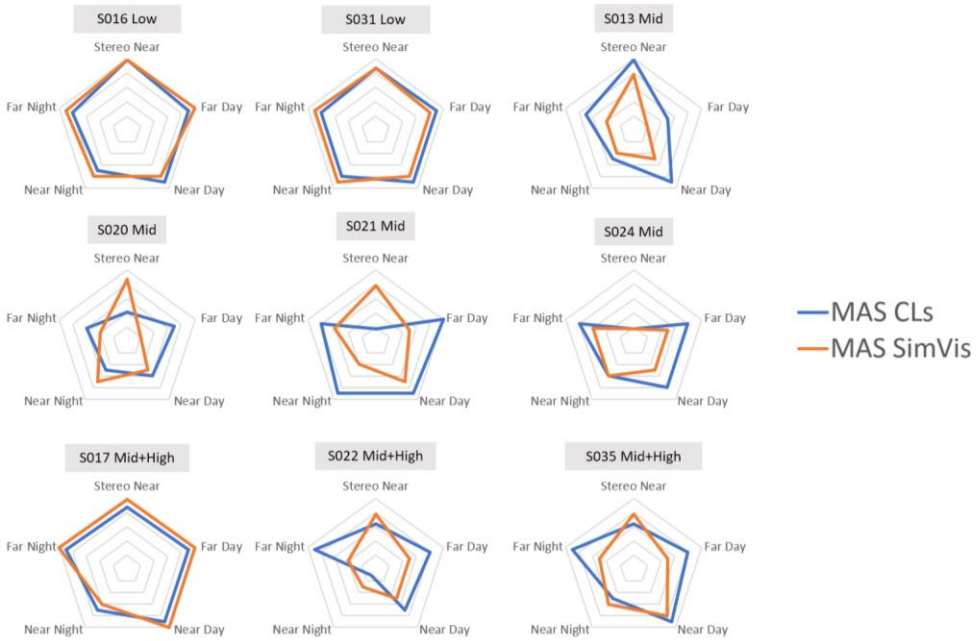

Figure 8.5 *Some examples for the binocular MAS-2EV polygons measured with SimVis Gekko (orange) and M-CLs (blue) for the low add lenses (low), medium add lenses (mid), and the combination of the medium and high add lenses (mid+high).*

Figure 8.6 shows the MAS-2EV Modulus excluding stereovision) for all measured patients, with the actual (blue) and the simulated M-CLs (orange) grouped by lens add. Standard deviations across day/night/near/far scores are represented as dashed (negative) bars.

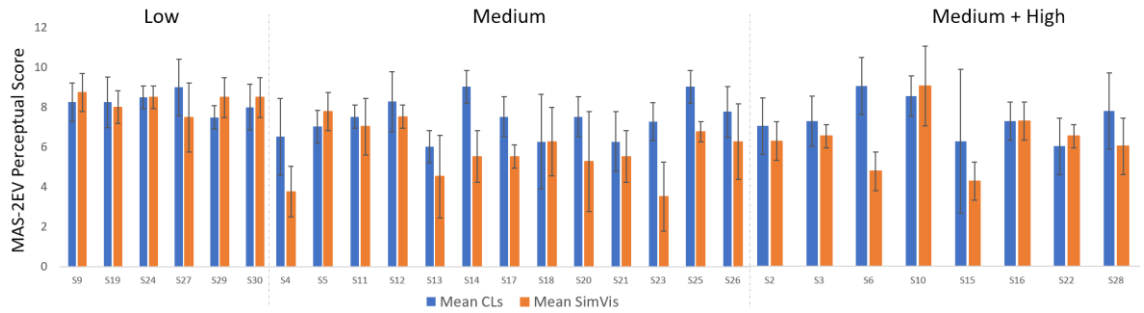

Figure 8.6 *Average perceptual score (all scores from MAS-2EV excluding stereovision) in all subjects, with M-CLs (blue) and simulated lenses (orange). Standard deviations are represented as black lines.*

The average PS for MAS-2EV with actual and simulated low add M-CLs were not statistically significantly different (8.25±0.99 and 8.29±1.01, respectively; p=0.91; paired-sample t-test). Higher add lenses produced lower average PS, with PS scores higher for actual M-CLs than for the simulated M-CLs: avg PS 7.37±1.18 for actual M-CLs and 5.77±1.37 for simulated M-CLs, for the medium add (statistically significantly different, p<0.001), and avg PS 7.38±1.62 for actual M-CLs and 6.31±1.05 for simulated M-CLs, for the medium+high add (not statistically different, p=0.1). PSs are consistently lower for night than day for all lens designs, both for actual M-CLs (10.50% lower) and simulated M-CLs (4.60% lower). However, the discrepancy between actual and simulated M-CLs is highest for day conditions (8.13±0.96 PS for actual M-CLs and 6.69±1.66 PS for simulated M-CLs).

There was a significant positive correlation of the metric between the actual M-CL and the SimVis Gekko simulator across all conditions and subjects ($p<0.01$; $r= 0.347$) within confidence intervals of ±2.80PS (Bland-Altman). 81.48% of subjects report a MAS-2EV score with the simulated M-CLs that is within 2 PS of the MAS-2EV score with actual M-CLs and a 62.96% within 1 PS.

8.3.5. ProVision Questionnaire with actual M-CLs vs SimVis Gekko-simulated M-CLs

ProVision questionnaire average scores are represented in Figure 8.7 for all subjects (organized by lens type) comparing actual M-CLs (blue bars) with simulated M-CLs (orange bars). Except for a few exceptions (i.e., S20, S32, S33, S15, S22) there was a very good correspondence between the ProVision scores with actual M-CLs and with simulated M-CLs (2-17 minimum to maximum points of difference). When discrepancies occur, in the ProVision questionnaire there was no bias towards actual or simulated M-CLs.

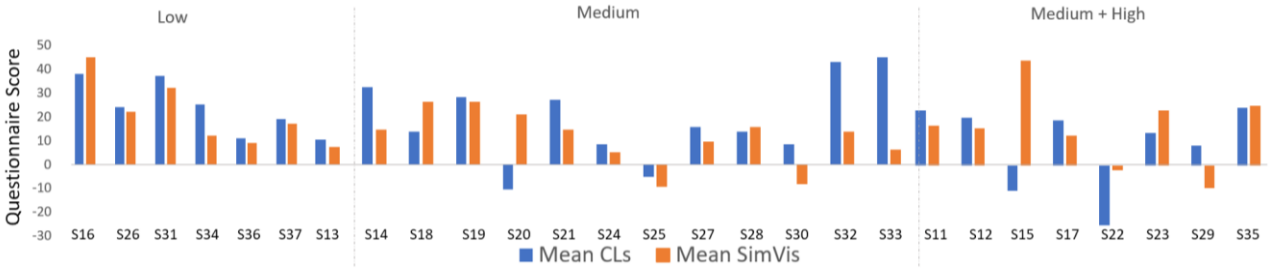

Figure 8.7 *ProVision questionnaire responses for all subjects, organized by lens simulation, wearing M-CLs (blue) and SimVis Gekko (orange).*

On average, both actual and simulated M-CLs showed the same trends. There was a better ProVision overall perception with the low add lens (25.67±10.42 PS for M-CL, 22.83±13.56 PS for SimVis Gekko), than with the medium lens (16.92±16.04 PS for M-CL, 10.46±10.60 PS for SimVis Gekko) or with the medium+high add lenses (8.63±16.95 PS for the actual lens, 15.00±15.74 PS for the simulator).

For the vision questionnaire responses, there was no statistically significant differences between actual and simulated lenses for neither add ($p=0.33$ for low add; $p=0.19$, for medium add; $p=0.44$, medium+high add). 81.48% of subjects report ProVision score with simulated M-CLs that is within 17.6 PS (equivalent to 2 PS in the MAS-2EV scale) of the ProVision score with actual M-CLs, the same percentage of subjects as in the MAS-2EV metric. 51.85% of subjects report a difference within an 8.8 PS (equivalent to 1 PS in the MAS-2EV scale).

8.3.6. Correlations between VA and MAS-2EV

VA measurement is the standard method to assess the quality of vision with M-CLs, even it is known that high contrast VA is a limited descriptor of the quality of vision. In comparison, MAS-2EV is a subjective metric to measure patient's perceived visual quality, something rarely used in the clinic. Figure 8.8 shows the measured logMAR VA versus the subjective scores obtained with

MAS-2EV, for far (spots) and near distance (asterisks), both with the fitted M-CLs (blue) and its simulation (orange), including all measured subjects (pilot and full studies). LogMAR VA and MAS-2EV scores were not correlated at far vision for neither actual M-CLs (p=0.49 r=-0.14) or simulated M-CLs (far p=0.96 r=0.008), nor at near vision with M-CLs (p=0.19 r=-0.2488) but it was significantly correlated at near vision with simulated M-CLs (p=0.02 r=-0.39).

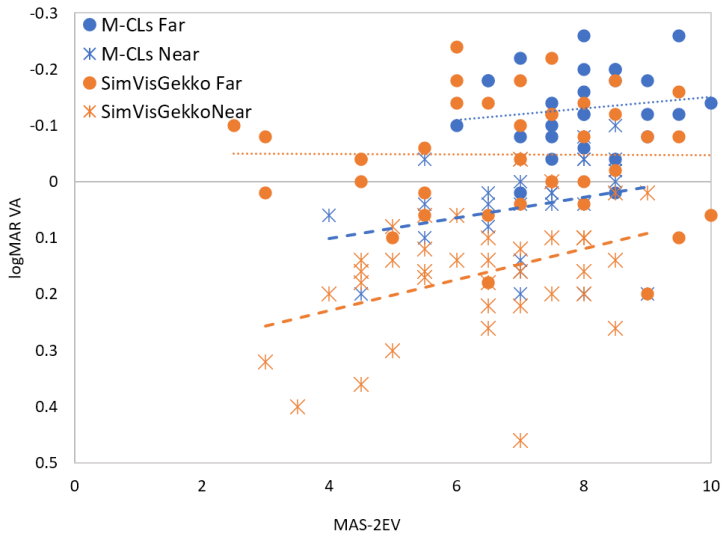

Figure 8.8 *Measured logMAR VA, represented in Y axis, versus the score recorded with the MAS-2EV metric, in the X axis, for all subjects (pilot and follow-up study) at far distance (spots) and near distance (asterisks) measured with the actual M-CLs (blue) and its simulation (orange) with their correlation.*

8.3.7. MAS-2EV and ProVision questionnaire correlations

Figure 8.1 (methods section) shows correlations between MAS-2EV scores and ProVision questionnaire scores including all measured subjects (pilot and full studies). MAS-2EV Modulus and ProVision questionnaire average score for all subjects was highly correlated (p=0.0037 r=0.5387 for actual M-CLs; p=0.037 r=0.3448 for simulated M-CLs).

ProVision questionnaire scores related with far distance vision (questions in yellow in Figure 8.1) were highly correlated with the mean MAS-2EV scores for far distance for day and night conditions (M-CL p=0.0074 r=0.5124; simulated M-CLs p=0.0001 r=0.6137). ProVision questionnaire scores related with near distance vision (questions in pink in Figure 8.1) were highly correlated with the mean MAS-2EV scores for near distance (M-CL p=0.0063 r=0.5211; simulated M-CLs p=0.0025 r=0.4879) for far distance for day and night conditions. ProVision questionnaire scores related with night vision (questions in blue in Figure 8.1) were highly correlated with the mean MAS-2EV scores for night vision at near and far (M-CL p=0.0005 r=0.6336; simulated M-CLs p=0.0077 r=0.4367).

8.4. Discussion

Multifocal contact lenses (M-CLs) are increasingly used for presbyopia correction. Selecting the optimal correction is a challenging procedure that entails long chair time and trial and error. Simultaneous visual simulators that allow the patient to experience vision with different

multifocal designs non-invasively could reduce the number of lenses tested on eye and therefore facilitate M-CL prescription.

In this study, we investigated the accuracy of representation of M-CL designs in a binocular simultaneous vision simulator operating under the principle of temporal multiplexing (SimVis Gekko, 2EyesVision) comparing visual perception and performance in patients with the simulated lenses and with the actual M-CLs on, in a clinical setting. VA measurements at different distances, MAS-2EV metric and a standard questionnaire were performed and different were analyzed.

Performance of actual M-CLs

Previous studies have investigated the same rotationally symmetric center near M-CLs used in the current study (1-day Acuvue Moist, Johnson & Johnson). A study measuring visual performance of the lens on eye after one week of wear in 57 presbyopic subjects [187] reported logMAR VA of -0.05 at far distance, 0.02 at intermediate and 0.12 at near distance. Another study [188] analyzed the visual performance on 275 patients after ten days of wearing the M-CLs reported logMAR VA values of −0.09 ± 0.1, −0.07 ± 0.08 and 0.04 ± 0.10 for far, intermediate and near distance respectively. The VA results obtained in this study (-0.13±0.07 at far, -0.06±0.08 at intermediate and 0.03±0.07 at near distance) compared well with the VA range of previous literature.

A previous study in our laboratory also investigated the same M-CLs. Vedhakrishnan et al. 2021 [189] compared the visual performance of these M-CLs with that obtained with the M-CLs simulated in a Spatial Light Modulator in a laboratory Adaptive Optics. Seven subjects, with paralyzed accommodation, reported monocular VA values with the M-CLs on eye of -0.05, 0.12 and 0.37 for far, intermediate and near distance respectively. In another recent study Vinas et al 2020 [113] measured DFVA curves in patients monocularly fitted with the M-CLs and through the Sim+Vis simulated lenses in an tunable lens incorporated in a testing channel of the Adaptive Optics visual simulator. The reported VA values with the fitted M-CLs were 0.12, 0.15 and 0.09 at far, intermediate and near distance respectively.

As in previous studies, we found the highest DOF increase with the higher add. This effect of the M-CLs depth-of-focus (DOF) expansion with increasing near addition was observed in previous studies with presbyopic subjects and young subjects with paralyzed accommodation. However, our DOF values (Figure 8.2) were slightly higher than those reported in previous studies. Potential reasons for the higher DOF could be the presence of some residual accommodation (as subjects with low add lenses, i.e., younger group presented a higher-than-expected DOF), and the effect of higher order aberrations. Unlike Vedhakrishnan et al and Vinas et al studies, the current study was performed binocularly. Binocular measurements could, on the one hand, stimulate residual accommodation as the system allowed for convergence and pupil constriction [6] and, on the other hand, a slight offset in far refraction correction could produce some monovision [67]. The pupil diameter was not measured in this study, and it could play and important role both in the

relative effect of the eye's native aberration on the performance of the M-CLs and on convergence.

Comparison of actual vs simulated lenses

The pilot study showed that there was no systematic bias in the defocus curves measured with defocus induced with trial lenses with respect to those measured using proximity targets. In the follow-up study M-CLs VA, MAS-2EV scores and ProVision questionnaire simulations were directly measured (with actual and simulated M-CLs) at far, intermediate and near distances. On average, the differences in VA between the simulated and the actual M-CLs were between 4 to 6 logMAR VA letters. The differences were lower for far distance (0.08±0.01) than for intermediate and near (0.12±0.01 and 0.10±0.01, respectively).

In a previous study, M-CLs were simulated as a spatial phase pattern in an SLM, the average differences in VA between actual and simulated M-CLs were -0.01, -0.03 and -0.1, for far, intermediate and near, respectively, for a 5-mm pupil diameter [189]. The differences were negligible with a small bias towards a better performance with the SLM. Subjects' pupils were dilated, and patients performed all the measurements through an artificial 5-mm pupil. A potential reason for the lower discrepancy is the constant pupil for actual and simulated CLs. Vinas et al using SimVis in an Adaptive Optics system reported differences of 0.02, 0.04, 0.08. In that study the Sim+Vis M-CLs were programmed for 4-mm, and an artificial pupil of 4-mm allowed measurements with both actual M-CLs and Sim+Vis-simulated M-CLs to be performed with the same pupil diameter. However, that the improved VA values with simulated-MCLs in our study (-0.08 at far distance, 0.06 at intermediate and 0.12 at near distance) compared to those found by Vinas et al [113] (0.14 logMAR VA at far, 0.18 at intermediate and 0.17 at near distance) could be due to binocular summation, as our measurements were done binocularly [190] and improved correction of dynamic effects in the tunable lens [130].

The observed trend of slightly better VA with M-CLs than with SimVis Gekko may be due to a range of known differences between the two. First, it should be noted that the SimVis Gekko lenses are programmed based on the theoretical M-CL power profile. There are several factors that may cause deviations from the theoretical phase/temporal pattern representation of the lenses, including CLs conformity to the cornea, contributions of the tear lens, and CL decentrations. In a center-near M-CL design, CL decentration may improve distance performance at the cost of reduced near performance.

Second, an anticipated source of difference between actual and simulated M-CL is pupil diameter. While the study was performed with natural pupils to represent a natural condition, the pupil diameter as well as its variation between light conditions, and convergence [191] is expected to vary across individuals, potentially exposing the subjects with an ample range of pupil diameters in the actual CLs condition. However, the M-CLs were programmed for a fixed pupil diameter of 4 mm in all conditions. Future developments may incorporate adjusting the pupil in the SimVis Gekko or matching the programmed lens with the natural pupil diameter of the subject, in each condition.

On the other hand, subjects reported a more stable vision with the simulator than with the CLs. Variability in visual performance with M-CL has been typically associated with CL decentration (typically 0.50 mm), and this may occur more frequently after blinking, and be affected by the lens design, base curvature and material properties [192]. Given the design of M-CL, lens decentration alters the effective lens area for far and near, with fluctuations affecting either positively or negatively visual performance during the visual task [193]. Unlike previous studies using a tumbling E letter (0.5 second/trial) [189], the methodology used in the current study with clinical eyecharts does not limit the time allowed to perform the task. Shifts in CL centration during the letter reading task may allow subjects to improve measured VA.

MAS-2EV

Quality of vision is multifactorial. Observers experience and must operate under a wide range of visual conditions (luminance, pupil diameter, etc…) and visual scenes [96]. It is recognized that high contrast VA is a limited descriptor of the quality of vision. Besides, the complexity and unfamiliarity of multifocal vision [95] require more comprehensive evaluation methods. Traditionally quality of vision is clinically assessed through questionnaires given to the patient to report his/her comfort and performance in different situations, relying on the patient's memory and subjective reporting. There is an ample range of visual quality questionnaires, generally adapted to specific eye conditions or treatments. The questions of the ProVision questionnaire, extracted from the CLUETM questionnaire developed by Johnson & Johnson, were selected specifically to assess vision with multifocal corrections [102], with questions referring to quality of vision in situations/visual tasks at far and near, and day and night. The images in the MAS-2EV platform [181] represent a range of visual situations (faces, street scenes, theater, driving, navigating a map, reading, halos at night, and stereo tasks) compatible with the ProVision questionnaire, so that the patients could respond to the questionnaire in the experimental session.

In this study we found that neither the ProVision questionnaire nor the MAS-2EV metric were statistically correlated ($p>0.05$; Figure 8.8) with the high contrast VA. This supports the notion that high contrast VA is a poor predictor of overall subjective image quality, as the world is rich with spatial frequency content, and many tasks are well supported by mid-range spatial frequencies, but great VA is more heavily dependent on high spatial frequencies. However, the correlation between the Provision questionnaire and the MAS-2EV metric was highly statistically significant ($p<0.05$-0.0005; Figure 8.1) both for actual and simulated M-CLs. This finding suggests that the MAS-2EV metric can be used as a fast and quantitative alternative to vision questionnaires, well suitable for use in the clinic. Furthermore, while the visual questionnaires are used to collect the patient's reported outcome to a certain treatment, when the MAS-2EV is applied in combination with the SimVis Gekko it is conceivable to anticipate the prospective performance of various possible lenses before fitting them in eye, with the potential to improve and largely reduce chair time in M-CLs fitting [181].

In the following chapter DFVA curves obtained in healthy presbyopic patients through SimVis Gekko simulated IOLs were compared to DFVA curves reported in the literature in patients implanted with those M-IOLs.

Chapter 9

M-IOL performance: SimVis Gekko simulations vs implanted lenses

In the current chapter, we used the SimVis Gekko to simulate three different commercial M-IOL designs using through-focus MTF on bench data from the literature. We used these simulations to measure through-focus visual acuity (DFVA) with the simulated lenses in presbyopic clear lens patients. The measured DFVA curves were compared to DFVA curves data in the literature obtained from post-operative patients implanted with the same M-IOLs.

This chapter is based on the paper by *Barcala et al. "Binocular defocus curves with different multifocal IOLs: SimVisGekko simulations vs clinical data in implanted patients" in preparation*. The co-authors of the study are Amal Zaytouny, Lucie Sawides, Carlos Dorronsoro, and Susana Marcos.

The author of this thesis (1) conceived the ideas along with Carlos Dorronsoro and Susana Marcos, (2) set the measurements protocol, (3) supervised the clinical measurements, (4) analyzed the data, and (5) prepared the manuscript (in collaboration with Susana Marcos).

This work was accepted to be presented as a free paper to the European Society of Cataract and Refractive Surgery (ESCRS) annual meeting (October 2021) that will take place in Amsterdam (Netherlands).

9.1. Introduction

There is an increasing number of IOLs designs used in cataract surgery or refractive lens exchange (see chapter 1), including monofocal, multifocal, and EDOF designs. Different designs aim at meeting specific needs in patients, such as optimal far vision, functional vision at far and near, or a constant vision in a range of focus. Post-operative vision outcomes are frequently studied to understand the performance of their lenses, and the extent to which they match lens design expectations. Ideally, one would like to show the patients pre-operatively their prospective vision with the different lenses, in an attempt to customize the IOL selection and manage expectations.

Defocus Visual Acuity curves (DFVA) are often used to assess visual performance in pseudophakic patients. In this method, trial lenses are placed in front of the eye to mimic different vergences and high contrast VA is measured at each simulated distance. Despite some drawbacks of this method, which is time-consuming, uses targets with a frequency content and high contrast that may not be fully representative of natural targets and may be subject to VA underestimation associated with magnification, it still represents the most comprehensive assessment of the performance of presbyopic corrections in patients [140–142]. DFVA curves are used to estimate depth-of-focus, and many reports compare post-operative DFVA curves with the different lens designs [139]. Naturally, comparisons can only be made in different groups implanted with different lenses, as each patient can only receive (get implanted) one single design.

Visual simulators solve the unmet need of giving the patients the experience of prospective vision with different IOL designs. As these devices are programmable and non-invasive, patients can try multiple lenses in a short period of time. In particular, DFVA measurements can be easily integrated in visual simulation. In on bench simulators (based for example on DM or SLM), the VA stimuli are presented in a monitor or mini display, incorporated in one of the channels of the instrument by beam splitters and mirrors. Those systems are typically provided with a Badal optometer which allows continuous change in focus or alternatively by placing trial lenses in a pupil plane [189,194,195]. In see-through simulators (such as the SimVis Gekko, operating under the principle of temporal multiplexing), measurements can be done using standard clinical eyecharts, and the vergence is changed by placing trial lenses in a dedicated holder in the device, in a plane close to a pupil conjugate [91,92,113,181].

The fidelity of the simulations has been proved in previous studies through comparisons of the visual performance with SimVis-simulated lenses (implemented in a channel in an adaptive optics system) and through real IOLs immersed in a cuvette and projected in the eye [91,195]. Additionally, comparisons of DFVA with simulated CLs and the real CLs show a high degree of similarity [113,180,189]. In those series of validations, the crystalline lens of the eye was present with the simulation and the physical intraocular or contact lens, therefore proving the concept as long as the role of the natural lens is minor, as seems to be the case [196]. In a previous study, Vinas et al. [92] used the SimVis Gekko v0.5 (2018 version) to simulate pre-operatively a trifocal diffractive IOL, the FineVision POD F (Physiol, Liege, Belgium). Binocular DFVA curves were

measured pre-operatively through the simulator and post-operatively in the same patients, after being implanted with the same M-IOL. DFVA with simulated and real IOLs showed similar shapes both in clear lens and cataract patients (shape similarity metrics of 0.87 and 0.68, respectively). While absolute VA values were, as expected, significantly better post-operatively than with the simulated lens pre-operatively in cataract patients (0.09±0.01 logMAR RMS difference on average), the shape of the DFVA was similar in pre-operative simulations and with implanted IOLs. Furthermore, in clear lens patients, there was a high correspondence in DFVA absolute values pre-operatively with the simulated IOLs and post-operative with the implanted IOLs (0.06±0.01 logMAR RMS difference). While this study is a direct proof of the goodness of the simulations, it was restricted to a given lens design. Furthermore, the manufacturer had made the lens design available, allowing calculations of the through focus visual Strehl of this lens, on which the SimVis programmed patterns are based. A more practical operation of the SimVis should not require proprietary knowledge of the lens design in order to simulate it.

In the current study, we used published through-focus MTF on bench data of three different lens designs (Tecnis Symfony, AcrySoft IQ PanOptix, FineVision POD F) to program the lenses on SimVis Gekko v2.0 (2020 version) visual simulators. We used these programmed lenses to perform DFVA measurements in presbyopic clear lens patients. The measured DFVA curves were compared to DFVA curve data in the literature from post-operative patients implanted with the same M-IOLs. The excellent match that we found between DFVA in clear lens patients with simulated lenses and those of pseudophakic patients with those lenses implanted provides further support to the use of visual simulations to predict post-operative vision.

9.2. Methods

Binocular DFVA curves were measured in presbyopic patients through SimVis Gekko simulating the following commercial M-IOLs: Tecnis Symfony (Johnson & Johnson); AcrySoft IQ PanOptix (Alcon) and FineVision POD F (Physiol). DFVA curves from presbyopic healthy subjects were compared with DFVA reported in the literature from patients implanted with the same M-IOLs.

9.2.1. Subjects and experiments

Seven patients were recruited at the Visual Optics and Biophotonics Lab (CSIC, Madrid) to participate in the study (age: 54±5 years; spherical error: 1.21±0.79 D; astigmatism ≤ 0.50 D). Their profiles are shown in Table 9.1 with individual data of gender, age, sphero-cylindrical refraction, binocular best-corrected logMAR VA at far distance and the near addition needed.

Subject_gender	Age	Rx (sph, cyl, axys)	logMAR VA	Near add
S001_M	48	OD: +1.50	-0.20	+1.25
		OS: +1.75		
S002_M	52	OD: +1.50	-0.20	+2.25
		OS: +2.25		
S003_F	59	OD: +2,25, -0,25x150º	-0.18	+2.25
		OS: +2.00		

S004_F	58	OD: -0.25, -0.50x80º	-0.18	+1.75
		OS: -0.25x135º		
S005_F	53	OD: +1.50	-0.20	+1.50
		OS: +1.25, -0.25x90º		
S006_F	57	OD: +0.75	-0.08	+1.75
		OS: +0.75, -0.50x150º		
S007_M	48	OD: +1.00, -0.25x170º	-0.16	+1.75
		OS: +1.00, -0.25x130º		

Table 9.1 *Individual data of gender (_M male; _F Female); age (years); Sphero-cylindrical refraction (Rx, sph and cyl in D, x astigmatic angle in degrees) in right (OD) and left (OS) eyes, binocular VA at far distance and near add needed.*

The experiment conformed to the tenets of the Declaration of Helsinki, with protocols approved by CSIC Ethics Committee.

9.2.2. SimVis Gekko IOLs simulations

The SimVis Gekko TM v2.0 (2020 version) visual simulator was used to simulate different binocular commercial IOL: (1) Monofocal far; (2) the extended depth of focus (EDOF) Tecnis Symfony (Johnson & Johnson, California, USA); (3) the trifocal AcrySoft IQ PanOptix (Alcon Laboratories, Texas, USA) and (4) the trifocal FineVision POD F (Physiol, Liege, Belgium).

The three presbyopia-correction IOLs were simulated by calculating the best estimated TFVS ratio that represents the best approximation of the real corrections, from the published through-focus modulation transfer function (TF-MTF) curves at 15cpd (or 50lpmm) [136]. The best estimated TFVS was obtained in the following steps:

(1) Published TF-MTF curves @15cpd, for three lenses under study, for different wavelengths (RBG) and for a 3mm pupil diameter, were extracted from Loicq et al. (2019) [197]. The authors used a PMTF (lambda-X) to measure the TF-MTF curves and using ISO1 cornea model (no spherical aberration).

(2) A polychromatic TF-MTF curve was obtained from the weighted average (using the luminance function V(λ)) [198] of the MTFs in the three wavelengths.

(3) The average TF-MTF was normalized by a factor corresponding to the diffraction-limited MTF value for a 3mm pupil diameter (factor 0.797).

(4) A Zero-Phase digital filter was applied to the normalized TF-MTF to obtain its shape. A low-pass finite impulse response digital filter was used with the following parameters: Pass Band Frequency 0.05 D^{-1}, Stop Band Frequency 0.2 D^{-1}, Pass Band Ripple 0.05 dB, Stop Band Attenuation 10 dB, and Kaiser window design method. The filtered signal corresponds to the best estimate of the TFVS. The real lens and estimated TFVS curves were compared to validate the method, using cross correlation in the entire defocus range from -5.00 D to +2.00 D.

Once we get the best estimated TFVS of the multifocal lens, the temporal coefficients are calculated. The temporal coefficients correspond to the time spent by the TL in each addition. A full explanation of the calculation of the temporal coefficients for a given lens from the TFVS, including the compensation of dynamic effects can be found in prior publications [120,132] and chapters 2 (section 2.1.4) and 3.

9.2.3. Measured DFVA curves

Binocular DFVA curves were measured under photopic conditions (≈85 cd/m2), with an ETDRS high contrast optotype located at 4 meters. Optical vergence is modified with trial lenses of different powers and the best logMAR VA was obtained at each defocus level.

The patient's sphero-cylindrical refraction was corrected by trial lenses placed in the dedicated slot in the SimVis Gekko device. Subsequently, DFVA curves were performed in a focus range from -4.00 D to +1.50 D around the best focus in 0.50D steps [185].

9.2.4. Literature DFVA curves

DFVA curves from patients implanted with Symfony, PanOptix and FineVision IOLs were compiled from recent scientific literature [139,199].

Results from 20 patients (68.2 ± 6.2 years old, 5 male/15 female) implanted with the Symfony were obtained from a study recently reported by Gil et al. [139]. The DFVA curves in that publication were measured by adding trial lenses from +1.50 D to -4.50 D, in 0.50 D steps over the best-corrected distance refraction, using an ETDRS chart placed at 4 meters under photopic conditions (85 cd/m2). The publication also reports the photopic pupil diameter measured using an infrared Colvard pupillometer (Oasis Medical Inc., San Dimas, CA) while patients were fixating a distant target: 3.3 ± 0.8 mm.

Results from 15 patients (64±6 years old) implanted with the PanOptix IOL and from 15 patients (68±8 years old) implanted with the FineVision IOL were obtained from published work by Ribeiro et al. [199]. The DFVA curves in that publication measured from +1.00 to -4.00 D (in 0.50 D steps) under photopic conditions (85 cd/m2) 3-months after the bilateral surgery with the lenses.

9.2.5. Data analysis

DFVA curves with simulated IOLs were compared across lenses in the same subject and on average. The average DFVA measured with a simulated IOL was compared to reported average DFVA in implanted patients with the same IOL (literature values). Comparisons were made in terms of Absolute VA at Far (0.00 D), at intermediate (-1.50 D) and at near (-2.50 D), in terms of DFVA curve shape similarity, and Depth-of-focus (DOF). The shape similarity metric was defined as the cross-correlation between the curves, along with the Root Mean Square (RMS) DFVA curve differences. DOF was defined as the dioptric range for which VA is 0.2 logMAR [186]. A paired-sample t-test was performed to study the differences across the simulated lenses designs for each subject. Differences between the simulated and the real DFVA curves were analyzed based on the standard deviations from the published data.

9.3. Results

9.3.1. DFVA curves with simulated IOLs

Figure 9.1 shows the individual DFVA curves measured through the SimVis Gekko simulated M-IOLs (monofocal in black, Symfony in orange, PanOptix in blue and FineVision in green).

On average, all M-IOLs degraded VA with respect to the monofocal at far (-0.12±0.08 for Symfony, -0.15±0.00 logMAR for PanOptix, -0.14±0.04 for FineVision), but all M-IOLs improved VA at intermediate (0.11±0.03 for Symfony, 0.04±0.05 logMAR for PanOptix, 0.01±0.03 for FineVision) and at near (0.13±0.07 for Symfony, 0.43±0.04 logMAR for PanOptix, 0.40±0.02 for FineVision) distances. The PanOptix and the FineVision IOL DFVA curves showed clear peaks at near (with maximum at -3.07±0.19 D and -2.64±0.24 defocus logMAR values, respectively), while the Symfony had a lower dioptric range above the 0.2 logMAR threshold but with a notably improved performance at intermediate distance (except for subject number 6, which showed a reduced VA for all distances with the Symfony and also for the other M-IOLs). On average across subjects who were tested with all four simulated IOLs, DOF was 2.21±0.27 D for the monofocal IOL, 2.93±0.67 D for the Symfony simulated-IOL, 4.21±0.95 D for PanOptix, and 3.71±0.99 D for FineVision across all the distances (from +0.50 D to -4.00 D). The differences across designs were statistically significant for each subject (p>0.05, paired-t-test).

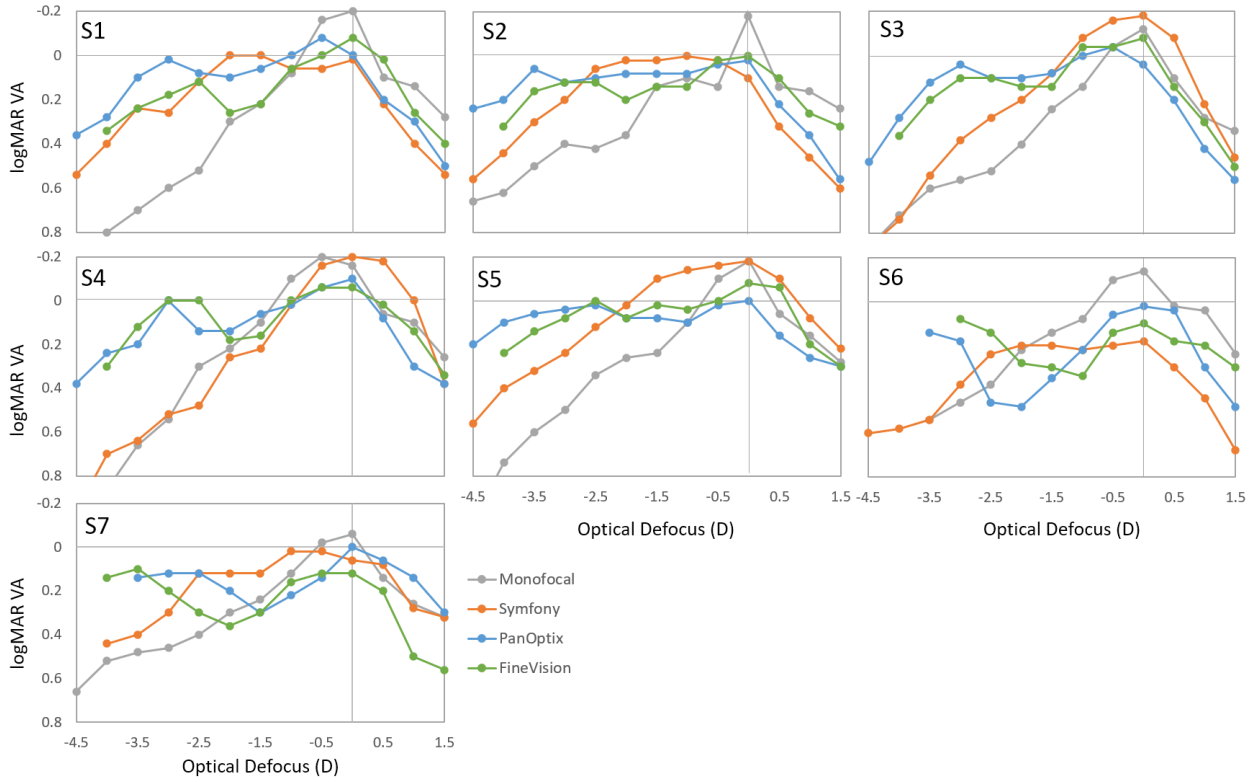

Figure 9.1 *Individual DFVA curves measured through the SimVis Gekko simulated M-IOLs: monofocal far (in gray), Symfony (in orange), PanOptix (in blue) and FineVision (in green).*

9.3.2. Comparison of DFVA curves with simulated M-IOLs and implanted M-IOLs

Figure 9.2A shows the DFVA curves for each simulated IOL (averaged across subjects and standard deviations), Figure 9.2B-C shows the DFVA curves for the simulated IOL (solid lines) and the DFVA in patients implanted with the corresponding IOL from literature reports (dashed lines), for Symfony (B, orange line, Gil et al 2020), PanOptix (C, blue lines, Ribeiro et al 2020), and FineVision (D, green line, Ribeiro et al 2020).

Binocular logMAR VA at far (0.00 D) were -0.03±0.16, 0.00±0.05 and -0.01±0.10 with the Symfony, PanOptix and FineVision simulated lenses, and -0.05, -0.01 and -0.01 with the implanted lenses, respectively. Differences in binocular logMAR VA between real and simulated M-IOLs were -0.05, -0.07 and 0.10 for intermediate distance (-1.50 D) and 0.04, -0.03 and 0.02 for near distance (-2.50 D) for Symfony, PanOptix and FineVision, respectively.

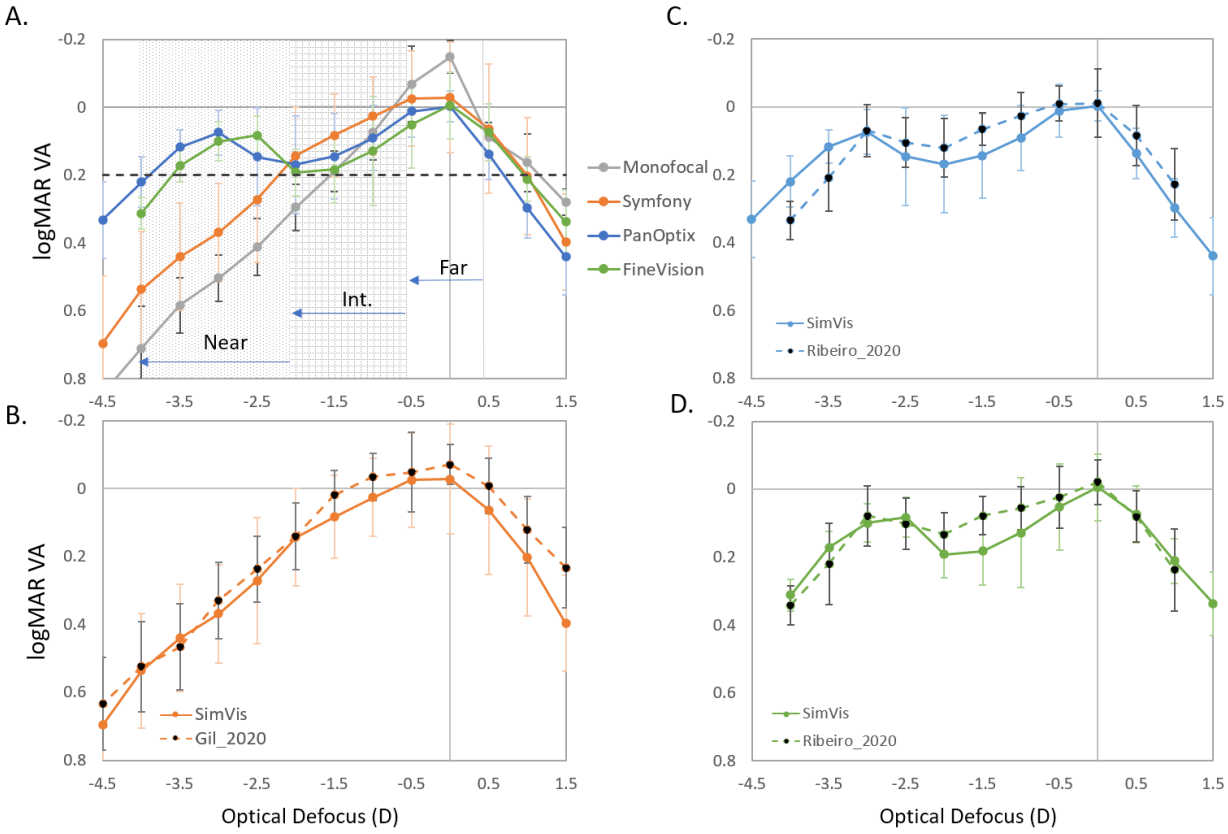

***Figure 9.2 A**. Mean DFVA curves measured through SimVis Gekko in presbyopic patients for monofocal far (black); Symfony (orange); PanOptix (blue) and FineVision (green). The dashed horizontal black line represents logMAR VA=0.2. **B**. DFVA curve for the simulated Symfony (solid orange line) overlapped with the reported DFVA curve by Gil et al. (dashed orange line). **C**. DFVA curve for the simulated PanOptix (solid blue line) overlapped with the reported DFVA curve by Ribeiro et al. (dashed blue line). **D**. DFVA curve for the simulated FineVision (solid green line) overlapped with the reported DFVA curve by Ribeiro et al. (dashed green line).*

There is a high similarity between the DFVA curves with SimVis Gekko-simulated IOLs and the implanted designs. The highest difference (0.10 logMAR) occurred on the positive side of the DFVA curve. The RMS DFVA curve differences for the range between +0.50 D to -3.50 D were

0.06, 0.05 and 0.05 logMAR for Symfony, PanOptix and FineVision. DFVA shape similarity metric was 0.99, 0.90 and 0.91 for Symfony, PanOptix and FineVision, respectively.

Figure 9.3 shows the mean DFVA curve across subjects through the SimVis Gekko simulation (solid line) for each lens design. The DFVA curves from the patients implanted with the same lens design are represented with the standard deviation and the area between the mean-across-subjects±standard-deviation has a gray background. Almost all defocus from the SimVis Gekko-simulations are within one standard deviation (90% of confidence) of the reported data from implanted patients, except for the -1.50 D defocus value with the PanOptix and FineVision simulations.

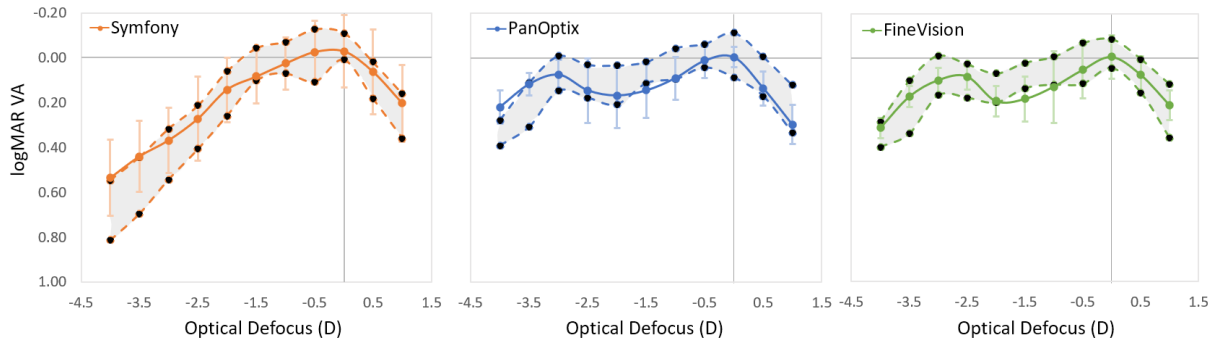

Figure 9.3 *Dashed lines represent the mean±standard-deviation from the published data from patients implanted with that lens design. The area in between has a gray background. The solid line represents the SimVis Gekko simulated DFVA curve. Symfony data is represented in orange, PanOptix in blue and FineVision in green.*

9.4. Discussion

In this study, SimVis Gekko v2.0 was used to simulate three different commercially available lens designs (Tecnis Symfony, AcrySoft IQ PanOptix, FineVision POD F). The lens designs were uploaded to the simulator using through-focus MTF on bench data from the literature. DFVA curves were performed in seven presbyopic subjects and compared to DFVA curves data in the literature from post-operative patients implanted with the same M-IOLs. Remarkably, published on bench through focus MTFs, and not the lens design, were used to generate the SimVis temporal coefficients used in the simulations.

The similarity and correlation between the simulated and the literature reported DFVA curves from implanted patients was high for all lens designs. RMS DFVA differences were 0.06, 0.05 and 0.05 logMAR for Symfony, PanOptix and FineVision. DFVA shape similarity metric was 0.99, 0.90 and 0.91 for Symfony, PanOptix and FineVision, respectively. The mean DFVA curves from the SimVis Gekko simulations are within the standard deviations of the reported DFVA curves from implanted patients.

We have shown that the SimVis Gekko simulations capture to a large extent the TF visual performance in patients implanted with the real IOLs. The great advantage of simulators is the capability of providing the patient the experience of vision through prospective corrections,

allowing to compare pre-operatively vision with multiple M-IOLs, binocularly, a comparison that is of course precluded post-operatively. In the same patient, we found significant differences in DFVA with the Symfony with respect to the FineVision or Panoptix. Symfony provided a flatter DFVA curve and a shorter DOF, in line with the frequent EDOF denomination of this lens. Also, DFVA curves for the FineVision and Panoptix were statistically significant different for all subjects ($p>0.05$, paired sample t-test).

Despite similar general trends for a given lens, DFVA with the same lens differs across patients. The standard deviations in the VA measured with simulated lenses (0.11 averaged across distances, patients and lenses) is comparable to the reported standard deviations post-operatively in patients implanted with these IOLs. These intersubjects' variability likely arises from differences in native aberrations patients baseline pupil diameter, as well as neural factors.

In a previous work, we compared DFVA pre-operatively with SimVis Gekko simulating the FineVision IOL, and post-operatively in the same patients implanted with that lens. The lower DFVA simulated-real IOL RMS difference in the earlier study (0.01 logMAR, in clear lens patients) in comparison with that found for the FineVision in the current study (0.05 logMAR) are likely due to the fact that a different cohort of patients was measured pre- and post-operatively. Potential reasons for the higher discrepancy include: differences in age between the patients in Vinas et al study and the presbyopic group in the current study (60.4±7.7 vs 54±5 years old), presumably affecting lens transparency, spherical aberration and residual accommodation. In fact, the slightly higher performance with the simulated lenses at near (particularly with the PanOptix) could result from some residual accommodation in the young presbyopic group.

An additional potential source of variation between the DFVA in our simulation study and the literature data is the pupil diameter. While in the clinical studies the measurements are performed with the natural pupil diameter, the lens designs are programmed in the SimVis Gekko for a fixed 3-mm pupil. Finally, simulations can only account for the lens design, whereas other surgical factors (lens centration, incision, among others) or design parameters of the lens outside the optical zone (IOL edges and haptic platform) may affect visual performance in the post-operative eyes.

We demonstrated that commercially available M-IOLs can be programmed in SimVis Gekko using publicly available data. The high correspondence of TF visual performance (both absolute and relative values) between presbyopic subjects tested with SimVis Gekko-simulated lenses and real patients implanted with the corresponding M-IOLs suggests that SimVis Gekko is a reliable simulator to capture the real vision through the FineVision, PanOptix and Symfony IOLs, allowing to study prospective differences in performance across designs pre-operatively.

In the next chapter, the combination of SimVis Gekko and MAS-2EV is used to estimate the suitability of these technologies in the presence of a cataract opacification.

Chapter 10

Visual simulations of presbyopic corrections through cataract opacification

In the current chapter, cataract patients evaluate their perceived visual quality with the modified MAS-2EV metric at far (4 m), intermediate (64 cm), and near distance (40 cm) with four binocular presbyopic corrections simulated with SimVis Gekko. The visual preferences are correlated with the scattering degree and correlated with the preference of the same patients after the cataract removal.

This chapter is based on the paper by *Barcala et al. "Visual simulations of presbyopic corrections through cataract opacification" submitted to Journal of Cataract & Refractive Surgery.* The co-authors of the study are Amal Zaytouny, Daniela Rego-Lorca, Julia Sanchez-Quiros, Ruben Sanchez-Jean, Jose Maria Martinez-de-la-Casa, Carlos Dorronsoro and Susana Marcos.

The author of this thesis (1) developed the clinical protocol (in collaboration with Carlos Dorronsoro), (2) submitted it to the ethical committee, (3) recruited the patients (in collaboration with Ruben Sanchez-Jean and Amal Zaytouny) (3) performed clinical measurements (in collaboration with Amal Zaytouny), (4) collected and analyzed the data, and (5) prepared the manuscript (in collaboration with Susana Marcos).

This work was presented as an oral contribution at the European Society of Cataract and Refractive Surgery (ESCRS) annual meetings in 2019 (held in Paris, France) and 2020 (online).

10.1. Introduction

Previous chapters (8 and 9) showed that visual simulators, in particular SimVis Gekko, capture the visual quality of real lenses. It has been demonstrated that visual simulators can be used to determine the degree of acceptance to a generic type of correction, to a particular commercial CL or IOL, or, if the ophthalmologist deems it appropriate, to compare two or more corrections with each other. Also, an advantage of this simulator is the ability to test binocular corrections and monovision.

Typically, pre-operative simulations of post-operative vision with IOLs are administered on phakic patients and are therefore valid as long as the role of the crystalline lens is minor. Artal et al. [196,200] showed that the aberrations of the crystalline lens played a secondary role in adaptive optics IOL visual simulations. Our previous work [92] using SLM-based and SimVis-based simulations in an optical bench, as well as the SimVis Gekko binocular simulator pre-operatively showed excellent correspondence in the same patients between the simulated trifocal IOL and post-operative performance with the implanted IOL. SimVis simulations and post-operative through-focus visual acuity (TFVA) curves matched in patients with clear lenses (RMS difference 0.06±0.01), while in patients with cataracts the TFVA had similar shapes pre- and post-operatively, just shifted by the effect of scattering (0.87 shape similarity curve metric). These results suggested that the SimVis simulations capture the relative through-focus performance of the multifocal lenses, and that the absolute performance could be projected by a single factor accounting for the VA improvement from the elimination of opacity. The temporal multiplexing principle in SimVis allows projecting on the retina the multifocal profile avoiding selective spatial occlusions that will occur in a spatial representation of the lens in other simulator modalities (for example using an SLM) in patients with cataracts.

Even if refractive clear lens exchange procedures are increasingly popular, the implantation of IOLs is still primarily performed on patients with cataracts. With the growing choice of IOLs at the patient's disposal, the cataract population would be largely benefited from experiencing visual quality with different IOLs, now possible with visual simulators. Even if the visual quality is reduced by the presence of the cataract, it would be valuable for the patients to be able to provide a relative assessment of the visual quality of different lenses at various distances, provided that the established relative ranking is accurate.

In this chapter, we further tested the applicability of visual simulations of presbyopic corrections in cataract patients with different levels of scattering. The patients scored their perceived visual quality with monofocal far, bifocal, monovision and modified monovision corrections with the SimVis Gekko pre-operatively and then post-operatively (after implantation of monofocal IOLs) with the same simulated correction. We studied the viability of the simulation testing as a function of cataract level and the effect of the presence of the cataract on visual score and correction ranking.

10.2. Methods

Patients (before and after cataract surgery) evaluated the perceived visual quality of real scene images with the Multifocal Acceptance Score to Evaluate Vision (MAS-2EV) metric at far (4 m), intermediate (64 cm) and near distance (40 cm) with four binocular presbyopic corrections simulated with SimVis Gekko: monofocal far, bifocal, monovision and modified monovision.

10.2.1. Patients

Thirty patients scheduled for bilateral cataract surgery with monofocal-far IOLs at the Hospital Clinico Universitario San Carlos in Madrid were recruited for this study. The inclusion criteria for the study included: age ranging between 50 and 85 years old; distance spherical equivalent from subjective refraction in the range of +4.00 D to -6.00 D in each eye and cylinder ≤2.50 D. Six patients did not meet the inclusion criteria due to high myopia and astigmatism and were discarded to continue the study measurements. Table 10.1 shows the demographic and refractive profiles of the twenty-four participating patients (average age: 70±10 y.o. Rx: -0.66±2.21 D, cyl: -1.24±0.65 D). Patients in cells shaded in grey were also measured post-operatively.

Subject_G	Age	Rx (sph, cyl x axys)	BCVA	Dominance	OSI	Mean OSI
S002_F	84	OD: -3.50	OD: 0.16	OD	OD: 7.2	11.55***
		OS: -1.75	OS: 0.40		OS: 15.9	
S003_F	58	OD: -0.50	OD: 0.70	OD	OD: 1.1	2.7**
		OS: +0.50, -1.00x60º	OS: 0.80		OS: 4.3	
S004_M	50	OD: -2.00	OD: 0.05	OS	OD: 11.6	11.75***
		OS: -1.50, -0.75x60º	OS: 0.30		OS: 11.9	
S006_F	72	OD: -2.50	OD: 0.20	OS	OD: 12.8	10.1***
		OS: -1.50, -0.50x180º	OS: 0.60		OS: 7.4	
S007_F	68	OD: -0.75	OD: 1.00	OD	OD: 1.1	1.1*
		OS: +0.75	OS: 0.90		OS: 1.2	
S008_F	72	OD: +4.00, -1.75x50º	OD: 0.16	OS	OD: 10	7.6**
		OS: +1.50, -0.75x10º	OS: 0.60		OS: 5.2	
S009_F	56	OD: -1.00,-1.75x70º	OD: 0.70	OS	OD: 2.6	1.95*
		OS: +1.75,-1.00x150º	OS: 0.80		OS: 1.3	
S010_M	80	OD: -0.50x30º	OD: 0.40	OS	OD: 8.3	6**
		OS: +1.50, -1.50x180	OS: 0.50		OS: 3.5	
S011_F	82	OD:+2.50,-1.00x100º	OD: 0.70	OS	OD: 2.7	1.9*
		OS: +3.00,-1.00x90º	OS: 0.80		OS: 1.1	
S012_M	74	OD: +0.50,-1.00x80º	OD: 0.60	OS	OD: 1.1	1.05*
		OS: +3.00,-1.50x70º	OS: 0.70		OS: 1.0	
S013_F	69	OD: -5.50,-1.00x170º	OD: 0.40	OS	OD: 14	7.6**
		OS:+1.00,-0.50x180º	OS: 1.00		OS: 1.2	
S014_M	56	OD: +1.00	OD: 1.00	OD	OD: 1.2	7.1**
		OS: -3.00,-2.50x90º	OS: 0.50		OS: 13	
S015_F	81	OD: -0.50,-2.00x60º	OD: 0.60	OD	OD: 6.5	6.05**
		OS: -0.75,-2.50x90º	OS: 0.60		OS: 5.6	

S016_F	80	OD: -0.50,-1.50x70º	OD: 0.50	OD	OD: 10	10.25***
		OS: +2.50,-2.00x90º	OS: 0.50		OS: 10.5	
S017_F	69	OD: -2.25,-1.25x125º	OD: 0.30	OS	OD: 13.2	10.4***
		OS: +0.25,-0.75x65º	OS: 0.30		OS: 7.6	
S018_F	64	OD: -4.50,-1.00x100º	OD: 0.70	OS	OD: 5.6	4.85**
		OS: -3.00,-0.50x80º	OS: 0.90		OS: 4.1	
S020_F	58	OD: +1.75	OD: 0.50	OS	OD: 4.3	5.5**
		OS: +1.00,-0.25x180º	OS: 0.70		OS: 6.7	
S021_F	71	OD: -5.50,-1.00x170º	OD: 0.50	OD	OD: 8.7	8.35***
		OS: -4.00,-0.75x170º	OS: 0.60		OS: 8	
S022_M	73	OD: -1.50,-0.50x130º	OD: 0.63	OD	OD: 1.7	1.7*
		OS: -1.00,-0.75x90º	OS: 0.80		OS: 1.7	
S023_M	66	OD: -0.50,-1.00x150º	OD: 0.4	OS	OD: 1.1	2.2**
		OS: -0.75,-0.50x140º	OS: 0.63		OS: 3.3	
S024_M	76	OD: -2.50, -2.00x90º	OD: 0.5	OS	OD: 6.3	9.5***
		OS: -1.00,-2.00x40º	OS: 0.6		OS: 12.7	
S025_F	77	OD: -0.50	OD: 0.80	OS	OD: 1.5	1.75*
		OS: +1.00	OS: 0.80		OS: 2	
S026_M	83	OD: -2.00,-1.00x10º	OD: 0.40	OD	OD: 15	11.35***
		OS: -0.75,-2.00x90º	OS: 0.50		OS: 7.7	
S027_F	64	OD: -0.50, -2.50x10º	OD: 0.60	OD	OD: 7.8	8.25***
		OS: -2.00x170º	OS: 0.60		OS: 8.7	

Table 10.1 *Profile of the participating cataract subjects. Columns stand for: subject ID, gender (F: female, M: male), age (years old), sphero-cylindrical refraction (sphere (sph) and cylinder (cyl) in D, and astigmatic angle in degrees) for the right (OD) and left (OS) eye, the monocular decimal best-corrected VA (BCVA), eye dominance, OSI index for each eye and mean OSI , severity identified by asterisks (*: small cataract; **: mild cataract; ***: severe cataract).*

10.2.2. Cataract Surgeries

Fifteen patients underwent bilateral cataract surgery implanted with monofocal IOLs targeting distance vision correction. Surgical procedures were performed by fifteen different surgeons under topical anesthesia. IOLs were implanted through a 1.80-mm valving and self-sealing clear corneal incision at 130 degrees, at about 1 mm anterior to the limbus. Three different monofocal IOLs were implanted, Akreos Adapt (Bausch&Lomb, USA) n=21 eyes, Zeiss CT Asphina (Carl Zeiss, Germany) n=8 eyes, and Tecnis Monofocal 1-piece aspheric IOL (Johnson & Johnson, USA) n=1 eyes. The IOL power ranged from 13 D to 23 D. The selected IOL was then implanted in the capsular bag with a single-use injection system, ViscojectTM 1.8 from Baushc&Lomb (used for the Akreos Adapt IOL) and BLUEMIXS® 180 from Zeiss (used for the Zeiss CT Asphina IOL). Optical biometry was conducted using IOLMaster 700 (Carl Zeiss, Germany). The Barret TK Universal II formula was used to select IOL power, with A-constants 118.5, 118.0 and 119.3 for the Akreos, Asphina and Tecnis IOLs, respectively.

The patients underwent standard post-operative clinical evaluations 1 day, 1 week and 1 month after unilateral surgery. Surgeries were performed 1.7±1.25 months apart between the first and second eye, except for four subjects (S003, S006, S021 and S025) that had 14.5±2.65 months between surgeries. Post-operative visual simulations were done 3-8 months after surgery of the

second eye, on average. A slit-lamp evaluation was performed at the time of post-operative measurement to ensure that no posterior-capsular opacification had been developed or to discard other potential complications/artifacts in the IOL such as whitening or calcification (which did not occur in any patient).

Table 10.2 shows the profile of the post-operative patients (average age: 70.33±9.24 y.o., implanted monofocal IOL and average residual subjective refractive error; sph.: -0.37±0.73D and cyl: -0.43±0.52 D). All patients achieved 0.90 or better decimal best-corrected VA (BCVA) for far distance, except for S006.

Subject_G	Age	Implanted IOL	Rx (sph, cyl x axys)	BCVA	Dominance
S002_F	85	Akreos Adapt	OD: -1.50 x 120º	OD: 0.90	OD
		Akreos Adapt	OS: -0.25	OS: 0.90	
S003_F	60	CT Asphina	OD: -1.00, -0.50 x 50º	OD: 1.00	OD
		CT Asphina	OS: +0.50, -1.00 x 60º	OS: 1.00	
S004_M	51	Akreos Adapt	OD: 0.00	OD: 1.25	OS
		Akreos Adapt	OS: 0.00	OS: 1.25	
S006_F	74	Akreos Adapt	OD: -3.25	OD: 0.8	**OD**
		Akreos Adapt	OS: -2.00, -1.50 x 80º	OS: 0.6	
S007_F	69	CT Asphina	OD: -0.50	OD: 1.00	OD
		CT Asphina	OS: -0.50	OS: 1.00	
S013_F	70	CT Asphina	OD: -0.75	OD: 1.25	**OD**
		Akreos Adapt	OS: -0.50	OS: 1.25	
S015_F	82	CT Asphina	OD: -1.50 x 80º	OD: 0.90	**OS**
		Akreos Adapt	OS: -0.25, -1.25 x 90º	OS: 0.90	
S017_F	70	Akreos Adapt	OD: -0.75	OD: 1.00	OS
		Akreos Adapt	OS: -0.50, -0.50 x 170º	OS: 1.00	
S018_F	65	Akreos Adapt	OD: -0.50, -0.50 x 110º	OD: 1.00	**OD**
		Akreos Adapt	OS: -0.50, -0.50 x 80º	OS: 1.00	
S020_F	59	CT Asphina	OD: -0.50, -0.50 x 90º	OD: 1.00	**OD**
		CT Asphina	OS: -0.50	OS: 1.00	
S021_F	73	Akreos Adapt	OD: 0.00	OD: 1.00	OD
		Akreos Adapt	OS: -0.50 x 180º	OS: 1.00	
S022_M	75	Akreos Adapt	OD: 0.00	OD: 1.00	**OS**
		Akreos Adapt	OS: 0.00	OS: 1.00	
S024_M	78	Akreos Adapt	OD: 0.00	OD: 1.00	OS
		Akreos Adapt	OS: +0.50	OS: 1.00	
S025_F	79	Tecnis Monofocal	OD: +0.50	OD: 1.00	OS
		Akreos Adapt	OS: -0.50 x 180º	OS: 1.00	
S027_F	65	Akreos Adapt	OD: -0.25, -1.00 x 180º	OD: 1.00	**OS**
		Akreos Adapt	OS: -1.00 x 180º	OS: 1.00	

Table 10.2 *Profile of the post-operatively subjects measured with their subject ID, gender (F: female, M: male), implanted monofocal IOL, age (years old), sphero-cylindrical residual refraction (sphere (sph) and cylinder (cyl) in D, x astigmatic angle in degrees) for the right (OD) and left (OS) eye, the monocular decimal VA) and eye dominance (surgery flipped ocular dominance highlighted in blue).*

10.2.3. Pre-operative cataract scattering

The Objective Scattering Index (OSI) obtained using the HD Analyzer (Keeler, Malvern, PA) was used to quantify the degree of opacification in cataracts. This instrument is based on the double-pass technique [201–203] that provides an objective clinical evaluation of the optical quality of the eye. In the double-pass technique, the light coming from a point of source forms the image on the retina, and it is reflected and passed through the eye's optics twice. OSI is calculated from the assessment of the amount of light that is on the outside of the patient's double-pass image, relative to the amount of light in its central part. The higher the OSI value, the greater the level of intraocular scattering.

According to the OSI manual user (version 2.7 – 2018), an OSI value of ≤1 is indicative of normal scattering, OSI between 1.5 and 4 for eyes with developing cataracts and OSI>4 for mature cataracts. Based on our measurements, we have classified the patients in three different groups based on the mean OSI index: small cataracts with OSI<2, mild cataracts 2>OSI<8 and mature cataracts when OSI is above 8.

The OSI measurements were obtained before cataract surgery of the first eye, in the same session as the visual simulations. The pre-operative OSI values in all patients are shown in Table 10.1.

10.2.4. Ocular dominance and binocular vision test

Sensory ocular dominance was determined by placing a +1.50 D lens alternatively in one eye, repeated three times [33]. The patients are indicated to look at lines above their best subjective far VA. The dominant eye is identified as the one with which the patient experiences a higher uncomfortably blurred visual percept upon introduction of the defocusing lens. The pre- and post-operative ocular dominance in all patients is shown in Table 10.1 and 10.2, respectively. Natural binocular vision was tested using a 4-dot Worth test to discard fusion dysfunction.

10.2.5. Simulated presbyopic corrections

Four binocular presbyopic corrections were tested, using SimVis Gekko v1.5: (1) Monofocal far in both eyes (FF); (2) Bifocal lenses in both eyes (BB); (3) Monovision (FN; dominant eye with monofocal far and non-dominant eye with monofocal near); and (4) Modified Monovision (FB; dominant eye with monofocal far and non-dominant eye with a bifocal lens). The bifocal correction represented a generic bifocal IOL with +2.50 D near add. The general bifocal correction simulates a 50/50 energy split between far and near vision. In this correction, the TL spends half of the time in an optical power corresponding to far vision and half of the time in an optical power corresponding to near vision (with 2.50 additional diopters), in cycles of 50Hz. The temporal coefficients driving the lens also correct for the dynamic effects of the TL, summarized in its impulse response measured with a high-speed focimeter [137]. The resultant through-focus optical quality curve exhibits two narrow peaks of Strehl Ratio centered at 0.00 D and 2.50 D. In

the monovision and modified monovision, the near add imposed in the non-dominant eye was 2.50 D, while the dominant eye was given a monofocal correction focused at far.

10.2.6. Modified MAS-2EV

The Multifocal Acceptance Score to Evaluate Vision (MAS-2EV™) is a metric presented in chapter 7 to evaluate the global quality of vision [181]. For this study, the MAS-2EV was modified, evaluating only the images for daylight conditions, and introducing an intermediate image at 64 cm of distance. Figure 10.1 shows MAS-2EV far, intermediate and near images used in the study. The images subtend 15.24 deg field, 20.55 deg field, and 30.96 deg field horizontally, for far, intermediate and near. Far images were displayed on a 43'' monitor (LG) and the intermediate and near on an iPad PRO of 12.9'' with Retina Display (Apple Inc). Measurements were performed under photopic conditions (≈85 cd/m2).

***Figure 10.1**. Set of MAS-2EV images presented at far distance (**A**), intermediate distance (**B**) and near distance (**C**) during daylight condition.*

Patients judged [177] the perceptual quality of images at far, intermediate and near (Perceptual Scores; PS: 0-10) through the SimVis Gekko simulating the IOL designs: Monofocal far (both eyes; FF); Bifocal (both eyes; BB); Monovision (far in the dominant eye and near in the contralateral eye; FN); Modified monovision (far dominant eye/bifocal contralateral eye; FB). Three repetitions were performed for each correction at each distance.

Near stereo-acuity targets are presented, consisting of a Random-dot anaglyph with different rectangles in different positions and with different crossed disparities (400 to 50 arcsec). The anaglyphs are presented in an iPad Pro 12.9" with Retina Display (by Apple Inc) and observed with cyan / red glasses. Near stereo-acuity was measured a single time for each correction at 40 cm.

10.2.7. Experimental protocol

The study was conducted at Hospital Clinico San Carlos, and the measurements were conducted by two experienced optometrists (XB and AZ). Measurements were performed under natural viewing conditions.

An experimental session included the following sequence: (1) subjective refraction; (2) eye dominance; (3) binocular vision; (4) OSI measurement; (5) MAS-2EV with SimVis Gekko. The same sequence of tests was done pre-operatively and then repeated three to eight months after the surgery of the second eye.

A preparatory trial using SimVis Gekko allowed the patient to set the range for their perceptual scoring by viewing the MAS-2EV far-day images through a simulated far-distance corrected monofocal lens (10 PS) and an additional 2.50 D monofocal lens (0 PS). The patient's sphero-cylindrical refraction was corrected by trial lenses placed in the dedicated slot in the SimVis Gekko.

Figure 10.2 summarizes the methodology followed in the study. The four binocular presbyopic corrections were tested using SimVis Gekko in random order. For a given correction, the stereopsis at near was first tested (yielding a 0-10 score). Then modified MAS-2EV scorings were obtained for far-day and near-day. The experiments conformed to the tenets of the Declaration of Helsinki, with protocols approved by the Hospital Clinico San Carlos Ethics Committee. The subjects signed an informed consent after receiving an explanation of the nature and implications of the study.

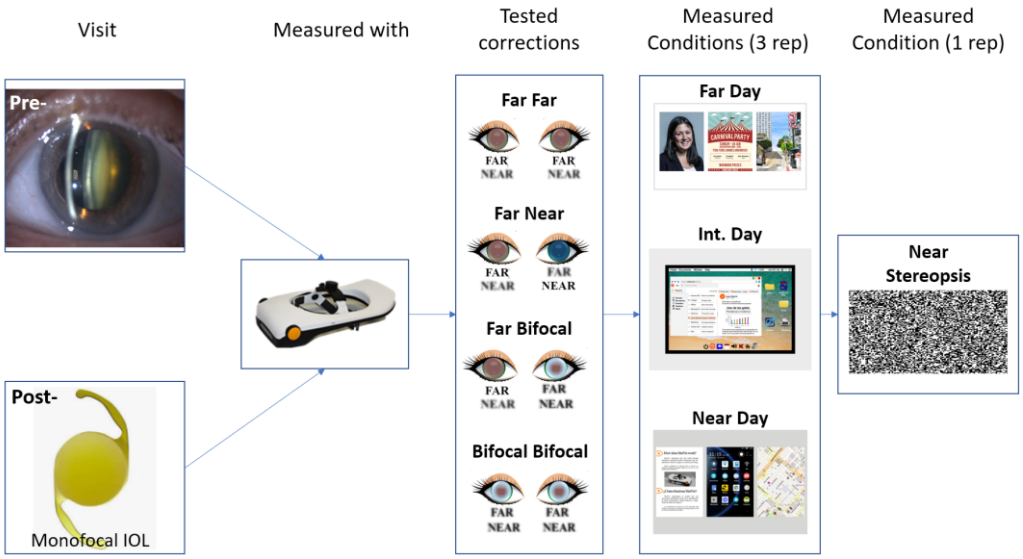

Figure 10.2 *Illustration summarizing the methods. Patients, before and after cataract surgery, were measured with four presbyopic corrections simulated through SimVis Gekko and performed the modified MAS-2EV.*

10.2.8. Data analysis

The following metrics were calculated from the MAS-2EV with all tested corrections (1) Visual degradation at far, defined as (PS Far for each presbyopic correction – PS Far FF)/PS Far FF; Visual benefit at near, defined as (PS Near for each presbyopic correction – PS Near FF)/PS Far FF. Pre-operatively, visual degradation at far and visual benefit at near were correlated with the OSI index (linear regression, Pearson's coefficient of correlation r, and p-value). MAS-2EV PS was analyzed for each distance separately and compared with OSI index and was also compared pre- and post-operatively to evaluate to what extent the pre-operative assessment of different presbyopic correction (through the cataract) matches the post-operative assessment of the same corrections (through a clear lens).

10.3. Results

10.3.1. SimVis Gekko simulations in cataract patients

The cataract patients spanned a wide range of scattering levels (OSI from 1.05 to 11.75, Table 10.1). There were also differences in OSI between eyes of the same patient. We found that VA was significantly correlated with OSI (r=-52, p=0.009). Also, the OSI difference between eyes was significantly correlated with the VA difference between eyes (r=-0.6, p=0.002).

Figure 10.3 shows the dependence of the perceptual score (PS) with the OSI index for far, intermediate and near distance. Since the PS were obtained binocularly, the mean OSI value (between right and left eye) was used. As expected, at far distance the PS decreased significantly with increasing OSI index for most corrections (FF r=-0.5 p=0.02; FN r=-0.4 p=0.05; FB r=-0.4 p=0.04). Conversely, the PS at near and intermediate is positively correlated with increasing OSI index with the monofocal far correction (r=0.5 p=0.007 for intermediate and r=0.6 p=0.002 for near distance).

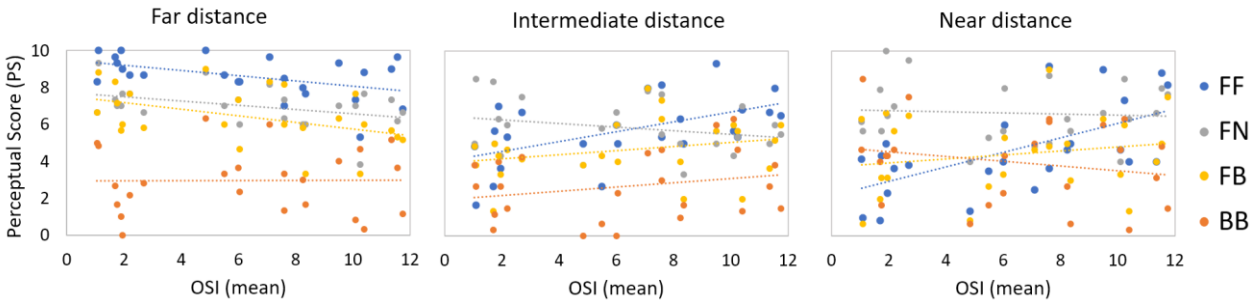

Figure 10.3 *Perceptual score as a function of the mean OSI index (mean between right and left eye) at far (left), intermediate (middle) and near distance (right) for monofocal far (FF) correction (blue), monovision (FN, in gray), modified monovision (FB, yellow) and bifocal in both eyes (BB, orange).*

Figure 10.4 shows the OSI dependence of the visual degradation at far distance for all presbyopic corrections. There was a constant visual degradation at far for a given correction, regardless of OSI. For OSI < 5 there was an average visual degradation of -36.4±27.2%, and for OSI > 5, an average visual degradation of -36.1±25.6%. The visual benefit at near distance provided by the presbyopic correction was apparent (23.3±27.6% on average across corrections) for an OSI < 5.

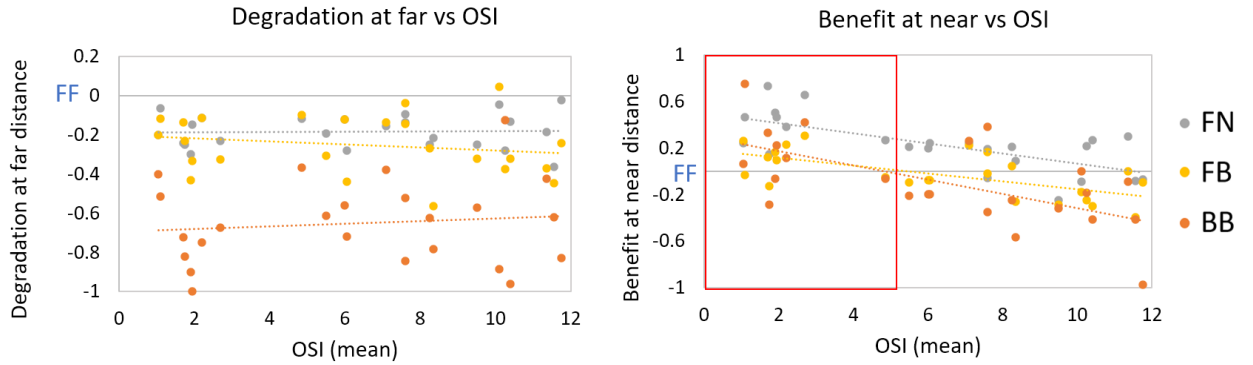

Figure 10.4 *Visual degradation at far distance (left graph) and visual benefit at near distance (right graph) according to the mean OSI index.*

10.3.2. Pre-operative and post-operative perceptual scores

Fifteen subjects were measured both pre-operatively and post-operatively. The OSI in this subset of patients ranged from 1.1 to 11.75 pre-operatively (Table 10.1, shaded cells). Surgery flipped ocular dominance in 46.67% of patients (Table 10.2, highlighted in blue). We found that 57.14% of the subjects with flipped ocular dominance had higher interocular OSI differences (range 2.4 - 12.8, mean of 4.33±6.49), and 42.86% of subjects had an interocular OSI difference ≤1.00.

On average across distances, corrections and subjects, scores increased by 0.66 points from the pre-operative to post-operative measurements. The increase in score was statistically correlated with OSI, since, as expected, the patients with the highest OSI scores provided the lowest scores pre-operatively.

Figure 10.5 shows the monofocal and presbyopic corrections, ranked from highest to lowest modified MAS-2EV scores, pre- (through the cataract opacification) and post-operatively (through the implanted IOL). Corrections are ranked according to the pre-operatively PS score (averaged across patients) at far. Even if there was a systematic increase of the scores after the cataract surgery similarly pre-operatively and post-operatively (2.48% for FF, 9.80% for FN, 9.96% for FB, and 3.90% for BB) patients ranked the perceived quality with these corrections in the same order pre- and post-operatively for each distance.

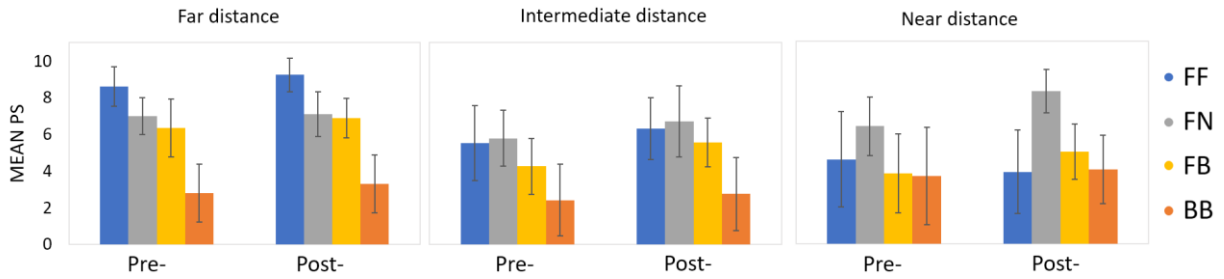

Figure 10.5 *Modified MAS-2EV Modulus (average of the four polygon vertices: near stereo and the three PS averaged across subjects) for each correction at far, intermediate and near distance compared before and after cataract surgery.*

Figure 10.6 shows the pooling of all individual PS for all corrections and distances, pre-operatively vs post-operatively. The high statistical correlation ($r=0.52$, $p<0.0005$) indicates that subjects are accurate at ranking the perceptual quality of the images with the different corrections even through a cataract opacification. We repeated the same analysis at all distances, therefore comparing the scores across corrections at a given distance pre- and post-operatively. At far, we found a high correlation between pre- and post- operative ($r=0.72$, $p<0.0005$) scores. The correlation between pre- and post- operative is slightly reduced at intermediate ($r=0.49$, $p<0.005$) but still highly significant. However, we did not find a significant correlation between the absolute PS scores pre-and post-operatively at near distance ($r=0.24$, $p=0.07$). For presbyopic corrections alone (i.e., excluding the far-far correction) we found statistically significant correlations between pre- and post-operative scores at all distances ($r=0.63$, $p<0.0001$; $r=0.50$, $p<0.0005$, $r=0.29$, $p=0.05$, for far, intermediate and near, respectively). The slope <1 in these

regressions (s=0.52 at all distances; s=0.72 at far; s=0.52 at intermediate and s=0.24 at near) is indicative of an increase in the absolute magnitude of the scores with surgery.

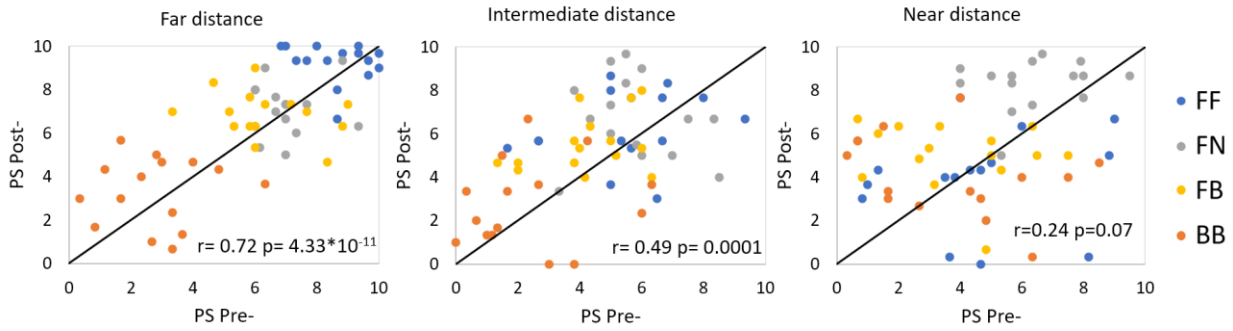

Figure 10.6 *Correlation between the PS pre- and pos-operatively across subjects and corrections for far, intermediate and near distance.*

10.4. Discussion

This study demonstrates the viability of visual simulators, particularly the SimVis Gekko, on cataract patients. The results allow establishing a cataract level threshold of usability and demonstrates that, in mild and moderate cataract patients the relative visual quality scores given to different presbyopic corrections pre-operatively are preserved when the cataract is removed. This indicates that visual simulators can be reliably used to guide the optimal presbyopic correction for a patient, even in the presence of cataracts.

A limitation of the study may have been the relatively large difference in opacification between the two eyes of the same patient (i.e., S002, S006, S013, S014, S017, S024 and S026). Since SimVis Gekko and MAS-2EV are naturally binocular measurements, we averaged the OSI between the left and right eye, to account for an overall reduction by the cataract, and to analyze the dependence of the perceptual scores with each correction on the OSI. Alternative analysis may have involved assuming that the perceived image quality is driven by the eye with the least degradation. In fact, previous work has found that binocular adaptation of blur is biased by the sharper of the two eye's retinal images in subjects with interocular differences of optical degradation [204]. The analysis is complicated by the fact that two out of the four tested corrections involve monovision. Monovision corrections are applied such that the dominant eye is corrected for far, and the non-dominant eye is corrected for near (and the bifocal correction, in modified monovision). In previous work on clear lens subjects, we found significant differences in MAS-2EV with monovision, simply flipping the eye in which the corrections are applied [205]. The shift in measured ocular dominance post-surgery suggests that the difference in opacity between the left and right eye may be limiting the identification of the dominant eye. In a previous study of Schwartz et al. [206], the ocular dominance was measured with the sighting dominance test before and after unilateral cataract surgery. They did not grade the cataract with any other metric but VA. Only 21% of patients had a change in ocular dominance, which was exclusively correlated to the best VA eye (in 80% of the subjects). We found a statistical correlation between OSI interocular difference and the difference in PS scores before and after

cataract surgery and/or ranking. The potentially temporary shift in ocular dominance due to the presence of cataracts is likely a contributor to the reduced performance of a given correction. Apart from OSI interocular differences and large OSI range in our samples, other differences between sessions and across patients may arise from differences in the period of time between eye surgeries (1 to 3 months in 73.3% of the subjects, and 11 to 18 months in 26.7% of the subjects), or susceptibility of the selected ocular dominance method to interocular differences of blur. Other sensory dominance methods [207] including those recently reported that use SimVis Gekko itself may be more accurate than the routine ocular dominance tests used in the clinic.

An interesting finding of our study is the ability of patients with cataracts to rank the different corrections through the cataract opacification (OSI from 1.05 to 11.75, $p>0.005$). Also, patients can judge the visual benefit at intermediate and near with the presbyopic corrections with OSI up to 5.

An unexpected result of the study is the fact the relatively high scores were given by cataract patients at intermediate and near distances with a monofocal far correction. We found that the PS at intermediate and near with the monofocal correction at far increases with the OSI index. This effect may be associated with an increase in blur tolerance in patients with a higher amount of scattering. The origin can be optical, as suggested by Artal et al, in a study showing beneficial optical interactions between aberrations and scattering [208]. On the other hand, increased perceived focus of blurred images is found in patients following neural adaptation to blur [209]. While to our knowledge, most of the previous literature refers to adapting images blurred by Gaussian blur, pure defocus or high order aberrations, it would not be surprising that similar mechanisms also apply to blur produced by cataract, which (as the other forms of blur) boils down to a loss in contrast.

In summary, visual simulations of IOLs are an excellent tool to explore prospective post-operative vision. The high correlation in the perceptual scores pre- and post-cataract surgery demonstrates that the SimVis Gekko can be used in cataractous patients.

Chapter 11

Conclusions

This thesis is divided into two main sections: the first part describes the development of methods and analyses to improve the SimVis Gekko technology and the TL control, and the second part reports the clinical measurements to validate the SimVis Gekko technology in clinical sites. The results of this thesis have an impact on the evaluation of presbyopia treatments and patient's subjective visual quality.

The main accomplishments of this thesis are:

1. An optimized control of tunable lenses working under temporal multiplexing. The high-speed focimeter developed allows the characterization of tunable lenses, that present a linear, repeatable, and predictable behavior. Also, the dynamic effects of the lenses could be compensated by modeling the input wave.

2. The evolution of the high-speed focimeter onto a low-cost and low-speed focimeter that provides an accurate characterization, calibration and experimental optimization of tunable lenses. This is the prototype of a calibration set-up for the clinical site.

3. The development of the Multifocal Acceptance Score Metric to Evaluate Vision (MAS-2EV) that complements the use of SimVis Gekko, to evaluate the global quality of vision of patients in a wide variety of situations (daylight, nighttime, far distance, near distance, and stereo vision).

4. SimVis Gekko tests in the clinic and direct comparisons between the simulations and the real lenses, M-CLs and IOLs, demonstrating that (1) the visual experience through the

simulator was equal to the visual experience with the real contact lenses on eye; and, additionally, that (2) the SimVis Gekko simulations reproduce the through-focus visual acuity curve reported in patients implanted with IOLs.

The specific conclusions of the studies presented in this thesis are:

1. The combination of the linear time-invariant model of the tunable lens and the fast focimeter presented enables, the direct characterization of the transient response of TLs and compensation of the temporal distortions introduced. This allows accurate control of the operation of TLs working at high speed. Based on this, a low-speed approach to TL optimization was proposed and demonstrated with satisfactory results.

2. A method to characterize and compensate the internal temperature effects of TLs was developed and demonstrated. The precision of the simulations was significantly improved after applying the experimental method proposed.

3. The optical quality evaluation system developed can measure and quantify the SimVis Gekko image quality. Experimental measurements matched theoretical predictions from optical design calculations. This system could guide the design, assembly, and fine adjustment of active afocal optical systems and visual simulators. The final version of SimVis Gekko is free of curvature and distortion. The 1x magnification factor along all the optical powers was experimentally demonstrated.

4. The MAS-2EV metric presents high repeatability (Alpha Cronbach's factor 0.95) and sensitivity, and requires short chair time (3 min for subject/condition/correction).

5. The high contrast VA (standard metric of success in the clinic) was not correlated neither with the MAS-2EV metric nor with standard questionnaire (CLUE). But the correlation between the questionnaire and the MAS-2EV metric were highly statistically significant ($p<0.05$-0.0005) both for real and simulated M-CLs.

6. With the first version of the instrument, there were statistically significant differences in VA between the SimVis Gekko (v1.0), and the M-CLs on eye. This result triggered new optical designs, new control techniques of the tunable lenses to improve the optical quality, and new optical benches to check the optical quality, all of them central in this thesis, and crucial in the value provided to eye care professionals and patients.

7. Commercial M-IOLs can be programmed in SimVis Gekko using publicly available data. DFVA curves of the FineVision, PanOptix, and Symfony IOLs, simulated with the SimVis Gekko

v2.0 using public information, matched perfectly the reported DFVA curves from implanted patients.

8. Cataract patients can rank different presbyopic corrections through cataract opacification (OSI from 1.05 to 11.75). Patients can judge the visual benefit at intermediate and near vision with the presbyopic corrections with OSI up to 5. The high correlation in the perceptual scores pre- and post-cataract surgery demonstrates that the SimVis Gekko can be used in cataractous patients.

Scientific activities during this thesis

1. Scientific publications

7. A.G. Lopez-de-Haro, X. Barcala, I. Martinez-Ibarburu, Y. Marrakchi, E. Gambra, V. Rodriguez-Lopez, L. Sawides, C. Dorronsoro. *Closed-loop experimental optimization of tunable lenses*. In preparation.

6. X. Barcala, A. Zaytouny, L. Sawides, C. Dorronsoro, S. Marcos. *Binocular defocus curves with different multifocal IOLs: SimVis Gekko simulations vs clinical data in implanted patients.* In preparation.

5. Y. Marrakchi, X. Barcala, E. Gambra, I. Martinez-Ibarburu, L. Sawides, C. Dorronsoro. *Characterization, prediction, and compensation of temperature effects in tunable lenses performance*. Submitted to Optics Express.

4. X. Barcala, M. Vinas, S. Ruiz, R. Hidalgo, D. Nankivil, T. Karkkainen, E. Gambra, C. Dorronsoro, S. Marcos. *Comparison of vision with a binocular visual simulator and the real multifocal contact lenses in a clinical site.* Submitted to Contact Lens and Anterior Eye.

3. X. Barcala, A. Zaytouny, R. Sanchez-Jean, D. Rego-Lorca, J. Sanchez-Quiros, J.M. Martinez-de-la-Casa, C. Dorronsoro, S. Marcos. *Visual simulations of presbyopic corrections through cataract opacification. S*ubmitted to Journal of Cataract & Refractive Surgery.

2. X. Barcala, M. Vinas, M. Romero, E. Gambra, J.L. Mendez-Gonzalez, S. Marcos, C. Dorronsoro. *Multifocal Acceptance Score to Evaluate Vision: MAS-2EV*. Sci. Rep. 11, 1397 (2021) https://doi.org/10.1038/s41598-021-81059-0

1. C. Dorronsoro, X.Barcala, E. Gambra, V. Akondi et al. *Tunable lenses: dynamic characterization and fine-tuned control for high-speed applications.* Opt. Express 27, 2085-2100 (2019). https://doi.org/10.1364/OE.27.002085

2. Patents

1. P201730854, C. Dorronsoro, E. Gambra, X. Barcala, V. Rodríguez López, S. Marcos. *Aparato para medir a alta velocidad la potencia óptica de lentes y método de medida.* June 28th, 2017, PCT extended PCT/ES2018/070464. Ownership: CSIC and 2EyesVision SL. Licensed to 2EyesVision, Spain.

3. Proceedings

2. L. Sawides, A. de Castro, C. Lago, X. Barcala, A. Zaytouny, S. Marcos, C. Dorronsoro. *SimVis simulations of multifocal IOL designs based on public-literature data*. Proc. SPIE 11871, Optical Design and Engineering VIII, 118710O https://doi.org/10.1117/12.2595035

1. X. Barcala, E. Gambra, L. Sawides, I. Martinez-Ibarburu, A. G. Lopez de Haro, Y. Marrakchi, C. Dorronsoro. *Optical quality evaluation for active afocal systems*. Optical Design and Engineering VIII Conference, 118710Q; https://doi.org/10.1117/12.2596921

4. Conferences

Personally presented

(authors are indicated by signature order, p=poster, t=talk)

[2021 – *t*] X. Barcala, A. Zaytouny, L. Sawides, F. Ribeiro, C. Dorronsoro and S. Marcos. *Binocular defocus curves with different multifocal IOLs: SimVisGekko simulations vs clinical data in implanted patients*. ESCRS 2021 (Amsterdam, Netherlands)

[2021 – *t*] X. Barcala, E. Gambra, L. Sawides, I. Martinez-Ibarburu, A. G. Lopez de Haro, Y. Marrakchi, C. Dorronsoro. *Optical quality evaluation for active afocal systems*. Optical Design and Engineering VIII Conference, SPIE 2021 (Madrid, Spain)

[2021 – *t*] X. Barcala, V. Rodriguez-Lopez, A. Zaytouny, C. Dorronsoro, E. Peli, S. Marcos. *Ocular dominance measurements and monovision corrections.* ARVO 2021 (online)

[2020 – *t*] X. Barcala, A. Zaytouny, R. Sanchez-Jean, D. Rego-Lorca, J. Sanchez-Quiros, S. Marcos, C. Dorronsoro. *Visual quality with pre-operative multifocal corrections simulated with SimVis Gekko in cataract patients*. ESCRS 2020 (online)

[2020 – *t*] X. Barcala, M. Vinas, F. Hidalgo, S. Ruiz, D. Nankivil, T. Karkkainen, K. Chehab, C. Dorronsoro, S. Marcos. *Comparison of vision with multifocal contact lenses and SimVis Gekko in a clinical site*. ARVO 2020 (online)

[2019 – *t*] X. Barcala, M. Romero, N. Garzon, F. Poyales, E. Gambra, S. Marcos, C. Dorronsoro. *Effect of cataract on pre-operative predictions of multifocal acceptance with SimVis Gekko*. ESCRS 2019 (Paris, France)

[2019 – *p*] X. Barcala, I. Martinez-Ibarburu, V. Rodriguez-Lopez, E. Gambra, C. Dorronsoro. *Image quality of tunable-lens based visual simulators*. IONS 2019 (Barcelona, Spain)

[2019 – *t*] X. Barcala, M. Vinas, E. Gambra, S. Marcos, C. Dorronsoro. *Perceptual differences across binocular corrections for presbyopia*. ARVO 2019 (Vancouver, Canada)

[2018 – *t*] X. Barcala Gosende, M. Romero, M. Vinas, J.L. Mendez-Gonzalez, E. Gambra, C. Dorronsoro, S. Marcos. *Repeatability of the multifocal acceptance score (MAS)*. ESCRS 2018 (Vienna, Austria)

[2018 – *t*] X. Barcala, E. Gambra, C. Dorronsoro, S. Marcos. *A high-speed focimeter to characterize the dynamic response of tunable lenses in the visual simulation of multifocal patterns*. VPO 2018 (Athens, Greece)

[2017 – *p*] X. Barcala, E. Gambra, C. Dorronsoro, S. Marcos. *Characterization of the dynamic response of tunable lenses with a high-speed focimeter.* IONS 2017 (Paris, France)

Presented by collaborators

(authors are indicated by signature order, p=poster, t=talk)

[2021 – *t*] L. Sawides, A. de Castro, C. Lago, X. Barcala, A. Zaytouny, S. Marcos, C. Dorronsoro. *SimVis simulations of multifocal IOL designs based on public-literature data*. Optical Design and Engineering VIII Conference, SPIE 2021 (Madrid, Spain)

[2020 – *t*] S. Marcos, X. Barcala, J.M. Martinez de la Casa, J. Garcia-Feijoo, N. Garzon, F. Poyales, C. Dorronsoro. *Multi-component assessment of perceived visual quality with presbyopic corrections using MAS-2EV*. ESCRS 2020 (online)

[2019 – *p*] V. Rodriguez-Lopez, X. Barcala, E. Gambra, L. Sawides, S. Marcos, C. Dorronsoro. *Can tunable lenses provide accurate multifocal simulations?* IONS 2019 (Barcelona, Spain)

[2019 – *t*] C. Dorronsoro, V. Rodriguez Lopez, X. Barcala, E. Gambra, V. Akondi, L. Sawides, Y. Marrakchi, E. Lage, W.S. Geisler, S. Marcos. *Perceptual and physical limits to temporal multiplexing simulation of multifocal corrections*. ARVO 2019

[2018 – *t*] V. Rodriguez-Lopez, X. Barcala, E. Gambra, S. Marcos, C. Dorronsoro. *High-speed focimeter to measure the dynamic response of tunable lenses*. IONS Scandinavia 2018 (Copenhagen, Denmark)

[2018 – *t*] V. Akondi, L. Sawides, Y. Marrakchi, E. Gambra, X. Barcala, S. Marcos, and C. Dorronsoro. *On-bench validations of tunable lens based multifocal visual simulations*. Oral communication. Imaging and Applied Optics (Orlando, USA)

[2017 – *t*] S. Marcos, M. Vinas, C. Dorronsoro, C. Benedi, S. Aissati, V. Akondi, X. Barcala, E. Gambra. *Visual simulations of real multifocal lenses in a multi-channel Adaptive Optics system*. ARVO 2017 (Baltimore, USA)

[2017 – *t*] S. Marcos, A. Radhakrishnan, M. Vinas, C. Benedi, S. Aissati, E. Gambra, D. Pascual, J.R. Alonso-Sanz, V. Akondi, J.L. Mendez-Gonzalez, X. Barcala, C. Dorronsoro. *Wearable see-thru binocular simulator of multifocal and monovision presbyopic corrections*. Wavefront Congress 2017 (San José, USA)

5. Books and chapters

[2021] M. Vinas, S. Aissati, X. Barcala, C. Benedí et al. *Discovering Light. Fun Experiments with Optics.* Editorial: SPIE, OSA Foundation and CSIC. Print ISBN: 9781510639355; PDF ISBN: 9781510639355 https://doi.org/10.1117/3.2579764

[2020] Enrique Gambra Urralburu, María Viñas Peña, Lucie Sawides, Xoana Barcala Gosende, Carlos Dorronsoro Díaz, Susana Marcos Celestino. *Simuladores Visuales*. In *Cirugía refractiva del cristalino*, editado por Luis Fernández-Vega and José F. Alfonso. Monografías de la Sociedad Española de Oftalmología. ISBN: 9788489085756

[2018] M. Vinas, S. Aissati, X. Barcala, C. Benedí et al. *Descubriendo la luz. Experimentos divertidos de óptica.* Editorial: Los libros de la catarata (CSIC). Madrid, Spain. ISBN: 9788490975367

6. Invited talks

[22/09/2021] X Barcala. The Multifocal Acceptance Score to Evaluate Vision (MAS-2EV). Visual Perception and Questionnaires Session. International Society of Presbyopia (ISOP).

[16/04/2021] X Barcala. SimVis Gekko Visual Simulator: a novel ophthalmic instrument developed from scratch. 17th International Young Scientist Conference "Developments in Optics and Communications" 2021 (online)

[30/10/2020] X Barcala. Simuladores visuales en la práctica clínica. Alicante Refractiva Internacional (ARI) 2020 (online)

7. Grants during this thesis

[2018-2021] Industrial PhD (IND2017/BMD7670) fellowship of the Madrid Regional Government, to develop this thesis project. Advisor: Prof. Susana Marcos. Visual Optics and Biophotonics Lab, Spanish National Research Council (CSIC). Company advisor: Dr. Carlos Dorronsoro. 2Eyes Vision.

[03 2021] ARVO Foundation Travel Grant 2021.

[06 2019] Full grant to assist to the International School on Light Sciences and Technologies (ISLiST) Core: Light in Sources, Health and Medicine; Universidad Internacional Menéndez Pelayo (UIMP)

8. Awards during this thesis

[06/12 2020] ARVO Global Mentorship Program. A six-month program that supports and sustains the interest of junior researchers with a focus on professional development within the field and engaging in ARVO (the Association for Research in Vision and Ophthalmology).

9. Other scientific activities

[2017-2021] Member of the IO-CSIC Student Chapter of the Optical Society of America (IOSA, https://sites.google.com/view/iosa-student-chapter-csic/). Treasurer from January 2018 to December 2018. Vice-President of the IOSA student chapter from January 2019 to December 2020. We organize internal seminars series of the IOSA student chapter, as well as invited talks and informal coffees with great researchers. We organize activities to promote the scientific knowledge among our local community. All the activities are funded by the OSA.

[2021] Reviewer for "Eye and Vision" journal. Springer Nature. ISSN: 2326-0254

[05 2020] Certified OSA Reviewer

[04 2020] Design and Interpretation of Clinical Trials Certification Course, Johns Hopkins University through Coursera.

[11 2020] Good Clinical Practice (GCP) Course for Clinical Trials Involving Devices & GCP Course for Clinical Trials Involving Investigational Medical Devices (international focus) from CITI (Collaborative Institutional Training Initiative) program.

[23/11/2018] Teaching assistant at the specialization course "Aprendiendo a enseñar ciencia de forma divertida. Curso de experimentos científicos para profesores" inside the competitive program "Cuenta la Ciencia" of CSIC General Foundation. (1 hour).

[10 2018] Specialization course "Fundamentos de óptica adaptativa para aplicaciones en tecnología de óptica visual y biofotónica" organized by the IO-CSIC

10. Other professional activities

On-site clinical demonstrations in international conferences: European Society of Cataract and Refractive Surgeons (ESCRS) 2018-2019, International Society Of Presbyopia (ISOP) 2018-2019, American Academy of Ophthalmology (AAO) 2019

Training in national and international hospitals and clinics: Pepose Vision (St. Louis, USA) Hospital da Luz (Lisbon), CHU Morvan of Brest (France), Center for Sight (London), Hospital Universitario Fundación Jiménez Díaz (Madrid), Clínica las Claras (Salamanca), ….

Clinical coordination of a multicentric study (Hospital da Luz, Lisbon, Dr. Filomena Ribeiro; CHU Morvan of Brest, France, Dr. Filomena Ribeiro; QVision Clinic, Almería, Dr. Joaquin Fernandez) with a CRO (Medeuronet and Medevice consulting).

Remote demonstrations worldwide during 2020-2021: USA (Rochester, Miami, Houston, South Dakota), Portugal, Spain, France, Switzerland, Chennai (India) and Nagoya (Japan).

Feedback collection from a Beta-tester program, clinical studies, on-site and remote demonstrations and sessions with key opinion leaders and experts.

Bibliography

[1] Fernandez-Vega L, Alfonso JF. Cirugía refractiva del cristalino. Sociedad Española de Oftalmología; 2020.

[2] de Castro A, Ortiz S, Gambra E, Siedlecki D, Marcos S. Three-dimensional reconstruction of the crystalline lens gradient index distribution from OCT imaging. Opt Express 2010;18:21905. https://doi.org/10.1364/oe.18.021905.

[3] Descartes R. Treatise of Man (translated by Hall TS). [Original work published in 1677]. Cambridge, MA: Hardvard University Press; 1977.

[4] Hartridge H. Helmholtz's theory of accommodation. Br J Ophthalmol 1925;9:521.

[5] Myers GA, Stark L. Topology of the near response triad. Ophthalmic Physiol Opt 1990;10:175–81.

[6] Ciuffreda KJ. Accommodation, the pupil, and presbyopia. Borish's Clin Refract 1998:77–120.

[7] Peña MV. Polychromatic Adaptive Optics to evaluate the impact of manipulated optics on vision. Universidad Complutense de Madrid; 2015.

[8] Duane A. Normal values of the accommodation at all ages. J Am Med Assoc 1912;LIX:1010–3. https://doi.org/10.1001/jama.1912.04270090254042.

[9] Kasthurirangan S, Glasser A. Age related changes in accommodative dynamics in humans. Vision Res 2006;46:1507–19. https://doi.org/10.1016/j.visres.2005.11.012.

[10] Glasser A, Campbell MCW. Presbyopia and the optical changes in the human crystalline lens with age. Vision Res 1998;38:209–29. https://doi.org/10.1016/S0042-6989(97)00102-8.

[11] Charman WN. The eye in focus: Accommodation and presbyopia. Clin Exp Optom 2008;91:207–25. https://doi.org/10.1111/j.1444-0938.2008.00256.x.

[12] Resnikoff S, Pascolini D, Etya'ale D, Kocur I, Pararajasegaram R, Pokharel GP, et al. Global data on visual impairment in the year 2002. Bull World Health Organ 2004. https://doi.org//S0042-96862004001100009.

[13] Eurostat. Surgical operations and procedures statistics n.d. https://ec.europa.eu/eurostat/statistics-

explained/index.php?title=Surgical_operations_and_procedures_statistics (accessed May 9, 2021).

[14] Holden BA, Fricke TR, Ho SM, Wong R, Schlenther G, Cronjé S, et al. Global vision impairment due to uncorrected presbyopia. Arch Ophthalmol 2008;126:1731–9. https://doi.org/10.1001/archopht.126.12.1731.

[15] Charman WN. Developments in the correction of presbyopia I: Spectacle and contact lenses. Ophthalmic Physiol Opt 2014. https://doi.org/10.1111/opo.12091.

[16] Morgan PB, Efron N, Woods CA. An international survey of toric contact lens prescribing. Eye Contact Lens 2013;39:132–7. https://doi.org/10.1097/ICL.0b013e318268612c.

[17] Sha J, Bakaraju RC, Tilia D, Chung J, Delaney S, Munro A, et al. Short-term visual performance of soft multifocal contact lenses for presbyopia. Arq Bras Oftalmol 2015;79:73–7. https://doi.org/10.5935/0004-2749.20160023.

[18] Morgan PB, Efron N, Woods CA. An international survey of contact lens prescribing for presbyopia. Clin Exp Optom 2011;94:87–92. https://doi.org/10.1111/j.1444-0938.2010.00524.x.

[19] Llorente-Guillemot A, García-Lazaro S, Ferrer-Blasco T, Perez-Cambrodi RJ, Cerviño A. Visual performance with simultaneous vision multifocal contact lenses. Clin Exp Optom 2012;95:54–9. https://doi.org/10.1111/j.1444-0938.2011.00666.x.

[20] Pérez-Prados R, Piñero DP, Pérez-Cambrodí RJ, Madrid-Costa D. Soft multifocal simultaneous image contact lenses: a review. Clin Exp Optom 2017;100:107–27. https://doi.org/10.1111/cxo.12488.

[21] Morgan PB, Efron N, Woods CA, Santodomingo-Rubido J. International survey of orthokeratology contact lens fitting. Contact Lens Anterior Eye 2019;42:450–4. https://doi.org/10.1016/j.clae.2018.11.005.

[22] Fedtke C, Ehrmann K, Thomas V, Bakaraju RC. Visual performance with multifocal soft contact lenses in non-presbyopic myopic eyes during an adaptation period. Clin Optom 2016;8:37.

[23] Fedtke C, Bakaraju RC, Ehrmann K, Chung J, Thomas V, Holden BA. Visual performance of single vision and multifocal contact lenses in non-presbyopic myopic eyes. Contact Lens Anterior Eye 2016;39:38–46. https://doi.org/10.1016/j.clae.2015.07.005.

[24] Charman WN. Developments in the correction of presbyopia II: Surgical approaches. Ophthalmic Physiol Opt 2014. https://doi.org/10.1111/opo.12129.

[25] Ambrósio R, Wilson SE. LASIK vs LASEK vs PRK: advantages and indications. Semin. Ophthalmol., vol. 18, Taylor & Francis; 2003, p. 2–10.

[26] Becker KA, Jaksche A, Holz FG. PresbyLASIK. Der Ophthalmol 2006;103:667–72.

[27] Alió JL, Chaubard JJ, Caliz A, Sala E, Patel S. Correction of presbyopia by technovision central multifocal LASIK (PresbyLASIK). J Refract Surg 2006;22:453–60. https://doi.org/10.3928/1081-597x-20060501-06.

[28] Arbelaez MC, Vidal C, Arba-Mosquera S. Clinical outcomes of corneal vertex versus central pupil references with aberration-free ablation strategies and LASIK. Investig Ophthalmol Vis Sci 2008;49:5287–94. https://doi.org/10.1167/iovs.08-2176.

[29] ZHELEZNYAK LEN. Ophthalmology/Femtosecond Lasers: LIRIC: Next-generation refractive laser

surgery. BioOptics World 2016;11.

[30] Buratto L, Apple DJ. Phacoemulsification: principles and techniques. Slack Incorporated; 2003.

[31] Meister DJ, Fisher SW. Progress in the spectacle correction of presbyopia. Part 1: Design and development of progressive lenses. Clin Exp Optom 2008;91:240–50.

[32] Han SC, Graham AD, Lin MC. Clinical assessment of a customized free-form progressive add lens spectacle. Optom Vis Sci 2011. https://doi.org/10.1097/OPX.0b013e31820846ac.

[33] Pointer JS. Sighting versus sensory ocular dominance. J Optom 2012;5:52–5.

[34] Zheleznyak L, Alarcon A, Dieter KC, Tadin D, Yoon G. The role of sensory ocular dominance on through-focus visual performance in monovision presbyopia corrections. J Vis 2015;15:17.

[35] Evans BJW. Monovision: A review. Ophthalmic Physiol Opt 2007. https://doi.org/10.1111/j.1475-1313.2007.00488.x.

[36] Burge J, Rodriguez-Lopez V, Dorronsoro C. Monovision and the Misperception of Motion. Curr Biol 2019;29:2586-2592.e4. https://doi.org/10.1016/j.cub.2019.06.070.

[37] Rodriguez-Lopez V, Dorronsoro C, Burge J. Contact lenses, the reverse Pulfrich effect, and anti-Pulfrich monovision corrections. Sci Rep 2020;10:1–16. https://doi.org/10.1038/s41598-020-71395-y.

[38] Fiala W. Bi-and multifocal intraocular lenses. J Emmetropia 2010;1:36–45.

[39] MacRae S, Holladay JT, Glasser A, Calogero D, Hilmantel G, Masket S, et al. Special report: American Academy of Ophthalmology Task Force consensus statement for extended depth of focus intraocular lenses. Ophthalmology 2017;124:139–41.

[40] Rampat R, Gatinel D. Multifocal and Extended Depth-of-Focus Intraocular Lenses in 2020. Ophthalmology 2020.

[41] Pérez-Escudero A, Dorronsoro C, Marcos S. Correlation between radius and asphericity in surfaces fitted by conics. JOSA A 2010;27:1541–8.

[42] Kim E, Bakaraju RC, Ehrmann K. Power Profiles of Commercial Multifocal Soft Contact Lenses. Optom Vis Sci 2017;94:183–96. https://doi.org/10.1097/OPX.0000000000000998.

[43] Venter JA, Pelouskova M, Collins BM, Schallhorn SC, Hannan SJ. Visual outcomes and patient satisfaction in 9366 eyes using a refractive segmented multifocal intraocular lens. J Cataract Refract Surg 2013;39:1477–84.

[44] Muñoz G, Albarrán-Diego C, Cerviño A, Ferrer-Blasco T, García-Lázaro S. Visual and optical performance with the ReZoom multifocal intraocular lens. Eur J Ophthalmol 2012;22:356–62.

[45] Gillmann K, Mermoud A. Visual performance, subjective satisfaction and quality of life effect of a new refractive intraocular lens with central extended depth of focus. Klin Monbl Augenheilkd 2019;236:384–90.

[46] Bellucci R, Curatolo MC. A new extended depth of focus intraocular lens based on spherical aberration. J Refract Surg 2017;33:389–94.

[47] Fernández D, Barbero S, Dorronsoro C, Marcos S. Multifocal intraocular lens providing optimized through-focus performance. Opt Lett 2013;38:5303–6.

[48] Vega F, Millán MS, Gil MA, Garzón N. Optical performance of a monofocal intraocular lens designed to extend depth of focus. J Refract Surg 2020;36:625–32.

[49] Alarcon A, Cánovas C, Koopman B, Weeber H, Auffarth GU, Piers PA. Enhancing the intermediate vision of monofocal intraocular lenses using a higher order aspheric optic. J Refract Surg 2020;36:520–7.

[50] Chang DF. Disruptive innovation and refractive IOLs: How the game will change with adjustable IOLs. Asia-Pacific J Ophthalmol (Philadelphia, Pa) 2019;8:432.

[51] Davison JA, Simpson MJ. History and development of the apodized diffractive intraocular lens. J Cataract Refract Surg 2006;32:849–58.

[52] Gatinel D, Pagnoulle C, Houbrechts Y, Gobin L. Design and qualification of a diffractive trifocal optical profile for intraocular lenses. J Cataract Refract Surg 2011. https://doi.org/10.1016/j.jcrs.2011.05.047.

[53] Maxwell WA, Lane SS, Zhou F. Performance of presbyopia-correcting intraocular lenses in distance optical bench tests. J Cataract Refract Surg 2009;35:166–71.

[54] Kretz FTA, Gerl M, Gerl R, Müller M, Auffarth GU. Clinical evaluation of a new pupil independent diffractive multifocal intraocular lens with a+ 2.75 D near addition: a European multicentre study. Br J Ophthalmol 2015;99:1655–9.

[55] Yang CM, Lim DH, Hwang S, Hyun J, Chung T-Y. Prospective study of bilateral mix-and-match implantation of diffractive multifocal intraocular lenses in Koreans. BMC Ophthalmol 2018;18:1–10.

[56] Schmickler S, Bautista CP, Goes F, Shah S, Wolffsohn JS. Clinical evaluation of a multifocal aspheric diffractive intraocular lens. Br J Ophthalmol 2013;97:1560–4.

[57] Cochener B, Group CS. Clinical outcomes of a new extended range of vision intraocular lens: International Multicenter Concerto Study. J Cataract Refract Surg 2016;42:1268–75.

[58] Weeber HA, Meijer ST, Piers PA. Extending the range of vision using diffractive intraocular lens technology. J Cataract Refract Surg 2015;41:2746–54.

[59] Cochener-Lamard B. Multifocal Intraocular Lenses: The Johnson and Johnson Family of Lenses. Multifocal Intraocular Lenses, Springer; 2019, p. 249–73.

[60] Poyales F, Garzón N, Poyales C, Poyales B. Clinical outcomes with a new model of extended depth of focus intraocular lens. Open J Ophthalmol 2018;8:161–70.

[61] Kanclerz P, Toto F, Grzybowski A, Alio JL. Extended depth-of-field intraocular lenses: an update. Asia-Pacific J Ophthalmol (Philadelphia, Pa) 2020;9:194.

[62] Reinstein DZ, Archer TJ, Gobbe M. Aspheric ablation profile for presbyopic corneal treatment using the MEL80 and CRS Master Laser Blended Vision module. J Emmetropia J Cataract Refract Corneal Surg 2011;2:161–75.

[63] Brar S, Ganesh S, Arra RR, Sute SS. Visual and Refractive Outcomes and Patient Satisfaction Following Implantation of Monofocal IOL in One Eye and ERV IOL in the Contralateral Eye with Mini-Monovision. Clin Ophthalmol (Auckland, NZ) 2021;15:1839.

[64] Ouchi M, Shiba T. Blended Vision Achieved by Combining High and Low Addition Power Diffractive Intraocular Lenses with Micromonovision: A Clinical Outcome. J Ophthalmol

2020;2020.

[65] Hayashi K, Sato T, Igarashi C, Yoshida M. Comparison of visual outcomes between bilateral trifocal intraocular lenses and combined bifocal intraocular lenses with different near addition. Jpn J Ophthalmol 2019;63:429–36.

[66] de Medeiros AL, de Araújo Rolim AG, Motta AFP, Ventura BV, Vilar C, Chaves MAPD, et al. Comparison of visual outcomes after bilateral implantation of a diffractive trifocal intraocular lens and blended implantation of an extended depth of focus intraocular lens with a diffractive bifocal intraocular lens. Clin Ophthalmol (Auckland, NZ) 2017;11:1911.

[67] Goldberg DG, Goldberg MH, Shah R, Meagher JN, Ailani H. Pseudophakic mini-monovision: high patient satisfaction, reduced spectacle dependence, and low cost. BMC Ophthalmol 2018;18:293. https://doi.org/10.1186/s12886-018-0963-3.

[68] Labiris G, Giarmoukakis A, Patsiamanidi M, Papadopoulos Z, Kozobolis VP. Mini-monovision versus multifocal intraocular lens implantation. J Cataract Refract Surg 2015;41:53–7.

[69] Muñoz G, Albarrán-Diego C, Javaloy J, Sakla HF, Cerviño A. Combining zonal refractive and diffractive aspheric multifocal intraocular lenses. J Refract Surg 2012;28:174–81.

[70] Gunenc U, Celik L. Long-term experience with mixing and matching refractive array and diffractive CeeOn multifocal intraocular lenses. J Refract Surg 2008;24:233.

[71] Tabernero J, Chirre E, Hervella L, Prieto P, Artal P. The accommodative ciliary muscle function is preserved in older humans. Sci Rep 2016. https://doi.org/10.1038/srep25551.

[72] Vega-Estrada A, del Barrio JLA, Alió JL. Accommodative Intraocular Lenses. Multifocal Intraocular Lenses, Springer; 2019, p. 355–66.

[73] Marcos S, Ortiz S, Pérez-Merino P, Birkenfeld J, Durán S, Jiménez-Alfaro I. Three-dimensional evaluation of accommodating intraocular lens shift and alignment in vivo. Ophthalmology 2014;121:45–55.

[74] Slagsvold JE. 3M diffractive multifocal intraocular lens: eight year follow-up. J Cataract Refract Surg 2000;26:402–7.

[75] Findl O, Leydolt C. Meta-analysis of accommodating intraocular lenses. J Cataract Refract Surg 2007;33:522–7.

[76] Pepose JS, Burke J, Qazi MA. Benefits and barriers of accommodating intraocular lenses. Curr Opin Ophthalmol 2017;28:3–8.

[77] Rosen E, Alió JL, Dick HB, Dell S, Slade S. Efficacy and safety of multifocal intraocular lenses following cataract and refractive lens exchange: Metaanalysis of peer-reviewed publications. J Cataract Refract Surg 2016;42:310–28.

[78] Pager CK. Expectations and outcomes in cataract surgery: a prospective test of 2 models of satisfaction. Arch Ophthalmol 2004;122:1788–92.

[79] Braga-Mele R, Chang D, Dewey S, Foster G, Henderson BA, Hill W, et al. Multifocal intraocular lenses: relative indications and contraindications for implantation. J Cataract Refract Surg 2014;40:313–22.

[80] Pajic B, Zakharov P, Pajic-Eggspuehler B, Cvejic Z. User friendliness of awearable visual behavior monitor for cataract and refractive surgery. Appl Sci 2020.

https://doi.org/10.3390/app10062190.

[81] Radhakrishnan A, Dorronsoro C, Marcos S. Differences in visual quality with orientation of a rotationally asymmetric bifocal intraocular lens design. J Cataract Refract Surg 2016. https://doi.org/10.1016/j.jcrs.2016.06.034.

[82] Vinas M, Dorronsoro C, Gonzalez V, Cortes D, Radhakrishnan A, Marcos S. Testing vision with angular and radial multifocal designs using Adaptive Optics. Vision Res 2017. https://doi.org/10.1016/j.visres.2016.04.011.

[83] Dorronsoro C, Radhakrishnan A, de Gracia P, Sawides L, Marcos S. Perceived image quality with simulated segmented bifocal corrections. Biomed Opt Express 2016. https://doi.org/10.1364/boe.7.004388.

[84] Mamalis N. Explantation of intraocular lenses. Curr Opin Ophthalmol 2000;11:289–95.

[85] Mamalis N, Brubaker J, Davis D, Espandar L, Werner L. Complications of foldable intraocular lenses requiring explantation or secondary intervention—2007 survey update. J Cataract Refract Surg 2008;34:1584–91.

[86] Gispets J, Arjona M, Pujol J, Vilaseca M, Cardona G. Task oriented visual satisfaction and wearing success with two different simultaneous vision multifocal soft contact lenses. J Optom 2011;4:76–84. https://doi.org/10.1016/S1888-4296(11)70046-2.

[87] Toshida H. Bifocal contact lenses: History, types, characteristics, and actual state and problems. Clin Ophthalmol 2008;2:869. https://doi.org/10.2147/opth.s3176.

[88] Rueff EM, Bailey MD. Presbyopic and non-presbyopic contact lens opinions and vision correction preferences. Contact Lens Anterior Eye 2017;40:323–8. https://doi.org/10.1016/j.clae.2017.03.010.

[89] Remón L, Pérez-Merino P, Macedo-de-Araújo RJ, Amorim-de-Sousa AI, González-Méijome JM. Bifocal and Multifocal Contact Lenses for Presbyopia and Myopia Control. J Ophthalmol 2020;2020:8067657. https://doi.org/10.1155/2020/8067657.

[90] Bennett ES. Contact lens correction of presbyopia. Clin Exp Optom 2008;91:265–78. https://doi.org/10.1111/j.1444-0938.2007.00242.x.

[91] Vinas M, Benedi-Garcia C, Aissati S, Pascual D, Akondi V, Dorronsoro C, et al. Visual simulators replicate vision with multifocal lenses. Sci Rep 2019. https://doi.org/10.1038/s41598-019-38673-w.

[92] Vinas M, Aissati S, Romero M, Benedi-Garcia C, Garzon N, Poyales F, et al. Pre-operative simulation of post-operative multifocal vision. Biomed Opt Express 2019. https://doi.org/10.1364/boe.10.005801.

[93] Pedrotti E, Carones F, Aiello F, Mastropasqua R, Bruni E, Bonacci E, et al. Comparative analysis of visual outcomes with 4 intraocular lenses: Monofocal, multifocal, and extended range of vision. J Cataract Refract Surg 2018. https://doi.org/10.1016/j.jcrs.2017.11.011.

[94] Sheppard AL, Shah S, Bhatt U, Bhogal G, Wolffsohn JS. Visual outcomes and subjective experience after bilateral implantation of a new diffractive trifocal intraocular lens. J Cataract Refract Surg 2013. https://doi.org/10.1016/j.jcrs.2012.09.017.

[95] Gil MA, Varon C, Rosello N, Cardona G, Buil JA. Visual acuity, contrast sensitivity, subjective

quality of vision, and quality of life with 4 different multifocal IOLs. Eur J Ophthalmol 2012. https://doi.org/10.5301/EJO.2011.8371.

[96] McAlinden C, Pesudovs K, Moore JE. The development of an instrument to measure quality of vision: The quality of vision (QoV) questionnaire. Investig Ophthalmol Vis Sci 2010. https://doi.org/10.1167/iovs.10-5341.

[97] Grzybowski A, Kanclerz P, Muzyka-Woźniak M. Methods for evaluating quality of life and vision in patients undergoing lens refractive surgery. Graefe's Arch Clin Exp Ophthalmol 2019. https://doi.org/10.1007/s00417-019-04270-w.

[98] Hays RD, Mangione CM, Ellwein L, Lindblad AS, Spritzer KL, McDonnell PJ. Psychometric Properties of the National Eye Institute-Refractive Error Quality of Life Instrument. Ophthalmology 2003. https://doi.org/10.1016/j.ophtha.2002.07.001.

[99] Atkinson MJ, Tally S, Heichel CW, Kozak I. PSS34 Qualitative Grounding for A New Patient Assessment Measure in Ophthalmology: The Functional Assessment of Visual Tasks (Vistas). Value Heal 2011. https://doi.org/10.1016/j.jval.2011.08.1499.

[100] Atkinson MJ, Tally S, Kozak I, Heichel CW, Kulischak J. PSS35 Validation of the Eighteen Item Functional Assessment of Visual Tasks (Vistas-18) Using A New Lens Prescription Methodology. Value Heal 2011. https://doi.org/10.1016/j.jval.2011.08.1500.

[101] Lundström M, Pesudovs K. Catquest-9SF patient outcomes questionnaire. Nine-item short-form Rasch-scaled revision of the Catquest questionnaire. J Cataract Refract Surg 2009. https://doi.org/10.1016/j.jcrs.2008.11.038.

[102] Wirth RJ, Edwards MC, Henderson M, Henderson T, Olivares G, Houts CR. Development of the contact lens user experience: CLUE scales. Optom Vis Sci 2016;93:801–8. https://doi.org/10.1097/OPX.0000000000000913.

[103] McAlinden C, Skiadaresi E, Moore J, Pesudovs K. Subscale assessment of the NEI-RQL-42 questionnaire with rasch analysis. Investig Ophthalmol Vis Sci 2011. https://doi.org/10.1167/iovs.10-67951.

[104] Vinas M, Dorronsoro C, Radhakrishnan A, Benedi-Garcia C, LaVilla EA, Schwiegerling J, et al. Comparison of vision through surface modulated and spatial light modulated multifocal optics. Biomed Opt Express 2017. https://doi.org/10.1364/boe.8.002055.

[105] Dorronsoro C, Radhakrishnan A, Alonso-Sanz JR, Pascual D, Velasco-Ocana M, Perez-Merino P, et al. Portable simultaneous vision device to simulate multifocal corrections. Optica 2016. https://doi.org/10.1364/optica.3.000918.

[106] Hardy JW, Lefebvre JE, Koliopoulos CL. Real-time atmospheric compensation. J Opt Soc Am 1977;67:360–9. https://doi.org/10.1364/JOSA.67.000360.

[107] Porter J, Queener H, Lin J, Thorn K, Awwal AAS. Adaptive optics for vision science: Principles, practices, design, and applications. vol. 171. John Wiley & Sons; 2006.

[108] Burns SA, de Castro A, Sawides L, Luo T, Sapoznik K. Robust adaptive optics systems for vision science. Adapt. Opt. Wavefront Control Biol. Syst. IV, vol. 10502, International Society for Optics and Photonics; 2018, p. 1050209.

[109] Liang J, Williams DR, Miller DT. Supernormal vision and high-resolution retinal imaging through adaptive optics. J Opt Soc Am A 1997. https://doi.org/10.1364/josaa.14.002884.

[110] Fernández EJ, Artal P. Membrane deformable mirror for adaptive optics: performance limits in visual optics. Opt Express 2003;11:1056–69.

[111] Vinas M, Dorronsoro C, Cortes D, Pascual D, Marcos S. Longitudinal chromatic aberration of the human eye in the visible and near infrared from wavefront sensing, double-pass and psychophysics. Biomed Opt Express 2015. https://doi.org/10.1364/boe.6.000948.

[112] Marcos S, Werner JS, Burns SA, Merigan WH, Artal P, Atchison DA, et al. Vision science and adaptive optics, the state of the field. Vision Res 2017. https://doi.org/10.1016/j.visres.2017.01.006.

[113] Vinas M, Aissati S, Gonzalez-Ramos AM, Romero M, Sawides L, Akondi V, et al. Optical and visual quality with physical and visually simulated presbyopic multifocal contact lenses. Transl Vis Sci Technol 2020;9:1–16. https://doi.org/10.1167/tvst.9.10.20.

[114] Rocha KM, Vabre L, Chateau N, Krueger RR. Enhanced visual acuity and image perception following correction of highly aberrated eyes using an adaptive optics visual simulator. J. Refract. Surg., 2010. https://doi.org/10.3928/1081597X-20101215-08.

[115] Otero C, Vilaseca M, Arjona M, Martínez-Roda JA, Pujol J. Repeatability of aberrometric measurements with a new instrument for vision analysis based on adaptive optics. J Refract Surg 2015;31:188–94. https://doi.org/10.3928/1081597X-20150224-03.

[116] Norrby S, Piers P, Campbell C, van der Mooren M. Model eyes for evaluation of intraocular lenses. Appl Opt 2007;46:6595–605.

[117] Wahl S, Song C, Ohlendorf A. Comparison of two devices to simulate vision with intraocular lenses. Clin Ophthalmol 2019. https://doi.org/10.2147/OPTH.S188890.

[118] Dorronsoro C, Marcos S. Instrument for simulating multifocal ophthalmic corrections. PCT/ES2010/070218, 2010.

[119] de Gracia P, Dorronsoro C, Sánchez-González Á, Sawides L, Marcos S. Experimental simulation of simultaneous vision. Investig Ophthalmol Vis Sci 2013. https://doi.org/10.1167/iovs.12-11219.

[120] Akondi V, Dorronsoro C, Gambra E, Marcos S. Temporal multiplexing to simulate multifocal intraocular lenses: theoretical considerations. Biomed Opt Express 2017. https://doi.org/10.1364/boe.8.003410.

[121] Papadatou E, Águila-Carrasco AJ Del, Marín-Franch I, López-Gil N. Temporal multiplexing with adaptive optics for simultaneous vision. Biomed Opt Express 2016;7:4102–13. https://doi.org/10.1364/BOE.7.004102.

[122] Blum M, Büeler M, Grätzel C, Aschwanden M. Compact optical design solutions using focus tunable lenses. In: Tissot J-LM, Raynor JM, Mazuray L, Wartmann R, Wood A, editors. Opt. Des. Eng. IV, vol. 8167, SPIE; 2011, p. 274–82. https://doi.org/10.1117/12.897608.

[123] Grulkowski I, Manzanera S, Cwiklinski L, Sobczuk F, Karnowski K, Artal P. Swept source optical coherence tomography and tunable lens technology for comprehensive imaging and biometry of the whole eye. Optica 2018;5:52–9. https://doi.org/10.1364/OPTICA.5.000052.

[124] Fahrbach FO, Voigt FF, Schmid B, Helmchen F, Huisken J. Rapid 3D light-sheet microscopy with a tunable lens. Opt Express 2013;21:21010–26. https://doi.org/10.1364/OE.21.021010.

[125] Jabbour JM, Malik BH, Olsovsky C, Cuenca R, Cheng S, Jo JA, et al. Optical axial scanning in

confocal microscopy using an electrically tunable lens. Biomed Opt Express 2014;5:645–52. https://doi.org/10.1364/BOE.5.000645.

[126] Jiang J, Zhang D, Walker S, Gu C, Ke Y, Yung WH, et al. Fast 3-D temporal focusing microscopy using an electrically tunable lens. Opt Express 2015;23:24362–8. https://doi.org/10.1364/OE.23.024362.

[127] Volpi D, Tullis IDC, Barber PR, Augustyniak EM, Smart SC, Vallis KA, et al. Electrically tunable fluidic lens imaging system for laparoscopic fluorescence-guided surgery. Biomed Opt Express 2017;8:3232–47. https://doi.org/10.1364/BOE.8.003232.

[128] Dorronsoro C, Alonso-Sanz JR, Marcos S. Miniature simultaneous vision simulator instrument. Patent WO 2015/049402 (09.04.2015), 2015.

[129] Watson AB. Temporal sensitivity. Handb Percept Hum Perform 1986;1:1–43.

[130] Dorronsoro C, Rodríguez-Lopez V, Barcala X, Gambra E, Akondi V, Sawides L, et al. Perceptual and physical limits to temporal multiplexing simulation of multifocal corrections. Invest Ophthalmol Vis Sci 2019;60:6465.

[131] Zhang H, Ren H, Xu S, Wu S-T. Temperature effects on dielectric liquid lenses. Opt Express 2014;22:1930–9.

[132] Akondi V, Sawides L, Marrakchi Y, Gambra E, Marcos S, Dorronsoro C. Experimental validations of a tunable-lens-based visual demonstrator of multifocal corrections. Biomed Opt Express 2018. https://doi.org/10.1364/boe.9.006302.

[133] Radhakrishnan A. Presbyopia corrections: optical, perceptual and adaptational implications 2019.

[134] Radhakrishnan A, Pascual D, Marcos S, Dorronsoro C. Vision with different presbyopia corrections simulated with a portable binocular visual simulator. PLoS One 2019. https://doi.org/10.1371/journal.pone.0221144.

[135] Chikri YM. Development of Electronics and Firmware for a Vision Simulation Device. Universidad Carlos III de Madrid, 2017.

[136] Sawides L, de Castro A, Lago CM, Barcala X, Zaytouny A, Marcos S, et al. SimVis simulations of multifocal IOL designs based on public-literature data 2021. https://doi.org/10.1117/12.2595035.

[137] Dorronsoro C, Barcala X, Gambra E, Akondi V, Sawides L, Marrakchi Y, et al. Tunable lenses: dynamic characterization and fine-tuned control for high-speed applications. Opt Express 2019. https://doi.org/10.1364/oe.27.002085.

[138] Self HC. Optical tolerances for alignment and image differences for binocular helmet-mounted displays. HARRY G ARMSTRONG AEROSPACE MEDICAL RESEARCH LAB WRIGHT-PATTERSON AFB OH; 1986.

[139] Gil MA, Varón C, Cardona G, Buil JA. Visual acuity and defocus curves with six multifocal intraocular lenses. Int Ophthalmol 2020;40:393–401. https://doi.org/10.1007/s10792-019-01196-4.

[140] Schwiegerling J, Lapid-Gortzak R, Balachandran C, Suryakumar R. Metric for assessing the functional range of vision of multifocal IOLs. Invest Ophthalmol Vis Sci 2019;60:3710.

[141] Buckhurst PJ, Wolffsohn JS, Naroo SA, Davies LN, Bhogal GK, Kipioti A, et al. Multifocal intraocular lens differentiation using defocus curves. Invest Ophthalmol Vis Sci 2012;53:3920–6.

[142] Pieh S, Kellner C, Hanselmayer G, Lackner B, Schmidinger G, Walkow T, et al. Comparison of visual acuities at different distances and defocus curves. J Cataract Refract Surg 2002;28:1964–7.

[143] Dorronsoro C, Gambra E, Barcala X, Rodriguez-Lopez V, Marcos S. Device for determining the optical power of lenses and measurement method. WO/2019/002656; PCT/ES2018/070464, 2017.

[144] Oku H, Hashimoto K, Ishikawa M. Variable-focus lens with 1-kHz bandwidth. Opt Express 2004;12:2138–49. https://doi.org/10.1364/OPEX.12.002138.

[145] López CA, Hirsa AH. Fast focusing using a pinned-contact oscillating liquid lens. Nat Photonics 2008;2:610–3. https://doi.org/10.1038/nphoton.2008.198.

[146] Berge B, Peseux J. Variable focal lens controlled by an external voltage: An application of electrowetting. Eur Phys J E 2000;3:159–63. https://doi.org/10.1007/s101890070029.

[147] Krupenkin T, Yang S, Mach P. Tunable liquid microlens. Appl Phys Lett 2003;82:316–8. https://doi.org/10.1063/1.1536033.

[148] Ren H, Wu S-T. Tunable-focus liquid microlens array using dielectrophoretic effect. Opt Express 2008;16:2646. https://doi.org/10.1364/oe.16.002646.

[149] Dong L, Agarwal AK, Beebe DJ, Jiang H. Adaptive liquid microlenses activated by stimuli-responsive hydrogels. Nature 2006;442:551–4. https://doi.org/10.1038/nature05024.

[150] Chronis N, Liu G, Jeong K-H, Lee L. Tunable liquid-filled microlens array integrated with microfluidic network. Opt Express 2003;11:2370. https://doi.org/10.1364/oe.11.002370.

[151] Moran PM, Dharmatilleke S, Khaw AH, Tan KW, Chan ML, Rodriguez I. Fluidic lenses with variable focal length. Appl Phys Lett 2006;88:1–3. https://doi.org/10.1063/1.2168245.

[152] Golnaraghi F, Kuo BC. Automatic control systems. 2nd ed. Complex Variables; 2010.

[153] Miccio L, Finizio A, Grilli S, Vespini V, Paturzo M, Nicola S De, et al. Tunable liquid microlens arrays in electrode-less configuration and their accurate characterization by interference microscopy. Opt Express 2009;17:2487–99. https://doi.org/10.1364/OE.17.002487.

[154] López CA, Lee CC, Hirsa AH. Electrochemically activated adaptive liquid lens. Appl Phys Lett 2005;87:1–3. https://doi.org/10.1063/1.2058209.

[155] Huang X, Cheng CM, Wang L, Wang B, Su CC, Ho MS, et al. Thermally tunable polymer microlenses. Appl Phys Lett 2008;92:2006–9. https://doi.org/10.1063/1.2945646.

[156] Schwiegerling J. Field Guide to Visual and Ophthalmic Optics. SPIE Press; 2004.

[157] Navarro R, Moreno-Barriuso E. Laser ray-tracing method for optical testing. Opt Lett 1999;24:951–3. https://doi.org/10.1364/OL.24.000951.

[158] Jarosz J, Mecê P, Conan J-M, Petit C, Paques M, Meimon S. High temporal resolution aberrometry in a 50-eye population and implications for adaptive optics error budget. Biomed Opt Express 2017;8:2088–105. https://doi.org/10.1364/BOE.8.002088.

[159] Annibale P, Dvornikov A, Gratton E. Electrically tunable lens speeds up 3D orbital tracking. Biomed Opt Express 2015;6:2181. https://doi.org/10.1364/boe.6.002181.

[160] Oku H, Ishikawa M. High-speed liquid lens with 2ms response and 80.3 nm root-mean-square

wavefront error. Appl Phys Lett 2009;94. https://doi.org/10.1063/1.3143624.

[161] Liu S, Hua H. Time-multiplexed dual-focal plane head-mounted display with a liquid lens. Opt Lett 2009;34:1642–4. https://doi.org/10.1364/OL.34.001642.

[162] Korposh S, James SW, Lee S-W, Tatam RP. Tapered optical fibre sensors: Current trends and future perspectives. Sensors 2019;19:2294.

[163] Optotune. Fast Electrically Tunable Lens EL-10-30 Series. Switzerland: 2021.

[164] Iwai D, Izawa H, Kashima K, Ueda T, Sato K. Speeded-up focus control of electrically tunable lens by sparse optimization. Sci Rep 2019;9:1–6.

[165] Wang Z, Bovik AC, Sheikh HR, Simoncelli EP. Image quality assessment: from error visibility to structural similarity. IEEE Trans Image Process 2004;13:600–12.

[166] Sara U, Akter M, Uddin MS. Image quality assessment through FSIM, SSIM, MSE and PSNR—a comparative study. J Comput Commun 2019;7:8–18.

[167] Ashtiani AO, Jiang H. Thermally actuated tunable liquid microlens with sub-second response time. Appl Phys Lett 2013;103:111101.

[168] Kawashima Y. Liquid lens with temperature compensated focus time. US20110200314A1, 2011.

[169] Patscheider R, Niedere D, Gebbers P, Borer D, Laning C, Smolka S. Temperature drift compensation for liquid lenses. US20180136372A1, 2016.

[170] Iskander DR. Computational aspects of the visual Strehl ratio. Optom Vis Sci 2006;83:57–9.

[171] Barcala X, Gambra E, Sawides L, Martinez-ibarburu I, Rofriguez-lopez V, Dorronsoro C. Optical quality evaluation for active afocal systems 2021. https://doi.org/10.1117/12.2596921.

[172] Millán MS, García-Varela MSM, Soteras JE, Cabré EP. Óptica geométrica. Grupo Planeta (GBS); 2004.

[173] Malacara D. Optical shop testing. vol. 59. John Wiley & Sons; 2007.

[174] Perra C, Massidda F, Giusto DD. Image blockiness evaluation based on sobel operator. IEEE Int. Conf. Image Process. 2005, vol. 1, IEEE; 2005, p. I–389.

[175] Manzanera S, Prieto PM, Ayala DB, Lindacher JM, Artal P. Liquid crystal Adaptive Optics Visual Simulator: Application to testing and design of ophthalmic optical elements. Opt Express 2007. https://doi.org/10.1364/oe.15.016177.

[176] Zheleznyak L, Kim MJ, MacRae S, Yoon G. Impact of corneal aberrations on through-focus image quality of presbyopia-correcting intraocular lenses using an adaptive optics bench system. J Cataract Refract Surg 2012. https://doi.org/10.1016/j.jcrs.2012.05.032.

[177] Radhakrishnan A, Dorronsoro C, Sawides L, Marcos S. Short-term neural adaptation to simultaneous bifocal images. PLoS One 2014. https://doi.org/10.1371/journal.pone.0093089.

[178] Nathan E. Contact Lens Practice: 3rd edition. Elsevier; 2017.

[179] Aller TA, Liu M, Wildsoet CF. Myopia control with bifocal contact lenses: A randomized clinical trial. Optom Vis Sci 2016. https://doi.org/10.1097/OPX.0000000000000808.

[180] Barcala X, Vinas M, Hidalgo F, Ruiz S, Nankivil D, Karkkainen T, et al. Comparison of vision with

multifocal contact lenses and SimVis Gekko simulations in a clinical site. Invest Ophthalmol Vis Sci 2020;61:579–579.

[181] Barcala X, Vinas M, Romero M, Gambra E, Luis J, Gonzalez M, et al. Multifocal acceptance score to evaluate vision : MAS - 2EV. Sci Rep 2021:1–15. https://doi.org/10.1038/s41598-021-81059-0.

[182] Johnson & Johnson Medical Ltd. 1-DAY ACUVUE® MOIST MULTIFOCAL FITTING GUIDE 2017:1–3. https://www.jnjvisioncare.co.uk/sites/default/files/public/uk/documents/2018-01_1dammf_fitting_guide_uk.pdf.

[183] College of Optometrists and The Royal College of Ophthalmologists. Contact lens fitting 2011. https://guidance.college-optometrists.org/guidance-contents/knowledge-skills-and-performance-domain/fitting-contact-lenses/ (accessed January 6, 2021).

[184] Ferris FL, Kassoff A, Bresnick GH, Bailey I. New Visual Acuity Charts for Clinical Research. Am J Ophthalmol 1982;94:91–6. https://doi.org/https://doi.org/10.1016/0002-9394(82)90197-0.

[185] Wolffsohn JS, Jinabhai AN, Kingsnorth A, Sheppard AL, Naroo SA, Shah S, et al. Exploring the optimum step size for defocus curves. J Cataract Refract Surg 2013;39:873–80. https://doi.org/10.1016/j.jcrs.2013.01.031.

[186] Collins MJ, Franklin R, Davis BA. Optical considerations in the contact lens correction of infant aphakia. Optom Vis Sci 2002;79:234–40. https://doi.org/10.1097/00006324-200204000-00010.

[187] Sha J, Tilia D, Kho D, Diec J, Thomas V, Bakaraju RC. Comparison of extended depth-of-focus prototype contact lenses with the 1-day ACUVUE MOIST MULTIFOCAL after one week of wear. Eye Contact Lens 2018;44:S157–63.

[188] Karkkainen T, Moody K, Clark R, Xu J, Hickson-Curran S. Evaluation of the visual performance of a new multifocal contact lens and the impact of refractive error. Contact Lens Anterior Eye 2018;41:S24–5.

[189] Vedhakrishnan S, Vinas M, El Aissati S, Marcos S. Vision with Spatial Light Modulator simulatingmultifocal contact lenses in an Adaptive Opticssystem. Biomed Opt Express 2021;12:2859–72. https://doi.org/10.1364/boe.419680.

[190] Home R. Binocular summation: a study of contrast sensitivity, visual acuity and recognition. Vision Res 1978;18:579–85.

[191] Plainis S, Ntzilepis G, Atchison DA, Charman WN. Through-focus performance with multifocal contact lenses: Effect of binocularity, pupil diameter and inherent ocular aberrations. Ophthalmic Physiol Opt 2013;33:42–50. https://doi.org/10.1111/opo.12004.

[192] Fedtke C, Ehrmann K, Thomas V, Bakaraju RC. Association between multifocal soft contact lens decentration and visual performance. Clin Optom 2016;8:57.

[193] Plainis S, Atchison DA, Charman WN. Power profiles of multifocal contact lenses and their interpretation. Optom Vis Sci 2013;90:1066–77. https://doi.org/10.1097/OPX.0000000000000030.

[194] Villegas EA, Alcón E, Artal P. Optical quality of the eye in subjects with normal and excellent visual acuity. Invest Ophthalmol Vis Sci 2008;49:4688–96.

[195] C. B-G, M. V, C. L, C. D. Optical and visual quality of real intraocular lenses physically projected on the patient's eye. Investig Ophthalmol Vis Sci 2020.

[196] Villegas EA, Manzanera S, Lago CM, Hervella L, Sawides L, Artal P. Effect of crystalline lens aberrations on adaptive optics simulation of intraocular lenses. J Refract Surg 2019;35:126–31.

[197] Loicq J, Willet N, Gatinel D. Topography and longitudinal chromatic aberration characterizations of refractive–diffractive multifocal intraocular lenses. J Cataract Refract Surg 2019;45:1650–9. https://doi.org/10.1016/j.jcrs.2019.06.002.

[198] Sharpe LT, Stockman A, Jagla W, Jägle H. A luminous efficiency function, V*(λ), for daylight adaptation. J Vis 2005;5:3.

[199] Ribeiro F, Ferreira TB. Comparison of clinical outcomes of 3 trifocal IOLs. J Cataract Refract Surg 2020;46:1247–52. https://doi.org/10.1097/j.jcrs.0000000000000212.

[200] Manzanera S, Lago CM, Hervella L, Sawides L, Villegas E, Artal P. Effect of crystalline lens' aberrations on AO-simulation of IOLs in phakic eyes. Invest Ophthalmol Vis Sci 2017;58:2497.

[201] Coletta NJ, Marcos S, Wildsoet C, Troilo D. Double-pass measurement of retinal image quality in the chicken eye. Optom Vis Sci 2003;80:50–7.

[202] Artal P. Calculations of two-dimensional foveal retinal images in real eyes. JOSA A 1990;7:1374–81.

[203] Artal P, Marcos SC, Navarro RF, Miranda I, Ferro M. Through focus image quality of eyes implanted with monofocal and multifocal intraocular lenses. Opt Eng 1995;34:772–9.

[204] Kompaniez E, Sawides L, Marcos S, Webster MA. Adaptation to interocular differences in blur. J Vis 2013;13:19.

[205] Barcala X, Rodríguez-Lopez V, Zaytouny A, Dorronsoro C, Peli E, Marcos S. Ocular dominance measurements and monovision corrections. Invest Ophthalmol Vis Sci 2021;62:1443.

[206] Schwartz R, Yatziv Y. The effect of cataract surgery on ocular dominance. Clin Ophthalmol (Auckland, NZ) 2015;9:2329.

[207] Seijas O, de Liaño PG, de Liaño RG, Roberts CJ, Piedrahita E, Diaz E. Ocular dominance diagnosis and its influence in monovision. Am J Ophthalmol 2007;144:209–16.

[208] Artal P. Image formation in the living human eye. Annu Rev Vis Sci 2015;1:1–17.

[209] Webster MA, Marcos S. Neural adaptation to blur. Handb. Vis. Opt., CRC Press; 2017, p. 307–20.